

Session 6

Materials and Components

OPERATING EXPERIENCE WITH THE DRAGON HIGH TEMPERATURE REACTOR EXPERIMENT

R.A. SIMON

*DRAGON Operations Branch/EC (retired)
Rue du Dragon 62A, BE-1640 Rhode-St.Genesse /Belgium*

and

P.D. CAPP

*DRAGON Operations Branch/UKAEA (retired)
20 Field Barn Drive, Weymouth, Dorset DT1 2AE/ UK*

ABSTRACT

The Dragon Reactor Experiment in Winfrith /UK was a materials test facility for a number of HTR projects pursued in the sixties and seventies of the last century. It was built and managed as an OECD/NEA international joint undertaking. The reactor operated successfully between 1964 and 1975 to satisfy the growing demand for irradiation testing of fuels and fuel elements as well as for technological tests of components and materials. The paper describes the reactor's main experimental features and presents results of 11 years of reactor operation relevant for future HTRs.

1. Introduction

The DRAGON Reactor Experiment (DRE) was the experimental reactor of the O.E.C.D High Temperature Reactor Project. This facility was uniquely suitable for testing the fuel, the fuel element designs and the structural materials not only for the HTR power reactor designs pursued by the Dragon Project itself, but also for the development of national power reactor projects like the THTR and the Fort St. Vrain HTGR. During the later years of operation, more than 60% of the available core positions were occupied by coated particle fuel experiments sponsored by the UKAEA, the CEA, Belgonucléaire and KFA. Although there were limitations in the geometry of irradiation experiments, requirements concerning the burnup, the neutron flux, the temperature and the coolant flow could be satisfied individually by selecting the core position and adapting the base of the fuel element. The precise irradiation conditions and the accurate measurement of the experiments performance were made possible by continuously monitoring various fuel element temperatures and sampling gas release from the fuel. These measurements were facilitated by the extremely low contamination of the primary circuit and the controlled area in general. The results of the many DRAGON irradiation tests have been incorporated in today's general data base on HTRs. The operational experience was reported in detail by B.G.Chapman [1]. This paper is also concerned with some less well publicised items.

2. The core

The core consisted of thirty-seven fuel elements, placed in a hexagonal array with an effective diameter of 1.08m. This hexagonal array was surrounded by 30 prismatic graphite columns of the "inner live" reflector, machined on one side to match the profile of the adjacent fuel element and on the other to form a circle of 1.5m diameter. The 24 control rods operated in holes in the inner live reflector. The overall length of a fuel element was 2.54m, of which 1.60m in the middle contained fuel (s.Fig.1) The remaining lengths at the top and bottom comprised the axial reflector and end fittings. The helium coolant entered the core from below and passed upward through channels between fuel rods. Maximum thermal power was 21.5 MW obtained with an inlet temperature of 350°C, an outlet temperature of 750 °C and a helium mass flow of 9.62 kg/s at 20 atm.

Fig.1 shows the cross section of a typical DRAGON fuel element: The six outer fuel rods (a) were held together at the top by a massive graphite block (b) which extended up to a reinforced lifting head (c); at the bottom a Nimonic ring held the six-rod assembly

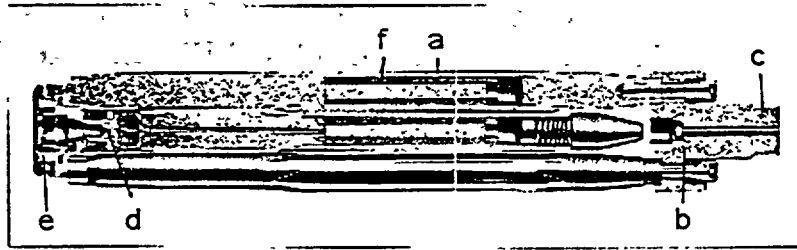


Fig 1. Standard DRE Fuel Element

together. The central rod accommodated the experimental section. This central rod was firmly attached to the metallic base of the fuel element, which accurately positions the fuel element in one of the 37 core positions by means of a central conical hole (d) sitting on the precisely fitting conical spike attached to the core bed plate. Each spike was equipped with a key bolt to align the orientation of fuel element and surrounded by 12 thermocouple terminals mating with contacts (e) under the fuel element base. In certain fuel elements the outer ring of six driver rings with the lifting head and bottom ring could be separated from the experimental central rod and the base by remotely unlocking the Nimonic bottom ring.

The six outer rods of a fuel element generally contained highly enriched UO_2 driver fuel which provided most of the reactivity of the core. The coated particles for this fuel were produced at the reactor site: the UO_2 kernels had a diameter of 0.8mm and had a triple (TRISO) layer of inner pyrocarbon, silicon carbide and outer pyrocarbon with a combined thickness of about 0.15mm. These coated particles were bonded together in a carbonaceous matrix to form the hollow cylinder "compacts" (f) characteristic for DRAGON driver fuel. The experimental coated particle fuel in the centre of the elements consisted of low enriched UO_2 , but also thorium and plutonium as oxide and carbide. Specimens for a variety of HTR fuel cycles were irradiated simultaneously in the experimental centre channels and in entire fuel element positions. The extensive DRE experience with irradiating coated particle fuel at extreme temperatures confirmed that a statistical approach is valid for failure prediction. Fig. 2 shows the measured Fission Product (FP) release (expressed as Release/Birth or R/B ratio) from a fuel with a temperature of $1800^\circ C$ compared to its release at an operating temperature of $1250^\circ C$. The significant feature is the exponential increase in release

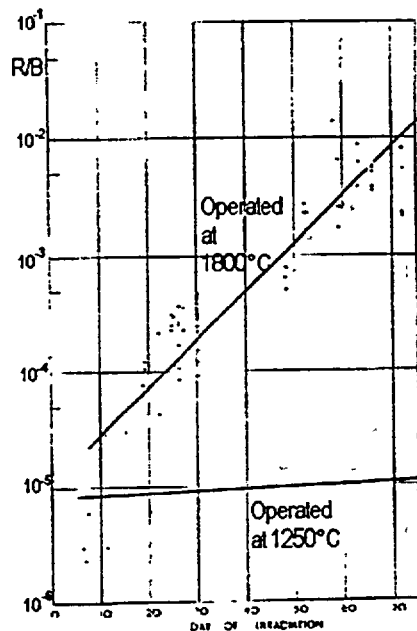


Fig 2: Fission Product Release/Birth Xe-133

indicating that in the case of unexpected overheating or other fuel failure, there is a slow build up of activity permitting location and removal.

As the sampling of released FP through the purge gas system was generally limited to the experimental central fuel rod in an element, a procedure for the identification of defective unpurged fuel was developed. This technique involves a slight reduction of the reactor power and the changing of the control rod pattern to a 20 rod 'curtain' with one rod fully inserted. The power and therefore the temperature from the element closest to the inserted rod dropped significantly and its FP release was reduced dramatically. This procedure was repeated for each control rod position. The effect was most important in the peripheral fuel elements, but still gave meaningful results one pitch away from the dipped rod. The FP isotope monitored in the outlet gas was the very short-lived Kr-90 (8.5 seconds half-life) and its sister Kr-87 (87 minutes), which reached equilibrium concentrations in the outlet gas in less than 2 hours after the control rod insertion. This technique could be applied to power reactors, where the symmetrical arrangements of control rods could allow the location of releasing fuel.

3. Power cycling

The experience with power cycling the reactor confirmed the excellent behaviour predicted in the safety analyses. The very small fuel particles embedded in a graphite matrix gave efficient heat transfer and the difference between peak fuel temperature and graphite surface temperature were small (about 200°C). During normal operation peak fuel temperatures did not exceed 1250°C. The physics of the HTR core provided the system with a strong negative temperature coefficient. Using this characteristic it was possible to control the reactor power by varying helium mass flow. The experiments clearly demonstrated that the power immediately followed the increase in helium mass flow, but that core and fuel temperatures did not rise as consequence of raising the reactor power from 75% to 90% in a few seconds.

Two core positions were modified in order to further study the effect of regular temperature cycling on various graphites and fuel assemblies. The sampling connections to the fuel element spikes were altered to permit the injection of a pulse of helium to the base of the element. This pulse was used to actuate a special valve that changed the coolant flow section to the element. Elements fitted with these valves and irradiated in these positions were temperature cycled frequently without perturbing the rest of the core.

4. Chemical reactivity of the core

In the initial concept of the reactor experiment purged fuel rods contained compacts of 'bare' uranium oxide pellets in a graphite matrix. It was envisaged that this fuel would release the fission product xenon and krypton as they formed to be purged out into a purification plant thus significantly reducing the neutron poisoning effects of these isotopes. The purge helium flowed through large fission product adsorption beds and on into three clean-up plants, to be used individually and regenerated as necessary. Early fuel tests Loop 'A' of the Pluto Heavy Water MTR at Harwell showed that, even at 1000°C, most of the krypton and xenon was retained in the fuel matrix. This encouraged the development of a revolutionary coated particle fuel that released less than 10^{-7} of the fission products. In practice the purification plants maintained ultra pure helium coolant conditions in the primary circuit of the reactor. Typical results of coolant chemical analysis during operation were (in vpm):

O ₂	N ₂	CO	CO ₂	CH ₄	H ₂ O	H ₂
0.1	0.05	0.05	0.02	0.1	0.1	0.1

This high purity coolant coupled with the advanced analytical system that had been developed permitted the study of the chemistry of the injection of very low concentrations (1-5 volume parts per million) of possible circuit contaminants. It became a routine procedure to determine the 'core chemical reactivity' by injecting a small quantity of water into each fresh fuel configuration. In addition experiments were carried out injecting small quantities of methane or carbon dioxide. Due to the absence of metallic corrosion and the almost perfect retention of the FP in the fuel there was practically no routine secondary waste.

5. Primary circuit

The primary heat removal circuit was contained entirely in the carbon steel pressure vessel with its six heat exchanger branches. It operated at reactor outlet temperatures of 750°C and inlet temperatures of 330-370°C. The operating pressure of the vessel was 20 ata. The coolant path of the primary heat removal circuit was arranged in a way that the vessel walls were in contact with the cold (330°C-370°C) reactor inlet stream only. The integrated fast neutron dose of the vessel walls at mid core height was in the order of 5×10^{18} n/cm² after ten years of power operation. The hot leg of the circuit consisted of a large plenum chamber above the core and six duct liners, which fed the reactor outlet coolant to the primary heat exchangers. The plenum structure was thermally insulated the hot side by two layers of 3 mm Nimonic sheet spaced 6 mm apart.

The helium inventory of the Dragon primary coolant system was about 355 kg of which, during operation, 175 kg were kept in the reserve stores and the dump tanks. Of the other half, 68 kg were circulating in the main heat removal circuit, the rest was slowly circulating through the Fission Product Removal Plant (36 kg), the Helium Purification Plant (19 kg) and the Transfer Chamber (45.5

kg). The heat sink contained the remaining 10 kg. The coolant losses from the primary circuit during operation were identified as accountable or unaccountable losses. Losses due to refuelling shutdowns (20-30 kg per shutdown) were mainly caused by changing the vessel contents from helium to air. The accountable losses consisting of coolant bled off for analysis or for other experimental and operational purposes amounted to about 1 kg per operating day. The unaccounted losses stemmed from leaks, maintenance work on instruments and ancillaries and "spillage" during insertion and operation of experimental probes. The safety philosophy relied upon the leak detection for an early warning of any conceivable major failure of the pressure vessel. A sensitive and reliable method of monitoring the leak rate from the primary circuit was, therefore, primarily a safety requirement. As any helium leaking from the primary circuit was rapidly dispersed in the large volume of the inner containment, the background concentration from accountable losses had to be kept at a low level so that any increase in the leak rate could be observed at an early stage. A continuous measurement of the helium concentration in the inner containment was provided by a highly sensitive mass spectrometer. As the leakage from the active part of the circuit was the most important parameter, the readings of an activity monitor measuring Kr-87 on the containment ventilation extract correlated to the primary circuit activity gave a measurement of the primary circuit active leak rate, normally about half of the total leak rate. Both instruments were recalibrated frequently. For an absolute determination of the overall leak rate a helium balance within the primary circuit was taken twice a week. During routine operation, the average helium leak rate was less than 0.2kg/day or 0.12 % of the circulating inventory. In the beginning of 1974, the leak rate during operation reached 2.0 kg/day and after months of searching a number of leaks were found in the stainless steel (SS) pipework leading to the helium purification plant. The leaks, almost invisible pores and crevices in the otherwise healthy lengths of pipe, were produced by chloride corrosion. All leaks occurred in narrow sections of the pipes that had been wrapped with PVC insulating tape during commissioning for the purpose of marking the various flow paths and components of the circuit. When the circuit operated at temperature roughly between 80 and 120°C, the innermost layer of PVC tape decomposed, leaving gaseous HCl trapped under the outer still intact layers of tape. (On pipe sections under 80°C the PVC tape remained stable and above ca. 120°C the complete wrapping cracked and fell off). After the discovery of the leaks caused by the chloride corrosion all accessible SS pipework was searched and more than 200 tape markings were removed. All sections of SS pipework that had carried tape markings were cleaned and sections that had operated above 80°C were replaced. The result was a drastic reduction of unaccounted helium losses to 0.2 kg/day.

6. Maintenance

The fission product release studies, both gaseous and metallic, indicated the comparative cleanness of the primary circuit but the in-core maintenance operations really proved the point. The original design made provision for the remote removal of, in addition to fuel elements, inner live reflector blocks, fuel support spikes and control rods and their winding heads. During the nine years of operation all of these procedures were carried out and the last two even became almost routine. The reflector block replacement carried out in 1973 proved to be a rather non-standard operation and it is worthwhile reiterating some of the lessons learned. Fig 3 shows one of the reflector blocks warped by the neutron flux.

After removal of the primary helium and its replacement with nitrogen the circuit was opened and no further precaution taken to exclude air. Without the easy access made possible by these open-air arrangements, relative freedom from contamination and the viewing opportunities afforded by a transparent coolant, the task might have been impossible. Experience during this refit showed that small simple tools were successful in many instances where more elaborate devices would have proved unnecessary or even introduced difficulty. The great benefit from the regular use of good viewing facilities (e.g. the core periscope) was demonstrated from start to finish of the operation.

Experience from Dragon of the levels of contamination of the primary circuit are of great interest particularly as Dragon's role in testing experimental fuels could be

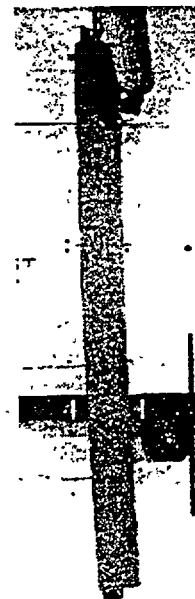


Fig 3.
Reflector Block

expected to yield pessimistic information. In fact radioactive contamination problems during the reflector change were remarkable by their absence. Continuous working around large open penetrations to the core was always possible without the need for air-hoods or respirators. Numerous devices such as television cameras, lights, handling tools, etc., were lowered into the core chamber, frequently rubbing against graphite and metal surfaces, yet on removal they showed very little contamination requiring no personal protection other than normal industrial fabric gloves.

The frequently expressed fears that prolonged contact between metal components in a high temperature, high purity helium environment could lead to self-welding seizure did not materialise. Even at the loaded and hot (about 650°C) interface of the Nimonic control rod shield tubes with the Monel 400 reflector head assemblies, resistance to disengagement was only that caused by normal frictional forces. Detailed evidence of contamination by dust-borne activation products were obtained from swabbing the metal surfaces of primary circuit components. On most of the areas examined a simple swab soaked in methanol removed the bulk of the activation products suggesting that these were in a non-adherent dust layer. Rowland [2] gave the typical ratio of activation products compared to Mn-54 averaged over a Dragon heat exchanger, these were Cr-51, 6; Co-60, 0.14; Zn-65, 1.0; Ag-110m, 3.2. These values were supported by subsequent examination of the thermocouple probes which showed Mn:Co ratios on the hot side 4:1 (700°C) and 'cold' side (320°C) 15:1. The deposits on the graphite surfaces were totally different; Mn-54 was present at very low levels compared to cobalt and it was not possible to detect Zn-65. If it had indeed been dust deposited on the blocks an alteration in the ratios would have been expected but both Mn-54 (from Fe) and Zn-65 should have continued to rise in activity (Zn-65 needs three years to reach saturation). It was therefore concluded that the activity on the graphite was not due to dust, but rather to contamination during machining.

7. Conclusions

The O.E.C.D. High Temperature Reactor Project has produced exhaustive performance data for a variety of fuels and coated particle fuel configurations during the eleven years of operating the Dragon Reactor Experiment. The extensive facilities for measuring temperature and analysing fission product release combined with the versatile control of coolant flow and neutron flux available for individual fuel elements made it possible to exactly reproduce the required experimental conditions and continuously monitor all relevant parameters.

The low release of FP to the primary circuit and the almost complete absence of corrosion not only improved the sensitivity of individual release measurements, but also allowed hands-on maintenance of non-activated components and personnel access to the containment building and during operation. Operation with the Dragon High Temperature Reactor Experiment has proven that the HTR is a highly stable reactor with good load following characteristics that the fuel can support overheating to an incomparable degree and that practically no secondary waste is generated.

All these results were documented by the Dragon Project and all reports made available to the sponsoring organisations, inter alia the O.E.C.D and the European Commission. It is time to bring these documents out of the archives and make them freely accessible for example on the www!

8. Acknowledgements

This paper should not only draw the attention of the present generation to the relevant results of yesteryear, but also remind the audience of the excellent scientific work accomplished by the members of a highly dedicated and competent international team. They shall not be forgotten.

9. References

- [1] B. G. Chapman, "Operational and Maintenance Experience with the Dragon Reactor Experiment", D.P. Report 884, May 1974.
- [2] P. R. Rowland, "New Methods for the Investigation of Radioisotope Transport in a Gas Cooled Reactor", D.P. Report 639, March 1969.

THE RELATIONSHIP BETWEEN IRRADIATION INDUCED DIMENSIONAL CHANGE AND THE COEFFICIENT OF THERMAL EXPANSION: A NEW LOOK

G. HALL, B.J. MARSDEN, A. FOK and J. SMART

*Nuclear Graphite Technology Research Group
University of Manchester, Oxford Road, Manchester - England*

ABSTRACT

In the 1960s, J.H.W. Simmons derived a theoretical relationship between the coefficient of thermal expansion (CTE) and dimensional changes in irradiated graphite. At low irradiation dose, the theory was shown to be consistent with experimental observations. However, at higher doses the results diverge. Despite this, modified versions of this theory have been used as the basis of the design and life prediction calculations for graphite-moderated reactors.

This paper revisits Simmons's theory, summarising the assumptions made in its derivation. The paper then modifies and applies the theory to the dimensional change and CTE change behaviour in isotropic nuclear graphite, making use of trends in irradiated behaviour recently derived using finite element analyses.

The importance of these issues to present HTR technology is that the life of HTR graphite components is related to their irradiated dimensional change behaviour. A more in depth understanding of this behaviour will allow suitable graphite material to be selected or new graphite types to be developed.

1. Introduction

Many nuclear reactors around the world use graphite as a neutron moderator and because the moderator can not be replaced in most of these reactors, the life of the moderator governs the working life of the reactor. The graphite material properties show considerable changes when subjected to fast neutron irradiation. Two of the most noticeable behaviours are the dimensional change and CTE of the graphite. The combined effect of these changes is often difficult to predict accurately for the design life of a reactor; the situation being further compounded by the effect of radiolytic oxidation in carbon dioxide cooled reactors.

Previous authors have investigated the relationship between CTE and dimensional change, a notable one being the relationship by Simmons^[1]. This relationship linked the macroscopic properties of the polycrystalline graphite to the properties of the crystallites, and at low doses, it shows good agreement to experimental data. However, the results diverge at higher doses, as the relationship does not predict the reversal of shrinkage (turnaround) exhibited in many graphites.

The objectives of this investigation were to re-examine the derivation of Simmons's work and to modify the relationship so turnaround could be predicted. The predictions would then be compared to experimental trends and results from a finite element method study also being conducted. The understanding of these relationships will aid the selection, design and development of new graphites.

2. Theory

2.1. Simmons's relationship

Simmons^[1] theorised that because some of the dimensional changes in irradiated graphite were caused by changes in the graphite crystal lattice, a relationship between the CTE and dimensional change with fast neutron irradiation could be formed. In order to derive such a relationship, several assumptions had to be made. First, polycrystalline graphite consists of a porous aggregate of graphite crystals, with each crystal having the correct graphite crystal symmetry and possessing identical properties (that it is a single-phase material). Second, small elemental volumes of polycrystalline graphite may be chosen such that stresses either induced internally or externally can be regarded as being uniform. Third, the volume of each element contains only graphite. Using the laws of thermodynamics, Simmons was able to show that

$$\frac{d\varepsilon_{xx}}{d\gamma} = A_x \frac{dx_c}{d\gamma} + (1 - A_x) \frac{dx_a}{d\gamma} \quad (1)$$

$$\alpha_{xx} = A_x \alpha_c + (1 - A_x) \alpha_a \quad (2)$$

where $\frac{d\varepsilon_{xx}}{d\gamma}$ is the rate of change of strain in the x direction of a polycrystalline graphite, $\frac{dx_a}{d\gamma}$ and $\frac{dx_c}{d\gamma}$ are the rate of dimensional change of a crystal, parallel and perpendicular to the hexagonal axis, α_{xx} is the CTE in the x direction of a polycrystalline graphite, α_a and α_c are the CTE of a crystal, parallel and perpendicular to the hexagonal axis, γ is irradiation dose, and A_x is the structure factor.

The CTEs of the crystal (α_a and α_c) and polycrystalline graphite (α_{xx}) are measured over the same temperature ranges. Therefore, by rearranging equation (2), A_x can be successfully obtained as a function of dose. However, the use of Simmons's relationship for dimensional change given in equation (1) has shown divergence in results. Therefore, a number of developments of the original relationship have been investigated^[2] but with limited success.

2.2. Modified Simmons relationship

To account for the relatively high strain dimensional changes, it is proposed that an extra term, B_x , should be introduced to modify A_x . This extra parameter will be applied to the whole of the dimensional change formula and therefore, the relationship will be of the form

$$\frac{d\varepsilon_{xx}}{d\gamma} = A_x B_x \frac{dx_c}{d\gamma} + (1 - A_x B_x) \frac{dx_a}{d\gamma} \quad (3)$$

$$\alpha_{xx} = A_x B_x \alpha_c + (1 - A_x B_x) \alpha_a \quad (4)$$

In irradiated graphite, the Young's modulus has been shown to be dependent upon dose (Fig 1). The change in Young's modulus, where E is the irradiated value and E_0 is the unirradiated value, is the combination of two distinct features, pinning and structural changes. The pinning term P accounts for the pinning of mobile dislocations and is considered to be instantaneous and constant. The structure term S allows for irradiation induced structural changes and is not instantaneous and changes with increasing dose. The relationship is

$$\frac{E}{E_0} = \left[\frac{E}{E_0} \right]_P \left[\frac{E}{E_0} \right]_S = P \cdot S \quad (5)$$

A working hypothesis is that for an isotropic polycrystalline graphite, the structure term B_x can be defined by the changes in the modulus structure term S with dose, and a constant, a

$$B_x = (S-1)ae^S + 1 \quad (6)$$

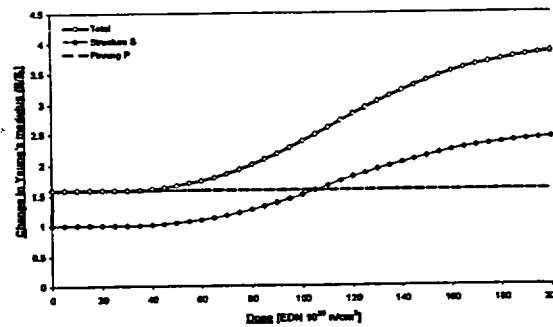


Fig 1. Components of the change in Young's Moduli

2.3. Finite element method

In conjunction with this work, there has been an investigation into the relationship between crystal and bulk graphite properties, specifically dimensional change and CTE, using the finite element method (FEM). Again, the assumption is that the crystal behaviour is the driving force behind the polycrystalline behaviour. A model of an idealised filler particle/crystal surrounded by a binder material has been developed and its behaviour, when subjected to loading conditions akin to those in a reactor, inserted into a polycrystalline model. In the isotropic case, the filler particles/crystals were randomly oriented and distributed throughout the polycrystalline model. This was then subjected to the same loading conditions as the crystal model, and its behaviour monitored. Comparison of these behaviours with experimental and theoretical results will hopefully give insight as to what is happening throughout the structure, and possibly, how the graphite material can be better represented.

3. Results

The dimensional changes of an isotropic polycrystalline graphite have been calculated using both Simmons's original and modified relationships. The required crystal (HOPG) and polycrystalline graphite (Gilsocarbon) data at 450°C were obtained from Brocklehurst and Kelly^[3] and Brocklehurst^[4] respectively.

A trend can be fitted to the experimental polycrystalline data of Brocklehurst and Kelly^[3] (Fig 2). Calculation of the dimensional change using Simmons's original relationship, equations (1) and (2), showed close relationship to the behaviour at low doses (Fig 2). If however, the modified relationship in equation (3) was used, the behaviour was close at high doses (Fig 2). In both cases, there was a gap between the experimental trend and the respective Simmons prediction. The dimensional change predicted using the FEM model was also similar to the experimental trend, although it did show some noticeable deviation from the actual values (Fig 2).

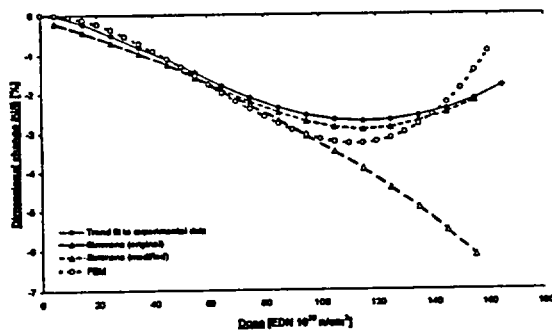


Fig 2. Predicted and observed dimensional changes of an isotropic polycrystalline graphite

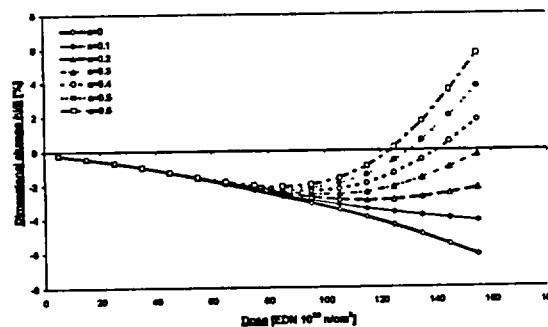


Fig 3. Effect of varying a in the modified Simmons relationship

In the Simmons (modified) results (Fig 2), the value of constant a in equation (6) was set at 0.2. Varying this value gave visibly different dimensional changes (Fig 3). When a was set to 0, the dimensional change exhibited no turnaround and coincided with that predicted using the original Simmons relationship. Increasing the value of a caused the dimensional change curves to demonstrate turnaround and to show a higher rate of expansion after turnaround.

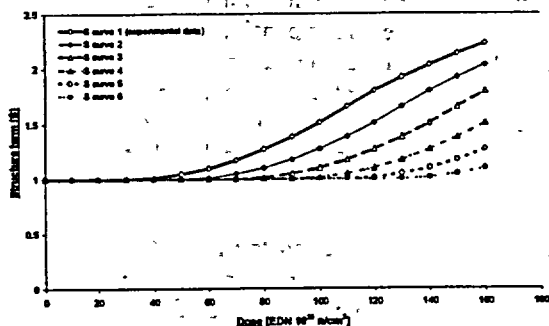


Fig 4. Structure term S used in the modified Simmons relationship

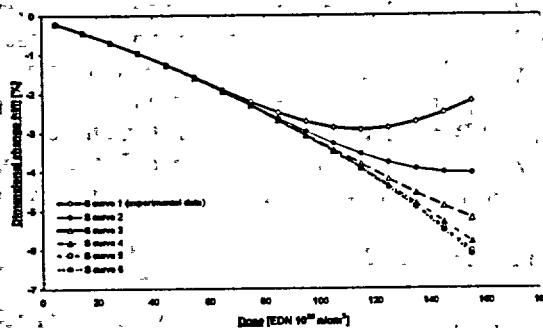


Fig 5. Effect of varying S in the modified Simmons relationship

Similarly, in all of the previous calculations using the modified Simmons relationship, the structure term S had been set to that given by experiment (S curve 1, Fig 4). If however, the values of S were varied by shifting the curve to the right (Fig 4), an identifiable change in results was observed (Fig 5). It should be noted that in the calculations, a was set to 0.2. When the original S values (S curve 1) were used, the dimensional change exhibited turnaround. As the curve was shifted to the right (S curve 2 and above), the respective dimensional change either displayed more shrinkage and delayed turnaround, or more shrinkage and no turnaround. The change in behaviour with each subsequent shift of the S curve became less i.e. the difference between the dimensional changes when using S curve 1 and S curve 2 was greater than that of S curve 2 and S curve 3, which in turn was greater than S curve 3 and S curve 4, and so forth.

4. Discussion

The original Simmons relationship predicted a dimensional change curve similar to that experimentally observed for an isotropic polycrystalline graphite at low doses (Fig 2). The difference between the two curves even at low doses can be attributed to the fact that in the experimental dimensional change data, there was a small amount of expansion at very low doses, followed by the shrinkage and turnaround. The Simmons relationship however, did not account for this initial expansion.

The original relationship was unable to predict the behaviour of the graphites at higher doses, but the modified Simmons relationship could (Fig 2). The extra term B_s , or more specifically S, is the main difference between the two relationships, and thus, the modulus structure term may be important when modelling graphite at higher doses. Again, there was a gap because of the experimental data's initial expansion at very low doses.

The FEM model gave a reasonable representation of the graphite; the overall trends were similar but the actual values were not always close (Fig 2). The reason for this was that there were many variables within the modelling procedure that could alter the results of the FEM model such as crack volume, material properties, and geometry. However, a current parametric study is investigating these and their effect on the model behaviour. This will hopefully lead to the development of a closer representation of the behaviour, and provide useful information as to what is happening at the microstructural level. An

unexpected but promising feature of the FEM results was that the model did show a small amount of expansion before shrinking, as demonstrated in the experimental data.

Changing the constant a in the modified relationship gave significant changes in the predicted behaviour. Setting the value to zero effectively returned the modified relationship to the original Simmons relationship and therefore, the dimensional change curve diverged from the experimental data (Fig 3). Increasing the value caused turnaround to occur at a lower dose and for the preceding expansion to be at a higher rate (Fig 3). Thus, the constant a may be comparable to the effect of temperature changes, heat treatment, porosity, grain size or some other parameter. One possibility may be that a is a function of density as Kelly and Brocklehurst^[5] observed that in an isotropic graphite, turnaround was delayed when the initial density was lower. At present, the modified relationship is only an empirical relationship, but further investigation is underway to examine the underlying hypothesis.

Variation of the S values used within the modified relationship also had a great effect on the predicted dimensional change (Fig 5). If the shifting of the S curve to right (Fig 4) is assumed to be a consequence of an ageing process, the subsequent changes in dimensional behaviour will also be a consequence of this. However, this requires more examination.

5. Conclusions

- a) The original derivation by Simmons of the relationship between irradiation induced dimensional change and CTE has been re-examined and shown to give a close approximation of the dimensional change with irradiation of polycrystalline, isotropic graphite at low doses.
- b) As the original relationship was unsuitable at high doses, an empirically based, modified relationship has been proposed and shown to give a good prediction of the polycrystalline, isotropic graphite up to high doses.
- c) A finite element method model has been developed and shown to have similar dimensional change behaviour to the experimental data. However, further investigation is required to understand how the model behaves as parameters are changed and to its significance to real graphite behaviour.
- d) Variation of the extra parameters (a and S) in the modified relationship may allow for the application of the relationship to different cases, although further investigation is required before this can be justified.

6. Acknowledgements

This work was funded by British Energy plc while conducting an EngD at the University of Manchester.

7. References

- [1] J.H.W. Simmons, A Relation Between Thermal Expansion And Dimensional Change For Polycrystalline Graphite, UKAEA, AERE R 3883, November, 1961.
- [2] J.E. Brocklehurst & B.T. Kelly, Analysis Of The Dimensional Changes And Structural Changes In Polycrystalline Graphite Under Fast Neutron Irradiation, Carbon, Vol. 31, No. 1, 1993, pp. 155-178.
- [3] J.E. Brocklehurst & B.T. Kelly, The Dimensional Changes of Highly-Oriented Pyrolytic Graphite Irradiated With Fast Neutrons At 430°C And 600°C, Carbon, Vol. 31, No. 1, 1993, pp. 179-183.
- [4] J.E. Brocklehurst, Irradiation Damage In CAGR Moderator Graphite, UKAEA, ND-R-1117 (S), July, 1984.
- [5] B.T. Kelly & J.E. Brocklehurst, Dimensional Changes In Graphite At Very High Doses, Carbon '72 Conference, Baden, July, 1972.

COMPARISON OF CYCLE EFFICIENCY, TURBINE EFFICIENCY AND RECUPERATOR HEAT TRANSFER SURFACE AREA BETWEEN DIRECT CYCLES OF CARBON DIOXIDE AND HELIUM

YASUYOSHI KATO, TAKESHI NITAWAKI and YASUSHI MUTO

*Research Laboratory for Nuclear Reactors
Tokyo Institute of Technology
O-okayama, Meguro-ku, Tokyo, 152-8550
JAPAN*

ABSTRACT

Compared to helium cycles, cycle efficiency is improved by about 4% with a carbon dioxide cycle with partial cooling. Higher efficiency is ascribed to reduced compression work resulting from its real gas effect and to reduced heat rejected to cooling water through partial cooling required from its temperature dependence of specific heat; both effects cannot be expected for helium cycles because helium behaves virtually as an ideal gas and has constant specific heat. Compared to helium cycles, carbon dioxide turbine efficiency is higher by about 1% and the turbine size is significantly smaller, but the recuperator size is larger. Assuming that opposing trends in size will offset, higher cycle efficiency will yield a lower expected power generation cost per unit electricity for the carbon dioxide cycle design than for a helium cycle design.

1. INTRODUCTION

Helium (He) is currently used as a working fluid of a closed gas turbine direct cycle for high temperature gas cooled reactors (HTGRs). Since the compressor consumes about 50% of power produced by the turbine in this cycle, main efforts to enhance cycle efficiency have focused upon reduction of compressor work by improving compressor efficiency and increasing turbine output by elevating turbine inlet temperature. Recuperator efficiency enhancement is also crucial to improve the cycle in the gas turbine system. If carbon dioxide (CO₂) is used as the working fluid, condensability and non-ideal gas behaviour around the critical point (31°C, 7.3MPa) of CO₂ will provide additional means for improving cycle efficiency which cannot be used for the He cycle. Our partial condensation CO₂ cycle is based on these additional means [1].

Work W of one mol real gas in isentropic compression processes is calculated as

$$W = - \int V dP = - \int zRT dP/P,$$

where V = gas volume, P = gas pressure, R = gas constant, and z = compressibility factor (fractional deviation from ideal gas = 1.0). Compressibility factor z is given as a function of reduced temperature Tr ($Tr=T/Tc$, Tc =critical temperature) and reduced pressure ($Pr=P/Pc$, Pc =critical pressure) [2]. At critical temperature and pressure, the z value dips sharply below the ideal line of unity and takes an extremely low value: as low as about 0.2. A low z value indicates that the gas is more compressible than the ideal gas. Since compressor inlet temperature (35°C) is very close to CO₂ critical temperature (31°C), compressor work is expected to be smaller and cycle efficiency is higher in a CO₂ cycle than that in a He cycle.

As coolant, CO₂ has other preferable properties in comparison to He: about 1.5 times higher heat transfer coefficient between coolant and fuel surfaces, about 2.5 times more effective decay heat removal under natural circulation conditions, about 3.6 times longer depressurization time [3], and about 24 times lower cost per unit volume.

Although CO₂ cycle efficiency was shown to be highest in a partial condensation cycle in previous studies [1], cycle efficiency, turbine size and adiabatic efficiency, and recuperator size are compared in this study between CO₂ and He in Brayton cycles because a cycle with condensation is not applicable to He due to its extremely low condensation temperature.

2. CYCLE EFFICIENCY

Cycle efficiency of a Brayton cycle is improved when the number of compression stages with intercooling is increased as shown in Figs. 1(a) through (c). However, contribution of each additional stage to cycle efficiency becomes less and less; use of more than three stages with two intercoolers cannot be justified economically. Hence, comparison of cycle efficiency is done in this study for one through two compression stages between He and CO₂ in closed gas-turbine direct cycles. It is difficult to apply the two-intercooler cycle to the He cycle because the length of the gas turbine rotor is much longer in a He cycle than in a CO₂ cycle; rotor dynamics design becomes much more difficult if an additional compressor is added.

Cycle configurations of Figs. 1(a) and (b) are adopted to actual designs of He cycle HTGRs [4],[5]. Cycle efficiencies of He and CO₂ cycles are almost identical in these usual Brayton cycle configurations as shown in Table 1, although they are not preferable for the CO₂ cycle as explained hereafter. Specific heat at constant pressure C_p of CO₂ is dependent on temperature and pressure, whereas C_p of He is constant and C_p of CO₂ in the recuperator is considerably lower in the high temperature-low pressure side (connected to the turbine outlet) than in the low temperature-high pressure side (connected to the compressor outlet). As a result, CO₂ cannot be pre-heated to such temperature at the core inlet as it provides maximum cycle efficiency. If flow is by-passed to the compressor before pre-cooling, as shown in Fig. 2(a), this temperature mismatch problem is avoided. Bypass flow reduces heat rejected to cooling water and thereby improves cycle efficiency by about 4% as shown in Table 1. A cycle with a bypass flow cycle is called hereafter a "partial cooling" cycle. Partial cooling is also achieved in the one-intercooler cycle by bypassing flow to the third compressor before the intercooler, as shown in Fig. 2(b). As expected from the constant C_p of He, bypass flow is not necessary for the He cycle, but it degrades cycle efficiency.

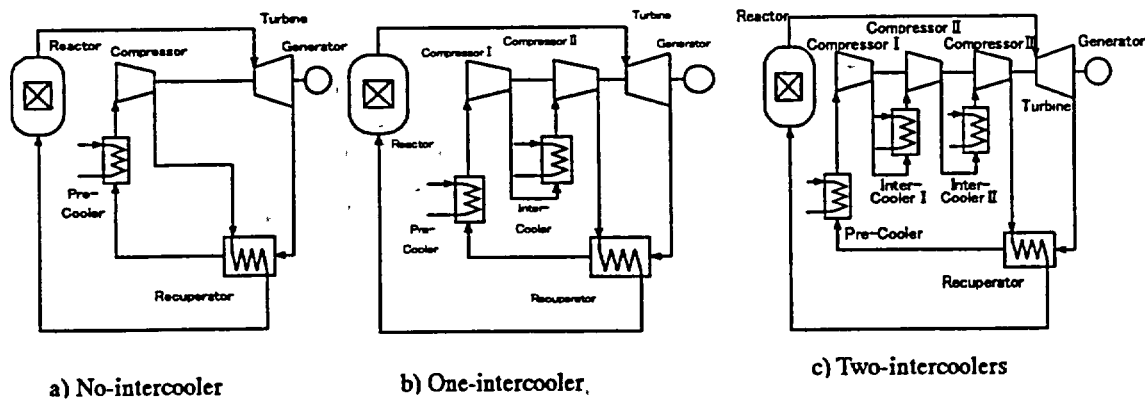


Fig. 1. Variation of Brayton cycles with number of intercoolers.

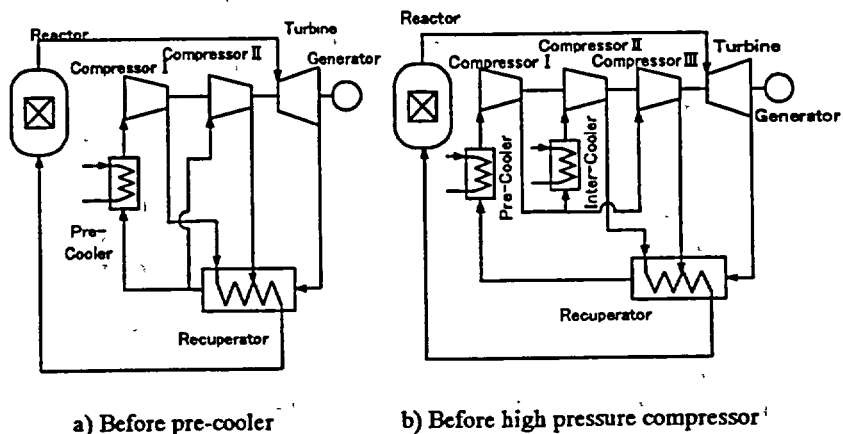


Fig. 2. Flow bypassing positions for partial cooling of CO₂ cycles.

The temperature mismatch problem is improved in the two-intercooler cycle given in Fig. 1(c) by allocating a few times larger compressor as a high pressure compressor than the low and medium pressure ones, and resultantly by providing a higher temperature at the high pressure compressor outlet or recuperator inlet.

Table 1. Cycle thermal efficiencies of He and CO₂ cycles.

Items		Cycle Thermal Efficiency (%)					
		No Intercooler		One Intercooler		Two Intercoolers	
		7MPa	12.5MPa	7MPa	12.5MPa	7MPa	12.5MPa
He	No Partial Cooling	45.3	45.1	47.5	47.4	48.4	48.3
CO ₂	No Partial Cooling	45.8	45.5	47.8	47.4	48.7	48.1
	Partial Cooling	49.2	49.7	51.4	51.9	-	-

Evaluated under the conditions: reactor outlet temperature = 800°C, turbine adiabatic efficiency = 90%, compressor adiabatic efficiency = 90%, recuperator effectiveness = 95%.

3. TURBINE DESIGN

Table 2 shows design conditions for turbine design. Turbine adiabatic efficiencies are evaluated using profile loss and secondary-flow loss models of Craig and Cox [6], and the Roelke tip-clearance loss model [7]. Results are shown in Table 3. Adiabatic efficiencies are 92.91%, 93.82%, and 93.78% for a He turbine with one inter-cooler, a CO₂ turbine of partial cooling with one intercooler, a CO₂ turbine with two intercooler cycle, respectively. Reduction of efficiency by about 1% in the He turbine is mainly attributed to a larger flow deflection angle at the turbine blade required by the 1.2 times larger loading coefficient than CO₂. As shown in Fig. 3, axial length is three times shorter for the CO₂ turbine while diameter is almost identical; the flow channel is nearly parallel for the He turbine, but diverging for the CO₂ turbine.

Table 2. Turbine design conditions.

Items	He Cycle	CO ₂ Cycle	
	one Intercooler	Partial Cooling	Two Intercoolers
Inlet Temperature (°C)	800		
Inlet Pressure (MPa)	7.0		
Outlet Pressure (MPa)	3.53	1.134	1.062
Mass Flow Rate (kg/s)	318.9	1218.6	1147.3
Rotational Speed (rpm)	3600		
Number of Stages	9	3	
Tip Clearance	0.008 (ratio to blade height)		
Loading Coefficient ψ	1.25	1.15	
Flow Coefficient φ	0.4	0.3	

$\psi = \Delta h / u^2$, $\varphi = C_x / u$, where Δh : enthalpy rise per stage,
 u : peripheral speed at mean blade radius, C_x : axial velocity.

4. RECUPERATOR DESIGN

Three kinds of heat exchangers are used in a Brayton cycle, a recuperator, pre-cooler, and intercooler. The recuperator is the most critical component for cycle efficiency, whose heat exchanger units are located in an annular space between the turbine rotor casing and pressure vessel. Compact

Table 3. Results of turbine design.

Items		He Cycle	CO ₂ Cycle	
		One Intercooler	Partial Cooling	Two Intercoolers
Peripheral Speed* (m/s)		338	312	317
Velocity * (m/s)	Nozzle Exit	426	330	334
	Blade Exit	362	331	335
Turbine Loss *	Nozzle**	0.0169	0.0221	0.0218
	Blade***	0.0405	0.0265	0.0260
Centrifugal Stress**** (MPa)		215	285	280
Adiabatic Efficiency (%)		92.91	93.78	93.82

* Values at the medium stage. ** Profile loss + secondary flow loss.
 *** Profile loss + secondary flow loss + tip clearance loss. **** Values at the last stage.

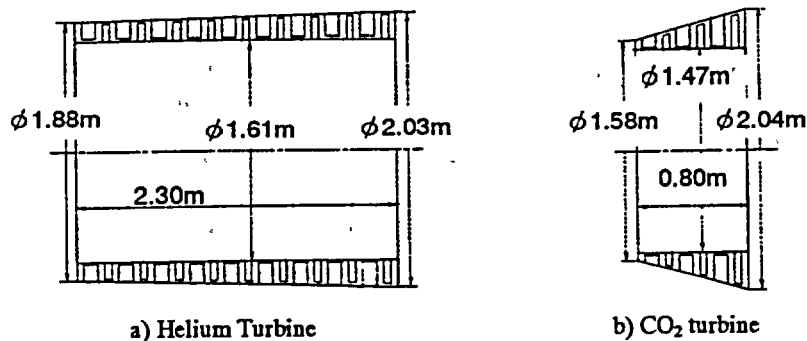


Fig. 3. Cross sectional views of He and CO₂ turbines.

plate-fin type recuperators are designed for He and CO₂ cycles to minimize the pressure vessel and attain thermal duty, thermal effectiveness of 95%, and pressure drop of less than 1.5% relative to system pressure. Heat transfer coefficient and pressure drop calculations are based on models proposed by Wieting [8].

Recuperator design is carried out using conditions given in Table 4; results are shown in Table 5. Compared with the He cycle, CO₂ cycles exhibit: significantly lower gas velocities; higher Reynolds numbers due to the approximately ten times higher CO₂ density; and a quarter the heat transfer coefficient due to thermal conductivity that is about one-sixth that of the He cycle. Consequently, total height and weight are significantly higher in the CO₂ recuperator than in the He recuperator. However, the recuperator can be accommodated inside the pressure vessel with height of about 30m and weight of about 100 tones. Assuming that increased recuperator weight in the CO₂ cycle is offset by decreased turbine size, the power generation cost per unit electricity is expected to be lower in the CO₂ cycle than for He cycles due to higher cycle efficiency.

5. CONCLUSIONS

Cycle thermal efficiency, turbine adiabatic efficiency and recuperator heat transfer surface area are compared between direct cycles of CO₂ and He cycles. A CO₂ cycle attains about 4% higher cycle efficiency by introducing partial cooling than the He Brayton cycles. Turbine size is significantly smaller in the CO₂ cycle than in the He cycle. Adiabatic efficiency is higher by about 1% for the CO₂ turbine than for the He turbine. On the other hand, recuperator heat transfer area and weight are rather smaller in the He cycle compared with those in CO₂ cycles. If these advantages and disadvantages cancel each other, CO₂ cycles would be superior to the He cycle because CO₂ offers cycle thermal efficiency which exceeds those of the He cycle by about 4%.

Table 4. Recuperator design conditions.

Items	He Cycle	CO ₂ Cycle		
	One Intercooler	Partial Cooling		Two Intercoolers
		#1	#2	
Number of Units	6			
Heat Duty (MW)	124.3	76.75	20.39	85.08
High Temperature Side				
Inlet Temperature (°C)	569.3	561.1	221.4	553.4
Inlet Pressure (MPa)	3.53	1.134	1.119	1.062
Mass Flow Rate (kg/s)	53.15	203.1	203.1	191.2
Low Temperature Side				
Inlet Temperature (°C)	95.3	206.0	110.2	121.3
Inlet Pressure (MPa)	7.15	7.14	7.17	7.15
Mass Flow Rate (kg/s)	53.15	203.1	184.1	191.2
Width x Length (m)	0.94 x 0.94			

Table 5. Results of recuperator design.

Items	He Cycle	CO ₂ Cycle		
	One Intercooler	Partial Cooling		Two Intercoolers
		#1	#2	
High Temperature Side				
Fin Height (mm)	1.1	1.4	2.8	2.4
Outlet Gas Temperature (°C)	119	223	121	148
Pressure Drop (MPa)	0.039	0.016	0.014	0.013
Low Temperature Side				
Fin Height (mm)	1.1	1.1	1.1	1.1
Outlet Gas Temperature (°C)	546	535	207	514
Pressure Drop (MPa)	0.023	0.006	0.021	0.012
Heat Transfer Area (m ²)	2792	6574	2151	3858
Heat Transmitted (MW)	124.3	76.75	20.39	85.08
Effectiveness (%)	95.1	95.3	90.6	93.9
Total Height (m)	5.06	18.98		9.82
Total Weight (ton)	16.6	54.2		26.7

References

- [1] Y. Kato, T. Nitawaki, and Y. Yoshizawa, *Proc. Int. Conf. on: Back-End of the Fuel Cycle: From Research to Solutions (GLOBAL 2001)*, Paris, France, Sept. 9-13, 2001, #028 (2001).
- [2] O. A. Hougen, K. M. Watson and R. A. Ragatz, *Chemical Process Principles, Part II, Thermodynamics*, John Wiley & Sons, pp. 579-591 (1960).
- [3] E. E. Lewis, *Nuclear Power Reactor Safety*, John Wiley & Sons, pp.398-402 (1977).
- [4] Y. Muto and S. Ishiyama, *J. Atomic Energy Soc. Japan*, **42**, pp. 1020-1027 (2000). (in Japanese)
- [5] www.saep.org/subject/nuclear/pbmr/pbmr.html
- [6] H. R. M. Craig and H. J. A. Cox, *Proc. Inst. Mech. Engrs.*, Vol. **185**, 32/71, paper and discussion, London, UK (1971).
- [7] R. J. Roelke, *Miscellaneous Losses in Turbine Design and Application, Vol. 2*, edited by A. Glassman, Special publication, SP-290, pp. 127-128 NASA, Washington, DC (1973).
- [8] A. R. Wieting, *Trans. ASME, J. Heat Transfer*, pp. 488-490 (1975).

STUDIES ON AIR INGRESS FOR PEBBLE BED REACTORS

Richard L. Moore, Chang H. Oh, Brad J. Merrill, and David A. Petti

Idaho National Engineering and Environmental Laboratory, Idaho Falls, ID, USA

ABSTRACT

A loss-of-coolant accident (LOCA) has been considered a critical event for helium-cooled pebbled bed reactors. Following helium depressurization, it is anticipated that unless countermeasures are taken air will enter the core through the break and then by molecular diffusion and ultimately by natural convection leading to oxidation of the in-core graphite structure and graphite pebbles. Thus, without any mitigating features a LOCA will lead to an air ingress event. The INEEL is studying such an event with two well-respected light water reactor transient response codes: RELAP5/ATHENA and MELCOR.

To study the degree of graphite oxidation occurring due to an air ingress event, a MELCOR model of a reference pebble bed design was constructed. A modified version of MELCOR developed at INEEL, which includes graphite oxidation capabilities, and molecular diffusion of air into helium was used for these calculations. Results show that the lower reflector graphite consumes all of the oxygen before reaching the core. The results also show a long time delay between the time that the depressurization phase of the accident is over and the time that natural circulation air through the core occurs.

1. Introduction

New and safer nuclear reactors (Generation IV reactors) are now in the early planning stages in many countries through out the world. One of the reactor concepts being seriously considered is the Pebble Bed Modular Reactor (PBMR) of which several preliminary reference designs have been developed [1,2]. To achieve public acceptability, these reactor concepts must show an increased level of inherent safety over current reactor designs, i.e., a system must be designed to eliminate any concerns of large radiological releases outside the site boundary. As such, the analysis of severe accidents such as an air ingress using well-validated computer codes such as MELCOR, RELAP5/ATHENA or other thermal-hydraulic codes specifically developed to analysis PBMR must be performed.

As a result of this new interest in Generation IV reactors the NRC held in October 2001, a two-and-a-half day workshop [3] on high temperature gas reactor safety and research issues, where a number of high priority issues were identified. Several issues that were identified include the development of thermal-hydraulic and safety analysis codes, the need for an adequate database to validate the codes and accident phenomenology for air ingress events and the resulting consequences.

Over the past three years the Idaho National Engineering and Environmental Laboratory (INEEL), through the use of Laboratory-Directed Research and Development (LDRD) funds, has collaborated with the Massachusetts Institute of Technology (MIT) to explore the use of the PBMR as a viable alternative to present reactor designs. As a small part of the overall funding we at the INEEL are investigating the use of proven thermal-hydraulic reactor accident codes such as MELCOR (with some modifications) to analyze the air ingress accident. The main advantage of using such codes (provided it can be shown that they are qualified for such analyses) is that they are available now and many of their thermal-hydraulic models have been validated against test data over the past twenty years. Thus, the needed validation and verification effort to qualify these codes for PBMR safety analyses and licensing activities should be greatly reduced.

This paper will address the air ingress accident associated with a reference PBMR design being developed by MIT and INEEL. We will show that the results generated using the safety analysis code MELCOR are consistent with experimental results reported in the literature [4]. RELAP/ATHENA results will be published later.

2. Accident and model description

The air ingress accident is considered to be an accident that poses a serious threat to the integrity of the fuel and subsequent the release fission products to the site boundary. For an air ingress accident to occur, we are postulating that the primary coolant inlet and outlet ducts experience a simultaneous complete double guillotine break between the reactor vessel and the high-pressure turbine, which is located in an adjacent auxiliary equipment room. This room will be referred to as the vault in this paper. Following rupture of the primary ducts, depressurization of the reactor will occur. The depressurization event last only a few seconds until the pressure in the reactor core comes to equilibrium with the pressure of the vault. Based on Japanese experimental data [4] and results in this paper, it is expected that little or no air will flow into the reactor core for many hours after the initiation of the accident.

A preliminary MELCOR model of a reference PBMR was developed to model a LOCA and subsequent air ingress event. MELCOR [5] is a severe accident code being developed at Sandia National Laboratory for the U. S. Nuclear Regulatory Commission to model the progression of severe accidents in light water nuclear power plants. However, due to the general and flexible nature of the code other reactor concepts such as the pebble bed reactor can be modeled. In this paper we are using a modified version of MELCOR 1.8.2. These INEEL modifications to MELCOR 1.8.2 were the implementation of multi-fluid capabilities [6] and the ability to model graphite oxidation. The multi-fluid capability allows MELCOR to use other fluids such as helium as the primary coolant.

A schematic of the reactor configuration under consideration is shown in Figure 1. The reactor was assumed to have a core diameter of 3.5 m and a active core height of 8.0 m yielding a total core volume of 76.9 m³. The core of the reactor was divided into three radial zones and eight axial zones for a total of 24 core control volumes. The core control volumes are cylindrical and are centered about the core centerline. The inner radial zone contains 69,700 non-heated pebbles. The two outer radial zones contain a total of 342,900 heat-generating pebbles producing a total of 270 MW of thermal energy.

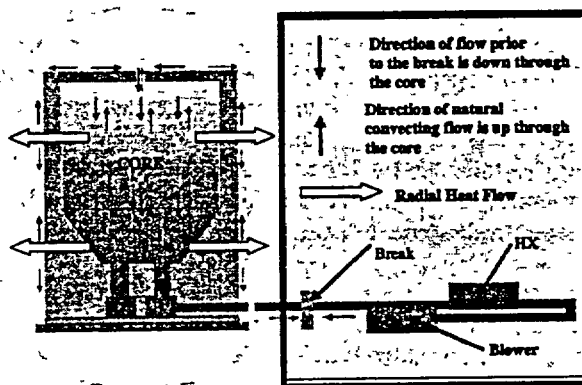


Fig. 1 Schematic of pebble bed reactor and vault

For nominal operating conditions the coolant enters the bottom of the reactor at 450 °C, flows up an annular flow channel located between the reactor side reflector and the reactor vessel. The coolant then flows radially along the top of the reactor exiting into a plenum above the core. From the plenum the coolant flows down through the core and exits the bottom of the core at 850 °C. The coolant then flows to the power conversion unit, which is represented simplistically by several control volumes. The double-ended rupture of both the inlet and outlet pipes as shown in Figure 1 is represented in the model as two valves that are connected to the vault and are opened at the beginning of the decompression accident. For this calculation the vault volume was estimated to be 27000 m³ and is assumed to be isolated from any outside air. When details of the vault geometry are available the vault volume will be updated.

The heat transfer from the pebbles is dominated by convection during nominal operation of the reactor. However, during the LOCA when the flow in the core decreases to near zero the heat generated by the pebbles is removed by conduction and radiation through the pebbles to the graphite reflector. The heat is then conducted through the reflector, radiated to the reactor vessel wall, conducted through the vessel wall, and then removed from the outside of the vessel by natural convection and radiation. The pebbles in the core were modeled as spherical heat structures, one heat structure per control volume. Radial conduction from each zone of the core was modeled as a homogenous cylindrical conduction. This conduction was then applied to the spherical heat structure by dividing the conduction terms by the number of pebbles in the zone. We have validated our modeling approach by matching our model against cylindrical transient heat conduction solutions. The heat transfer from the one structure was then multiplied by the number of pebbles in the control volume to obtain the overall heat transfer from all the pebbles in the volume.

Since this is a preliminary calculation, the heat transfer from the outer surface of the graphite reflector to the outside heat sink was modeled as radiation heat transfer through two radiation shield representing the reactor vessel wall and the vault wall. In other words the thermal conductance of the two walls were neglected, as was the natural convection from the reactor vessel to the environment abjection to the vessel. Axial conduction in the core and in the lower graphite reflector was also modeled. The air ingress event is assumed to occur after the reactor has been operating for many hours at steady state conditions.

2.1 Oxidation Model

As stated above, the main objective of this study was to evaluate the capability to model the oxidation of the reactor graphite structure (reflector and core) due to an air ingress accident. The graphite oxidation kinetics shown in Figure 2 was implemented in MELCOR. The present model is based on graphite oxidation rates obtained experimentally at the INEEL by O'Brien et al., as reported in Reference [7].

The rate equation is based on the oxygen concentration in air at standard atmospheric conditions. Thus, in the MELCOR model as a first order approximation, the oxidation rates are assumed to vary linearly with the oxygen partial pressure. It is also assumed that only CO_2 is produced during the oxidation process. The heat generated from the exothermic reaction is deposited directly into the surface node of the graphite layer being oxidized.

3. Results

The LOCA was initiated by opening the two valves that connect the hot and cold legs to the vault. The blower was tripped and the reactor was scrammed at the beginning of the accident. The simultaneous double-ended rupture of the hot and cold legs causes a rapid depressurization of the primary coolant system. The pressure in the reactor equalizes with the vault pressure at 0.15 MPa in \approx 1.5 seconds.

The mass flow rate of air through the core is shown in Figure 3. After the depressurization phase of the LOCA, the mass flow rate of air through the core due to natural convection is essentially zero until approximately 214 hrs. At this time, the flow suddenly increases from zero to 0.080 kg/sec indicating

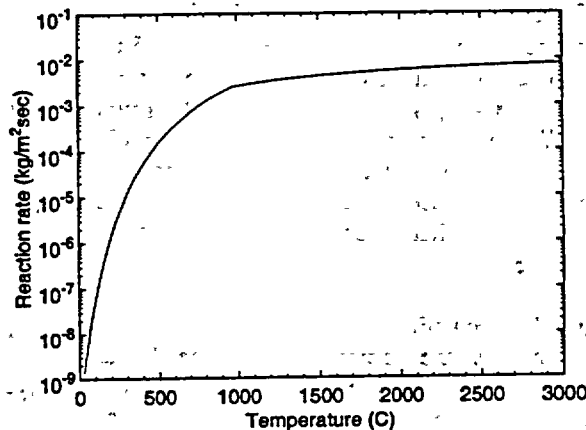


Fig. 2 Graphite oxidation rate as a function of graphite surface temperature

the onset of natural circulation through the core. The flow rate through the core remains between 0.080 kg/sec and 0.075 kg/sec from 214 to 400 hours, the time when the transient was terminated.

After the depressurization stage, hot helium occupies the core, the upper plenum, and the inlet annulus regions of the reactor with cool heavy air at the entrance of the pipe breaks. In this configuration there is insufficient buoyancy force to support natural convective flow. Thus, little or no mass flow of air from the containment to the core and from the core to the containment occurs for a number of hours. During this phase of the accident, air from the containment is mainly transported to the reactor by molecular diffusion. This delay in the onset of natural convection is supported by Japanese and German experimental high-temperature gas-cooled reactors air ingress results [4, 8].

The mole fraction of air (nitrogen) in the core and upper plenum of the reactor calculated by MELCOR gradually increases (shown in Figure 4) until the buoyancy force is large enough to initiate natural circulation. As depicted in the figure, the mole fraction of nitrogen in the core gradually increases from zero at the beginning of the accident to ≈ 0.45 by means of molecular diffusion and what little natural convection that exists just before the onset of natural convection. When natural convection starts, the mole fraction of oxygen immediately starts to decrease with a corresponding increase of carbon dioxide in the vault. This indicates that oxidation of the graphite in the reactor is occurring.

When natural circulation of the air from the containment begins the temperature of the lower reflector graphite located below the core immediately experiences a sharp rise in surface temperature as shown in Figure 5. This rise in temperature is the result of surface oxidation of the graphite. As shown in the figure the temperature of the lower graphite surface starts to increase, going from less than 500 °C to a maximum of 890 °C in 34 hours. At 248 hours the lower reflector graphite starts to cool off because the concentration of oxygen in the feed stream has been depleted to the point where the heat removal by the convective flow and radial conduction is greater than the energy generated by oxidation. The lower upper portion of the reflector graphite just below the core experiences very little oxidation because the graphite below this region depletes all the oxygen. The first layer of pebbles in the core experiences little or no oxidation during the ≈ 200 hours when oxygen is flowing to the bottom of the reactor. In fact the results indicate that the first layer of pebbles immediately starts to cool off due to the natural convection flow.

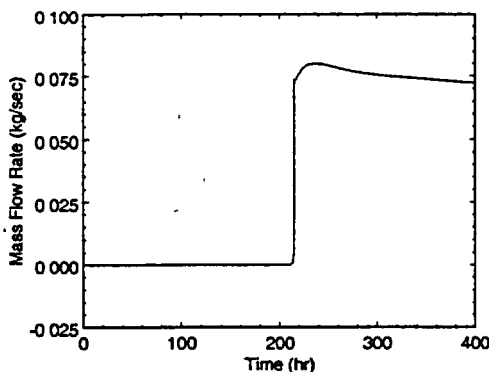


Fig. 3 Mass flow rate through the core

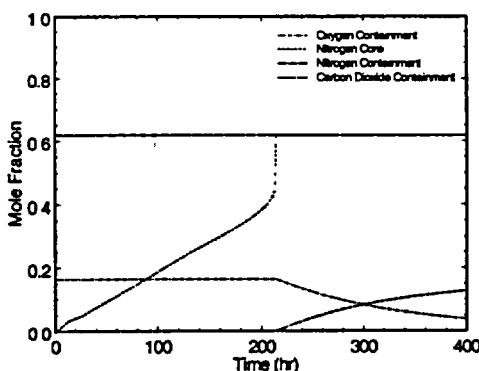


Fig. 4 Mole fraction of gas components in the reactor and containment

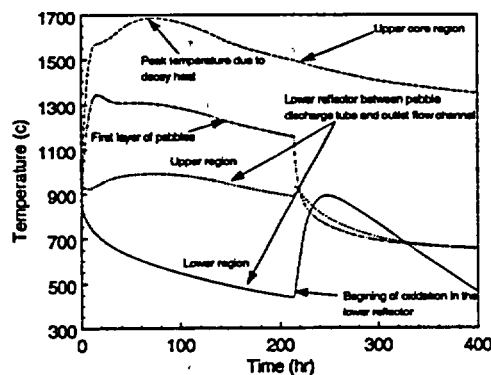


Fig. 5 Temperature history of core and lower reflector region

The maximum temperature that the pebbles in the core experience during the transient is 1685 °C. As shown in the figure, this peak temperature occurs early in the transient and is due to decay heat. This peak temperature is greater than the allowable fuel particle temperature of 1600 °C but with a more detailed model and better exterior boundary conditions the maximum core temperature is expected to fall below the maximum allowable fuel particle temperature.

4. Conclusions

The preliminary results presented in this paper indicate that oxidation of the PBMR pebbles will probably not be a major concern for release of large amounts of fission products in any air ingress event. The oxidation of lower reflector graphite appears to consume all the available oxygen before it can reach any of the fuel in the core. This is a result of the mass flow rate due to natural circulation being very small. Sensitivity calculations are planned where the availability of oxygen in the vault will be varied and different oxidation rates will be used.

The onset of natural convection appears to take days to occur. Thus, if required countermeasures can be taken to mitigate the consequences of an air ingress accident. The prediction of the timing of the onset of natural circulation depends on how well the code used is able to predict the molecular diffusion of the air through the helium in the core. This phenomenon is strongly dependent on the flow characteristics through the core (e.g. friction losses) and subsequent thermal response. Therefore we plan to benchmark MELCOR against the Japanese experimental results presented in Reference 6. With the benchmarking complete, we will then take what we have learned and apply it to our PBMR model. It appears that present day safety analysis codes such as MELCOR can with a few modifications be used to analyze reactor accidents associated with the PBMR.

5. References

- [1] D. Nicholls, "The Modular Pebble Bed Reactor," *Nuclear News*, September 2001, pp.35-40.
- [2] Idaho National Engineering and Environmental Laboratory and Massachusetts Institute of Technology, 1999, Strategic Nuclear Research Collaboration: FY-99 Annual Report, INEEL/EXT-99-00649, July 1999.
- [3] Summary Report, Workshop on High-Temperature Gas Cooled Reactor Safety and Research Issues, USNRC, Washington DC (Adams Accession ML013650004) October 10-12, 2001.
- [4] M. Hishida and T. Takeda, "Study on air ingress during an early stage of a primary-pipe rupture accident of a high-temperature gas-cooled reactor," *Nuclear Engineering and Design* 126 (1991) pp.175-187
- [5] R. O. Gauntt, R. K Cole, S. H. Hodge, S. B. Rodriguez, R. L. Sanders, R. C. Smith, D. S. Stuart, R. M. Summers, and M. F. Young, "MELCOR Computer Code Manuals," NUREG/CR-6119, Vol 1, Rev. 1, SAND97-2397-2398, 1997.
- [6] B. J. Merrill, R. L. Moore, S. T. Polkinghorne, and D. A. Petti, "Modifications to the MELCOR code for application in fusion accident analyses," *Fusion Engineering and Design*, 51-52, (2000) pp555-563.
- [7] M. H. O'Brien, B. J. Merrill, and S. N. Ugaki "Combustion Testing and Thermal Modeling of Proposed CIT Graphite Tile Material," EGG-FSP-8255 September 1988, Idaho National Engineering Laboratory.
- [8] J. Schaar, W. Frohling, H. Hohn, "Status of the Experiment NACOR for Investigation on the Ingress of Air into the Core of an HTR-Module," Nuclear Energy Agency "Workshop on High Temperature Engineering Research Facilities and Experiments", Petten, Netherlands, November 12-14-1997.

6. Acknowledgment

Work supported through the INEEL Long-Term Research Initiative Program under DOE Idaho Operations Office Contract DE-AC07-99ID13727.

NUCLEAR EMERGENCY RESPONSE PLANNING AND PREPAREDNESS FOR THE HTR-10

J. QU and Z. WU

*Institute of Nuclear Energy Technology
Tsinghua University, Energy Science Building, 100084 Beijing-China*

ABSTRACT

The 10 MWth high-temperature gas-cooled test reactor (termed HTR-10) went into criticality at the Institute of Nuclear Energy Technology (INET) of Tsinghua University in December 2000. As required by China nuclear safety authorities, we had developed nuclear emergency response plan and relevant technical procedures for the implementation of protective actions should an accident occur. This paper presents the technical basis for the development of the HTR-10 nuclear emergency plan. Firstly, it describes briefly the requirements of the China nuclear safety authorities about the nuclear emergency planning and preparedness for research reactors. Then, the paper focuses on the technical development of initiating conditions (ICs) and emergency action levels (EALs) for HTR-10. The ICs and EALs developed are tabulated in this paper. Finally, a brief presentation about the on-site emergency response exercise carried out before the first fuel loading on HTR-10 and other emergency preparedness activities conducted or being planned are given in this paper.

1. Emergency Classification System

Similar to the emergency classification system for nuclear power plants, the emergency states that may happen on research reactors can be classified into four categories, i.e. emergency standby, plant emergency, site area emergency and general emergency based on the features and consequences of potential events or accidents, which are characterized by emergency action levels.

In the current China nuclear safety regulations, emergency action levels for research reactors are defined in terms of the air concentration of or radiation exposure from the effluents released at the site boundary (Table 1). However, it is often a big challenge to estimate the concentration or radiation dose in the event of an accident. In fact, it is in general required that proper mitigating measures should be carried out to avoid or decrease the release of radioactive material into the environment before the release actually occurs. The experience and lessons learnt from the emergency management of nuclear facilities have shown that the operability of the emergency action levels as given in Table 1 is relatively poor. Because of this, the National Nuclear Safety Administration (NNSA) requires that quantitative emergency action levels be established in the emergency response planning for research reactors. They should be developed based on the initiating conditions or events defined in the safety analysis. They should be straightforward and easy to use, such as instrument readings, equipment states or other directly observable information and phenomena etc. Clearly, this kind of action levels facilitates quick recognition and determination of emergency classes.

2. Quantification of Emergency Action Levels

Emergency action levels are used as the technical criteria or parameters for the classification of

emergency states, such as instrument readings and alarm settings etc. The purpose is to facilitate recognition and determination of the emergency states and hence take prompt and effective protective actions to avoid or mitigate the potential consequences should an accident occur.

Table 1 Emergency Classification System for Research Reactors ^[1]

Emergency Classes	Action Levels
Emergency standby	<ul style="list-style-type: none"> Actual or projected radiological effluents at the site boundary exceeding 10 DAC* when averaged over 24hrs, or 0.15mSv whole body dose accumulated in 24hrs. Report or observation of severe natural phenomenon, such as earthquake and hurricane etc.
Plant emergency	<ul style="list-style-type: none"> Actual or projected radiological effluents at the site boundary exceeding 50 DAC* when averaged over 24hrs, or 0.75mSv whole body dose accumulated in 24hrs. Actual or projected radiation levels at the site boundary of 0.2mSv/h for 1 hour whole body or 1mSv thyroid dose.
Site area Emergency	<ul style="list-style-type: none"> Actual or projected radiological effluents at the site boundary exceeding 250 DAC* when averaged over 24hrs, or 3.75mSv whole body dose accumulated in 24hrs. Actual or projected radiation levels at the site boundary of 1.0mSv/h for 1 hour whole body or 5mSv thyroid dose.
General emergency	<ul style="list-style-type: none"> Sustained actual or projected radiation levels at the site boundary exceeding 5mSv/h whole body. Actual or projected dose at the site boundary in the radioactive plume exposure pathway exceeding 10mSv whole body or 50mSv thyroid.

DAC: Derived Air Concentration

In HTR-10 emergency response plan three emergency classes are identified. It includes emergency standby, plant emergency and site area emergency. The corresponding initiating events and emergency action levels are listed in Table 2. The methodology for development of emergency action levels for nuclear power plants was taken as a reference in this task ^[2]. It should be noted, however, that it is generally not possible to develop quantified indicators for all initiating events that may result in emergency states. Therefore, qualitative judgment about the safety status and eventual progression of reactor system is also needed in many cases.

3. Determination of Emergency Planning Zones

In China the emergency planning zones for research reactors are determined primarily using the criteria given in Table 3. The radionuclide inventory in a research reactor core is generally much less than that in commercial nuclear power plants. Consequently, the quantity of radioactive material that may be released into the environment in an accident and hence the potential impact on the population living in the vicinity would be significantly smaller compared with an accidental release from a large-scale nuclear power plant. The principal purpose of establishing emergency planning zones around a research reactor is to be able to take effective protective actions to avoid or mitigate the radiation exposure from the passing radioactive plume to the workers and the public members who are occasionally on-site or near the site boundary in the event of an accident.

Table 2 HTR-10 Initiating Events and Action Levels

Emergency Classes	Initiating Events and Action Levels
Emergency standby	<ul style="list-style-type: none"> • Loss of off-site or on-site AC power supply, and failure of the diesel generating unit supplying power to designated loads within 60 min; • Failure of engineered safety features or fire protection system, and the Technical Specifications requiring reactor shutdown. • Abnormal opening of certain safety valve or pressure relief valve, and failure of closing as system pressure decreasing to a preset value; • Failure of the indications and alarm signals for more than two reactor safe shutdown parameters in the control room, and loss of protection function for one of them; • The mean concentration of airborne radioactive effluents into the environment over 30 min exceeding 10 times of the routine discharge concentration; • The specific activity of the coolant inside the primary circuit during 5 min exceeding 10 times of the preset alarm threshold; • Loss of pressure accident caused by tube rupture in primary circuit; • The decreasing speed of the liquid level due to abnormal leakage of liquid nitrogen system exceeding 5 times of the normal speed.
Plant emergency	<ul style="list-style-type: none"> • The mean concentration of airborne radioactive effluents into the environment over 30 min exceeding 100 times of the mean discharge concentration; • Decrease in pressure by 20% in 5 min due to abnormal leakage of the waste gas processing and storage system; • Decrease in liquid level by 2 cm due to abnormal leakage of the storage tank in the tritiated water collection system; • Loss of feed water supply without trip; • Uncontrolled lifting-up of a control rod during power operation without trip; • Water ingress into reactor core due to SG tube rupture, and the safety valve in the pressure relief system of the primary circuit in open position; • Loss of off-site and on-site power without scram; • Failure of all indicators and alarm signals for reactor safe shutdown; • The specific activity of the coolant inside the primary circuit during 5 min exceeding 100 times of the preset alarm threshold.
Site area emergency	<ul style="list-style-type: none"> • The maximum dose expected on the site resulting from the effluents exceeding the lower intervention level for taking sheltering (5mSv whole body dose or 50mSv thyroid dose); • Double-ended break of the hot gas duct (air ingress accident) • The specific activity of the coolant inside the primary circuit during 5 min exceeding 500 times of the preset alarm threshold, and the safety valve in open position.

Table 3 Recommended Radius of Emergency Planning Zone for Research Reactors ^[1]

Thermal Power (P)	Radius of Emergency Planning Zone (m) (Centered at reactor)
$P \leq 2\text{MW}$	Operations boundary
$2\text{MW} < P \leq 10\text{MW}$	100
$10\text{MW} < P \leq 20\text{MW}$	400
$20\text{MW} < P \leq 50\text{MW}$	800
$P > 50\text{MW}$	To be determined on a case-by-case basis

Besides the HTR-10, there are two other research reactors at INET. They are the twin-core shielding research reactor, each with a thermal power of 1MW, and the 5MW district heating experimental reactor. According to the recommendations given in Table 3, the outside wall of the building in which the shielding research reactor is located could be chosen as boundary of the emergency planning zone for this reactor. For HTR-10 and the 5MW district heating experimental reactor we could establish an emergency planning zone with a radius of 100m for each of them. For the sake of effective management, we have taken the site boundary of INET as the emergency planning zone for all the three reactors instead of setting up separate emergency planning zones for these reactors.

According to the criteria given in IAEA TECDOC-953 ^[3], an urgent protective action zone with a radius not less than 500m and a long-term protective action zone with a radius not less than 5km would be required for HTR-10. It means that off-site emergency response planning would be needed. Although the principles proposed for establishing adequate emergency response capabilities are sound and comprehensive and the corresponding technical steps reasonable and operable, we are of the opinion that in this document the safety features of a nuclear facility are not explicitly emphasized in the quantitative criteria suggested for defining the magnitude of emergency planning zones. Apparently, it is reasonable to establish different size of emergency planning zones for nuclear facilities with different safety features. The safety analysis done for HTR-10 has shown that this reactor is of advanced inherent safety features. Reactor states that could result in high radiation doses or significant radioactive releases are of extremely low probability of occurrence ^[4]. Based on those considerations, we find it would not be necessary to extend the emergency planning zone for HTR-10 beyond the site boundary of INET.

4. Emergency Preparedness Activities

To be able to respond promptly and effectively to emergency situations in case of an accident, a comprehensive and integrated emergency response plan has been developed ^[5]. On the basis of this, an on-site emergency response center has been established. In addition, information network connecting relevant emergency organizations will also be put in place in the near future, in particular the data network connection between the HTR-10 control room and the response center. Each of the emergency organizations has compiled their emergency response implementing procedures. They have also conducted relevant training and exercise activities.

A convincing demonstration of emergency response capability is a mandatory requirement for the issuance of fuel loading license in China ^[6]. Therefore, an on-site emergency exercise for HTR-10 was carried out shortly before the first fuel loading. The hypothetical accident scenario was water ingress into primary loop. The initiating event supposed was SG hot tube rupture.

The whole exercise progressed from emergency standby via plant emergency to site area emergency and lasted for 1.5 hours. All the emergency organizations of INET were involved in this

event. They performed their tasks satisfactorily under the direction of the on-site emergency response center. Protective actions, including sheltering and evacuation of part of the site personnel and public members (students), were smoothly conducted.

The NNSA staff supervised the whole exercise on the site and convened a technical evaluation meeting thereafter. They concluded that the exercise was a great success. They also made some suggestions for further improvement of the INET emergency response capabilities.

5. Conclusions

The emergency response capability established for HTR-10 is an integral part of the whole safety management system aiming at the safe operation of the reactor. The development of quantified emergency action levels represents a key issue in this aspect. Because of the limitation in the knowledge of the safety performance of high temperature gas-cooled reactors, the initiating events and action levels presented in this paper are preliminary. They will be further elaborated in the future as more experience is accumulated in this field.

References

- [1] NNSA. Emergency Response Planning and Preparedness for Research Reactors. HAD002/06. 1991
- [2] NUMARC. Methodology for Development of Emergency Action Levels. NUMARC/NESP007. 1992
- [3] IAEA Method for the Development of Emergency Response Preparedness for Nuclear or Radiological Accidents. IAEA-TECDOC-953. 1997
- [4] INET. The Final Safety Analysis Report for HTR-10. Institute of Nuclear Energy Technology of Tsinghua University, 2000.
- [5] J. Qu and Z. Wu et al. Nuclear Emergency Response Plan for the Nuclear Facilities at the Institute of Nuclear Energy Technology of Tsinghua University. INET-1959. 2000
- [6] NNSA. Safety Requirements for Operation of Research Reactors. HAF202. 1995

HTR: Confinement / Containment Question

Dr. G. Brinkmann,
Framatome ANP GmbH, NGES3
Freyeslebenstraße 1
91058 Erlangen, Germany

and

Ms. Sophie Esther,
Framatome ANP SAS,
Cedex 06
69456 Lyon, France.

ABSTRACT

One of the major discussed questions today is:

Does an HTR need a containment – pressure retaining – or is it possible – licensable – to have only a so called confinement?

The answer depends on the design of the HTR and there especially on the fuel, the layout of the core, primary circuit and the reactor building. The calculations of the radiological releases strongly rely on the assumptions made for the source term definition, e.g. fuel particles failure rates (during normal and accidental conditions) the diffusion data, the dust data and the deposition / lift off mechanisms.

It can't be generalized – HTRs only need a confinement. The results of the accident analyses have to demonstrate with an adequate safety margin that the special HTR design has low radiological consequences during postulated accident conditions. Then this special HTR may not be required to have a pressure resistant containment (conventional PWR type containment).

Introduction

During a lot of conferences and discussions on HTRs around the world it seems that often the question confinement / containment is only treated in a philosophical way. So there are a lot of opinions:

- Nuclear power plants in general need a PWR type containment.
- HTRs don't need a PWR type containment, but let us call it a vented containment.
- HTRs never need a containment – we have to find another word.

In most of the discussions the confinement / containment question is coupled with the question of barriers against external events, especially after Sept. 11th 2001. But this coupling makes only sense, if the barrier against radioactive releases is identical to the barrier against external events, and that depends on the design of the plant.

So talking about confinement / containment first the barrier concept against radioactive releases has to be defined.

Barrier Concept

First barrier: The HTRs use fuel elements in which the fuel is located in many small fuel particles each coated with two high-density layers of pyrocarbon and one layer of silicon carbide. One characteristic safety feature of the HTRs is that radioactive substances produced during nuclear fission are confined within the fuel particles during all operating and accident conditions in such a way that there can be no significant release of radioactivity from these fuel particles. This safe confinement of radioactivity is assured by the design of the fuel particles coatings and the inherent upper limit of approx. 1600 °C on the maximum possible fuel temperature under accident conditions. The silicon carbide layer in particular is demonstrably so dense up to a temperature of 1600 °C that no radiologically significant quantities of gaseous metallic fission products are released from intact particles.

For the design purposes and safety licensing requirements, however, it has to be postulated that a small portion of coated particles in the core (10^9 up to 10^{11}) have manufacturing, radiation or accident induced defects.

So the quality of the first barrier has to be defined by a Failed Particle Fraction Curve as a function of the particle temperature and depending on the irradiation (burn up).

Second barrier: The primary gas envelope (primary boundary) forms the second barrier against the release of radioactive substances. The components should be designed in such a way that through wall cracks can be rolled out. Because of the quality assurance measures taken, unisolable breaks in the connecting piping should be highly improvable – otherwise each break in the helium systems would lead to a depressurization of the primary system.

So the quality of the second barrier has to be defined, and also the borders – so that breaks outside of this primary gas envelope are of less interest for radiological releases.

Nevertheless during the licensing procedures a break in a connecting pipe (inside the primary gas envelope, unisolable) the released gas borne activity in the primary coolant, the portion of the released activity deposited on surfaces of the primary system and a portion of released dust has to be defined. In the second phase of this event (core heat up) the following is needed for the calculations:

- Decay heat removal – transport of the cavity cooler
- Temperature of the core as a function of time
- The fractions of the fuel particles as a function of time depending on temperature
- The activity release out of the core
 - release out of the particle transport in the coolant
- The activity release out of the broken pipe
 - pipe diameter, plate out inside the primary system.

Third barrier: The third barrier – here called confinement envelope – should act in conjunction with other barriers to minimize the radiological impact on the environment during normal and accident conditions.

So depending on the quality of the first barrier, the assumptions and calculations due to the second barrier the question – what is the confinement envelope – may differ for each HTR in particular, based on the layout and design of the core, the primary circuit and the reactor-building or the compartments e.g. reactor cavity.

HTR Module

In the HTR Module (Siemens design in the 80ies) the following features fulfill confinement functions:

- Reactor building (leak tightness 50 vol.-% / day)
- Secured subatmospheric pressure system

- Building pressure relief system, HVAC system isolation.

For the confinement envelope it was stated:

- Normal operation: no filtering.
- At overhauls: filtering by exhaust air filtering system (aerosols).
- During major depressurization accident (unisolable DN65 line): Unfiltered venting through two dampers to vent stack.
- Other depressurization accidents: Possibility of filtering by subatmospheric pressure system (iodine filter).
- Environmental impact of all accidents far below limits described in Article 28.3 of the German Radiological Protection Ordinance even without active measures taken or filtering; consequently no PWR containment necessary.

During the licensing procedure for the HTR Module this concept for the confinement envelope (described in the Safety Analysis Report) was accepted by the TÜV Hanover, working as the authorized expert of the government of Lower Saxony and later on behalf of the BMFT (Federal Minister of Research and Technology). Even so it was confirmed by the RSK (Reactor Safety Commission) on behalf of the German Federal Government in their recommendations on the safety concept of the HTR Module ("The RSK has no safety related objections to the confinement envelope concept. It is suitable for ensuring compliance with the requirements of the Radiological Protection Ordinance in normal operation and under upset and accident conditions").

Conclusions

For the nowadays designs of HTRs – PBMR and GT-MHR-(uranium) – a pressure resistant containment (PWR type) is not planned. Looking at the design and the layout of the core etc. of these reactors it should be possible to show that they only need a confinement envelope – whatever the features are to fulfill the functions. But nevertheless the accident analyses must demonstrate with an adequate safety margin that the radiological consequences are far below the governmental dose limits.

LESSONS LEARNED DURING THE SAFETY ASSESSMENT OF THE THTR FOR FURTHER DEVELOPMENTS AND ASSESSMENTS OF HTR

R. SARTORI

*Department of Machine Technology, Stress Analysis, Nuclear Technology
RWTHV Anlagentechnik GmbH, Kurfürstenstr. 58, D-45138 Essen*

and

K. HOFMANN

Subdivision Energy and Environment

ABSTRACT

During the assessment of the THTR the inherent safety characteristics of the HTR reactor brought changed requirements for the design of the safety systems.

The safety assessment was conducted taking account of the major design criteria available, such as

- fail-safe design of the prestressed concrete pressure vessel, which resulted in a modified safeguard against excess pressure and less stringent requirements for the in-service inspections,
- the strongly negative temperature coefficient, which resulted in modified requirements for the shut-down system,
- the high design temperature of the fuel elements, which resulted in modified requirements for the emergency cooling systems,
- the low power density and high storage capacity of the core and core internals, which resulted in modified requirements for the time behaviour of the residual heat discharge systems.

1. Introduction

RWTÜV, based in Essen, the Federal Republic of Germany, is the body engaged by the licensing authority as the main expert organisation for the safety assessment of the THTR (Thorium High Temperature Reactor). This contract has now been in effect for approximately 30 years and encompasses an assessment during the

- design phase
- manufacturing and erection phases
- commissioning
- operation and
- decommissioning and safe enclosure

A major problem when beginning the assessment was the lack of reliable technical rules and guidelines for the THTR-specific reactor concept. The German BMI Safety Criteria for Nuclear Power Plants are valid for all reactor types, especially for light water reactors, but they do not take into consideration the specific characteristics of the HTR. For the THTR therefore first a "THTR planning basis" and then the "Safety Criteria for HTR" were developed.

Below safety-specific solutions are highlighted for the HTR on the basis of the HTR's inherent safety features, namely:

- strongly negative temperature coefficient
- high design temperature of the fuel elements
- the chemical and physically neutral cooling gas helium
- low power density
- high temperature storage capacity

2. Overpressure Relief System

In the rules for pressure vessels, equipment is generally required to safeguard against excess pressure, unless it is demonstrated for all design cases that the design pressure is not exceeded. In the case of an HTR there is an additional requirements that no primary coolant be discharged - even if there is an incident. Such safety valve systems must therefore consist of redundant devices to ensure that, on the one hand, any unintentional opening and remaining open can be prevented by shutting off a valve and, on the other, that any failure of a safety valve is also controllable. Such a valve station is very elaborate and also requires a considerable in-service inspection effort.

With an HTR it can be demonstrated, on the basis of the low power density and the related storage capacity, that a pressure safeguard can be dispensed with. This applies for the design basis accidents, the plant being equipped with an after heat removal system of reliable and redundant design or with an only passive after heat removal system.

If this after heat removal system is not designed as a solely passive system - as was the case with the THTR - and it is not possible to demonstrate adequately calculated reliability, accident management procedures are provided for. In view of the high storage capacity and the related, existing time until higher pressures and temperatures are reached in the primary circuit, it is possible to take manual measures in order to lower pressure by relieving the primary gas in the He accumulator or for a manual start-up of a special after heat removal system. The time available for the measures amounts to a number of hours. During the assessment of the systems' reliability it was found that there are no secured failure rates for components specifically erected for operation under high purity helium or at high temperatures. Relevant tests must be planned here for the system design in order to be able to satisfy the requirements regarding sound probabilistic safety analyses.

3. First core charge

With a pebble-bed reactor the first loading is, in contrast to that for an LWR reactor, a very time-consuming and laborious procedure, and it is very difficult to implement in the case of a multi-zone core structure with the operational fueling installation. An application was therefore made in the case of the THTR to perform the first charge manually and even before completion of the plant as a whole, in order to save construction time. The assessment revealed that a simple back-up reactor protection system with neutron detectors is sufficient to ensure reliable control in the case of reactivity disturbances. Once again the low power density and high heat storage capacity played an important part. After heat removal systems or activity inclusion systems are not necessary.

4. Shutdown Systems

The basic requirements regarding two shutdown systems also apply for the shutdown systems of an HTR. Of course the THTR also had two shutdown systems. For the 1st such system for emergency shutdown a deviating design was provided for. The requirement for the design of the emergency shutdown system is that the reactor be rendered subcritical from any operating state and any accident situation, even in the case of a single fault. It keeps the reactor core subcritical long enough to ensure that specified limits for the system are not exceeded. Manual interventions (manual shutdown) must be avoided for at least half an hour.

These requirements lead in the case of an HTR with immediate after heat removal or on the basis of the temperature equalisation processes and the strongly negative temperature coefficients to the provision of so much shutdown reactivity that the redevelopment of criticality from a hot start is hardly possible. This also leads in each case to extended shutdown breaks. To avoid this, for an

emergency shutdown defined as the worst possible operating case (approx. 1-2 days after an extended shutdown break) from power operation without the presence of the J 135 and Xe 135 equilibrium and without after heat production from an extended stationary operation, the shutdown reactivity was such that redevelopment of criticality is possible in less than half an hour. But since half an hour must be assumed so that a manual shutdown using the other shutdown system can be taken into account in the analysis, the case of the development of criticality was therefore to be examined. With a conservative calculation there was a shortfall of 0.5 nile shutdown reactivity. The redevelopment of criticality was analysed with this shortfall. The calculation revealed that the requirement of the regulations for compliance with specified limit values was met and the values present were clearly below the limits. A power production peak of approx. 20 % of the nominal power arose for less than 100 s and the longer-term core power was less than 5 %. The gas temperatures were only a little above the operational cold gas temperatures. This therefore meets the related requirements regarding an emergency shutdown system and at the same time an emergency shutdown system adapted to the circumstances of an HTR is present.

5. Activity release

Even the overall release of activity with the ventilation system was well below the licensed annual limits, but to fulfill the ALARA principle there were provided aerosol filters in all ventilation paths. By this the problem of release of dust to the environment in a HTR were solved.

6. Conclusion

On the basis of the individual examples it was shown that it is possible to achieve to a satisfactory extent the safety objectives even if there is a lack of HTR-specific regulations. The special features inherent to HTR are utilised. The related experience gained with the THTR can still be fully utilised with other concepts as well.

Posters

Thermal Characteristics' Research of Circular High Temperature Gas-Cooled Reactors Under Loss-Cooling and Depressurization Crisis

TIECHANG QIN and ZUYING GAO

*Branch 103, Institute of Nuclear Energy Technology,
Tsinghua University, Beijing, P.R.China, 100084*

ABSTRACT

When the power of single modular high temperature reactor was raised more than 200 MW with the method of expanding the core's volume or adding the power density, the maximum temperature of the fuel spheres would exceed the limitation of 1600°C because the core could not transfer the decay heat to the outside in time. Circular high temperature reactor takes advantages of the flowing rules of spheres in the core and set up a column, which is filled with graphite spheres. Because the graphite spheres' region is not consisted of fuel and provides a low-temperature heat storage region, the radial heat conducting resistance can be cut down to the level which can transfer decay heat to outside in time under the loss-cooling and depressurization crisis so that the fuel spheres' maximum temperature will not exceed the limitation of 1600°C on condition of any crises.

1. Introduction

Modular High Temperature Gas-cooled Reactor is one generation of newly developed reactor, which has better inherent safety. The power level of single reactor is restricted by the following factors:

- 1) The limitation of the fuel's maximum temperature: When the power of single modular high temperature reactor was raised more than 200 MW with the method of expanding the core's volume or adding the power density, the maximum temperature of the fuel spheres would exceed the limitation of 1600°C because the core could not transfer the decay heat to the outside in time.
- 2) The limitation of the neutron radiation on the graphite reflectors: Due to the limitation of the modular HTR's dimension, the reactor's power level can be heightened only by means of increasing the power density which will lead to the increase of the neutron radiation on the graphite reflectors. Because the graphite reflectors cannot be replaced during their lifetime, the neutron radiation must be restricted under its permission limitation.
- 3) The mixing of cool and hot gas: For the circular reactor, the central area is not consisted of the fuels, so the gas temperature discrepancy between the central area and the fuel area will be quite distinct, which will lead to the corruption of some parts along the gas flowing track.

In 1982, Professor Wang Dazhong put forward the idea of circular high temperature reactor, which broke through the research barricade of increasing the HTR's power level. Circular high temperature reactor takes advantages of the flowing rules of spheres in the core and sets up a column, which is filled with graphite spheres^{[1][2][3]}. Because the graphite spheres' region is not consisted of fuel and

provides a low-temperature heat storage region, the radial heat conducting resistance can be cut down to the level which can transfer decay heat to outside in time under the loss-cooling and depressurization crisis so that the fuel spheres' maximum temperature will not exceed the limitation of 1600°C on condition of any crises. During the practical engineering designing, the problem how the relative parameters affect the reactors' whole performance is worth careful studying.

This paper utilized the reactor's analysis software of THERMIX simulative calculation program, and studied the characteristic rules of the circular high temperature reactors. The first step is to set up the simulative calculation model and gets out the results of the reactor's stationary condition. The second step is to get hold of the dynamic results when the reactor is under the loss-cooling and depressurization Crisis condition.

2 Model Explanation

2.1 Direct Cycle and Indirect Cycle

The selection of direct cycle and indirect cycle plays a key role on the design of reactors. Because the discrepancy between the two cycles is quite distinct, which leads to the difference of the system components and performance, it requires us to define the type of cycle first.

The following two situations are the detailed description of this problem: There are two HTRs with power of 250MW, the circular area's inner diameters of which are both 100 cm. One is the direct cycle and the inlet and outlet temperature are respectively 350°C and 900°C. Other is indirect cycle and the inlet and outlet temperature are respectively 250°C and 750°C. The other parameters are all same. The calculation results are:

(Note: 1.The Time-Tmax refers to the time when the maximum temperature appears. 2. The Tini refers to the initial temperature of the maximum temperature at the beginning of the crisis. 3. The Tmax refers to the maximum temperature)

Outer Diameter m	3.2	3.4	3.6	3.8
Power Density MW/m ³	3.6550	3.1981	2.8238	2.5128
Tini °C	965.3	961.0	951.8	952.1
Tmax °C	1453.1	1440.5	1427.7	1410.2
Time-Tmax	48.0	51.0	54.5	58.0
Outlet Temperature Difference	480.26	475.74	466.26	470.44

Table1 Direct cycle calculation results (350°C-900°C)

Outer Diameter m	3.2	3.4	3.6	3.8
Power Density MW/m ³	3.6550	3.1981	2.8238	2.5128
Tini °C	815.8	808.2	799.7	800.8
Tmax °C	1414.1	1400.5	1387.1	1368.9
Time-Tmax	56.5	59.5	63.5	70.0
Outlet Temperature Difference	441.43	434.45	426.09	431.06

Table2 Indirect Cycle calculation results (250°C-750°C)

From the previous two tables, we conclude that:

1. The maximum temperature of indirect cycle is about 40°C less than that of direct cycle.
2. The initial temperature of the indirect cycle is about 150°C less than that of the direct cycle.

The maximum temperature is the most important factor. Because the type of cycle only leads to a

slight variance, we only consider the situation of the direct cycle in our later discussion. If the conclusion of this situation was used to the designing of the indirect cycle, it will improve the reactor's whole safety performance. The final goal of reactor's safety designing is to eliminate the negative effects of nuclear energy utilization under the extreme accidental crisis. We must comprehensively take the safety and economy into account and get to a conclusion, which can simultaneously satisfy the requirements of safety and economy.

2.2 Convection

During the practical loss-cooling and depressurization crisis, natural convection is one of the heat-transferring methods. So we need make out how the natural convection influence these crises and whether it is positive or negative, which will also be very important in the designing of HTRs.

Theory and experiments point out that convection will carry away some heat, which will decrease the fuel's maximum temperature under loss-cooling and depressurization crisis. Fig 1 describes the maximum temperature dynamic process under the condition of the accident.

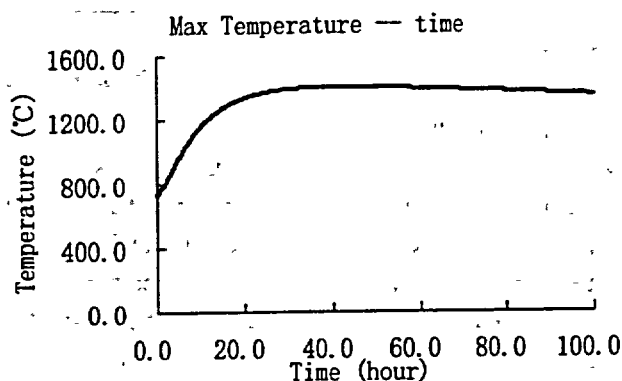


Fig 1. 200MW HTR without convection

1 describes the maximum temperature dynamic process under the condition of the accident. The gas's inlet and outlet temperature are respectively 250 °C and 750 °C. We consider the maximum temperature's dynamic process during the 100-hour period after the beginning of the accident.

From the previous results, we concluded that the maximum temperature is definitely reduced due to the influence of the convection under the loss-cooling and depressurization crisis. The detailed values are listed in the table 3:

	Convection	No Convection
Tini °C	726.9	726.9
Tmax °C	1371.8	1402.8
Time-Tmax hour	53.9	41.9

Table3 Convection's Influence on the Maximum temperature Under Crisis

From table 3, the convection makes the maximum temperature reduce with 31 °C. From a variety of relative calculations, we can also get to the similar result that the convection reduces the maximum temperature and the reduction is always about 30 °C. However it is negligible that the influence of the descent of 30 °C on the maximum temperature, we only consider the non-convection situation in the future calculations which will make the discussion much clearer and the result will expand the safety scope under the crisis condition.

2.3 Inlet Temperature

The gas inlet temperature is one of the reactor's main input parameters. We consider the maximum temperature of the dynamic process under the loss-cooling and depressurization crisis. Although these are peculiar examples, the results represent the universal conclusions

Apparently, as the inlet temperature's increasing, the initial temperature of the maximum temperature tends to be decreasing and the maximum temperature tends to be increasing. The occurring time of the maximum temperature is about the 35th hour after the beginning of the crisis. The previous results can be explained that:

1. Under the preconditions of fixed power and outlet temperature, the adding of the inlet temperature will lead to the augmentation of gas flux. Thus, due to the improvement of heat-transferring efficiency, the higher gas flux will carry away much more heat than

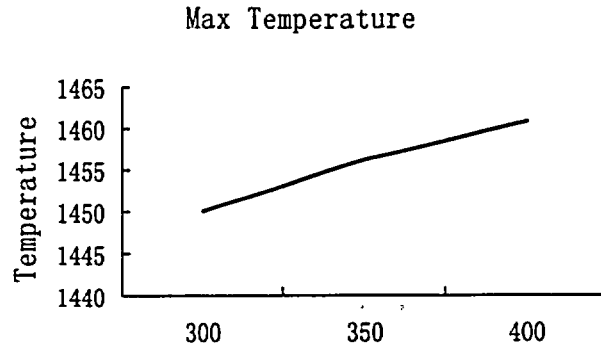


Fig 2. the different inlet temperatures influence

- the lower gas flux situation does at the beginning of crisis, which will result in the decreasing of the initial maximum temperature. So the higher the inlet temperature, the lower the initial temperature of the maximum temperature under the loss-cooling and depressurization crisis.
2. As the inlet temperature's rising and the outlet temperature keeps constant, the average temperature of the reactor is added, which will increase the heat storage of the reactor. After the happening of the crisis, the relatively higher heat storage will lead to the higher maximum temperature. On the other hand, the distribution of the reactor's core temperature gradually tends to be uniform. That is, the heat storage tends to be equal, which results in the much more gentle increasing of the maximum temperature.
3. If the geometrical and physical parameters keep constant, the heat storage ability can be regarded as unchangeable and the thermal performance is also immovable, so the dynamic response of the maximum temperature also keeps changeless. In another word, the occurring times are all approximately equal.

Summarily, the inlet temperature's influence on the maximum temperature after the crisis is very small, so we no longer consider the variance of inlet temperature and regard that the inlet temperatures are always 300°C. Table 4 listed the principal parameters of the circular HTRs which we are studying.

Items		Values
Power	MW	200, 250, 300, 300
Height	m	9.43m
Power Density	MW/m ³	3.0
Inner Diameter	m	0.8, 1.0, 1.2, 1.4, 1.6, 1.8
Outer Diameter	m	3.2, 3.4, 3.6, 3.8
Work Fluid		Helium
Cycle		Direct Cycle
Convection		No Convection
Inlet Temperature	°C	300

Table 4 Principal parameters of Circular HTRs

3 Calculation Results and Analysis

3.1 The dimension of the circular area's influence

We take the example of 250MW circular HTR. The inlet and outlet temperature is respectively 300°C and 900°C. On the occasion of loss-cooling and depressurization crisis, the maximum temperature's variance is directly proportional to the expanding of the inner diameter of the circular HTR. The method of expanding the inner diameter can effectively reduce the maximum temperature. The inner diameter of circular area expands every

10cm and the maximum temperature decreases about 30°C, which is very helpful to improve the reactor's safety performance. Fig 3 describes the influence of the inner diameter on the maximum temperature under the condition of loss-cooling and depressurization crisis

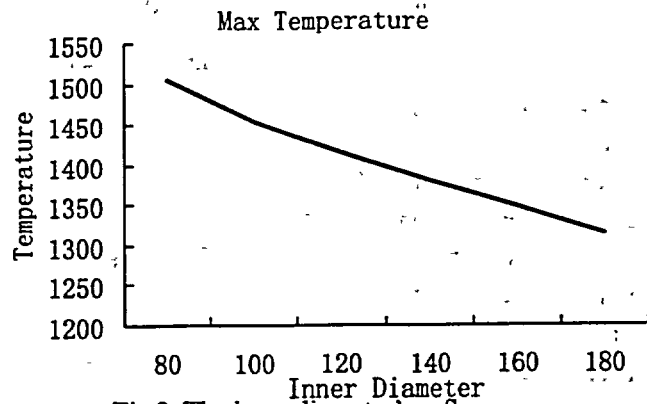


Fig 3. The inner diameter's influence

However, under the condition of loss-cooling and depressurization crisis, as the increasing of circular area's inner diameter, the maximum temperature tends to increase too, which means that the reactor's inner thermal condition will deteriorate and the neutron flux will boost up on the condition of reactor's normally running situation. So, in the future discussion, we will only consider the three inner diameters: 80cm, 100cm and 120cm.

3.2 Outer Diameters of Circular Areas

From the previous discussion we knew that the increasing of inner diameter can decrease the maximum temperature under extreme crisis, but it will deteriorate the thermal performance. This result can be attributed to the adding of the average power density of the reactor, so one of the feasible resolution is to expand the outer diameter of the reactor, which can reduce the power density effectively. On the other hand, circular HTR can dramatically reduce the maximum

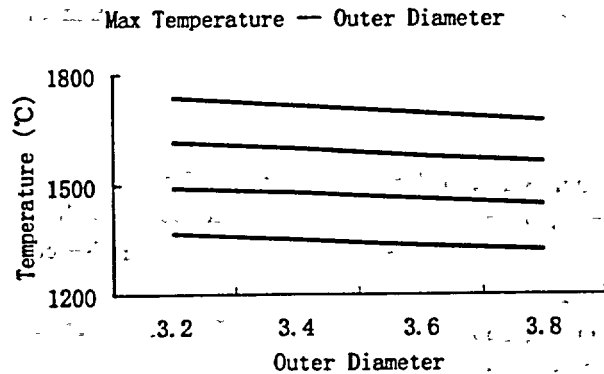


Fig 4. The influence of outer diameters and different power temperature under crisis situations. This is the reason why circular design can increase the power of HTRs.

In Fig 4, we conclude that: it is accordant with the theoretical analysis that the influence of the reactors' outer diameter on the maximum temperature under the condition of loss-cooling and depressurization crisis. That is, expanding of the outer diameter will decrease the maximum temperature, and at the same time it will effectively improve the thermal performance and remarkable reduce the neutron flux. Considering the factors of safety and calculation precision, we set up 1450°C as the temperature evaluating criteria. We require that the maximum temperature must be less than 1450°C under the crisis conditions.

3.3 The relations between the maximum temperature and reactor's power density

Fig 5 describes the relations between the maximum temperature and the reactor's power density under the condition of loss-cooling and depressurization crisis. The power level is 300MW. the inlet and outlet temperatures are respectively 350°C and 900 °C . In fact, the principal factor, which dominates the crisis maximum temperature, is the power density of the reactors. Fig 5 just illustrates that the less the power density, the lower the maximum temperature.

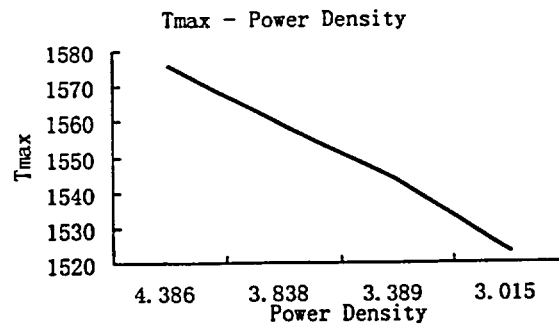


Fig 5. Power Density Influence on the maximum temperature

4 Conclusion

Summarily, during the dynamic process after the beginning of the loss-cooling and depressurization crisis,

1. The maximum temperature of the indirect cycle is 40°C less than that of the direct cycle.
2. Convection makes the maximum temperature a descending of 30°C
3. As the inlet temperature's increasing, the crisis initial temperature tends to descend and the maximum temperature tends to ascend. The happening time of the maximum temperature is about the 35th hour after the beginning of the loss-cooling and depressurization crisis .
4. The influence of the inlet temperature on the crisis maximum temperature is quite slight.
5. Under the condition of loss-cooling and depressurization crisis, the variance of the maximum temperature is directly proportional to the variances of the inner diameter of the circular area. In detail, the inner diameter expands every 10 cm, the maximum temperature descends 30°C.

References

- [1] Zhang Ximin, Heat Transferring Mechanics (The Third Edition) , Building Industry Press 1993.
- [2] Yu Rongxian, Power Mechanics of Factory, SouthEast Publishing House, 1992.
- [3] Wang Dazhong, Investigation of A High-temperature Reactor with A Central Region Of Graphite-Sphere, 1982.
- [4] Jiang Zhiqiang, 350MW Modular HTR's Designing Research and Gas Mixing Experiment Study, Tsinghua University Press. 1991.
- [5] Ma Changwen, the new method of nuclear utilizing, Science Publishing House of P.R.China, 1997.
- [6] Yu Pingan , Thermal Analysis of Nuclear Reactors, Nuclear Energy Publishing House of P.R.China,1986.
- [7] Alvin H.Weinberg, The First Nuclear Era, Nuclear Energy Publishing House,1996.
- [8] Willian W.Bathe, Fundamentals of Gas Turbines.

**A COMBINED EXPERIMENTAL AND FINITE ELEMENT
ANALYSIS OF MANETHI STEEL FRACTURE PROPERTIES**

K. Ahmed and M. Ghonim, Atomic Energy Authority, Egypt

Paper will be handed out separately

E. BREUIL
Novatome Framatome ANP
10 rue Juliette Récamier, 69006 Lyon - France

and

R. EXNER
Borsig Energy GmbH
Hans Joachim Balcke Strasse 46049 Oberhausen - Germany

HTR-E Project. High-Temperature Components and Systems

The HTR-E European project (four years project) is proposed for the 5th Framework Programme and concerns the technical developments needed for the innovative components of a modern HTR with a direct cycle. These components have been selected with reference to the present projects (GT-MHR, PBMR) :

- the helium turbine, the recuperator heat exchanger, the electro-magnetic bearings and the helium rotating seal.
- the tribology. Sliding innovative components in helium environment are particularly concerned.
- the helium purification system. Recommendations on impurities contents have to be provided in accordance with the materials proposed for the innovative components.

The main outcomes expected from the HTR-E project are the design recommendations and identification of further R&D needs for these components. This will be based :

- on experience feedback from European past helium test loops and reactors
- on design studies, thermal-hydraulic and structural analyses
- and on experimental tests

1. Introduction

The main objective of the work performed for HTR-E is to develop innovative technologies which are needed for the components and systems of a modern HTR with a direct cycle and then contribute to the competitiveness, safety and acceptability of such reactors. The competitiveness of such reactors is based on the use of these technologies for each high efficiency components and systems which allow, at the end, to reach a net plant efficiency of around 50 %. Similarly, high performances components and systems in terms of thermo-mechanical resistance, lifetime, maintenance, behaviour in case of failure,... are required to demonstrate the safety and to contribute to the acceptability of such reactors.

The critical and innovative components and systems have been selected by reference to the present projects with a direct cycle concept (GT-MHR, PBMR) as shown on fig. 1 and 2.

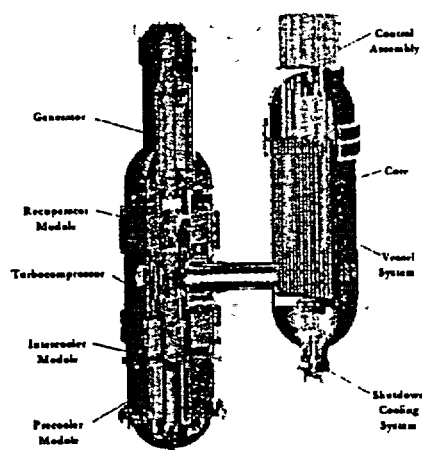


Fig 1. GT-MHR MODULE

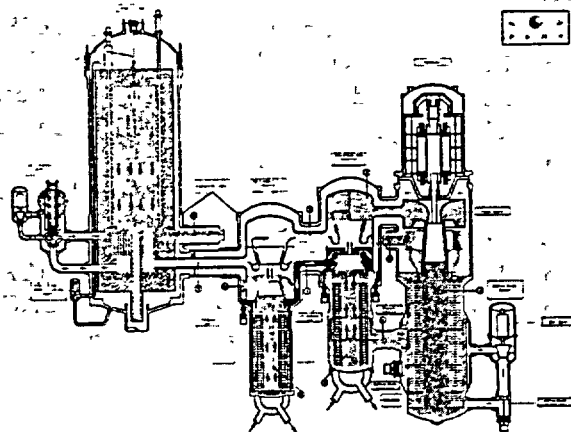


Fig 2. PBMR module

The key components and systems selected for HTR-E are :

- the helium turbine,
- the helium/helium heat exchanger called recuperator,
- the large capacity magnetic bearings,
- the helium leak-tightness rotating seal,
- the tribology,
- the helium purification system.

Design recommendations and identification of further R&D needs for these components will be provided taking into account :

- the experience feedback from European past helium test loops and reactors (EVO, HHV, KVK, Dragon, AVR and THTR) but also from reactors outside Europe (Peach Bottom, FSV, HTTR, HTR-10), and also from other technologies (FBR, AGR, PNP plant,...),
- the design studies, thermal-hydraulic and structural analyses with CFD and FEM codes (DACAT, BLADES, CAST3M, Fluent, STAR CD, ANSYS, NASTRAN, MLDyn codes),
- and the tests performed on experimental facilities (CLAIRE high temperature heat exchangers test facility from ESTHER platform of CEA, FLP 500 test facility for AMBs of Zittau university, tribological test facilities).

The work will be carried out over a period of four years split into two main phases of two years. The first phase concerns the experience feedback, the specifications and design studies and the second one the validation, the tests, the identification of further R&D needs and recommendations for the main components and systems of a modern HTR with a direct cycle. The budget is 3,5 million Euro (50% funded by EC).

The partners involved in the HTR-E project are : Framatome ANP, CEA, Zittau university, NRG, FZJ, EA, NNC, Jeumont, S2M, Ansaldo, von Karman institute, Heatric, EVO, Aubert et Duval, Borsig Energy GmbH.

2. Turbine

The direct cycle concept is the main feature of a competitive and safe modern HTR. Then the feasibility of a high efficiency helium turbine, inserted in the primary cycle, is the most important technological key issue for the components of a modern HTR. There is however no industrial experience for the HTR typical operating conditions (helium gas, 850°C, 100-300 MWe range, long time operating conditions with high reliability...).

An important work program is proposed in HTR-E. It is complementary to the material development work program carried out in the HTR-M project. It consists in :

Phase 1 : SPECIFICATIONS-STATE OF THE ART-PRELIMINARY DESIGN

- Design use, system review, integration and ISIR (GT-MHR and PBMR type reactor),
- Review of existing technologies from past HTR experience and other industries,
- HHV data and turbine inlet thermal insulation,
- EVO design data and measurements for specified load cases,
- HTR-M results analysis,
- Design study (turbine and thermal insulation at the inlet)

Phase 2 : DESIGN ANALYSES

- Thermal and thermo-mechanical analysis (CAST3M, ANSYS codes),
- Aerodynamic design-CFD calculations (DACAT and BLADES codes, inverse method),
- Experimental tests program definition

3. Recuperator Heat eXchanger (HX)

The recuperator is a helium/helium heat exchanger inserted in the primary circuit to recuperate a part of the remaining energy at the turbine outlet to preheat the helium at the core inlet. This component is specific to the direct cycle and its main function is to increase as high as possible the efficiency of the cycle. The competitiveness of a modern HTR is directly linked to the feasibility of this key component particularly loaded in Temperature and Pressure difference. The work program consists in :

Phase 1 :

SPECIFICATION OF TYPICAL OPERATING CONDITIONS (GT-MHR and PBMR type reactor)

REVIEW AND IDENTIFICATION OF EXISTING TECHNOLOGIES

- Technological survey of high temperature heat exchangers used in industry : conventional shell and tube units as well as helical finned tube and compact plate heat exchangers will be considered,
- Consultation of manufacturers specialised in large heat exchangers,
- Engineering studies on 2 or 3 basic concepts, CFD calculations (Fluent, STAR CD code), thermo-mechanical analyses (ANSYS code), see fig.3 and 4 two potential concepts for recuperator application,
- Selection of reference concepts; the development and test program of the next phase will be established.

Phase 2 : FEASIBILITY STUDY AND VALIDATION TESTS

- Definition of small scale units for high temperature testing (participation of HX manufacturers)
- Adaptation of the test rig (CLAIRE loop of the ESTHER platform) and preliminary testing
- Validations tests
 - Steady state testing under actual flow conditions and ambient pressures
 - Transient testing (cycling at high temperatures)

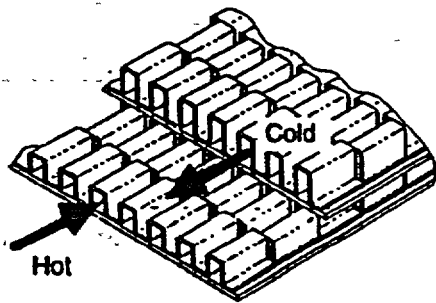


Fig 3. Plate fin concept

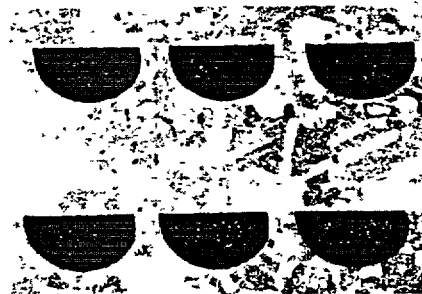


Fig 4. Micro channel concept (HEATRIC)

4. Electro Magnetic Bearings (EMBs)

These components are used to support the rotating shafts of turbo-compressors or turbo-machine inserted in the direct cycle of a modern HTR. This kind of support has been selected for a modern HTR to avoid the risk of leakage and fluid ingress in the primary circuit induced by the concept of mechanical and lubricated bearings (bad experience feedback in US and German former HTRs). So, the magnetic bearings for rotors support are considered as key components with regards to the safety and competitiveness of a modern HTR. The work program consists in :

Phase 1 :

FUNCTIONAL REQUIREMENTS-LOAD ANALYSIS-FEASIBILITY STUDIES

- Functional requirements
- Definition of the functional requirements under normal and emergency operating conditions for Active Magnetic Bearing and Catcher Bearings
- Load analysis. The bearings loads are determined by analysis of HTR loads, Finite Element Methods (ANSYS code) and Real Time Simulation (MLDyn code).
- Permanent MB feasibility study
- Catcher bearings feasibility study

CONCEPT PROPOSAL-MECHANICAL ANALYSES

- Concept proposal for bearings and diagnosis. Depending on the special requirements and the results of the load analysis a concept will be designed for Active Magnetic Bearings (including controller, sensor and power electronics), Catcher Bearings and Diagnosis Systems.
- Mechanical analyses. The magnetic, thermal, and structural behaviour of the magnetic bearing system (start-up, shut-down, unbalance, emergency shut-down) will be determined by means of transient Finite Element Methods (ANSYS code) under the load cases previously defined.

Phase 2 : EXPERIMENTAL VALIDATION-RECOMMENDATIONS

- Experimental validation AMB (FLP 500 test facility, see fig. 5 and 6). The main aims of experimental part are the validation of the designed system and dynamic behaviour as well as the investigation of single effects. Further parts are to test the algorithms of the diagnosis system and catcher bearings.
- Recommendations and statements

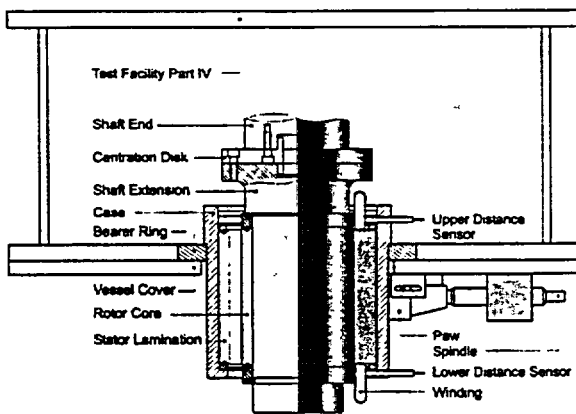


Fig 5. FLP500 test facility

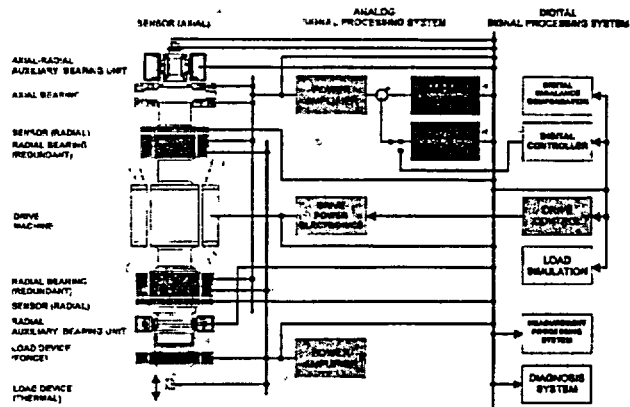


Fig 6. FLP500 EMBs and load device

5. Helium rotating seal

The helium rotating seal is associated with a rotor of the turbo-machine penetrating through the primary vessel. In this case the generator is located outside the primary circuit that simplifies the maintenance operations and allows to use mechanical bearings for the support. So this concept can be considered as an alternative of a fully immersed rotor in primary helium and consequently fully supported by magnetic bearings. The feasibility of such a seal is a key issue to increase the competitiveness of a modern HTR by reducing the maintenance campaign duration. The work program (Phase 1 only) consists in :

STATE-OF-THE-ART AND SPECIFICATIONS

State-of-the-art and specifications concerning helium leak rates in previous or similar projects, classification of the potential leakage areas of a "typical" HTR design, existing technologies and their performances

FEASIBILITY STUDY

- Canned magnetic bearings. Single effect analysis for Canned Active Magnetic Bearings on basis of theoretical and experimental investigations
- Dry system. In connection with the analysis of the existing devices, a suitable concept of dry system as regards the HTR conditions will be defined, and justified by theoretical analysis.
- Liquid, gas, ferro-fluid barrier. In connection with the analysis of the existing devices, a suitable concept of the system as regards the HTR conditions will be defined, and justified by theoretical analysis.
- Dry system. Stability and leakage analysis (STAR CD code). The objective of this task is to determine whether the selected dry seal designs meet the requirements for functionality and structure integrity
- Experimental tests program definition

6. Tribology

Sliding and new components (stator seals, hot gas duct seal,...) of a modern HTR with direct cycle are particularly concerned. It must be noted that a bad operating of these sliding components will dramatically impact the safety and availability of the reactor. The work program consists in :

Phase 1 :

UPDATING OF THE STATE OF THE ART

- Review of tribological problems on a HTR
- Review and identification of typical tribology conditions of components
- Review of the existing materials and coatings

PROPOSAL OF ELEMENTARY CONFIRMATION OR ORIENTATION TESTS

Phase 2 : ELEMENTARY TESTS – COMPENDIUM OF RECOMMENDATIONS

- Tests with representative tribological and environmental conditions. Tests will be performed on a selection of materials and antagonistic couples, in representative configurations (sliding + fretting, sliding + bearing (gears)), and in representative conditions : HTR non pure Helium, 500-750°C, 70 bars.
- Redaction of a compendium of recommendations

7. Helium purification system

The performances of this system impact directly the safety of a modern HTR as it controls the level of impurities in the primary helium. It is a key system to limit the corrosion risk of the graphite and materials of all components of the primary cycle. The work program (Phase 1 only) consists in :

ANALYSIS OF HELIUM ENVIRONMENTS IN FORMER HTRS.

Available literature and data from former HTR projects will be collected and archived in electronic form. Additional relevant knowledge from other sources (HTTR, HTR-10, Magnox, AGR, helium test loops) will be included in a state-of-the-art report.

SPECIFICATIONS FOR THE HELIUM IMPURITIES CONTENT.

Specifications and recommendations for the helium impurities content and the control system will be provided for a modern HTR with direct cycle (GT-MHR and PBMR type reactor). The possible range of impurities in helium (H₂O, H₂, CO₂, CO, CH₄) and graphite particles has to be defined taking into account the risk of corrosion, erosion of the materials. Feedback experience of the Helium purification system will be recovered and analysed. These data will be useful to the selection of grades for high temperature materials tests in HTR-M and also to the tribological tests in helium environment.

CALCULATION OF DECAY HEAT REMOVAL TRANSIENT BY PASSIVE MEANS FOR A DIRECT CYCLE MODULAR HTR

A. WOAYE-HUNE and S. EHSTER

Framatome-ANP/ 10, rue Juliette Récamier 69456 Lyon cedex06

ABSTRACT

In the frame of the modular HTR design assessment, the decay heat removal during accident conditions is one of the main problems to investigate in order to demonstrate the passive safety of the concept. The aim of the present paper is to present one methodology using a numerical simulation approach to assess the thermal consequences on HTR core and structures during a Loss Of Forced Convection configuration. The detailed methodology is presented, and different parametric studies are performed to assess the parameters sensitivity. These first results allow to define the leading parameters which will be retained in the frame of a future HTR passive safety function optimisation.

1. INTRODUCTION

The objective of this paper is to present the thermal calculations performed by Framatome-ANP on the Gas Turbine Modular Helium Reactor (GT-MHR) in the configuration of Loss Of Forced Convection (LOFC) accident (IAEA benchmark, CRP3, 1997).

The objectives are to implement a numerical methodology using the STAR-CD computer code (reference [1]) and to investigate the possible optimisations. The aim of the numerical analysis is to evaluate the maximum fuel temperature during accident configuration when the reactor is cooled by the reactor cavity cooling system (RCCS). In a second step parametric studies are performed to assess the parameters sensitivity. Based on these first results, leading parameters are highlighted, they will be retained in the frame of a future HTR passive safety function optimisation.

2. SYSTEM DESCRIPTION

The Nuclear Power Plant assumed in the present case is a GT-MHR power plant (reference [2]).

The main characteristics are:

- Modular Reactor located in an underground containment building
- Thermal power: 600 MW
- Helium temperature at the core inlet/outlet: 490°C / 850°C
- Helium flow rate through the core: 320 kg/s
- Helium pressure at the core pressure chamber: 7.2 MPa
- Annular core shape with hexagonal graphite blocks
- Reactor Cavity Cooling System surrounding the reactor vessel to ensure the decay heat removal

In normal operation, the heat is transferred via a hot pipe duct to the Power Conversion System (PCS) located in a neighbouring concrete cavity.

In the present study, only the Reactor Cavity including the Reactor Vessel and its internals are considered.

3. MAIN ASSUMPTIONS

During the normal operation, the heat is extracted from the core by a forced helium flow rate. The hot helium is then transferred to the PCS. In the present analysis (accidental conditions), the normal helium flow rate path is suppressed. The decay heat is extracted by passive means from the core assuming the radiation and conduction heat transfer in the reactor vessel, radiation and natural convection in the reactor concrete cavity (see figure 2). The calculations are performed with the assumption of a LOFC followed by a rapid depressurisation and scram. The geometry and physical parameters are consistent with data provided in IAEA-TECDOC-1198 and 1163 (references [2] and [3]).

4. MODELLING ASSUMPTIONS

4.1 THE COMPUTATIONAL STAR-CD CODE:

The general purpose code Star-cd for fluid mechanics and heat transfer (reference [1]) is used. The main characteristics of this software are listed below:

- 3 dimensional code
- A finite volume formulation
- Unstructured grid capabilities including advanced features: local refinement, non-conformant grids with arbitrary interfaces. Meshes are mainly hexahedrons and prisms
- Matrices inverted by bi-conjugate gradient method with preconditioning
- PISO algorithm for pressure linked equations (the pressure solver is semi-implicit: pressure fields are corrected at every iteration in order to achieve both momentum and continuity balances)
- Numerical schemes up to third order

The Navier-Stokes and energy equations are solved in primary variables (velocity, pressure and temperature). For this specific study, computations are run in transient regime.

4.2 GEOMETRY

The geometry is based on data provided in references [2] and [3]. The table 1 sums up the main geometrical parameters.

4.3 PHYSICAL PHENOMENA AND NUMERICAL MODEL

Due to the geometry of the reactor vessel, a 2D axi-symmetrical model is established. The hexagonal arrangement of the core is approximated as an annular shape with average radius.

The model includes the core, the internal and external graphite reflectors, the core barrel, the lower plenum, the floor metallic support, the upper core restraint, the upper shroud, the internal and external vessels, the helium contained in the reactor vessel and the air contained in the reactor concrete cavity. The radial gaps (2 mm) between graphite blocks are explicitly accounted for. Each fuel block layer is modelled by a cells layer with equivalent physical properties to account for the compact and the helium channels not explicitly modelled here. The equivalent properties of fuel block are calculated using another model (2D-plane approach) with compacts and He channels explicitly accounted for. The cross duct and the vertical and radial vessel external supports are neglected.

The model is composed of 3595 nodes and 1765 cells including 1107 fluid cells. The figure 1 presents the finite volume model implemented. During the transient analysis, the thermal transfer by convection into the reactor vessel is neglected in the established model. This assumption is severe for the maximum core temperature assessment. During the transient, the air hydraulic velocity field in the concrete cavity is assumed to be constant and equal to the one calculated during the steady state calculation. This assumption is also conservative for the maximum core temperature assessment (slightly conservative only since the heat extraction is mainly due to radiation), but it decreases strongly the Star-cd numerical resolution delay.

4.4 DATA AND BOUNDARY CONDITIONS

Core Power distribution and evolution: The power distribution is displayed into the three layers of the active core part. During the transient the decay heat evolution is time dependent, decreasing from 30MW (5% of nominal power) at $t=0$ h, to 1.74 MW (0.29% of nominal power) at $t=100$ h (exponential decrease). The table 2 presents the decay heat evolution. It is assumed that during the transient, the power distribution into the core remains homothetic to the one existing at the nominal stage.

Physical properties : The physical properties used for the calculations are summarised in the following table 2. The graphite characteristics are those corresponding to the irradiated H451 (fluence of about $7 \cdot 10^{21}$ n/cm²). In the calculations the graphite is assumed to have an isotropic behaviour. The steel grades assumed are 10Cr9MoVNb for the Reactor Vessel and 03Cr21Ni32Mo3Nb for the inner vessel and core barrel.

Table 2

	ρ (kg/m ³)	C_p (J/kg/K)	λ (W/mK)	emissivity ϵ	μ (Pa.s)
Helium (1MPa)	ideal gas	5198	$f(T)$, ~ 0.29 at 490°C		
air (1 MPa)	ideal gas	1006	0.026		$1.8 \cdot 10^{-5}$
graphite H451	1740	1840	$f(T)$	0.9	
RV steel	7800	520	33	0.8	
Inner Vessel steel	7800	570	24	0.8	

T (°C)	400	600	800	1000	1200	1400	1600	1800
λ graph block (W/mK)	27	31.5	35.2	38.2	40.6	42.3	43.3	43.6
λ eq core block (W/mK)	15.6	17.7	19.4	21	22.3	23.3	24.1	24.6
λ fuel compact (W/mK)	33	27	24	22	20	19	18	17.5

Boundary conditions : The upper and lower boundaries of the model are assumed to be adiabatic (severe assumption). The external radial boundary (wall) which represents the RCCS shell cooled by the water circuit is assumed to have a prescribed linear distributed temperature from 30°C at the lower part to 90°C at the upper part, in consistency with IAEA benchmark.

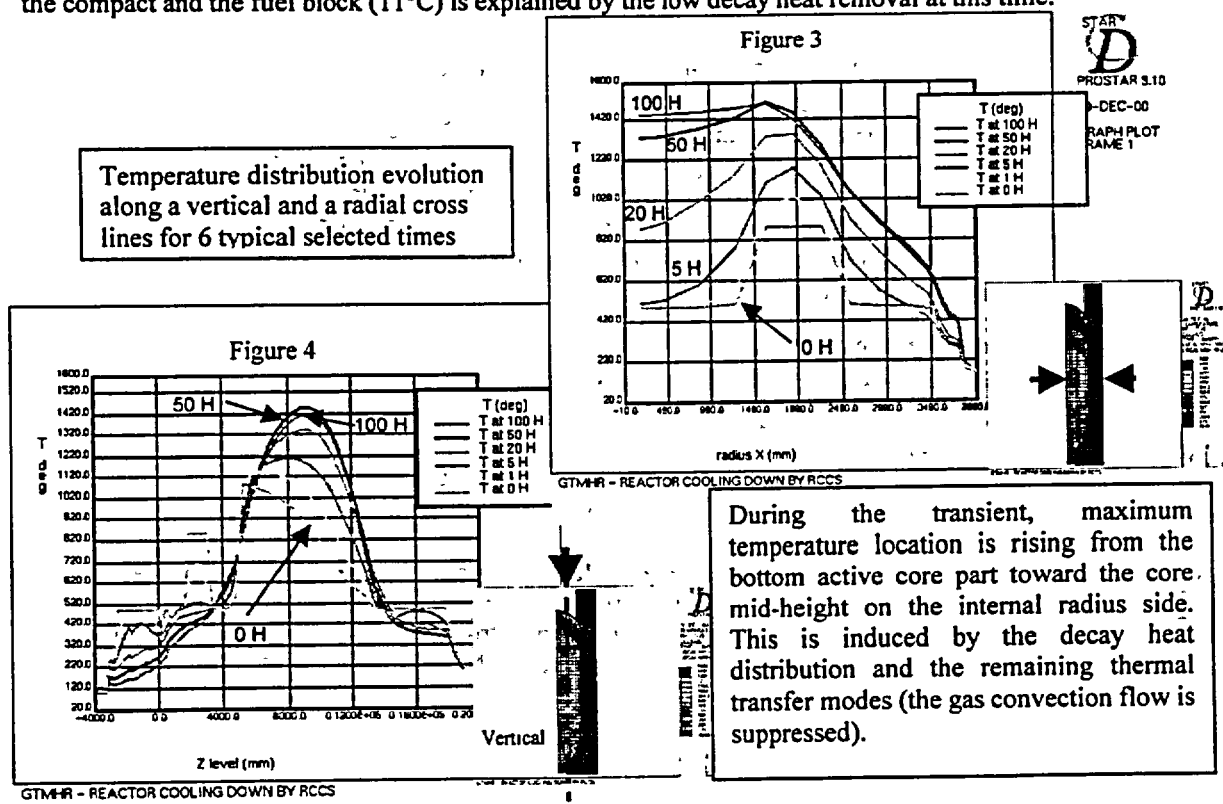
Calculations procedure : The calculations are performed in two stages. The first one is a steady state to calculate the initial thermal field in the whole numerical domain. The results of this first stage will be defined as initial conditions for the second stage. The second stage is a transient calculation performed over a total duration of 100 hours. This one is supposed to cover the time needed to reach the maximum temperature on the different parts of reactor structures.

5. RESULTS

The results show that the maximum temperature obtained on fuel compacts remains below the limit of 1600°C for which no fuel damage is expected. Figures 3 and 4 present the temperature profiles evolutions along horizontal and vertical cutting lines. Figures 5 and 6 present the temperature distribution and the evolution curves, the maximum temperature is obtained after 72 hours.

An additional calculation performed in steady state (severe two-dimensional plane approach with an explicit compact discretization, see figure 7) shows that the fuel block maximum temperature is representative of the fuel compact maximum temperature. The small temperature difference between the compact and the fuel block (11°C) is explained by the low decay heat removal at this time.

Temperature distribution evolution along a vertical and a radial cross lines for 6 typical selected times



During the transient, maximum temperature location is rising from the bottom active core part toward the core mid-height on the internal radius side. This is induced by the decay heat distribution and the remaining thermal transfer modes (the gas convection flow is suppressed).

6. PARAMETRIC STUDIES

In order to evaluate the sensitivity to input data and assumptions, several additional parametric calculations are carried out to assess their effects on the fuel compact temperature. Based on the different results, potential optimisations will be proposed.

In all mentioned parametric cases, only one parameter is changed at a time when compared with the reference case presented previously.

The studied parameters and justifications are:

- The steel emissivity of reactor vessel effect ($\epsilon = 0.5$ instead of 0.8): the emissivity values may vary during reactor lifetime and the value of 0.8 may not be guaranteed for such steel material or alternative one which may be possibly selected and retained during vessel optimisation design.
- The graphite thermal conductivity: this physical material property is very difficult to pin down since it depends on the temperature, the graphite type and also on the irradiation and annealing effects. The available data base is also poor, specially for irradiated graphite. The graphite conductivity retained in this parametric case is the one proposed in reference [4]. These properties values seem to be very severe when compared with the few data bases available, but they will indicate the envelop range for the core block temperature.
- The initial temperature field in graphite at steady state before the scram: this parametric calculation is justified by the strong assumption applied for initial temperature field in the reference case calculation (internal and external reflector temperature roughly equal to inlet helium temperature). The parametric calculation (pure thermal conduction in the graphite reflectors corresponding to a configuration with no helium flow leakage through the gaps between the blocks) leads to severe results since the initial temperature field is necessary lower than this one. A full steady state calculation with helium convection will allow to assess the actual initial thermal field at steady state (calculation to be performed in the future).
- The decay heat evolution, increased by 10% over all the transient: this parametric calculation is performed to evaluate the possibility to increase the reactor power.
- The thermal inertia of fuel assemblies reduced by 20% (in active core part): this parametric calculation is performed to assess the thermal inertia effect. Indeed, in the reference case the helium channels have been neglected and the associated thermal inertia has been replaced by graphite. This parametric calculation case is then more representative of the actual case (more severe).

The results show that:

- The steel surface emissivity has a low effect on maximum core temperature, but has a strong influence on the core barrel and vessel,
- The graphite thermal conductivity, the decay heat curve and the thermal initial conditions have a strong influence on maximum core temperature (e.g. the decay heat increased by 10% leads to T maximum on core increased by 5.6 % ($\Delta T = +85^\circ\text{C}$)),
- The thermal inertia of active core has a small influence on the core temperature.

The table 3 sums-up the different results. For the HTR design and specially for the decay heat removal during accident conditions, the graphite physical properties definition is of the highest importance. Due to the principal radiative thermal transfer mode, the graphite selection should be combined with adapted steel with highest emissivity properties as possible. Unfortunately these requirements will be in opposition with thermal insulation considerations needed for the efficiency in normal operation. Further safety - thermal - mechanical analyses are to be performed to retain a final compromise.

Table 3: Parametric results

Case number	1	2	3	4	5	6	7
Title	Ref. case	$\epsilon = 0.5$	λ_{graph} decrease with T	T init field central part free	Decay heat increased by 10%	Active core thermal inertia reduced by 20%	Results of ref [3] for comparison
T max block (°C)	1525	1555	1713	1604	1610	1544	1490
time (H)	71	78	85	59	71	67	71
Tmax core barrel (°C)	690	816	674	722	723	702	715
time (H)	84	94	94	73	84	77	60
Tmax reac vessel (°C)	460	528	442	478	478	462	442
time (H)	86	100	97	75	86	80	75
Pmax extracted by RCCS (MW)	1.9	1.6	1.76	2.08	2.02	1.91	2
Tmax compact (°C)	1536 (=1525+11)						

7. FUTURE STUDIES

The numerical simulations allow to perform many parametric calculations to evaluate the efficiency and potential optimisation axes for future HTR development. Besides, the STAR-CD detailed internals reactor vessel modelling allows a precise assessment of the equipment thermal transients. Additional calculations will be performed to complete this first analysis: use of new material properties when available, e.g. irradiated modern graphite conductivity, study of the natural convection effect on the structure temperatures in the case without depressurisation, concrete temperature in case of RCCS unavailability.

8. CONCLUSION

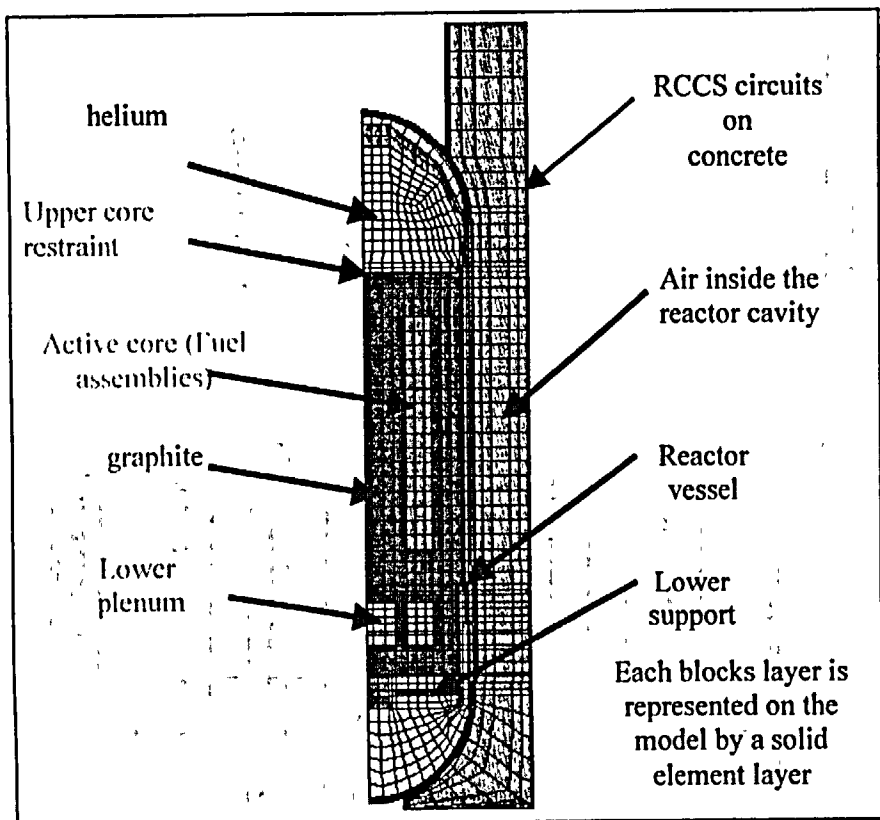
The numerical methodology implemented by Framatome-ANP for thermal calculations on the Gas Turbine Modular Helium Reactor (GT-MHR) in the configuration of Loss Of Forced Convection is now validated and available for future design studies. The approach gives consistent results when compared with existing benchmarks (reference [3]). Leading parameters are highlighted, they will be retained in the frame of a future HTR passive safety function optimisation. The analyses have revealed the steel emissivity and graphite conductivity highest importance. A combination of optimised graphite and steel grades selection have to be done for the accident configuration in consistency with mechanical strength and thermal efficiency considerations during normal operation.

9. REFERENCES

- [1] STAR-CD manuals, version 3.100. Computational dynamics limited, London, 2000.
- [2] IAEA TECDOC 1198 Current status and future development of modular high temperature gas cooled reactor technology (February 2001).
- [3] IAEA TECDOC 1163 Heat transport and afterheat removal for gas cooled reactors under accident conditions (January 2001).
- [4] S.J. Ball - Oak Ridge National Laboratory letter 11 Feb 97
CRP-3 TECDOC Submittal for description of GT-MHR Plutonium Burner Benchmark.

Reactor Power (MW)	600	Vessel outer diameter (m)	7.7
Fuel compact diam (mm)	12.5	Vessel thickness (m)	0.2
Number of fuel blocks	102	Gap between reactor vessel and RCCS (m)	2
Number of cooling channels in fuel block	108	Cooling channel diameter (mm)	16
Core height (m)	8	Gap between blocks (mm)	2
Inner / outer core average radius (m)	2.96 / 4.84	Hexahedral fuel block width (m)	0.36

Figure 1: Numerical model



GTMHR - REACTOR COOLING DOWN BY RCCS

Table 2		Heat decay evolution															
T (H)	0.0001	0.08	0.125	0.5	1	1.5	2	3	5	7.5	11	22	44	72.5	96	100	
Heat decay %	5	2.5	2	1.6	1.2	1.1	1	0.9	0.75	0.65	0.6	0.5	0.4	0.33	0.3	0.29	
P (MW)	30	15	12	9.6	7.2	6.6	6	5.4	4.5	3.9	3.6	3	2.4	1.98	1.8	1.74	

STAR

 PROSTAR 3.10
 22-DEC-00
 VIEW
 0.000
 -1.000
 0.000
 ANGLE
 0.000
 DISTANCE
 15305.18
 CENTER
 2820.000
 305.197
 8508.575
 EHHIDDEN PLOT

Heat removed from core through reactor vessel to the RCCS

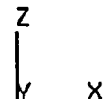
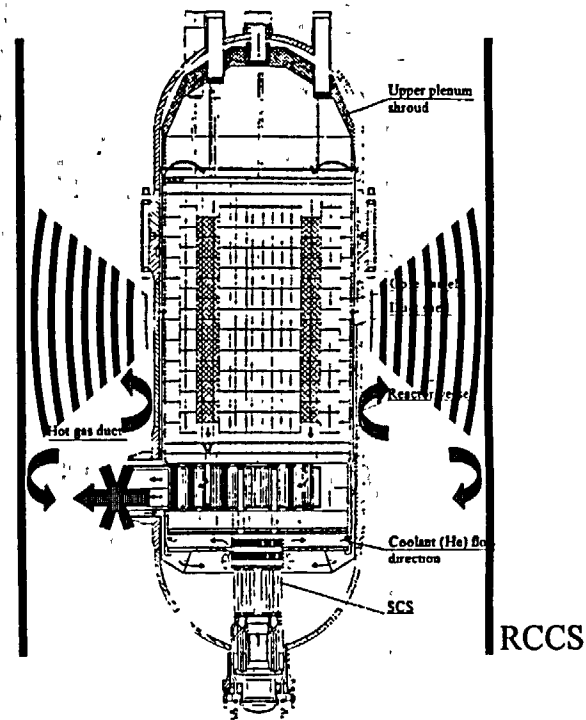
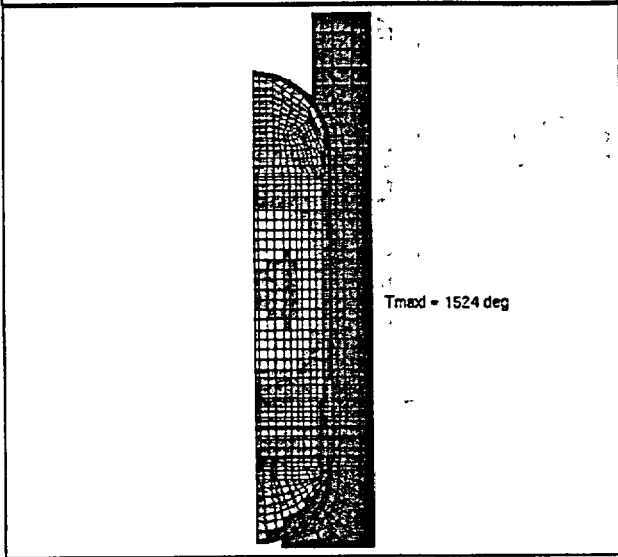


Figure 2
 Passive cooldown



Temperature consequences on core and structures ?

Figure 5: Temperature field at T = 72 H

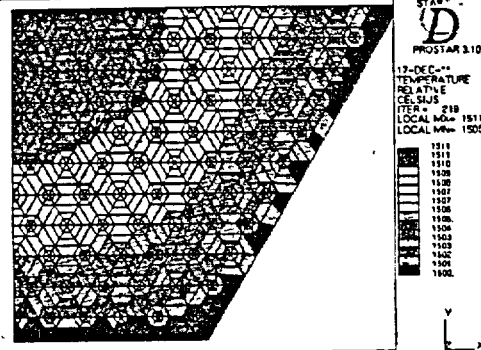


GTMHR - REACTOR COOLING DOWN BY RCCS

STAR
D
PROSTAR 3.10
20-DEC-00
TEMPERATURE
RELATIVE
CELSIUS
TIME = 255600
LOCAL MX = 1524
LOCAL MN = 90.29

1800
1491
1381
1272
1163
1054
944.3
835.0
725.7
616.4
507.1
397.8
288.6
179.3
70.00

Figure 7: Temperature field in hexahedral fuel block



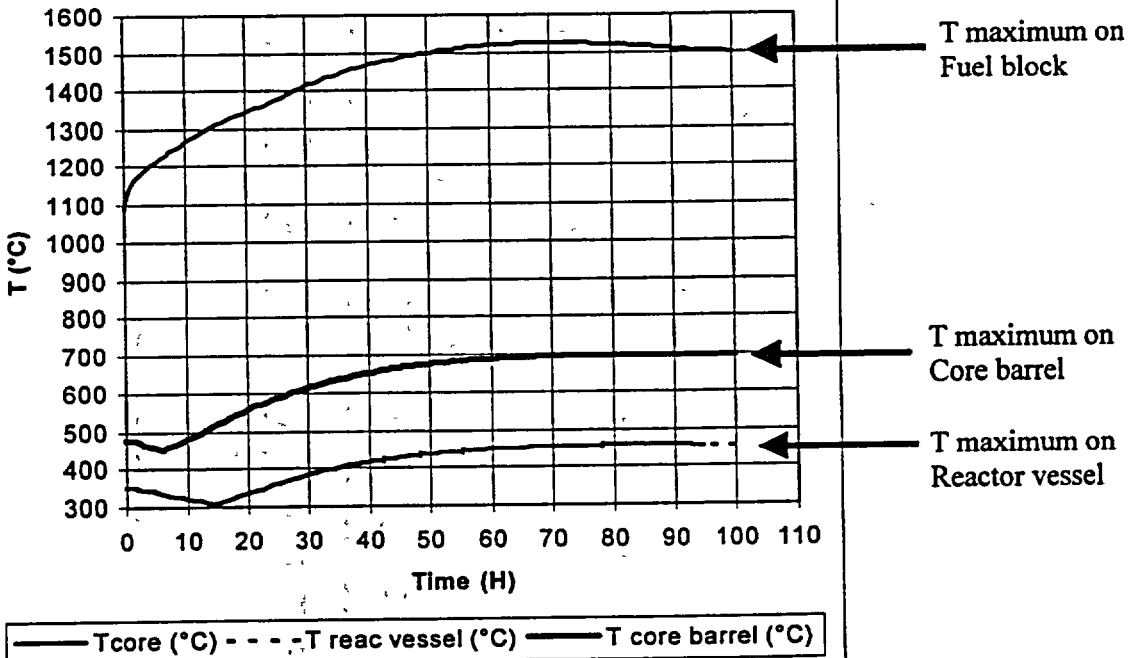
Temperature on fuel compacts is evaluated assuming another 2D plan model with the following assumptions:

- Steady state calculation (severe)
- Temperature imposed = 1500°C at core block boundary (issued from the previous 2D axi transient calculation).
- Power decay distribution in fuel compact at T=71 h (2 MW).
- Axial offset for power distribution = 1.28 (calculation in maximum flux plane)

Final result gives an offset temperature of 11°C between block and fuel compact temperatures, at this time.

The maximum Temperature location may change during the transient

Figure 6: Ref case (n°1) - Temperature evolution (depressurised)



THE MEASUREMENT OF BURN-UP LEVEL IN THE HTR-10

LUO ZHENGPEI, LIU WENFENG, HAN SONG and LI FU

Institute of Nuclear Energy Technology, Tsinghua University, Beijing 100084, P R China

ABSTRACT

Without shutting down the HTR-10, each fuel ball unloaded from the core must be measured. A fuel ball should be recycled into the core when its burn-up is less than $72,000\text{MWd/tu}$. Since the measurement of burn-up for a ball containing $0.9\text{g }^{235}\text{U}$ at most must be nondestructive, a γ spectroscopy method for the fission product ^{137}Cs is typically chosen. Without an accurate calibrating source, it is impossible to achieve the goal that the accuracy of measurement is up to 2%.

The method measuring burn-up without external source uses the ratio of ^{134}Cs to ^{137}Cs and gets bogged down in something unusual that both successful and failed examples have alternated in publications.

The inner calibrating method is proposed in the paper. It is necessary to solve the following problems: a). The simple relationship between $^{134}\text{Cs}/^{137}\text{Cs}$ and burn-up is held only in a specified range. How to use it for a spent ball? b). Can the migration of fission product be ignored? c) How to deal with the neutron spectrum? The paper gives the idea to be tried on the HTR-10.

1. Introduction

The core fuel management of the HTR-10 is marked by fuel load/unload without shutting down the reactor. That increases the availability factor of reactor and helps attain the purpose of making full use of fuels that the average burn-up level (BU) of spent ball is higher than $80,000\text{MWd/tu}$. Each fuel ball unloaded from the core must be measured and judged. Then it should be re-cycled into the core if its BU is less than $72,000\text{MWd/tu}$.

To get these features of fuel management, a facility has to be setup for measuring the HTR-10's BU . The facility should consist of two parts (Wimmers and etc, 1982): One is the fuel loading/unloading system and the other is the instrumentation for measuring burn-up level. During the operation of the reactor, the former system draws off a single ball from the discharging cone in the bottom of the core with pulsed gas and transports it to the proper measuring position along a pipe. And the fuel ball will stay at the measuring position until receiving a judging command from the instrumentation. According to the judgment made through the measurement results, the ball either returns into the core along the pipe or is taken away from the reactor. Separated by the wall of the gas-tight pipe, the instrumentation measures the BU for each ball held at the measuring position through a collimator. This facility is used to guarantee that any ball whose BU is higher than $72,000\text{MWd/tu}$ can not be re-loaded into the core to prevent the ball from destruction under further irradiation in the core.

2. γ spectroscopy method for ^{137}Cs

The BU in MWd/tu is proportional to the ratio of number of split atom to that of heavy metal initially

loaded (i.e. *fima*), because that the average energy E_f released per fission is about 197Mev (or $0.365 \times 10^{-21}\text{MWd}$).

$$BU = \frac{V_b}{G_b} 10^6 E_f \int \Sigma_f \Phi dt \quad (1)$$

Here V_b and G_b are respectively the volume in cm^3 and the weight in g of initially loaded mass of heavy metal in a fuel ball. It is quite evident that the BU is proportional to $\int \Sigma_f \Phi dt$ and directly related to the amount of fission products (Hsue and etc, 1978). Since the measurement of BU for a ball containing $0.9\text{g } ^{235}\text{U}$ at most must be nondestructive, a γ spectroscopy method for the specified fission product is typically chosen. A specified fission product ^{137}Cs is selected on the following reasons: a). near equal fission-yields for ^{235}U and ^{239}Pu ; b). low neutron-capture cross-section, especially for epi-thermal neutron; c). long half-life that does not care about Φ 's fluctuation in irradiation period; d). large fission-yield; e). high-energy gamma rays to minimize attenuation. The number of ^{137}Cs atom N_7 formed by fission is related with the BU through the following relation:

$$V_b \int \Sigma_f \Phi e^{-\lambda_7 t} dt = \frac{N_7}{Y_7} \quad (2)$$

Here Y_7 and λ_7 are the fission-yield and decay constant of ^{137}Cs .

Because of the radioactivity of ^{137}Cs , N_7 is measured via the γ -ray without destructing the ball.

$$BU = Ke^{\lambda_7 t_1} R_7 \quad (3)$$

and

$$K = \frac{10^6 E_f}{G_b \lambda_7 Y_7 R I_7 f \Omega \varepsilon} \quad (4)$$

Here t_1 is the cooling time. R_7 is the counting rate of the detector for $0.661642\text{Mev } \gamma$ of ^{137}Cs .

Thus it is possible to obtain the BU in MWd/tu from the measured counting rate R_7 provided that the proportional constant K in Eq.(3) is known. In general, the constant K can be obtained by using a calibrating ball with a known BU to Eq.(3) once. By using the W-Ni-Fe collimator with the solid angle 2.5×10^{-7} , the R_7 is about 1000cps for a spent ball and it takes about $10\sim 20$ seconds to meet its statistical fluctuation less than $\pm 1\%$. There is a calibrating source with 5% error in the HTR-10, thus the measurement method of BU with 8% error is the spectroscopy method for only γ ray of ^{137}Cs .

3. Inner calibrating method

To go deep into the accuracy, we found that it is difficult to obtain a calibrating ball with error less than 2% , except by using a mass-spectrometer what the HTR-10 is not provided with. For example, even though we obtain a radioactive source ^{137}Cs with 2% error and put it in the center of a graphite ball same as the fuel ball, its accuracy will deteriorate by the distribution of radioactivity within the ball. When we use Eq.(4) with the constants referred to the publications and design, some of them have the error larger than 2% , such as Y_7 , f , Ω and ε . Then through their product, it is impossible to calculate BU with only 2% error. In this case, we try to use an inner calibrating method as follows.

3.1 $^{134}\text{Cs}/^{137}\text{Cs}$ can not discriminate out a spent ball

We know that the radioactivity ratio of ^{134}Cs to ^{137}Cs from the same ball is tightly related with the ball's BU . For simplicity, suppose $\phi = \phi_0 = \text{constant}$ and be the same below. After exposure period T , the ratio R_4/R_7 of counting rates for ^{134}Cs and ^{137}Cs follows as (Wang, 1990)

$$\frac{R_4}{R_7} \approx \frac{\lambda_4 Y_3 R I_4 \sigma_3}{2 \lambda_7 Y_7 R I_7} \phi_0 T = \frac{\lambda_4 Y_3 R I_4 \sigma_3}{2 \lambda_7 Y_7 R I_7} \cdot \frac{G_b 10^{-6} e^{(\lambda_7 - \lambda_4) t}}{V_b \Sigma_f E_f} BU \quad (5)$$

Where σ_3 is the micro cross-section for ^{133}Cs . The subscripts 3, 4, and 7 denote ^{133}Cs , ^{134}Cs and ^{137}Cs respectively.

From Eq.(5), the BU of this fuel ball is obtained from the measurement of R_4/R_7 . Does it solve the difficulties lacking in accurate calibrating source? No, the answer is negative! At first, Eq.(5) is not true when T is so long that the fuel ball becomes spent (Ezure, 1990). Then we get bogged down in something quite unusual that both successful and failed examples have alternated in publications (Wang, 1990; Hsue, 1978; Ezure, 1990).

In order to use $^{134}\text{Cs}/^{137}\text{Cs}$ successfully, we conclude that the following conditions must be met:

- Eq.(5) is held only in a specified range.
- The migration of ^{137}Cs can be ignored.
- All neutrons within the core are thermal ones.

It is impossible to meet all these conditions for the HTR-10. So it is doubtful whether $^{134}\text{Cs}/^{137}\text{Cs}$ can be used to discriminate out the spent ball without a calibrating source.

3.2 Inner calibrating source

We can make some clever moves to deal with these conditions. The temperature threshold of migration effect of ^{137}Cs is above 1500°C and much higher than the ball's center-temperature in the HTR-10, so the condition b is met. The neutron energy spectrum is rather energetic in the HTR-10, however, the condition c is met after a so-called "neutron spectrum correction" described in next section was made. For the condition a , it comes from that Eq.(5) is an approximation when the $\exp(-\lambda_4^* T)$ is taken only as $1 - \lambda_4^* T$. Here $\lambda_4^* = \lambda_4 + \sigma_3 \phi$. Then Eq.(5) is correct to the extent of 1% error only when $\lambda_4^* T < 0.1146$ that corresponds to about $T=110\text{days}$ at the rating power of reactor. That calls attention to use the ratio $^{134}\text{Cs}/^{137}\text{Cs}$ as an inner calibrating-source when T is between 10 and 110 days. Even for only one ball, the constant K is obtained from Eq.(3). Since there are many such inner calibrating-sources, they give us the freedom to make an additional choice in statistics and from the suitable operation conditions in comparison with the K , which is determined via the radioactive calibrating source. Once the average K is determined, it can be used for Eq.(3) hereafter, because it does not vary from days to days.

3.3 Neutron-spectrum correction

The epi-thermal neutrons occupy a rather large portion in the HTR-10 core. Since the epi-thermal cross-section for ^{137}Cs is very small but not for ^{133}Cs , when ϕ_0 is regarded as thermal neutron flux, Eq.(3) is still right but Eq.(5) isn't. If ϕ_0 in Eq.(5) is treated as the thermal neutron flux, an effective cross-section for ^{133}Cs must be used to take account of the neutron spectrum. Unfortunately, the effective cross-section is an uneven function of positions within the core and changes with average BU s. It is impossible to give the effective cross-section a determinate value. For example, in spite of its random flow within the core, we suppose that fuel balls move down at constant velocity along 5 vertical routes, the effective cross-sections are calculated as

Route	1	2	3	4	5
Beginning of lifetime	19.612	19.347	18.552	17.308	15.199
End of lifetime	25.605	24.985	23.413	21.156	17.620

They are different from each other and contrast with 5.88 barns for thermal neutron. The problem we face is which value should be used in Eq.(5)?

In order to make the neutron-spectrum correction, for the same ball we measure the radioactivity of another fission-product ^{154}Eu that is sensitive to epi-thermal neutron too. Because the exposed experience for ^{153}Eu is all the same as that for ^{133}Cs and is linearly related with their cross-sections, it is possible to eliminate the effects of integrated epi-thermal neutron fluxes by each other. The simplified relation is as follows

$$BL = \frac{2 \times 10^6 V_b E_f \Sigma_f}{G_b \sigma_{3th} (1 - \frac{\sigma_{3r} \sigma_{Eth}}{\sigma_{3th} \sigma_{Er}})} \left[\frac{Y_7 R_I \lambda_7 R_A}{Y_3 R_I \lambda_4 R_7} - \frac{Y_7 R_I \lambda_7 R_E}{Y_E R_I \lambda_E R_7} \right] \quad (5)$$

Where the subscripts E , th and r denote Eu , thermal neutron and epi-thermal neutron respectively. Others are the same as above. Thus BU can be calculated from the measured counting rates R_A , R_7 and R_E .

4. The scheme of measuring burn-up level

4.1 Monitor ^{137}Cs to obtain the burn-up level in the whole range

Exposed in the reactor core operating at the rating power for a period of time T , the fuel ball goes to the measuring position. The counting rate R_7 for ^{137}Cs measured by the detector is as follows:

$$R_7 = \lambda_7 \epsilon f \Omega Y_7 R_I \phi \Sigma_f^0 V_b \left(\frac{e^{-\lambda_7 T} - e^{-\phi \Sigma_f^0 T}}{\phi \Sigma_f^0 - \lambda_7} \right) e^{-\lambda_7 t_1} \quad (6)$$

Where R_I is the relative yield of 0.661642MeV γ for fission-product ^{137}Cs . f , ϵ and Ω are the absorption coefficient, detector efficiency and solid angle respectively. Σ_f^0 is the initial fission macro cross-section. ϕ is the thermal neutron flux. t_1 is the "cooling" (elapsing) time.

4.2 The 0.661642MeV γ ray is resolvable

There are three factors to extract the 0.661642MeV γ ray of ^{137}Cs from the γ rays of reactor, especially the 0.664551MeV γ ray of ^{143}Ce , 0.6651MeV γ ray of ^{131m}Te and 0.6677MeV γ ray of ^{132}I . The first one is the energy-resolution of the detector. The second one is the portions including the fission yield and relative emission portion. The last one is the specified fission-product's attenuation caused by the 40days cooling time t_1 . By taking account of all three factors, the 0.661642MeV γ ray of ^{137}Cs is resolvable perfectly. And so do the 0.6046MeV γ ray of ^{134}Cs and 0.723264MeV γ ray of ^{154}Eu .

4.3 Using the inner calibrating source

During $T=10-110$ days, the constant K is calibrated by using the inner calibrating source. Once this constant is obtained, it can be used for Eq.(3) hereafter.

5. The design of measuring system

Only the 0.661642MeV γ ray of ^{137}Cs is selected among the fission-products' γ ray spectrum and the others will be rejected even though they have energies very close to it. Thus a γ spectroscopy with high energy-resolution is used and the $FWHM$ of its $HPGe$ detector is 1.7keV for the resonance peak of ^{137}Cs and the ratio of peak to Compton is above 50. Its bias voltage is 1500v. A transistor-reset preamplifier is dedicated to measurements at high counting rates. The spectroscopy is a type of digital

signal processor where the pulse is formed as a trapezoid with $0.4 \mu s$ top-width to make its throughput achieve $60kcps$. The whole probe (detector and preamplifier) is vacuum-sealed and cooled by liquid-nitrogen to lower its electronic noise to $RMS < 4.5 \mu v$ and is put into a Lead-shielded cavity to lower its background to about $0.3cps$ while the reactor is operating at full power. Since the probe and its spectroscopy is placed at $-15M$ level far away from the core and their control, process and analysis are taken place on the ground surface, it is necessary to set up a local area network to connect those components.

6. Postscript

The above equations are deduced when the reactor is operated at a constant neutron flux level. When the HTR-10 is operated at a constant power, the corresponding equations change only a little and their similar relationships are available.

Acknowledgements

Supported by the Natural Science Foundation of China (Project number 19875028)

References

1. M. Wimmers, P. Pohl and K. Kruger, 1982, The New Facility for Measuring Burn-up has Come into Operation (German), AVR, KFA, Juelich, German, D-7500.
2. S.T. Hsue, T. W. Crane, W.L. Talbert and J. C. Lee, 1978, Nondestructive Assay Methods for Irradiated Fuels, U.S.A., LA-6923.
3. T. K. Wang, 1990, Fuel Burn-up Determination Based on the Measurement of a Short Lived Fission Product, Nuclear Technology, v.91, pp. 413~418.
4. H. Ezure, Evaluation of Depletion and Production of U, Pu, TransPu and fission products in JPDR-1 Fuel, Nuclear Technology, v.91, pp.311~343, (1990)

OVERVIEW OF LEI INVESTIGATIONS ON HEAT TRANSFER AND FLOW STRUCTURE IN GAS-COOLED SPHERES PACKINGS AND CHANNELS

J. VILEMAS, E. USPURAS, S. RIMKEVICIUS, A. KALIATKA, R. PABARCIUS

*Lithuanian Energy Institute
Breslaujos 3, LT-3035 Kaunas - Lithuania*

ABSTRACT

In this paper experimental investigations on heat transfer and hydrodynamics in various gas-cooled channels over wide ranges of geometrical and performance parameters performed at Lithuanian Energy Institute are presented. Overview introduces long-term experience on investigations of local and average heat transfer, hydraulic drag in various types of sphere packings, in smooth, helical tubes and annular channels equipped with smooth/rough or helical inner tubes, such bundle of twisted tubes, as well as turbulent flow structure and the effects of variable physical properties of gas heat carriers on local heat transfer in channels of different cross sections. Lithuanian Energy Institute has accumulated long term experience in the field of heat transfer investigations and has good experimental basis for providing such studies and following analytical analysis.

1. Introduction

Engineering progress in the conversion of thermal or chemical energy into other forms involves searching for new methods of conducting these processes at higher temperatures, which allows for improvement of the efficiency of thermodynamic or thermochemical systems. In the majority of cases, the working fluids or coolants in such systems are gaseous, and exchange of thermal energy between them occurs through a solid wall. To be able to manufacture equipment with acceptable weight, size, and performance, one must significantly augment the heat-transfer processes, which is attained by producing large temperature differentials and also by various other methods of intentional enhancement of heat transfer: the packed beds of spheres, use of artificial roughness, turbulization or swirling of the flow, reducing the thickness of boundary layers or increasing the velocity gradient in them, etc. A great deal of attention has been paid to the enhancement of heat transfer in equipment such as gas-cooled nuclear reactors under power-plant conditions.

Lithuanian Energy Institute (LEI) has accumulated long-term experience on heat transfer, friction and flow structure investigations in packed beds of spheres and variously shaped gas-cooled channels. LEI activities cover experimental and computational works on the effects of variable physical properties of gas heat carriers, on local heat transfer and hydraulic drag in channels of different cross sections, on turbulent flow structure, and on the heat transfer mechanism in the stabilized heat transfer region in a tube.

2. Gas-cooled packings of spheres

In the nuclear reactors spheres could be used as fuel, while cylinders – as control rods. Sphere packings strongly agitate the flow passing through them. Therefore, interest in heat transfer from spheres in packings and fillings of various kinds is understandable. The flow turbulence affects not only the spheres per se but also the surfaces adjacent to them. The heat transfer from the spheres and from a cylinder as well as hydraulic drag and flow mixing factors are investigated in air flow at LEI. The local heat transfer at various positions of cylinders length and perimeter as well as the effect of the sphere packings on the cylinder heat transfer were evaluated.

Various types of packings from the spheres are considered in performed experiments. One kind of them is regular rhombic or random packing, which is arranged between axial streamlined cylinders [1]. The rhombic packing was oriented so that spheres along cylinder were arranged in columns, with clearances that have periodically-varying cross sections running in the vertical direction between them. Near the cylinder surface, the clearances formed by larger flow sections were filled with displacers. In the case of a random filling of the spheres, there were no displacers. Heat transfer from the cylinder immersed in a random filling of spheres was investigated on two different experimental sections. In the first case, the cylinder under consideration made up an element of a longitudinally streamlined bundle with cylinders arranged in a triangular array with the spacing $s/d_{cyl}=1.63$. In the second case, the experimental section represented an annulus filled with spheres and containing the investigated inner cylinder. The annulus of outside to inner diameter ratio was 2.84. In all cases considered, both with a regular packing of the spheres and with their random filling, the cylinder-to-sphere diameter ratio was $d_{cyl}/d=4.29$, the height of assemblies was $H/d=36$, and the porosity - 0.42.

Heat transfer from the cylinder was studied under the second-kind of boundary conditions ($q_w=const$) in air flow with $Re = (0.3 \text{ to } 12) \cdot 10^3$, determined from the sphere diameter and filtration rate (velocity of the incoming flow in front of the sphere packing). Both local and perimeter-average heat transfer coefficients from the cylinder vs. Re and the length of the heated part of the cylinder immersed in the sphere packing were determined. Because the cylinder heat transfer stratifies streamwise, a relative length of the heated part of the cylinder immersed in a sphere packing is incorporated in the relation for heat transfer. The following relations were obtained for the perimeter-average heat transfer coefficients from the cylinder in a bundle with an intercylinder space filled with packings of spheres [1]:

$$Nu = 0.0584 \cdot Re^{0.89} (x/d)^{-0.1} \text{ - in the case of regular (rhombic) sphere packing, and}$$

$$Nu = 0.096 \cdot Re^{0.83} (x/d)^{-0.07} \text{ in the case of random sphere packing.}$$

In the case with the annulus, the cylinder heat transfer is a little higher, and its dependence on Re and on the cylinder height is more noticeable:

$$Nu = 0.094 \cdot Re^{0.88} (x/d)^{-0.16}$$

Given relations describe the experimental data with a $\pm(3 \text{ to } 4)\%$ standard deviation.

It should be pointed out that our data are consistent with the results of other authors [2] dealing with the average heat transfer from a cylinder surrounded by a random filling of spheres (Fig.1). This indicates that in LEI experiments there was no effect of the bundle cylinders or of the outer tube of the annulus on the heat transfer from the cylinder considered. As evident from the results of the investigations, the heat transfer from the cylinder with a random packing of spheres is higher than that with a regular packing. Importantly, this is not related to the increase of the assembly hydraulic drag. Also it was determined that heat transfer from a tube immersion in a sphere packing increases by more than a factor of five by comparing the obtained data with heat transfer in circular tubes [3] (Fig. 1).

Heat transfer from the spheres was studied under the boundary condition $T_w=const$. This condition was assured by the construction of the spheres-heaters (Fig. 2).

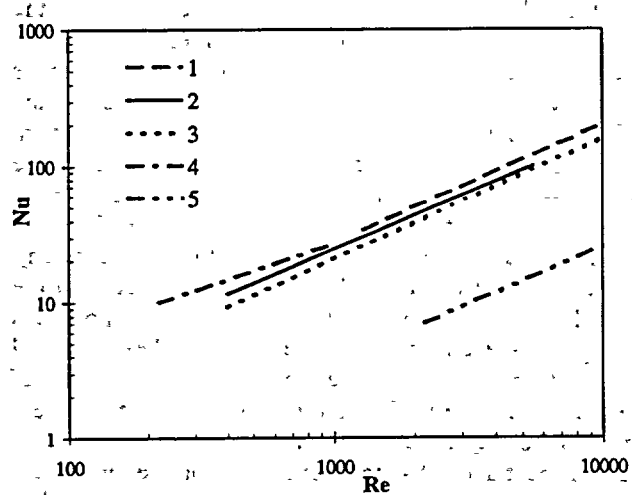


Fig. 1. Heat transfer in various types of sphere packings ($x/d=15$)

1 - inner cylinder of the annular filled with random packing of a spheres; 2 - cylinder in a bundle with an intercylinder space filled with random packing of a spheres; 3 - cylinder in a rhombic packing of spheres; 4 - cylinder in a sphere filling [2]; 5 - circular tube with no spheres [3]

The spheres-heaters were made from the cooper with high thermal conductivity. The temperature was measured in 3 or 4 points on the sphere surface.

The investigations are performed by the local modeling, which allows to obtain the heat transfer characteristics in different places of the packing. The influence of heat transfer by the conductivity, radiation, and natural convection was minimized in the performed experiments. In order to minimize the heat losses by the conductivity the ebonite or plastic spheres with low conductivity were placed around the spheres-heaters. The isolating plugs were embedded in the walls of the experimental sections at the contact points with spheres-heaters. The heat transfer by the radiation was less than 1 % due to low temperatures on the spheres-heaters surfaces (less than 330 K). The heat transfer by the natural convection was neglected due to the high Re values.

The investigations of the heat transfer from the spheres in the case of random packing were performed at the same experimental section as heat transfer from the cylinder in a bundle described above. The heat transfer from the spheres was investigated in two cross sections of random packing $H/d=10$ and 25. The four spheres-heaters were located in each cross section. The positions for the spheres-heaters were selected so that to find the maximal differences in the heat transfer from the spheres. Despite of this, the differences in the heat transfer from the spheres were not large, and the following relation summarizes the experimental data for all 8 locations with the standard deviation of 6 %:

$$Nu = 0.89 \cdot Re^{0.63}$$

The additional experimental section was designed for the heat transfer from spheres investigations in the rhombic packing. The cross section of this experimental section is presented schematically in the left hand top corner of the Fig. 3. Two kinds of the experimental sections were investigated – with displacers (see right hand side of the cross section) and without them. The displacers were used in order to avoid the free channels that are formed at the cylindrical surfaces (see left hand side of the cross section). The heat transfer from the spheres was investigated in the different locations of the packing (pos. 1-4). The positions for the spheres-heaters were selected so, that they cover all typical locations in the cross section. The investigations of the heat transfer were performed in two layers streamwise – in the 2nd and 6th layers of spheres pacing.

The experimental results demonstrated that the displacers improve the heat transfer on 20-40% (Fig. 4). The differences in the heat transfer of spheres in different places of the packing with displacers are less than in the packing without displacers. This allows to summarize the heat transfer from spheres results for all rhombic packing with displacers by one relation $Nu = 0.6 \cdot Re^{0.7}$.

Beside the investigations of heat transfer from the cylinder and from the spheres, the experimental investigations of the hydraulic drag and for all kinds of the packings described above were performed. The fluid mixing was investigated in the regular rhombic and random packings of spheres, which are arranged between axial streamlined cylinders [4]. Additionally, the experimental investigations were conducted for

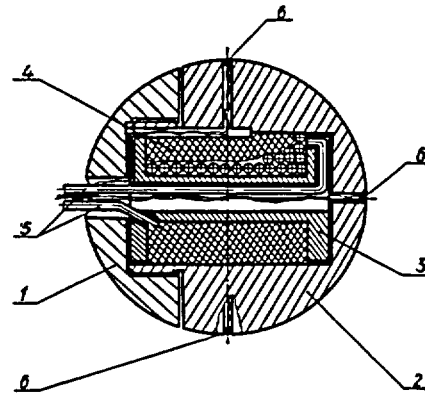


Fig. 2. Construction of the sphere-heater
1 – sphere cover; 2 – sphere body;
3 – heater coil; 4 – windings of coils;
5 – wires; 6 – point of temperature measurement

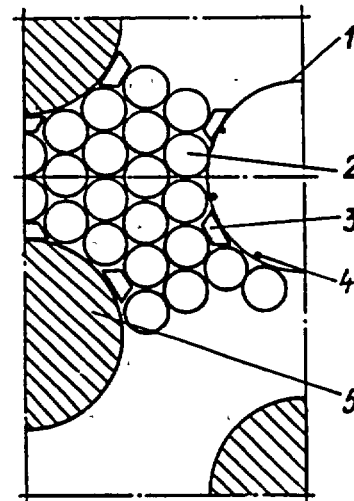


Fig. 3. Experimental section for heat transfer investigation from the spheres
1 – cylinder calorimeter; 2 – sphere;
3 – displacer; 4 – point of temperature measurement; 5 – bundle of cylinders

packings of spheres placed in thin annular slots. The equations for porosity, hydraulic drag and heat transfer from spheres were derived from the experimental results [5].

3. Smooth and rough channels

Studies of heat transfer and hydrodynamics in variously shaped gas-cooled channels have been ongoing in LEI for a long time now. Initial attention was focused on the effect of variability of physical properties in the boundary layer on heat transfer and drag in flow over smooth and rough surfaces. High-temperature systems with gaseous working fluids operate as a rule at high-temperature differences.

At LEI was accumulated a great deal of experience in investigating the heat transfer and friction of a smooth cylinder in axial flow placed in a large-diameter circular pipe. It was decided that the accumulated data be employed for detailed investigation of heat transfer, friction, velocity, and temperature distributions in the highly non-isothermal boundary layer that forms on smooth and rough cylinders in axial flow, and that a single procedure be employed for determining the effect of

different factors on heat transfer. Such studies allow more comprehensive investigation of the inlet regions of annular ducts, which is particularly important for improving the designs of various heat exchangers with short flow passages. The analysis of velocity and temperature distribution in the boundary layer that forms on the initial zone of a smooth annular duct, and of the effect of the variability of physical properties and surface curvature on heat transfer and friction was done [6, 7, 8].

The production of artificial roughness is one of the effective methods for the enhancement of convective heat transfer, particularly at high heat loads, since the roughness elements turbulize the wall layer in which the bulk of the thermal resistance is concentrated. However subsequent studies centered on investigating the specifics of enhancement of heat transfer on rough surfaces and in rough channels at high-temperature gradients in the boundary layer was the subject matter of a large number of experimental and a number of analytic studies performed at LEI [6, 8, 9].

4. Complex-geometry channels bundle

Heat-transfer systems of circular elements of different diameter in axial flow and annular channels are extensively employed. Basically these are densely packed bundles of twisted tubes of nuclear reactors, blankets of thermonuclear reactors, cooling channels of various industrial devices, etc. Such heat exchangers have a number of advantages which manifest themselves differently depending on the given operating conditions. The undisputed advantage of compact bundles consists of their resistance to vibrations and their significantly more intensive mixing of the working fluid between the channels than occurs in bundles of straight tubes in longitudinal flow.

Early stage LEI investigations cover the experimental and theoretical study of the heat transfer inside an oval helical tube [10], study of the unsteady process of heat carrier in a helical tube bundle when heat carrier flow-rate is increased/decreased [11]. The following comprehensive studies of heat transfer, hydraulic drag, and turbulent structure of longitudinal flow over bundles in annular channels with a helically shaped inside pipe with different helix pitches and different cross-sectional shapes are summarized in [6]. A great deal of attention is given to investigating the local characteristics over the

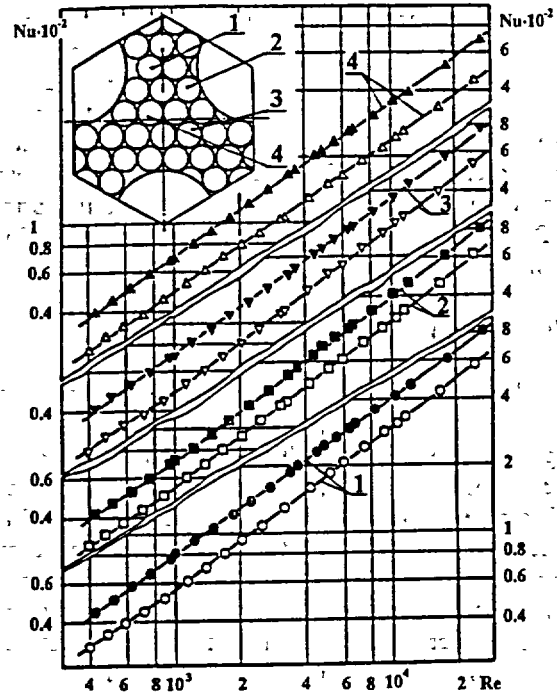


Fig. 4. Heat transfer from the spheres

perimeter and length of the tubes, clarifying the factors responsible for the observed specifics of flow over these surfaces, and making practical recommendations for their utilization. A physically validated model of flow in bundles of twisted tubes was developed.

The latest our experiments in bundles of twisted tubes were performed over a wide range of Re ($3 \cdot 10^2$ to $2 \cdot 10^5$), twisting pitches ($s/d_0=6.2-25$) and cross-sectional shapes (two-, three- and four lobes) [8]. The bulk of the experiments for investigating the effect of parameters such as the twisting pitch, cross-sectional shape of the twisted tube, relative bundle length, variable physical properties of the gaseous working fluid, and Re, were performed with a 19-, 37- and 151-tube sections. After comprehensive analytic and experimental studies generalized predictive equations suitable for practical use were proposed.

5. Conclusions

On the basis of durable experimental results for heat transfer, hydrodynamics and flow structure obtained for various gas-cooled types of sphere packings, as well as for smooth, helical tubes and annular channels equipped with smooth/rough or helical inner tubes, such bundle of twisted tubes, were clarified specifics of the manifestation of the effect of the variability of physical properties on transport processes in each specific case, to find the physical causes for the differences observed as compared with smooth or straight channels, and to obtain sufficiently general relationships for practical calculations. Conditions were determined at which the enhancement of the heat transfer at high-temperature differences are more significant than those at small differences. It shows that Lithuanian Energy Institute has accumulated long term experience in the field of heat transfer investigations and has good experimental basis for providing such studies and following analytical analysis.

6. References

- [1] S. Rimkevicius, V. Survila, R. Jankauskas, The Effect of Sphere Packing on Heat Transfer From a Longitudinally Streamlined Cylinder, *Heat Transfer Research*, Vol. 25, No. 4, 1993, p.507-510.
- [2] G.G. Gartvich, A.V. Lebetsev, V.A. Pavshuk and N.D. Segal, Determination of the Coefficient of Heat Transfer between a Sphere Filling and a Heat-Exchange Pipe VANT, *Ser. Atomno-Vodorodnaya Energetika i Tekhnologiya*, Vyp. 1, 1988, pp. 45-47.
- [3] V.I. Subbotin, M.Kh. Ibragimov, P.A. Ushakov, V.P. Bobkov, A.V. Zhukov and Yu.S. Yuriev, *Gidrodinamika i teploobmen v atomnykh energeticheskikh ustanovkakh (osnovy raschyota)/Hydrodynamics and Heat Transfer in Atomic Power Units (Calculation Basics)*. Atomizdat Press, Moscow, 1975.
- [4] S. Rimkevicius, V. Survila, A. Bagdonas, R. Jankauskas, Hydraulic drag and fluid mixing in packed beds of cylinders and spheres, *J. Energetika*, 1990, No. 2, p.64-73 (In Russian).
- [5] S. Rimkevicius, V. Survila, R. Jankauskas, Heat transfer and hydraulic drag packed beds of spheres, placed in thin annular slots with axial fluid flows, *J. Energetika*, 1990, No. 2, p.74-89 (In Russian).
- [6] J. Vilemas, B. Cesna, V. Survila, *Heat transfer in Gas-Cooled Annular Channels*, Hemisphere, Washington. D.C., 1987.
- [7] J. Vilemas, E. Uspuras, V. Simonis, Turbulent Momentum and Heat Transfer in Channel Gas Flow at High Heat Loads. A Review, *Int. J. Experimental Thermal and Fluid Science*, No. 4, 1991, p.375-388.
- [8] J. Vilemas, V. Simonis, J.E. Adomaitis, *Heat Augmentation in Gas-Cooled Channels*, Begell house, Florida, 1994.
- [9] J. Vilemas, V. Simonis, The Effect of Temperature Factor on the Transition From Partially to Fully Rough Flow Conditions, *Int. Comm. Heat Mass Transfer*, Vol. 15(1), 1988, p.121-124.
- [10] L. Asmantas, M. Nemira, V. Trilikauskas, Coefficient of Heat Transfer and Hydraulic Drag of Twisted Oval Tube. *Int. J. Heat Transfer Sov. Res.*, Vol. 17(4), 1985, p.103-109.
- [11] B.V. Dziubenko, G.A. Dreitser, A. Kaliatka, Mechanisms of unsteady mixing of heat carrier with its flowrate variation and flow swirling. I. Calculation methods and experimental study of transient processes. *Int. J. Heat Mass Transfer*, Vol. 41(3), 1998, p.645-651. II. Results and analysis. *Int. J. Heat Mass Transfer*, Vol. 41(3), 1998, p.653-661.

OVERVIEW OF LEI INVESTIGATIONS ON HEAT TRANSFER AND FLOW STRUCTURE IN GAS-COOLED SPHERES PACKINGS AND CHANNELS

J. VILEMAS, E. USPURAS, S. RIMKEVICIUS, A. KALIATKA, R. PABARCIUS

*Lithuanian Energy Institute
Breslaujos 3, LT-3035 Kaunas - Lithuania*

ABSTRACT

In this paper experimental investigations on heat transfer and hydrodynamics in various gas-cooled channels over wide ranges of geometrical and performance parameters performed at Lithuanian Energy Institute are presented. Overview introduces long-term experience on investigations of local and average heat transfer, hydraulic drag in various types of sphere packings, in smooth, helical tubes and annular channels equipped with smooth/rough or helical inner tubes, such bundle of twisted tubes, as well as turbulent flow structure and the effects of variable physical properties of gas heat carriers on local heat transfer in channels of different cross sections. Lithuanian Energy Institute has accumulated long term experience in the field of heat transfer investigations and has good experimental basis for providing such studies and following analytical analysis.

1. Introduction

Engineering progress in the conversion of thermal or chemical energy into other forms involves searching for new methods of conducting these processes at higher temperatures, which allows for improvement of the efficiency of thermodynamic or thermochemical systems. In the majority of cases, the working fluids or coolants in such systems are gaseous, and exchange of thermal energy between them occurs through a solid wall. To be able to manufacture equipment with acceptable weight, size, and performance, one must significantly augment the heat-transfer processes, which is attained by producing large temperature differentials and also by various other methods of intentional enhancement of heat transfer: the packed beds of spheres, use of artificial roughness, turbulization or swirling of the flow, reducing the thickness of boundary layers or increasing the velocity gradient in them, etc. A great deal of attention has been paid to the enhancement of heat transfer in equipment such as gas-cooled nuclear reactors under power-plant conditions.

Lithuanian Energy Institute (LEI) has accumulated long-term experience on heat transfer, friction and flow structure investigations in packed beds of spheres and variously shaped gas-cooled channels. LEI activities cover experimental and computational works on the effects of variable physical properties of gas heat carriers, on local heat transfer and hydraulic drag in channels of different cross sections, on turbulent flow structure, and on the heat transfer mechanism in the stabilized heat transfer region in a tube.

2. Gas-cooled packings of spheres

In the nuclear reactors spheres could be used as fuel, while cylinders – as control rods. Sphere packings strongly agitate the flow passing through them. Therefore, interest in heat transfer from spheres in packings and fillings of various kinds is understandable. The flow turbulence affects not only the spheres per se but also the surfaces adjacent to them. The heat transfer from the spheres and from a cylinder as well as hydraulic drag and flow mixing factors are investigated in air flow at LEI. The local heat transfer at various positions of cylinders length and perimeter as well as the effect of the sphere packings on the cylinder heat transfer were evaluated.

Various types of packings from the spheres are considered in performed experiments. One kind of them is regular rhombic or random packing, which is arranged between axial streamlined cylinders [1]. The rhombic packing was oriented so that spheres along cylinder were arranged in columns, with clearances that have periodically-varying cross sections running in the vertical direction between them. Near the cylinder surface, the clearances formed by larger flow sections were filled with displacers. In the case of a random filling of the spheres, there were no displacers. Heat transfer from the cylinder immersed in a random filling of spheres was investigated on two different experimental sections. In the first case, the cylinder under consideration made up an element of a longitudinally streamlined bundle with cylinders arranged in a triangular array with the spacing $s/d_{ci}=1.63$. In the second case, the experimental section represented an annulus filled with spheres and containing the investigated inner cylinder. The annulus of outside to inner diameter ratio was 2.84. In all cases considered, both with a regular packing of the spheres and with their random filling, the cylinder-to-sphere diameter ratio was $d_{ci}/d=4.29$, the height of assemblies was $H/d=36$, and the porosity - 0.42.

Heat transfer from the cylinder was studied under the second-kind of boundary conditions ($q_w=const$) in air flow with $Re = (0.3 \text{ to } 12) \cdot 10^3$, determined from the sphere diameter and filtration rate (velocity of the incoming flow in front of the sphere packing). Both local and perimeter-average heat transfer coefficients from the cylinder vs. Re and the length of the heated part of the cylinder immersed in the sphere packing were determined. Because the cylinder heat transfer stratifies streamwise, a relative length of the heated part of the cylinder immersed in a sphere packing is incorporated in the relation for heat transfer. The following relations were obtained for the perimeter-average heat transfer coefficients from the cylinder in a bundle with an intercylinder space filled with packings of spheres [1]:

$$Nu = 0.0584 \cdot Re^{0.89} (\chi/d)^{-0.1} \text{ - in the case of regular (rhombic) sphere packing, and}$$

$$Nu = 0.096 \cdot Re^{0.83} (\chi/d)^{-0.07} \text{ in the case of random sphere packing.}$$

In the case with the annulus, the cylinder heat transfer is a little higher, and its dependence on Re and on the cylinder height is more noticeable:

$$Nu = 0.094 \cdot Re^{0.88} (\chi/d)^{-0.16}$$

Given relations describe the experimental data with a $\pm(3 \text{ to } 4)\%$ standard deviation.

It should be pointed out that our data are consistent with the results of other authors [2] dealing with the average heat transfer from a cylinder surrounded by a random filling of spheres (Fig.1). This indicates that in LEI experiments there was no effect of the bundle cylinders or of the outer tube of the annulus on the heat transfer from the cylinder considered. As evident from the results of the investigations, the heat transfer from the cylinder with a random packing of spheres is higher than that with a regular packing. Importantly, this is not related to the increase of the assembly hydraulic drag. Also it was determined that heat transfer from a tube immersion in a sphere packing increases by more than a factor of five by comparing the obtained data with heat transfer in circular tubes [3] (Fig. 1).

Heat transfer from the spheres was studied under the boundary condition $T_w=const$. This condition was assured by the construction of the spheres-heaters (Fig. 2).

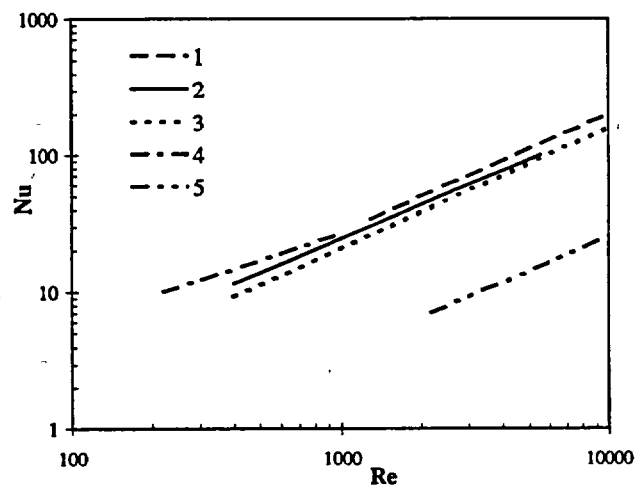


Fig. 1. Heat transfer in various types of sphere packings ($\chi/d=15$)

1 - inner cylinder of the annular filled with random packing of a spheres; 2 - cylinder in a bundle with an intercylinder space filled with random packing of a spheres; 3 - cylinder in a rhombic packing of spheres; 4 - cylinder in a sphere filling [2]; 5 - circular tube with no spheres [3]

The spheres-heaters were made from the cooper with high thermal conductivity. The temperature was measured in 3 or 4 points on the sphere surface.

The investigations are performed by the local modeling, which allows to obtain the heat transfer characteristics in different places of the packing. The influence of heat transfer by the conductivity, radiation, and natural convection was minimized in the performed experiments. In order to minimize the heat losses by the conductivity the ebonite or plastic spheres with low conductivity were placed around the spheres-heaters. The isolating plugs were embedded in the walls of the experimental sections at the contact points with spheres-heaters. The heat transfer by the radiation was less than 1 % due to low temperatures on the spheres-heaters surfaces (less than 330 K). The heat transfer by the natural convection was neglected due to the high Re values.

The investigations of the heat transfer from the spheres in the case of random packing were performed at the same experimental section as heat transfer from the cylinder in a bundle described above. The heat transfer from the spheres was investigated in two cross sections of random packing $H/d=10$ and 25. The four spheres-heaters were located in each cross section. The positions for the spheres-heaters were selected so that to find the maximal differences in the heat transfer from the spheres. Despite of this, the differences in the heat transfer from the spheres were not large, and the following relation summarizes the experimental data for all 8 locations with the standard deviation of 6 %:

$$Nu = 0.89 \cdot Re^{0.63}$$

The additional experimental section was designed for the heat transfer from spheres investigations in the rhombic packing. The cross section of this experimental section is presented schematically in the left hand top corner of the Fig. 3. Two kinds of the experimental sections were investigated – with displacers (see right hand side of the cross section) and without them. The displacers were used in order to avoid the free channels that are formed at the cylindrical surfaces (see left hand side of the cross section). The heat transfer from the spheres was investigated in the different locations of the packing (pos. 1-4). The positions for the spheres-heaters were selected so, that they cover all typical locations in the cross section. The investigations of the heat transfer were performed in two layers streamwise – in the 2nd and 6th layers of spheres pacing.

The experimental results demonstrated that the displacers improve the heat transfer on 20-40% (Fig. 4). The differences in the heat transfer of spheres in different places of the packing with displacers are less than in the packing without displacers. This allows to summarize the heat transfer from spheres results for all rhombic packing with displacers by one relation $Nu = 0.6 \cdot Re^{0.7}$.

Beside the investigations of heat transfer from the cylinder and from the spheres, the experimental investigations of the hydraulic drag and for all kinds of the packings described above were performed. The fluid mixing was investigated in the regular rhombic and random packings of spheres, which are arranged between axial streamlined cylinders [4]. Additionally, the experimental investigations were conducted for

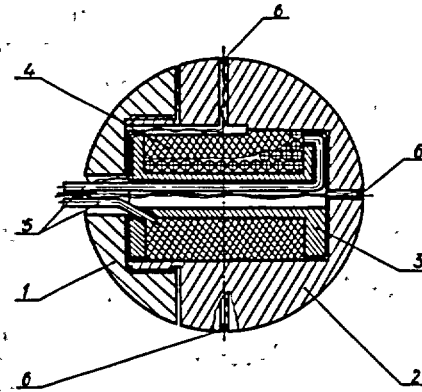


Fig. 2. Construction of the sphere-heater
1 – sphere cover; 2 – sphere body;
3 – heater coil; 4 – windings of coils;
5 – wires; 6 – point of temperature measurement

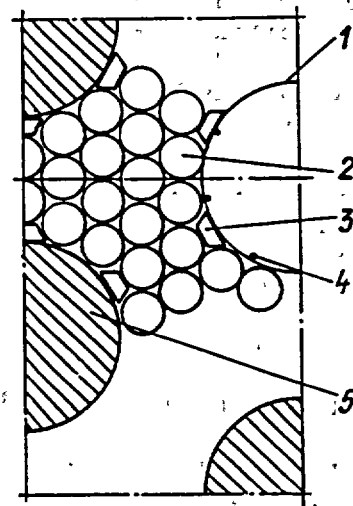


Fig. 3. Experimental section for heat transfer investigation from the spheres
1 – cylinder calorimeter; 2 – sphere;
3 – displacer; 4 – point of temperature measurement; 5 – bundle of cylinders

packings of spheres placed in thin annular slots. The equations for porosity, hydraulic drag and heat transfer from spheres were derived from the experimental results [5].

3. Smooth and rough channels

Studies of heat transfer and hydrodynamics in variously shaped gas-cooled channels have been ongoing in LEI for a long time now. Initial attention was focused on the effect of variability of physical properties in the boundary layer on heat transfer and drag in flow over smooth and rough surfaces. High-temperature systems with gaseous working fluids operate as a rule at high-temperature differences.

At LEI was accumulated a great deal of experience in investigating the heat transfer and friction of a smooth cylinder in axial flow placed in a large-diameter circular pipe. It was decided that the accumulated data be employed for detailed investigation of heat transfer, friction, velocity, and temperature distributions in the highly non-isothermal boundary layer that forms on smooth and rough cylinders in axial flow, and that a single procedure be employed for determining the effect of different factors on heat transfer. Such studies allow more comprehensive investigation of the inlet regions of annular ducts, which is particularly important for improving the designs of various heat exchangers with short flow passages. The analysis of velocity and temperature distribution in the boundary layer that forms on the initial zone of a smooth annular duct, and of the effect of the variability of physical properties and surface curvature on heat transfer and friction was done [6, 7, 8].

The production of artificial roughness is one of the effective methods for the enhancement of convective heat transfer, particularly at high heat loads, since the roughness elements turbulize the wall layer in which the bulk of the thermal resistance is concentrated. However subsequent studies centered on investigating the specifics of enhancement of heat transfer on rough surfaces and in rough channels at high-temperature gradients in the boundary layer was the subject matter of a large number of experimental and a number of analytic studies performed at LEI [6, 8, 9].

4. Complex-geometry channels bundle

Heat-transfer systems of circular elements of different diameter in axial flow and annular channels are extensively employed. Basically these are densely packed bundles of twisted tubes of nuclear reactors, blankets of thermonuclear reactors, cooling channels of various industrial devices, etc. Such heat exchangers have a number of advantages which manifest themselves differently depending on the given operating conditions. The undisputed advantage of compact bundles consists of their resistance to vibrations and their significantly more intensive mixing of the working fluid between the channels than occurs in bundles of straight tubes in longitudinal flow.

Early stage LEI investigations cover the experimental and theoretical study of the heat transfer inside an oval helical tube [10], study of the unsteady process of heat carrier in a helical tube bundle when heat carrier flow-rate is increased/decreased [11]. The following comprehensive studies of heat transfer, hydraulic drag, and turbulent structure of longitudinal flow over bundles in annular channels with a helically shaped inside pipe with different helix pitches and different cross-sectional shapes are summarized in [6]. A great deal of attention is given to investigating the local characteristics over the

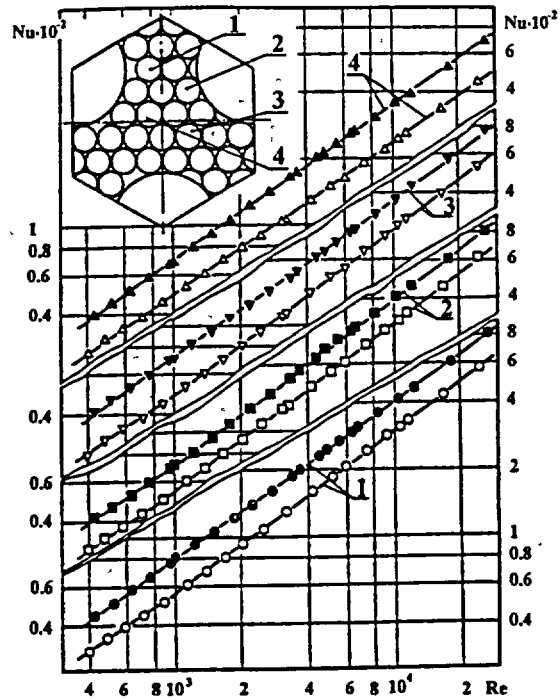


Fig. 4. Heat transfer from the spheres

perimeter and length of the tubes, clarifying the factors responsible for the observed specifics of flow over these surfaces, and making practical recommendations for their utilization. A physically validated model of flow in bundles of twisted tubes was developed.

The latest our experiments in bundles of twisted tubes were performed over a wide range of Re ($3 \cdot 10^2$ to $2 \cdot 10^5$), twisting pitches ($s/d_0=6.2-25$) and cross-sectional shapes (two-, three- and four lobes) [8]. The bulk of the experiments for investigating the effect of parameters such as the twisting pitch, cross-sectional shape of the twisted tube, relative bundle length, variable physical properties of the gaseous working fluid, and Re, were performed with a 19-, 37- and 151-tube sections. After comprehensive analytic and experimental studies generalized predictive equations suitable for practical use were proposed.

5. Conclusions

On the basis of durable experimental results for heat transfer, hydrodynamics and flow structure obtained for various gas-cooled types of sphere packings, as well as for smooth, helical tubes and annular channels equipped with smooth/rough or helical inner tubes, such bundle of twisted tubes, were clarified specifics of the manifestation of the effect of the variability of physical properties on transport processes in each specific case, to find the physical causes for the differences observed as compared with smooth or straight channels, and to obtain sufficiently general relationships for practical calculations. Conditions were determined at which the enhancement of the heat transfer at high-temperature differences are more significant than those at small differences. It shows that Lithuanian Energy Institute has accumulated long term experience in the field of heat transfer investigations and has good experimental basis for providing such studies and following analytical analysis.

6. References

- [1] S. Rimkevicius, V. Survila, R. Jankauskas, The Effect of Sphere Packing on Heat Transfer From a Longitudinally Streamlined Cylinder, *Heat Transfer Research*, Vol. 25, No. 4, 1993, p.507-510.
- [2] G.G. Gartvich, A.V. Lebetsev, V.A. Pavshuk and N.D. Segal, Determination of the Coefficient of Heat Transfer between a Sphere Filling and a Heat-Exchange Pipe VANT, Ser. Atomno-Vodorodnaya Energetika i Tekhnologiya, Vyp. 1, 1988, pp. 45-47.
- [3] V.I. Subbotin, M.Kh. Ibragimov, P.A. Ushakov, V.P. Bobkov, A.V. Zhukov and Yu.S. Yuriev, *Gidrodinamika i teploobmen v atomnykh energeticheskikh ustanovkakh (osnovy raschyota)/Hydrodynamics and Heat Transfer in Atomic Power Units (Calculation Basics)*. Atomizdat Press, Moscow, 1975.
- [4] S. Rimkevicius, V. Survila, A. Bagdonas, R. Jankauskas, Hydraulic drag and fluid mixing in packed beds of cylinders and spheres, *J. Energetika*, 1990, No. 2, p.64-73 (In Russian).
- [5] S. Rimkevicius, V. Survila, R. Jankauskas, Heat transfer and hydraulic drag packed beds of spheres, placed in thin annular slots with axial fluid flows, *J. Energetika*, 1990, No. 2, p.74-89 (In Russian).
- [6] J. Vilemas, B. Cesna, V. Survila, *Heat transfer in Gas-Cooled Annular Channels*, Hemisphere, Washington, D.C., 1987.
- [7] J. Vilemas, E. Uspuras, V. Simonis, Turbulent Momentum and Heat Transfer in Channel Gas Flow at High Heat Loads. A Review, *Int. J. Experimental Thermal and Fluid Science*, No. 4, 1991, p.375-388.
- [8] J. Vilemas, V. Simonis, J.E. Adomaitis, *Heat Augmentation in Gas-Cooled Channels*, Begell house, Florida, 1994.
- [9] J. Vilemas, V. Simonis, The Effect of Temperature Factor on the Transition From Partially to Fully Rough Flow Conditions, *Int. Comm. Heat Mass Transfer*, Vol. 15(1), 1988, p.121-124.
- [10] L. Asmantas, M. Nemira, V. Trilikauskas, Coefficient of Heat Transfer and Hydraulic Drag of Twisted Oval Tube. *Int. J. Heat Transfer Sov. Res.*, Vol. 17(4), 1985, p.103-109.
- [11] B.V. Dziubenko, G.A. Dreitser, A. Kaliatka, Mechanisms of unsteady mixing of heat carrier with its flowrate variation and flow swirling. I. Calculation methods and experimental study of transient processes. *Int. J. Heat Mass Transfer*, Vol. 41(3), 1998, p.645-651. II. Results and analysis. *Int. J. Heat Mass Transfer*, Vol. 41(3), 1998, p.653-661.

A HIGH TEMPERATURE REACTOR FOR SHIP PROPULSION

P. LOBET and R. SEIGEL

Ecole de application militaires de l'énergie atomique
Cherbourg Naval - France

and

A.C. THOMPSON, R.M. BEADNELL and P.A. BEELEY

HMS SULTAN, Nuclear Department
Gosport, Hampshire PO12 3BY - UK

ABSTRACT

The initial thermal hydraulic and physics design of a high temperature gas cooled reactor for ship propulsion is described. The choice of thermodynamic cycle and thermal power is made to suit the marine application. Several configurations of a Helium cooled, Graphite moderated reactor are then analysed using the WIMS and MONK codes from AEA Technology. Two geometries of fuel elements formed using micro spheres in prismatic blocks, and various arrangements of control rods and poison rods are examined. Reactivity calculations through life are made and a pattern of rod insertion to flatten the flux is proposed and analysed. Thermal hydraulic calculations are made to find maximum fuel temperature under high power with optimized flow distribution. Maximum temperature after loss of flow and temperatures in the reactor vessel are also computed. The temperatures are significantly below the known limits for the type of fuel proposed. It is concluded that the reactor can provide the required power and lifetime between refueling within likely space and weight constraints.

Introduction

There has recently been renewed discussion [1],[2] of nuclear power for merchant ships. In [1] reference was made to the consolidated nuclear steam raising plant, a water cooled design for which much relevant data exists. In [2] a high temperature gas cooled reactor coupled directly to a gas turbine is advocated, but information on such a system is lacking. Much experience [3] with the proposed fuel exists but it has not been shown that a compact reactor with a long refueling interval and controllability for marine use can be designed. The present study aims to produce a preliminary design of HTR suitable for marine use, which operates within the known temperature limits of the fuel.

Power requirements

The first part of the study determines the thermal power required from the core. Considerations of turbine maintenance and operator culture leads to the choice of steam turbine as the power conversion system. A cycle using super-heated steam at 550 °C at the turbine inlet is analysed to find its efficiency. The gas circulators are assumed to be similar to those described in [4]. An assessment of the power required for propulsion, hotel load and coolant circulation when

the efficiency of the power cycle is taken into account leads to a requirement for 180 MW thermal from the reactor. The overall plant parameters are given in table 1.

Table 1 Overall plant parameters

Thermal power	180 MW
Primary coolant (Helium) flowrate	86 kg/s
Helium core inlet/outlet temperatures	350 °C / 753 °C
Helium pressure	45 bar
Steam pressure	40 bar

Core design

To design the core, two software packages from AEA Technology are employed. The first, MONK [5], is based on the Monte-Carlo method. This stochastic method is mainly used for calculations of criticality. Calculations of k effective and burn-up are performed, requiring considerable computer time. The library used is the JEF2.2 or the UKNDL. The second package is WIMS [6], a deterministic code that solves the equation of Boltzmann. Some modules are based on collision probabilities, others on the Sn method in 1 or 2 dimensions. The code is used in this study to perform rapid burn-up and k_{inf} calculations on simple geometries, before using the Monte-Carlo code MONK on whole core models.

The use of prismatic graphite blocks is imposed at the start of the project. A previous study had considered a pebble bed and concerns exist about the motion of the pebbles and recycling pebbles in the marine environment. Two ways of incorporating the basic fuel microspheres into element are therefore considered, alternate fuel rods and coolant holes in the hexagonal graphite blocks and hollow fuel rods within coolant passages in the graphite moderator blocks. Similar elements have been used in the Fort St Vrain and Dragon [7] reactors respectively. Using WIMS and MONK the effect of rod size and pitch on k infinity at various burnups is explored. The WIMS model uses a single element surrounded by annuli of graphite and helium. The MONK model has a single hexagonal graphite block in reflecting boundaries. The dragon type element is chosen for further analysis because it is more closely linked to the coolant for heat transfer. This should result in superior dynamic behaviour when confronted with the varying power demands of the marine application.

The size of the core is determined by setting a maximum power density of 3.0 MW/m³ which previous studies suggest will limit the temperature during loss of flow accidents. Another constraint is the space available in a typical ship. This has been represented by a 10.0 m cube within which the core, pressure vessel and shielding are required to fit. Using the Dragon type hexagonal blocks this leads to a core of 169 blocks each holding 19 fuel elements with a radius of 3.3 m and a height of 3.0 m. This is shown in figure 1.

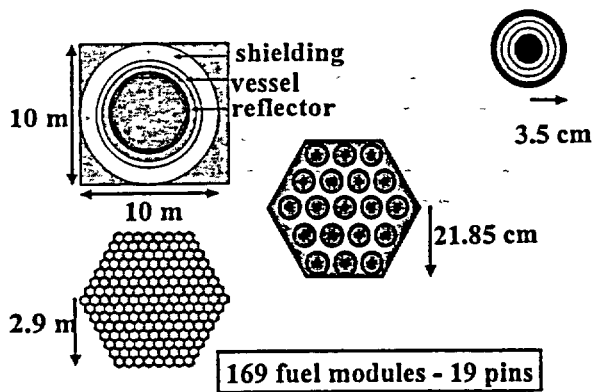


Figure 1 Overall core configuration

The use of burnable poisons to produce an even reactivity over a long core life is studied using WIMS for infinite array calculations and MONK for whole core calculations. Using WIMS a design of poison rod is developed which gives k_{inf} close to 1.15 over a life of 30000 MWd/T. The poison pins are placed in the central hole of each graphite block and have a concentration of gadolinium which increases in four steps from 1% at the outer radius of 3.5 cm to 4% at the inner radius of 1.5 cm. This design is then analysed in a whole core model using MONK and produces k effective close to 1.1 over the core life.

Three patterns of control rods are analysed using MONK before choosing an arrangement of seven rings of six hexagons each containing a large circular section rod and 12 standard fuel channels. One of these rings is at the center and one at each corner of the core. The control rod material is Hafnium and the diameter 12.0 cm. A calculation of the power profile across the core, shows the influence of these rods. Four rod configurations are analysed based on three rod groups. Group 1 are the six rods in the core center and group 3 are the two rods in each outer ring which lie on a radial line to the corners of the core. Group three are the remaining four rods in each outer ring. This grouping can be modeled using 1/12th of the core which can be seen in figure 2.

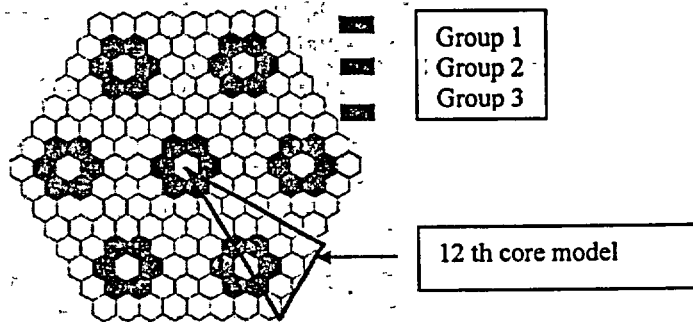


Figure 2 Core plan and rod groups

The final configuration has group 1 inserted 2.0 m into the 3.0 m high core, group 3 are fully inserted and the core is controlled by group 2 which are inserted 1.0 m at the start of life. This gives a radial power profile a peak to average value of 1.08 and an average power per assembly of 1.06 MW at full power. Axial power profiles are calculated by the same MONK analysis. This calculates the power in 50 cm axial sections of each hexagonal column in the core. The maximum power in such a section is twice the average power and is found in the region under the central control rods. The k_{eff} value with all rods withdrawn is 1.117 and with each group alone fully inserted it is 1.0998, 1.0725 and 1.0625. For all rods inserted $k_{eff} = 0.916$ and max value for any two rods withdrawn is 0.951.

Calculation of the temperature coefficients of reactivity for the fuel and for the moderator are made at the beginning and end of life shows that a single value closely describes the behaviour between 30 °C and 1300 °C with a second value between 1300 °C and 1700 °C.

The effect of poisons following reduction of power from full power is explored by performing a burnup calculation at a constant temperature of 900 °C. A reduction in reactivity of 1400 pcm occurs after 3-4 days which can be compensated by withdrawing group 2 rods. A similar calculation for a reactor scram and temperature fall to 30 °C shows recovery of reactivity but confirms that the reactor can still be kept sub-critical even if two rods fail to drop.

The principal features of the core are summarized in table 2.

Table 2 Principal features of the core

Radius of fuel micro sphere	0.457 mm
Spacing between micro spheres	1.0 mm
Number of micro spheres per element	771300
Radius of fuel element	$R_i : 1.875 \text{ cm} / R_o : 2.50 \text{ cm}$
Radius of Helium channel	$R_i : 1.325 \text{ cm} / R_o : 3.50 \text{ cm}$
Pitch of elements	8.0 cm
Volume % of fuel in element	9.36 %
Number of fuel elements	2790
Number of hexagonal assemblages	169
Assemblage size - center to flat	21.85 cm
Core size - center to flat	2.9014 m
Reflector radius	3.8 m
Core height	3.0 m
Power density	2.51 MW/m ³
Number / diam. of control rods (Hf)	42 / 12.0 cm
Number / diam. burnable poison rods (Gd ₂ O ₃)	127 / 7.0 cm

Thermal Hydraulics

The thermal hydraulics of the reactor is examined to ensure that the maximum fuel temperature in operation is below 1100 °C and after a depressurisation accident is less than 1600 °C. Programs are written in the general scientific computing package MATLAB [8] to calculate the temperature in the fuel matrix, at the centre of a microsphere and in the pressure vessel in the steady state, and also for the transient following loss of convective cooling.

The steady state calculation analyses a representative fuel element for each of the 169 prismatic blocks in the core. A numerical integration in the axial direction for the coolant

temperature is performed using the power profiles generated by MONK. This is linked to analytical expressions for the radial temperature differences which involves finding the power split to the internal and external coolant channels of the hollow fuel elements. The temperature rise through a microsphere is added to the maximum temperature in the fuel matrix. With equal flow rates in all channels the maximum temperature is above 1100 °C. The program is developed to optimize the flow distribution so that the temperature is below 1100 °C everywhere without an excessive number of different rates. Eleven flow groups are found giving the maximum fuel temperatures shown in figure 3.

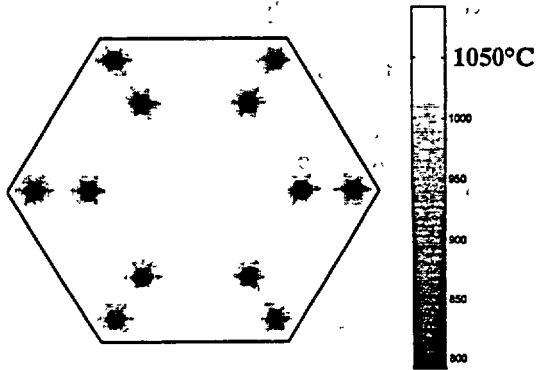


Figure 3 Maximum fuel temperatures in the core

Further additions to the program allow the temperature in the steel pressure vessel to be calculated. This is externally cooled by natural circulation and on the inside separated from the core by Helium returning from the cold leg and flowing upwards before entering the core. A maximum temperature of 388 °C is found at full power with little variation in the axial direction. This is below the limit of 500 °C for phase transition.

The transient calculation uses a finite volume solution of the conduction equation with implicit time integration. A 10cm axial slice at the hottest level in the core is modeled. This is divided into six radial regions representing the core, reflector, first thermal shield, Helium layer, second thermal shield and pressure vessel. These are represented by a 25x42 (r θ) grid of cells. Initial core temperatures shown in figure 3 are applied with corresponding values in the outer regions. A representative decay heat input is applied and an outer temperature of 50 °C. The calculation is continued until the maximum temperature condition which occurs after 17 hours is found. At this point the maximum temperature is 1253 °C, well within the limit of 1600 °C proposed at the start of the study.

Shielding

Calculations of the performance, size and disposition of the secondary machinery and of the shielding are also made. These may be the subject of a separate paper.

Conclusions

The advantages of high temperature Helium cooled reactors can be realized in a design which is adapted to the marine propulsion application. A design of sufficient

power yet with low power density will fit within the space likely to be available. A long interval between refueling with an enrichment of .5% can be obtained by using burnable poisons. Calculations confirming this for a scheme using Gadolinium oxide rods have been made. Maximum fuel temperatures at full power can be kept below 1100 °C by distributing the Helium flow in a manner which has been calculated. The maximum temperature after a loss of coolant flow can be limited to 1300 °C for the design proposed.

References

- [1] D J Palmer & J Tuttle, "The Economic and Political Feasibility of a Large High Speed Nuclear Merchant Vessel in the 21st Century", The Nuclear Engineer Vol 42, no 4, Aug 2001, p 121.
- [2] G A K Crommelin & H van Dam, "The NEREUS approach to broaden applications of nuclear technology", ICENES 2000, Sept 2000, p217.
- [3] H Nickel, K Hofmann, W Wacholz and I Weisbrodt "The helium-cooled high temperature reactor in the Federal Republic of Germany: safety features, integrity concept, outlook for design codes and lincencing procedures" Nuclear Engineering and Design 127 (1991) p181 .
- [4] P Buhner, Ch Duttke, J Engel and D Glass, "Research program and test loop for the prototype of a HTR coolant gas circulator with magnetic bearings", Nuclear Engineering and Design 137 (1992) p83.
- [5] MONK Users Manual, AEA Technology, 2000.
- [6] WIMS Users Manual, AEA Technology , 2000.
- [7] J L Head and A N Kinhead "Graphite fuel element structures for high temperature gas cooled reactors", Nuclear Engineering and Design 18 (1972) p115.
- [8] "Using MATLAB Version 6" The MathWorks Inc. 2000.

© British Crown Copyright 2002/MOD

Published with the permission of Her Britannic Majesty's Stationery Office.

MATERIALS FOR THE HIGH TEMPERATURE REACTOR

D. BUCKTHORPE

Reactor System & Advanced Technology, NNC Ltd., Knutsford, UK

R. COUTURIER

Commissariat à l'Énergie Atomique (CEA.), Grenoble, France

B. VAN DER SCHAAF

Nuclear Research and Consultancy Group (NRG), Petten, Netherlands

B. RIOU

Framatome ANP, Lyon, France

H. RANTALA

European Commission, Joint Research Centre (JRC), Institute for Energy, Petten, Netherlands

K. KUEHN

Forschungszentrum Juelich GmbH (FZJ.ESS), Juelich, Germany

A. BUENAVENTURA

Empresarios Agrupados Internacional S A (EASA.MD), Madrid, Spain

B-C. FRIEDRICH

Framatome ANP (GmbH), Germany

ABSTRACT

Research activities are in progress on the modular HTR technology, supported by the European Commission within its 5th Euratom Framework Programme. Two Projects (HTR-M & HTR-M1) consider the selection and development of materials for the reactor vessel, high temperature control rod and turbine, and graphite core. They involve two areas of activity covering a literature review and database and materials testing including irradiation tests in the High Flux Reactor at Petten. This paper describes the activities of the combined HTR-M / M1 programme and some results from the first year. The paper also looks towards the planning of some key tests due to begin in 2002.

Introduction

High temperature and gas-cooled reactors have been developed within Europe over many decades and considerable expertise exists within the European Community countries in this technology. There has been renewed interest in modular and direct cycle concepts in recent years and European Community Framework Programmes have been launched to consolidate and advance this modular HTR technology in Europe [1]. Coordinated projects are underway to investigate important technological issues associated with HTR development in key some technical areas (HTR-F, HTR-M, HTR-N, HTR-E, HTR-L). They cover issues on Fuel, Materials, Nuclear Physics, Equipment, and Licensing. The projects involve partnerships between principal industrial and research organisations from different countries of the European Union, and have the individual aim to develop and consolidate European expertise and experience in each of the individual areas. A European HTR Technology Network (HTR-TN) has also been launched to coordinate and encourage work-shared actions within European companies and to serve as a channel for international collaboration [2]. This network involves over 20 organisations from industry, research and development, utilities, universities together with the Joint Research Centre (JRC) of the European Commission. These

companies have agreed to work collectively on longer-term issues to establish a firm basis for continued development of HTR's in Europe. The technological issues important to two recent industrial projects PBMR and GT-MHR are used as basis.

The project on materials (denoted HTR-M & M1) deals with the selection and development of materials for the reactor pressure vessel, high temperature resistant alloys for the internal structures and turbine and graphite for the reactor core. The work began in November 2000 and involves eight partners from five European countries. This paper gives an update of the progress of the work for the HTR2002 conference and discusses some of the initial results. The main elements of the programme have previously been reviewed [3,4] and are shown in Figure 1.

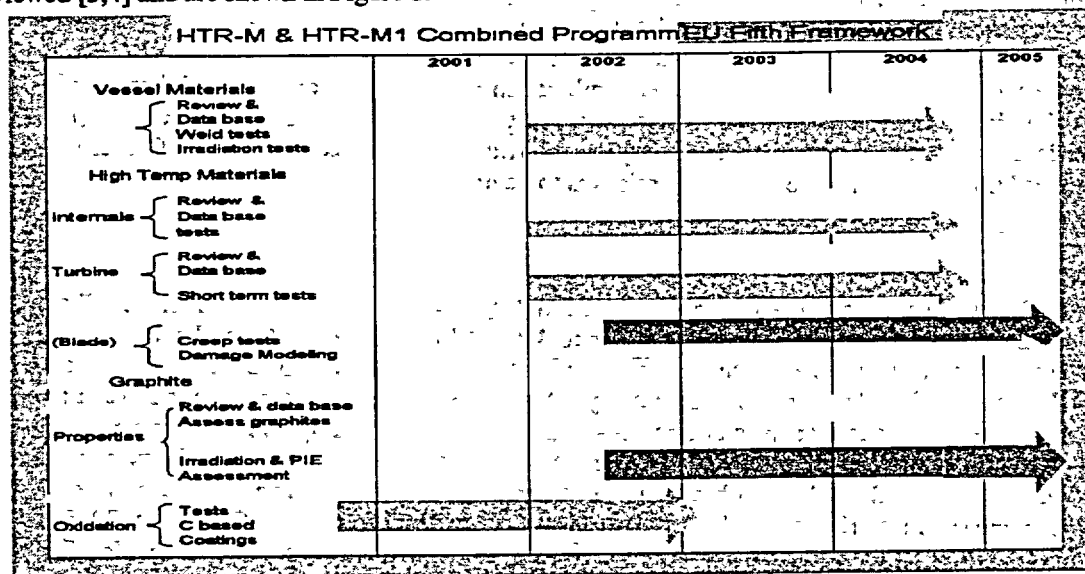


Fig. 1 Description of Overall HTR Materials Programme

HTR M & M1 Projects

The main objectives of the HTR Materials projects are to develop:

- ⇒ HTR vessel materials and data in the areas of design analysis, structural integrity analysis and materials properties under irradiated and non-irradiated conditions including testing on welds.
- ⇒ Materials for the high temperature regions of the HTR under simulated environments for both reactor internals and for the turbine
- ⇒ Graphite materials data identifying new graphites suitable for HTR and performing important testing and formulating a database of available information.
- ⇒ Graphite oxidation and consequences of severe air ingress with core burning including the development of HTR models and data, protective coatings and innovative C-based materials.

The project involves two main areas of investigation:

Review and data base

The vessel materials can operate at temperatures as high as 450°C and information is required on manufacturing, environment (neutron-irradiation fluence, operational temperature, and helium environment) and welding. The primary circuit components operate at temperatures of 850-900°C and metals and ceramic materials are being considered for the reactor internals, core support, etc. with high strength alloys for the turbine. Graphite acts as a moderator and structural component and has important safety implications because of structural and other property changes that occur when it is irradiated. Information on all these components is crucial and design and material property data under HTR relevant

conditions are to be reviewed and compiled for candidate materials of different HTR concepts, in relation to both normal and accident conditions.

Materials testing

For the vessel some tests on a chosen grade of steel taken from typical welded vessel joints are to be carried out under irradiated and non-irradiated conditions. The test pieces will be irradiated in the Petten High Flux Reactor prior to performing the mechanical testing. For the high temperature control rod and the turbine components some short term and medium term testing of important material options under simulated HTR environments are to be carried out. The tests concern fracture, creep and creep fatigue conditions in air and helium environments. For graphite the tests will be carried out to determine properties and oxidation. Many existing graphites used in previous core designs are no longer manufactured commercially, and currently available grades are limited to a few specific sources of raw materials. Alternative graphite grades with a better combination of desirable properties will therefore be irradiated in the HFR and tested to determine variations in physical and mechanical properties up to low/medium doses. Also test work associated with graphite oxidation on the consequences of severe air ingress with core burning and advanced C-based options is to be performed

Review and Database

Vessel Steels

Most designs of future plant make use of either an LWR type steel or Modified 9Cr 1Mo. These materials have similar strength levels at temperatures up to 370°C. Modified 9Cr1Mo steel allows higher temperatures with only a gradual reduction in design strength at temperatures up to 450°C and above 450°C allowable stresses for all materials fall off rapidly. The main structural integrity concerns are at the vessel welds, at thicker sections, hot spots and regions important to functionality. Fracture, fatigue and creep-fatigue (depending on temperature) are the main damage mechanisms with compatibility aspects (metal loss and carburisation) unlikely to have an impact on material choice. The data base is being assembled to include such materials as C-Mn steels (as used in the UK Magnox and AGR types), SA 508 Grade 3 Class 1 (LWR) or its European equivalent, 2¼ Cr-1Mo steel as used on HTTR and Modified 9Cr1Mo. Aspects such as provisions, products & parts, test and design data and environment are to be covered. Significant amounts of data exist for these steels and the main focus is on comparisons and assembling relevant design data. Mod 9Cr 1Mo steel showed the most uncertainty on data and fabrication experience with respect to HTR characteristics. It also potentially has the wider applicability. Mod 9Cr 1 steel was therefore selected for the test programme in the High Flux Reactor (HFR).

High Temperature materials

Materials for the control rod and turbine (blades and discs) are being investigated. Carbon-carbon composites offer advantages in strength, ductility and increased thermal resistance over metal alloys, giving potential for improved reactivity control during shutdown and for allowing the normal operating temperatures of future reactors to be increased [5]. For the turbine high temperatures and long term endurance are key issues. Criteria for material selection are typically to be based on a safe operation period of up to 60,000 h at 3000 rpm (50 Hz), with upper temperature limits in the range 850 to 950°C. The main criteria to be considered are creep and the influence of environment. Manufacturing considerations are also a major factor for the disc. Candidate alloys for the disc must be capable of production of large defect free ingots with good forging properties and proven thermal stability. The need for cooling is another major issue since the review has shown temperature limits for suitable disc materials to be below 750°C. For blades corrosion is a concern. Helium atmospheres from decomposition of methane under extremely low oxygen partial pressures are heavily carburising and can cause a significant shortening of the material creep life and accelerated creep crack growth rates. The presence of alloying elements such as cobalt (which is in most of the currently available turbine disc and blade materials) may be difficult to avoid. The main issues are the potential for plate out and lift off of particles and their activation and prevention of them flowing through the core. The review and data base work has identified a few potential materials and these are being considered for the experiments.

Graphite

The graphite core is a key component that affects safety and operability of the reactor. It provides structural support, coolant channels, moderation, and shielding while operating in a high temperature helium environment. Its performance is critically dependent on the graphite properties, which are irradiation dependent. The most important considerations are component integrity and changes in core geometry, both of which are affected by the dimensional change. Many of the graphites used in previous core designs are no longer available. The main questions are on the availability of the coke and manufacturing procedure. There are only three manufacturers left in the world. The decline in the ability to manufacture nuclear grade graphite in large quantities in the UK is an example of this. Two large plants, one owned by Anglo Great Lakes (AGL now SGL) and the other by British Acheson Electrodes Ltd (BAEL, later known as Union Carbide and presently called UCAR) manufactured all the Gilsocarbon graphite used in the UK's AGRs. Neither plant now exists. Today's HTGR projects - HTTR (Japan) and HTR-10 (China) - use a Japanese graphite (IG-110). This graphite, with its high strength, should be taken into account for exchangeable core components where low fast neutron fluences and hence low total doses apply. The proposal is to approach each of the three remaining manufacturers to see what graphites they can offer. The work on the review and collection of graphite properties is considering the accessible information on the IAEA database, internal information and published information at seminars and conferences. The IAEA database was established to help the development of International programmes on graphite moderated reactors, assist safety authorities in assessment of safety aspects and serve as a source of scientific information for nuclear and non-nuclear technology. The database is considered to have data that is relevant to the irradiation temperature and neutron fluence domains for new HTR's

Materials testing

Vessel Steel

The test programme for the vessel steel will concentrate on qualification of Mod 9Cr 1 Mo. For this purpose an irradiation test of thick welded joints is being prepared. The tests involve the use of the Lyrarig, giving accurate control of the temperatures and use of a helium atmosphere. The heaters in the rig will be used to correct the temperature levels obtained from gamma heating. Post irradiation tests will include tensile, creep, Charpy and CT toughness tests. The fabrication and characterisation of the welded specimens involves tests on 40 and 150mm thick plate. The thinner plate specimens provide a means for trials using different weld bead lengths and different weld parameters before producing the final weld specimens with the thicker plate. The conditions used will simulate the accumulated dose at the end of life. For the tests the lowest temperature condition is being considered as higher temperatures are expected to act to anneal out any irradiation damage effects. Work has started in defining the tests for post-irradiation and reference properties and final test selections and boundary conditions. The procurement of the material and fabrication of the thick section welded test pieces will be done following completion of the characterisation tests. The test programme details are expected to be finalised by mid 2002 to allow the actual test programme to start towards the end of 2002.

High Temperature materials

Experiments on these materials will involve short and intermediate term tests. High temperature short-term mechanical/ creep tests are planned for the control rod material. Short term tensile/ creep tests (air, helium) up to 850°C are planned for the blade materials (2 grades) and fatigue and creep/ fatigue tests up to 750°C in air and helium for the disc material (1 grade). The duration of the intermediate creep tests is expected to be >5000 h. The tests on the blade material will include aged and notched samples. The test matrix and proposals for the test conditions will as far as possible bound the temperature and transient cases experienced by the turbine. The details of the test programme and necessary heat treatments will be finalised during 2002. Possible candidate materials for the blade and disc tests are cast IN738 and IN792 DS which give a good creep resistance. For the disc U720 has a potential for operation up to 700°C and IN706 at 650°C. Discussions are underway with suppliers to confirm initial choices and availability.

Graphite

The irradiation experiment will use a test rig that allows two distinct temperature levels to be obtained. Measurements will be on dimensional changes, Young's modulus, CTE and thermal conductivity. The final conditions of the experiment have yet to be confirmed. The current programme must use currently available graphites since the development of a new material would take 3-5 years. Ideally the test conditions for the experiment would be those that give data for candidate graphites up the peak end of life fluence. This requires a significant effort over a long time scale, typically 10 years. The target flux in the current four year programme will be as high as possible.

The graphite oxidation work involves three experimental tasks relevant to safety analysis and licensing. Tests on graphite oxidation using THERA and INDEX facilities are well advanced. Measurements have been taken on the kinetics of graphite in oxygen for temperatures between 550 and 750°C and partial pressures of between 2 and 20kPa. Oxidation resistance of three-selected Carbon-Fibre-Composites (CFC's) developed for the Fusion Reactor have also been measured on THERA in air and oxygen (800°C): A 3D CFC containing about 9 at-% of silicon showed reactivity reduced by a factor of 2 compared with similar but non-silicon containing material. Oxidation attack concentrates on the matrix instead of the fibers. Further tests in steam are planned for 2002. Results from the high flow rate test rig INDEX are expected in mid 2002. Experiments are also planned for irradiated and non-irradiated CFC materials (up to 1dpa) that will look at strength, dimensional change, thermal diffusivity and heat capacity. Experiments to determine the thermal conductivity of such CFC materials have been made in non-irradiated material with tests on irradiated samples to be completed in 2002.

Summary and Conclusions

This paper reviews research activities on the HTR-Materials projects in support of the modular HTR technology within Europe. Overall the project is progressing to programme with review and data base investigations in hand and planning for experiments started. Graphite oxidation experiments are well underway and results available. The next phase of the work will involve decisions on materials and the setting up of the tests on the vessel material, the disc and blade high temperature alloys, and for the graphite irradiation tests to enable them to start as early as possible in the programme.

Acknowledgements

The projects HTR-M & HTR-M1 mentioned in this paper are being co-sponsored under the Fifth Framework programme of the European Atomic Energy Community ("Euratom"), contracts FIKI-CT-2000-0032 and FIKI-CT-2001-20135. The information provided herein is the sole responsibility of the authors and does not reflect the Community's opinion. The Community is not responsible for any use that might be made of the data appearing in this publication.

References

- [1] J Martin-Bermejo, M. Hugon, G. Van Goethem
Research activities on High Temperature Gas-cooled Reactors (HTRs) in the 5th EURATOM RTD, Framework Programme. Smirt 16, Washington, Aug 2001
- [2] W. Von Lensa, D. Hittner, J. Guidez, F. Sevini, A. Chevalier, M. T. Dominguez, G. Brinkmann, T. Abram, J. Martin- Bermejo. "The Role of International Collaboration within the European High-Temperature Reactor Technology Network (HTR-TN)" Seminar on HTGR Application and Development, Beijing, China, March 19-21, 2001.
- [3] D. Buckthorpe, R. Couturier, B. van der Schaaf, B. Riou, H. Rantala, R. Moormann, F. Alonso, B-C. Friedrich, Materials for the High Temperature Reactor, 16th SMiRT Conference, Washington, USA, on 12-17th August 2001)
- [4] D. Buckthorpe, R. Couturier, B. van der Schaaf, B. Riou, H. Rantala, R. Moormann, F. Alonso, B-C. Friedrich, Investigation of High Temperature Reactor (HTR) Materials, NEA/OECD, 2nd Information Exchange meeting on High Temperature Engineering, Paris, on 10-12 October 2001
- [5] Development of carbon/ carbon composite control rod for HTTR (II) - Concept, specification and mechanical test of materials - JEARI research 98-003.

THE NUMERICAL DETERMINATION OF THE VARIATION IN THE POROSITY OF THE PEBBLE-BED CORE

C.G. DU TOIT

*School for Mechanical and Materials Engineering
Potchefstroom University for CHE, Private Bag X6001, Potchefstroom 2520, South Africa*

ABSTRACT

The pebble-bed reactor can be considered as a packed bed reactor. The mechanisms of fluid flow and heat transfer in such a bed are sensitive to the porosity distribution of the bed. In this paper numerical procedures are presented to evaluate the axial and radial variations of the porosity in a cylindrical packed bed. The application of the procedures is illustrated by analyzing the porosity distribution in the pebble-bed core, which was generated using a discrete element approach. The typical oscillatory variation in porosity near the wall is observed. It is also found that significant local variations in the porosity can occur.

1. Introduction

The core of the pebble-bed reactor, currently being designed in South Africa, will consist of a central cylindrical collection of graphite balls surrounded by an annular collection of fuel balls. The reactor will be a MEDUL type reactor, which means that graphite and fuel balls will be added regularly at the top of the reactor and removed at the bottom of the reactor. The flow rate of the balls is envisaged to be in the order of 5000 balls per day which is approximately 0.013% of the total number of balls in the core. The pebble-bed reactor can therefore, as a first approximation, be considered as a fixed or a packed bed reactor.

The design of a packed bed reactor is based upon mechanisms of heat and mass transfer, and the flow and pressure drop of the fluid through the bed of solids. The mechanisms in turn are all sensitive to the porosity of the packed bed. Therefore, knowledge of the porosity distribution within a packed bed is important to any rigorous analysis of the transport phenomena in the bed [1]. In a packed bed reactor the porosity varies sharply near the wall, since the geometry of the packing is interrupted there. As a result the velocity profile inside a packed bed is severely distorted near the wall, reaching a maximum in the near-wall region. This was confirmed by Vortmeyer and Schuster [7] who evaluated the steady-state flow profiles in rectangular and circular packed beds. They solved the Brinkman equation by an equivalent variational method and approximated the radial variation of the porosity with a smooth exponential expression. This phenomenon can have a significant impact on heat and mass transfer in packed beds [2]. The variation in the porosity of the core near the wall of the pebble-bed reactor has been recognized [3], but the effect that it has on the flow and temperature distribution has not been taken into account [4].

As part of an investigation into the movement of the spheres through a pebble bed, Bedenig [3] also determined the porosity of the bed. By slowly filling a model of a pebble bed with water, he could determine the variation of the porosity of the bed as a function of the height from the bottom of the reactor. The results show that the porosity near the bottom is large and rapidly diminishes away from the bed until it attains an average or bulk value approximately five sphere diameters away from the bottom. However, the data were not detailed enough to exhibit the well-known periodic variation in the porosity away from a containing wall. This effect was demonstrated by the experimental study of Goodling *et al.* [1]. They studied the radial porosity distribution in resin filled cylindrical beds packed with spheres, by machining down annular rings. This was also confirmed by the investigation of Sederman *et al.* [5]. They used a Magnetic Resonance Imaging technique to study the radial porosity distribution in cylindrical packed beds filled with water. Furthermore, Goodling *et al.* [1] observed that the radial porosity distribution exhibited an exponential variation combined with a damped oscillation. Cohen and Metzner [6] proposed a mathematical expression for the oscillatory variation. Vortmeyer

and Schuster [7] also did some calculations using an oscillatory porosity variation in accordance with the results they obtained. They assumed the Ergun relation for pressure loss to be locally valid according to the drastic variation in porosity. However, Du Toit [8] has found that the validity of this assumption may be debatable if the origin of the Ergun relation is considered.

It is therefore important that in the design and analysis of the pebble-bed reactor, the occurrence of flow distortion should be investigated and that the scale of the effect that it has on all the associated phenomena in the reactor be determined. For this an intimate knowledge of the variation of the porosity is required. In this paper procedures are discussed that were developed to analyze the variation in the porosity in the axial and radial directions numerically.

2. Theory

To perform the analyses, the coordinates and the size of the spheres constituting the packed bed are required. The spheres are assumed to be uniform. The quality of the data can first of all be evaluated by investigating the overlap between the spheres. Ideally there should be no overlap. The distance d_{ij} between spheres i and j can be calculated as

$$d_{ij} = \sqrt{(x_i - x_j)^2 + (y_i - y_j)^2 + (z_i - z_j)^2} \quad (1)$$

where x_i, y_i, z_i and x_j, y_j, z_j are the coordinates of the centers of the spheres. The overlap d_o is then given as

$$d_o = \begin{cases} d_p - d_{ij} & \text{for } d_{ij} < d_p \\ 0 & \text{for } d_{ij} \geq d_p \end{cases} \quad (2)$$

where d_p is the diameter of the spheres.

The variation in the porosity in the axial direction can be determined from the ratio between the area occupied by the spheres and the cross sectional area of the reactor (cylinder) at each axial cross section considered. The axial porosity ε_z at the level z is therefore given as,

$$\varepsilon_z = 1 - (\sum A_x) / A_c \quad (3)$$

where A_c is the cross sectional area of the cylinder. The area A_x of the cross section of the sphere i in the plane z is given as

$$A_x = \pi [r_p^2 - (z_i - z)^2] \quad \text{for } |z_i - z| < r_p \quad (4)$$

where r_p is the radius of the spheres.

The variation in the porosity in the radial direction can be determined from the ratio between the area occupied by the spheres and the circumferential area of the cylindrical plane at each radial position considered. The radial porosity ε_r at the radial position r is therefore given as,

$$\varepsilon_r = 1 - (\sum A_r) / A_r \quad (5)$$

where A_r is the circumferential area of the cylindrical plane and is given by

$$A_r = 2\pi r (z_h - z_l) \quad (6)$$

and z_h and z_l are the upper and lower limits of the cylinder or part of the cylinder considered. The area A_r of the cross section of the sphere i in the cylindrical plane is given as

$$A_r = 2(\sum \Delta z_j) r \theta_c / n_\theta \quad \text{for } |z_i + r_p| > z_l \quad \text{or} \quad |z_i - r_p| < z_h, \quad \text{and} \quad |r_i - r| < r_p \quad (7)$$

where r_i is the radial distance from the axis of the cylinder to the center of the sphere and n_θ the number of integration intervals. Let the x' direction be defined by the line from the axis of the cylinder to the center of the sphere. The coordinates (x'_c, y'_c) of the points where the cylindrical plane intersects the perimeter of the center plane, perpendicular to the axial direction, of the sphere can be calculated as

$$x'_c = (r^2 - r_p^2 + r_i^2) / 2r_i, \quad (8)$$

and

$$y'_c = \pm \sqrt{r^2 - (x'_c)^2} \quad (9)$$

The angle θ_c between the x' direction and the line connecting the axis of the cylinder and the intersection point(s) is given by

$$\theta_c = \pm \cos^{-1}(x'_c/r) \quad (10)$$

The ordinates z_{cj} of the perimeter of the cross section A_j relative to the center plane of the sphere can be obtained as

$$z_{cj} = \sqrt{r_p^2 - r^2 - r_i^2 + 2rr_p \cos \theta_j} \quad \text{for } -\theta_c \leq \theta_j \leq \theta_c \quad (11)$$

Further

$$z_{uj} = z_i + z_{cj} \quad \text{for } z_{uj} < z_h, \quad \text{else } z_{uj} = z_h \quad (12)$$

and

$$z_{bj} = z_i - z_{cj} \quad \text{for } z_{bj} > z_i, \quad \text{else } z_{bj} = z_i \quad (13)$$

Finally the height (or width) Δz_j of the cross section A_j at the angle θ_j is given as

$$\Delta z_j = z_{uj} - z_{bj} \quad \text{for } z_{bj} < z_{uj}, \quad \text{else } \Delta z_j = 0 \quad (14)$$

3. Application and results

The application of the procedures is illustrated by analyzing the porosity of a numerical model of a test cylindrical packed bed and the porosity of a numerical model of the pebble-bed reactor. In both cases the numerical models were generated using the discrete element method [9].

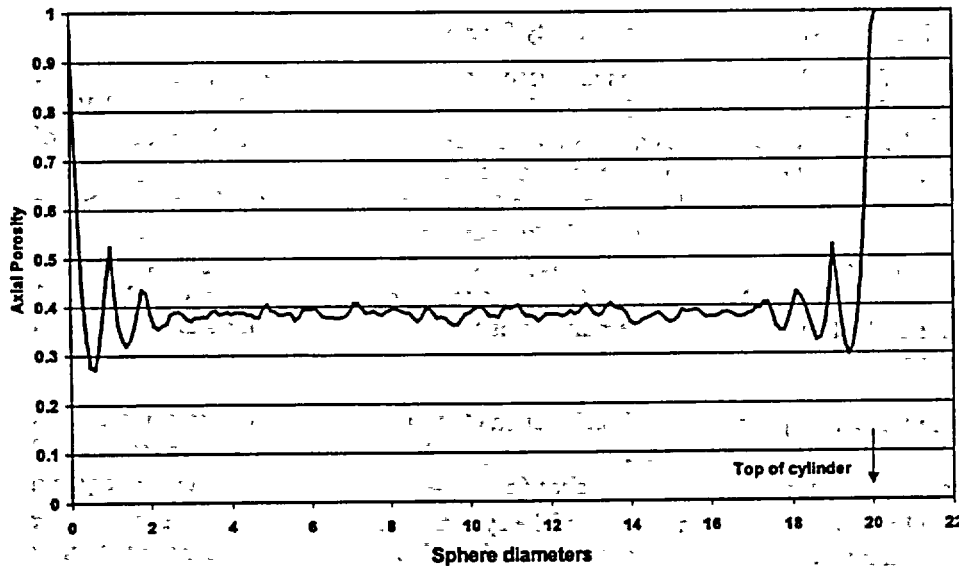


Figure 1. Axial variation in porosity for test cylindrical packed bed.

The test cylindrical packed bed had a diameter of 0.0714 m and a height of 0.0952 m and was filled with 4117 lead spheres with a diameter of 0.00476 m. An analysis of the overlap between the spheres has indicated that the average overlap is 2.08% and the maximum overlap is 7.87%. It has been found that there are 149 overlaps $> 0\%$ and $\leq 0.1\%$, 2256 overlaps $> 0.1\%$ and $\leq 1\%$, 3445 overlaps $> 1\%$ and $\leq 2\%$, 3117 overlaps $> 2\%$ and $\leq 3\%$, 1713 overlaps $> 3\%$ and $\leq 4\%$, 670 overlaps $> 4\%$ and $\leq 5\%$, 152 overlaps $> 5\%$ and $\leq 6\%$, 17 overlaps $> 6\%$ and $\leq 7\%$, and 5 overlaps $> 7\%$ and $\leq 8\%$. Not indicated in the numbers is that a number of spheres also penetrated through the solid surfaces.

The axial variation in the porosity for the test cylindrical packed bed is shown in Figure 1. The typical oscillatory variation in the porosity near a solid surface can be seen at the bottom. The oscillations are damped out after about five sphere diameters from the bottom after which the porosity hovers around 0.39, which was specified as the bulk porosity. The typical oscillatory variation in the porosity is also observed at the top of the cylinder. This indicates that all the spheres were not dropped freely into the cylinder, but that at least some of the spheres were squeezed or forced into the cylinder. This was indeed the case.

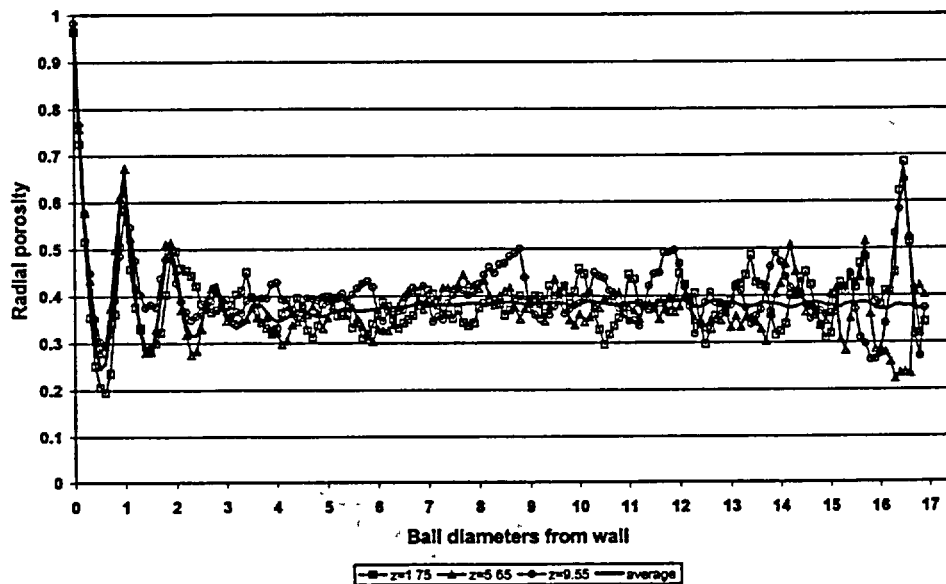


Figure 2. Radial variation in porosity for pebble-bed reactor.

The cylindrical section of the pebble-bed that was analyzed, had a height of 8.29 m and a diameter of 3.75 m, whilst the entire bed was filled with 95356 graphite uniform balls with a diameter of 0.10 m. The positions of the spheres were obtained from a “snapshot” that was taken of a DEM simulation of the moving bed. An analysis of the overlap between the spheres has indicated that the average overlap is 1.01% and the maximum overlap is 20.68%. It has been found that there are 10152 overlaps > 0% and ≤ 0.1%, 140589 overlaps > 0.1% and ≤ 1%, 90070 overlaps > 1% and ≤ 2%, 21903 overlaps > 2% and ≤ 3%, 2884 overlaps > 3% and ≤ 4%, 334 overlaps > 4% and ≤ 5%, 42 overlaps > 5% and ≤ 6%, 6 overlaps > 6% and ≤ 7%, 2 overlaps > 7% and ≤ 8%, 2 overlaps > 8% and ≤ 9%, and 1 overlaps > 20% and ≤ 25%. Not indicated in the numbers is that a number of spheres also penetrated through the solid surfaces.

The radial variation in the porosity for the cylindrical section of the pebble-bed is shown in Figure 2. It should be noted that the curves represent the average porosity in the tangential direction at each radial position. Four curves are shown, i.e. for a very thin slice ($z_k - z_l = 10\mu\text{m}$) near the bottom, a very thin slice in the middle, and a very thin slice near the top of the cylindrical section, and then the average for the full height of the cylindrical section. The typical damped oscillatory variation in the porosity near the wall, particularly in the case of the average, can be seen and is in good agreement with what had been found by Goodling et al. [1] and Sederman et al. [5]. It should be noted that the results of Goodling et al. [1] and Sederman et al. [5] are also representative average values. An analysis of the lower third of the cylindrical section, of the middle third and then of the upper third also exhibited the same trends as the average taken over the full height. A close look at the first three curves reveals that locally the radial porosity varies significantly around the average value. Especially near the axis of the cylinder the porosity can be significantly higher, or lower, than the bulk value which is in this case ± 0.385 . Nearer to the wall the variation around the average is much less. A possible explanation for this phenomenon can be the following. At the larger radii there is more space for the spheres and it is therefore easier to form a reasonably regular packing. At the smaller radii the space becomes less and the packing therefore also becomes more irregular leading to the values that are observed. Another

observation that can be made, is that at the bottom of the cylindrical section the minimum porosity near the wall is slightly less than the theoretical minimum of 0.2146. This is probably indicative of the effect of the overlaps that occur. However, this also suggests that the first layer of the packing is almost perfectly cubical in the radial direction next to the wall in this region. This can be attributed amongst others to the compressive force exerted by the spheres above. In the middle and near the top of the cylindrical section, however, the nature of the packing next to the wall seems to be less cubical.

4. Conclusion

In the design and analysis of the pebble-bed reactor, the occurrence of flow distortion should be investigated and the scale of the effect that it has on all the associated phenomena in the reactor should be determined. For this an intimate knowledge of the variation of the porosity is required. In this paper procedures that were developed to analyze the variation in the porosity in the axial and radial directions numerically, have been discussed. The application of the procedures has been illustrated by analyzing the porosity of a numerical model of a test cylindrical packed bed and the porosity of a numerical model of the pebble-bed reactor. In both cases the numerical models were generated using the discrete element method. The typical oscillations in porosity near the walls have been observed. However, it has been found that significant local variations in the porosity can occur. This can have a marked effect on the local variations in the flow distribution and heat transfer that may occur. These routines will allow the analyst to perform a careful analysis of the local variations in the porosity of the pebble-bed. By analyzing a number of consecutive "snapshots" the way in which the porosity varies over time can also be assessed. This knowledge can then be used to determine the local variations in the flow velocities and the temperatures as a result of the non-uniform distribution in the porosity.

5. References

- [1] J.S. Goodling, R.I. Vachon, W.S. Stelpflug and S.J. Ying, Radial porosity distribution in cylindrical beds packed with spheres, *Powder Technology*, 35, 23-29, 1983.
- [2] S.M. White and C.L. Tien, Analysis of flow channelling near the wall in packed beds, *Wärme- und Stoffübertragung*, 21, 291-296, 1987.
- [3] D. Bedenig, *Experimentelle Untersuchungen zum Strömungsverhalten eines Kugelhaufens im Hinblick auf den Brennelementkreislauf im Core eines Kugelhaufenreaktors*, Institut für Reaktorentwicklung, Kernforschungsanlage Jülich GmbH, 1966.
- [4] K. Verfondern, *Numerische Untersuchung der 3-dimensionalen stationären Temperatur- und Strömungsverteilung im Core eines Kugelhaufen-Hochtemperaturreaktors*, Jül - 1826, Institut für Reaktorentwicklung, Kernforschungsanlage Jülich GmbH, 1983.
- [5] A.J. Sederman, P. Alexander and L.F. Gladden, Structure of packed beds probed by Magnetic Resonance Imaging, *Powder Technology*, 117, 255-269, 2001.
- [6] Y. Cohen and A.B. Metzner, Wall effects in laminar flow of fluids through packed beds, *AIChE Journal*, 27, 705-714, 1981.
- [7] D. Vortmeyer and J. Schuster, Evaluation of steady flow profiles in rectangular and circular packed beds by a variational method, *Chemical Engineering Science*, Vol. 38, pp. 1691-1699, 1983.
- [8] C.G. du Toit, The pebble-bed reactor: effect of wall channelling on the flow in the core, *Proceedings 1st International Conference on Heat Transfer, Fluid Mechanics and Thermodynamics, Kruger Park, South Africa, Paper DC1*, April 2002.
- [9] M. Mitchell, Private communication, 2001.

ANALYSIS OF OPERATIONAL TRANSIENTS IN A FLUIDIZED BED NUCLEAR REACTOR

A. AGUNG, D. LATHOUWERS, T.H.J.J. VAN DER HAGEN, H. VAN DAM

*Interfaculty Reactor Institute, Delft University of Technology,
Mekelweg 15, 2629 JB Delft, The Netherlands*

and

C.C. PAIN, C.R.E. DE OLIVIERA, A.J.H. GODDARD

*Department of Earth Science and Engineering, Imperial College of Science, Technology and Medicine,
Prince Consort Rd, London SW7 2BP, United Kingdom*

ABSTRACT

A theoretical model describing the coupling of neutronics, thermohydraulics and fluidization in a fluidized bed nuclear reactor is presented. Simulations of operational transient conditions are performed, viz. a decrease of coolant flow rate and a change of coolant inlet temperature. These simulations show that the fuel temperature remains below the maximum allowable temperature of TRISO fuel, therefore ensuring a safe operational transient. The maximum reactivity is inherently limited and is rapidly compensated by the passive feedback mechanism.

1. Introduction

FLUBER is a conceptual design of a fluidized bed nuclear reactor that consists of TRISO coated fuel particles contained in a graphite-walled cylinder. The core cavity has a cross sectional area of 1 m² and a height of 6 m. The thickness of the axial and radial graphite reflectors is 1 m. Helium is used both as fluidization gas as well as coolant. The outer diameter of the fuel particles is 1 mm and the enrichment of the fuel kernel is fixed at 16.76%. When the helium flow is low enough, the core is packed and subcritical due to a lack of moderation. As the flow is increased, the core expands and reactivity is increased due to the influence of the graphite reflectors. In previous work, a geometric design was used where the reactivity attained a maximum at a certain flow rate and where the reactor became subcritical at high flow rates. The maximum attainable power was rather limited. In the present work, we choose a geometric design where the power attains its maximum at full core expansion. The power that can be reached in this way is somewhat higher than in the previous design.

A recent paper [1] discussed a startup transient that was simulated for an instantaneous increase of flow rate from 4 to 11 kg/s and showed that although the total power of the reactor may reach high values, the fuel temperature is well below safety limits at all times. The current paper describes several operational transients in FLUBER using the point dynamics model with coupled neutronics, thermal-hydraulics and fluidization interaction, which is intended as an improvement to the model presented by Kloosterman et al. [2] and as a reduced model to the fully coupled multidimensional one [3].

2. Model

The fluidization process is described by using the Richardson and Zaki (RZ) correlation which relates the fluidization velocity, $U_{g,s}$, to the bed porosity, ϵ ,

$$U_{g,s} = U_{\infty} \epsilon^n \quad (1)$$

where U_{∞} is the particle terminal velocity and n is a constant. The void fraction is assumed to relax

towards the steady state value as given by RZ with a timescale τ ,

$$\frac{d\varepsilon}{dt} = \frac{1}{\tau}(\varepsilon_{\infty} - \varepsilon) \quad (2)$$

The timescale is proportional to the bed height and inverse proportional to the gas velocity which corresponds to the time of propagation of a disturbance through the bed.

The energy equation for the fuel particles is

$$m_p C_{p,p} \frac{dT_p}{dt} = P_i + Q \quad (3)$$

and that for the gaseous coolant is

$$m_g C_{p,g} \frac{dT_g}{dt} = G_{in} C_{p,g} (T_{in} - T_{out}) - \frac{dm_g}{dt} (T_{out} - T_g) - Q \quad (4)$$

where P_i is the total power, G_{in} is the inlet mass flow rate of the helium, T_{in} and T_{out} are the inlet and outlet temperature of the helium, the subscripts p and g denote particle and gas respectively. Within the current point model an axially linear gas temperature distribution is employed [2], describing the relation of T_{out} to T_{in} and T_g . The interfacial heat transfer, Q , is based on the Nusselt relation for a single particle. Observe that the mass of particle in the above equations is constant, whereas the mass of coolant includes only that part in the active core region, which varies during a transient.

The basic equations for the point kinetics model is

$$\frac{dP_p}{dt} = \left[\frac{\rho - \beta}{\Lambda} \right] P_p + \sum_{i=1}^{N_p} \lambda_i C_i + \frac{S}{\Lambda} \quad (5)$$

the precursor concentrations further satisfy

$$\frac{dC_i}{dt} = \frac{\beta_i}{\Lambda} P_p - \lambda_i C_i, \quad i = 1, \dots, N_p \quad (6)$$

and the decay heat is formulated as

$$\frac{dP_{d,n}}{dt} = \frac{\gamma_n}{Q_f} P_p - \lambda_n P_{d,n}, \quad n = 1, \dots, N_d \quad (7)$$

where P_p is the prompt fission thermal power, P_d is the delayed component, ρ is the reactivity, β denotes the delayed neutron fraction, Λ is the neutron generation time, C_i is the precursor concentration of class i , λ is its corresponding decay-constant, S is the independent neutron source, expressed in power units and Q_f is the prompt recoverable energy per fission. In the present work 6 precursor groups and 15 decay heat groups are employed. There are two components of reactivity feedback existing in the fluidized bed fission reactor: (a) feedback due to variation of the bed height, ρ_{ref} , and (b) feedback from temperature effects, ρ_T :

$$\rho(\varepsilon, T_p) = \rho_{ref}(\varepsilon) + \rho_T(\varepsilon, T_p) \quad (8)$$

Two different formulations are used for the temperature feedback (i) a steady state formulation where the reflector temperature is assumed to be in between that of the core and room temperature, and (ii) a transient formulation where the reflector is assumed to stay at its initial temperature. This leads to the following statements

$$\rho_{T,ss} = \alpha_{d,t}(\varepsilon)(T_p - T_{ref}) \quad (9)$$

$$\rho_{T,tr} = \alpha_{d,t}(\varepsilon)(T_i - T_{ref}) + \alpha_{d,c}(\varepsilon)(T_p - T_i) \quad (10)$$

where α_{dt} and α_{dc} are the total and core temperature coefficients respectively. T_{ref} is the temperature at which the standard reactivity curve is known, and T_i is the fuel temperature at the inception of the transient. The present design of the reactor uses 170 kg of uranium and the reflector has an embedded absorber ring containing 20 ppm of natural boron located at the bottom of the core. Figure 1 shows the static reactivity and Doppler coefficients as a function of the bed porosity, together with fitted curves that have been used in the subsequent simulations. These static calculations have been performed with the criticality code KENO-Va.

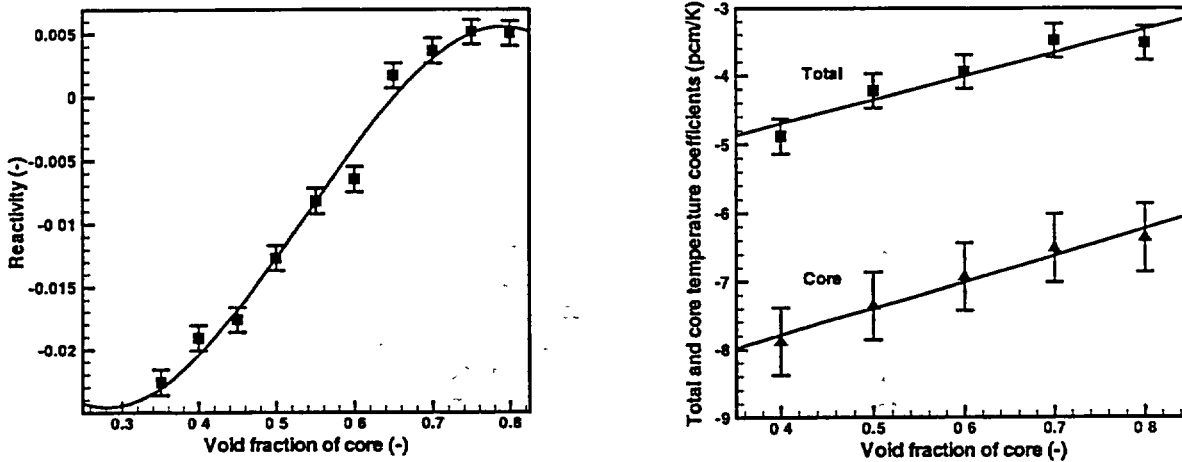


Figure 1. Reactivity (left) and temperature coefficients (right) as a function of the bed porosity. Reference temperature of the fuel is 693 K and the total mass of uranium in the bed equals 170 kg.

3. Results

Figure 2 shows the steady state conditions for the fuel temperature and the total power based on an inlet helium temperature of 543 K. The reactor starts to produce power at a flow rate of about 4.6 kg/s and rises towards its maximum at 14 kg/s. The curve for the fuel temperature follows that of the reactivity and reaches its maximum earlier. Around 14 kg/s, the porosity of the bed reaches its maximum value (height of the bed equals the height of the cylinder) and beyond that the model becomes invalid. The temperature of the coolant (not shown) is almost equal to that of the fuel particles due to the excellent heat transfer.

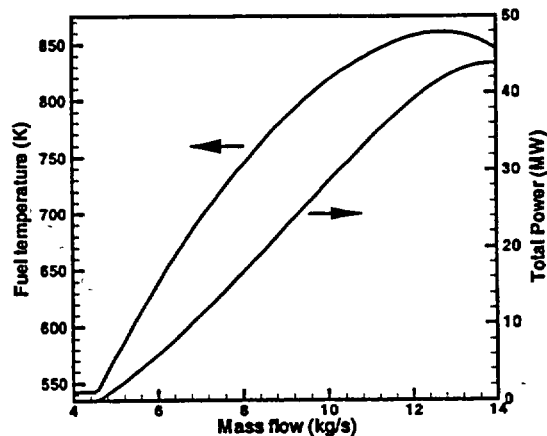


Figure 2. Fuel temperature and total power as a function of the coolant mass flow rate in steady state conditions.

Two kinds of operational transients were simulated to investigate the effect to the fluidized bed nuclear reactor, i.e. a decrease in the flow rate and a change in the helium inlet temperature. These transients are considered to represent a broad range of possible operational transients.

In the first case, the flow rate is instantaneously decreased at time 0 from 11 kg/s to 8 kg/s after the reactor reaches the steady state condition at 11 kg/s. This transient, for example, can occur as a result of a pump disturbance or as an intended decrease of power output. Results of this transient are shown in Figure 3.

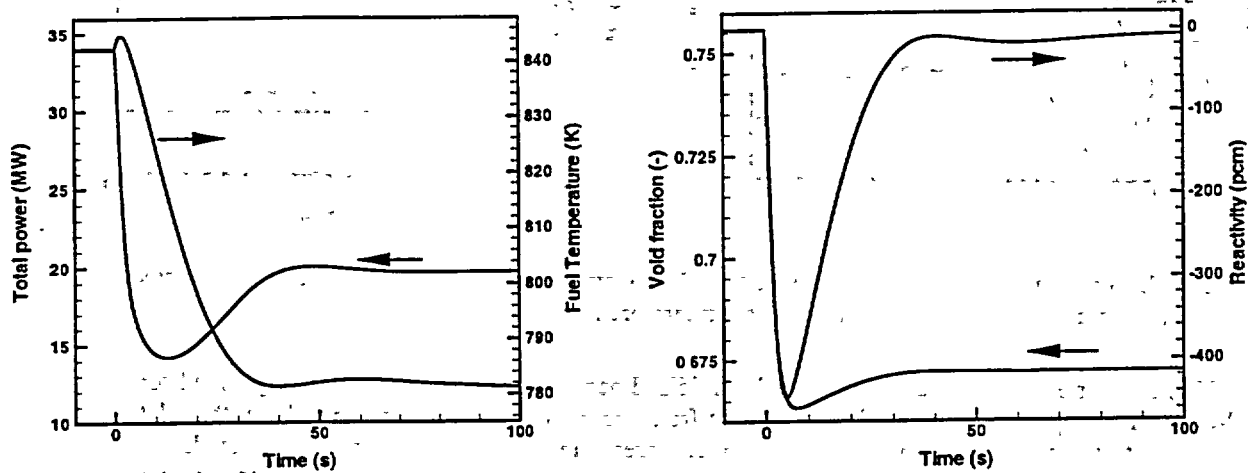


Figure 3. Total power and fuel temperature (left) and porosity and reactivity of the core (right) versus time during a decrease of flow rate from 11 kg/s to 8 kg/s.

As the flow rate decreases, the porosity of the core decreases very rapidly. Concurrently the cooling capacity of the helium decreases and during the first few seconds, the fuel temperature increases. This combined event affects the reactivity that further decreases steeply. As the heat generated in the core decreases, the fuel temperature begins to drop. It is clear that the reactivity (and consequently the total power) will increase through the Doppler feedback to a new equilibrium state. It should be observed that the fuel temperature jump is minor during the first few seconds of the transient.

In the second case, the helium inlet temperature is instantaneously decreased at time 0 by 100 K after the reactor reaches the steady state condition at 11 kg/s. Results of this transient are shown in Figure 4.

As the coolant temperature decreases, the helium density increases but the mass flow rate is kept constant, giving a decrease in the superficial velocity. Consequently the bed starts to contract, resulting in a sudden decrease in reactivity. After this, the decrease of the fuel temperature causes a rise in reactivity due to temperature feedback, creating a rise in power output.

A reverse event similarly occurs when the inlet temperature increases by 100 K (not shown in this paper). The fuel temperature rises up to about 870 K (an increase of about 50 K) within the first 20 seconds before it drops to a new equilibrium point.

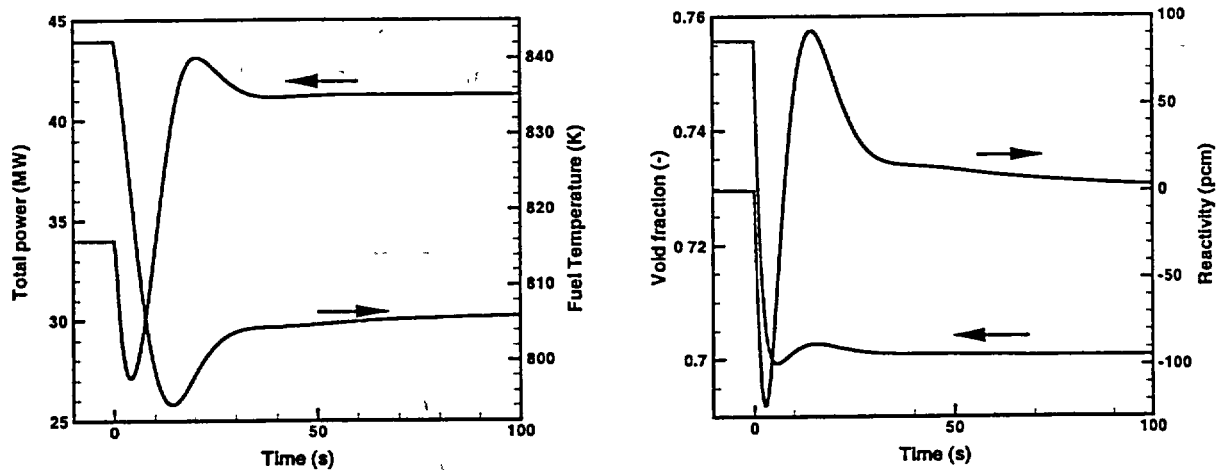


Figure 4. Total power and fuel temperature (left) and porosity and reactivity of the core (right) versus time during a decrease of helium inlet temperature from 543 K to 443 K.

This kind of transient shows the behavior of the fluidized bed nuclear reactor which is very useful for load-following purposes. When the heat extracted from the helium increases in the turbine, the inlet temperature to the core decreases and it leads to an increase in the reactor power to accommodate a larger power demand. Conversely when the load demand decreases, the inlet temperature to the core increases and furthermore the power generated in the core decreases.

Both types of simulations show a rapid response of the reactor to the introduced perturbation and always end up in a new equilibrium state without compromising the safety margin of the fuel.

4. Conclusions

A theoretical model has been presented for describing the coupled thermo-fluid dynamics, and neutronics in a fluidized bed nuclear reactor. The neutronics model is a point kinetics model including decay heat. The thermo-fluid dynamics is based on a relation between fluidization velocity and porosity of the bed, combined with global thermal balance equations.

Numerical studies of operational transients, viz. a step change in coolant mass flow rate and a coolant inlet temperature transient, show that the maximum fuel temperature remains below the safety margin of TRISO fuel. Furthermore, the maximum reactivity that can be introduced in all transients, is inherently limited and is rapidly compensated by the passive feedback mechanism.

5. References

- [1] D. Lathouwers, A. Agung, T.H.J.J. Van Der Hagen, H. Van Dam, C.C. Pain, C.R.E. De Oliveira, A.J.H. Goddard, Dynamics Modeling and Stability Analysis of a Fluidized Bed Nuclear Reactor, accepted for *SMORN8*, 2002.
- [2] J.L. Kloosterman, V.V. Golovko, H. Van Dam, and T.H.J.J. Van der Hagen, Conceptual Design of a Fluidized Bed Nuclear Reactor, *Nucl. Sci. Eng.* 139, 118, 2001.
- [3] C.C. Pain, J.L.M.A. Gomes, M.D. Eaton, C.R.E. De Oliveira, A.P. Umpleby, A.J.H. Goddard, H. Van Dam, T.H.J.J. Van der Hagen, D. Lathouwers, Space-dependent Kinetics Simulation of a Gas-cooled Fluidized Bed Nuclear Reactor, Submitted to *Nuclear Technology*, 2002.

CONCEPTUAL DESIGN OF A PASSIVE, INHERENTLY SAFE EMERGENCY SHUTDOWN ROD FOR HIGH-TEMPERATURE REACTOR APPLICATIONS

A. M. OUGOUAG, W. K. TERRY, and R. R. SCHULTZ

*Idaho National Engineering and Environmental Laboratory
P. O. Box 1625, Idaho Falls, ID 83415-3885 - United States*

ABSTRACT

The concept of a passive, inherently safe, and fail-safe design for an emergency control rod is presented. The functioning of the rod is based solely on inexorable physical laws. The operation of the rod in its emergency function does not require the intervention of a human operator, nor does it rely on any signal from a monitoring or safety system. Although the concept could be applicable to a variety of reactors (provided a normal temperature range is specified), in this paper, the concept is applied to the emergency shutdown of a pebble-bed reactor. The preliminary study presented here demonstrates that the proposed Electro-Magnetic Optimally Scramming Control Rod (EM-OSCR) naturally operates *when needed*. The rod is held out of the core region by the force of an electromagnet. The force is generated by a current carried by a conductor, a portion of which passes near or through the reactor core region. When the temperature in the conductor increases because of an increase in temperature in the reactor, the conductor resistivity increases. This, in turn, leads to a current decrease. When the current decreases below the level necessary to hold the rod up, the rod is released and it falls into the core under the effect of gravity.

1. Introduction

Recently, the pebble-bed reactor (PBR) concept has been receiving a great deal of renewed interest. For example, a consortium led by the South African Utility Eskom is studying the possibility of development and deployment of reactors of this type [1]. This renewed interest is motivated, in part, by the pebble-bed promise of safety features superior to those of the current generation of light water reactors (LWRs). Such passive safety features have been demonstrated experimentally in the German AVR project [2]. In particular, the PBR was shown to be safe against a loss of forced cooling (LOFC) without scram but without depressurization [3] and against depressurization with the simultaneous loss of forced cooling (DLOCF) but with scram [4]. The most severe scenario of the same type would be a depressurized loss of forced cooling without scram. Such a scenario has not been tested experimentally but has been modeled for a prismatic High Temperature Gas-Cooled Reactor (HTGR) [5]. In all cases, these HTGRs are shown to be safe. Yet, in all cases redundant safety systems for emergency shutdown and for maintaining the shutdown state are expected to be required. Passive (i.e., not requiring any intervention by a mechanism or by an operator) or inherent (i.e., relying on inexorable physical laws) systems will probably be preferred. Since in the PBR concept strong negative temperature feedback is expected to be the most likely shutdown mechanism in the LOCA events, control rods would be required only for maintaining sub-criticality following the eventual cooling down of the core. Since in a PBR the reactor core cooling process would take considerably longer than the time of descent of a rod into the core, the redundant shutdown rods would be effective even if they dropped into the core relatively slowly, as discussed later.

In this paper, a passive and inherently actuated control rod concept for emergency shutdown and for redundant, post-cooling reactivity hold-down is presented. Although the emergency shutdown concept is illustrated for a PBR, it is applicable to other types of reactors, provided a "normal" operating temperature range is specified. Preliminary analysis shows that the design can be made to be fail-safe, as the rod or rods would drop into the core under all failure conditions.

In the next section, a synopsis of the EM-OSCR is presented. The following section discusses the mechanism that holds the rod out of the core during normal operations and the means available for fine-tuning and adjusting the holding force. The evaluation of the neutronic performance of a set of EM-OSCR rods is then presented. The falling time, or time to descent into the core, is modeled and evaluated in the following section. The last section is a discussion of the paper is a discussion of the concept, its fail-safe features, and a summary of the principal findings.

This preliminary study shows that the EM-OSCR concept is feasible and that OSCR rods can be an effective passive and inherent system for the scrambling of gas-cooled reactors and for the prevention of re-criticality following drops in temperature. In the analyses presented here, it is assumed that the reactor under consideration is similar in thermal design and other physical features to the Pebble-Bed Modular Reactor (PBMR) currently undergoing design in South Africa [1].

2. Synopsis of the EM-OSCR Concept

The EM-OSCR concept is illustrated in Figure 1. The EM-OSCR control rod is intended to remain outside the core region during normal operations and to drop into the core under the influence of inexorable natural laws when the temperature in (or near) the core exceeds a pre-set value. The control rod is held out of the core region by an electromagnet (E-M). The electrical supply line to the E-M includes a portion that passes in or near the core. That portion is made of a material of known temperature-dependent resistivity. As the temperature in the core rises above a prescribed set point, the temperature in the in-core conductor rises, and hence the resistance. This in turn decreases the current that powers the E-M, and therefore the E-M lift force. When the lifting force drops below the weight of the control rod assembly, the rods drop into the core by gravity. No switch, no signal, and no operator intervention are needed to actuate the control rod.

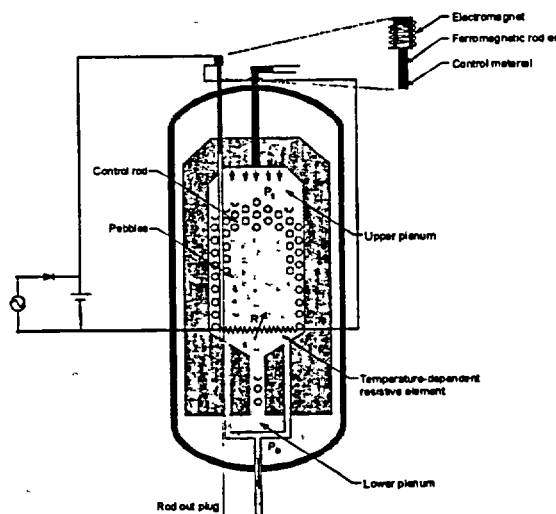


Figure 1. EM-OSCR Concept

Fuses within the circuit limit or interrupt the current, as needed. Failure modes such as loss of power to the E-M or disruption of the continuity of the conductor line are fail-safe as they result in the rod being dropped into the core.

3. Lifting Force Evaluation

The concept described in the previous section has been modeled for a steel in/near-core conductor segment. In the model it is assumed that the bulk of the conductor line from the electricity source to the core region and then from the core region to the E-M does not undergo temperature changes. In contrast, the portion of conductor within the core region changes temperature in response to changes in the core temperature, and in proportion to those changes. This assumption is plausible, since changes within the core region are expected to be prompt, whereas outside they would not be. Outside the core region, temperature changes would also occur, but the scrambling response would be needed before such changes arise from the effect of heat conduction to the outside electrical conductors. With these assumptions, the electrical resistance, $R(T)$, of the E-M circuit can be written as

$$R(T) = R_0 + R_c(T), \quad (1)$$

where R_0 is the resistance of the balance of the circuit (outside core region) at normal operating temperature and R_c is the resistance of the portion of circuit within the core region as a function of the temperature T . The temperature dependence of R_c is given by

$$R_c(T) = \rho_0 [1 + \alpha(T - T_0)] \frac{L}{A}, \quad (2)$$

where it has been assumed that in the range of interest (within 50 °C of the nominal operating temperature) the conductor resistivity is a linear function of temperature. In equation 2, the resistivity at normal operating temperature is denoted by ρ_0 , the normal operating temperature is T_0 , and the temperature coefficient of resistivity is α . L is the length of conductor wire and A is its cross sectional area. Using equations 1 and 2 and Ohm's law, one determines the current flow in the E-M circuit for any given temperature. From the current I (expressed in amperes), the E-M force is obtained. It is given by [6]

$$F = s \left(\frac{NI}{ac} \right)^2 + \frac{CsNI}{a}, \quad (3)$$

where c is the leakage factor, C is the E-M pull in pounds per square inch per ampere-turn per inch, a is the air gap in inches, s is the cross section area of the core or plunger of the E-M in square inches, N is the number of coil turns in the solenoid, and l_s is the length of the solenoid. It is assumed that the wiring is made of cooper everywhere, except in the core region, where it is assumed that soft steel is used. The values assumed for the various parameters are shown in Table 1. For simplicity, it is assumed that all parameters remain valid and unchanged throughout the applicable temperature range. With these values, the pull force is found to be about 8.11-lbf at 900 °C. At 950 °C, the pull force drops to 7.70 lbf, and at 1000 °C, it is 7.33 lbf. Thus, as temperature increases from 900 °C to 950 °C or to 1000 °C, the E-M no longer develops the force necessary to hold an 8-lb rod in place and the rod falls under the influence of gravity. At the maximum value of the pull, the current is about 1 ampere. In that situation, the power dissipation in the entire circuit is under 5 watts, a negligible contributor to heating.

Table 1. Parameter values for EM pull model.

Symbol	Property	Value
c	EM leakage factor	2600
C	Pull factor	0.01 (lbf/in ² -Amp-turn-in)
l_s	Air gap	0.9 mm
s	Area of plunger cross section	2 in ²
N	Number of turns in solenoid (one layer)	200
	Length of solenoid	14.4 in
V	Voltage	5.5 V
D	Coil diameter	4.79 in
d_{Cu}	Diameter of Cu wire (excluding insulation)	1.434 mm
d_{Fe}	Diameter of soft steel wire (excluding insulation)	1 mm
L	Length of Cu wire in E-M	76.8 m
L'	Length of Cu wire outside E-M	30.5 m
L''	Length of soft steel conductor in/near core (non active coil)	10 m
ρ_{Cu}	Resistivity of Cu at 20 °C	1.76E-6 Ω-cm
α_{Cu}	Cu temperature coefficient of resistivity	0.004
ρ_{Fe}	Resistivity of soft steel at 20 °C	1.59E-5 Ω-cm
α_{Fe}	Soft steel temperature coefficient of resistivity	0.0016

4. Neutronics Performance

In this section, the results of a preliminary assessment of the scramming effectiveness of the EM-OSCR are presented. From the results of the previous section, it is clear that either a single control rod or a set of control rods of mass up to 8 pounds each could be held outside the core with a small current and little energy dissipation. The rod or rods would fall into the core when the temperature exceeds the nominal operating conditions by 50 °C. The effectiveness of one such rod or of a set of rods is evaluated for a hypothetical, though realistic,

PBR. For this demonstration, an MCNP model of this PBR was constructed. The PBR is of a size suitable for power plant use. Parameters characterizing the reactor and shutdown system are given in Table 2. The reactor model is identical to one recently used to study a similar concept [7] that relies on the presence or absence of flow and/or pressure for its operation.

The core was assumed to be uniform in composition, based on pebbles in which "TRISO" coated UO₂ microspheres are embedded in a spherical graphite matrix inside a shell of pure graphite. The pebbles are assumed to be packed in the core with a packing fraction of 0.61, which is a typically observed value. The fuel concentration is adjusted to produce a critical core when the control rods are suspended above the reflector. In this study, the four control rods were arbitrarily located at 90-degree intervals on a circle 75 cm in diameter, centered on the core axis. The model assumes a uniform core. This assumption introduces two sources of inaccuracy (ignoring the actual axial composition distribution of the asymptotic core loading pattern and ignoring the heterogeneity of the core). The extent of the effects of these inaccuracies is discussed in that work and in a previous study [7, 8], and it is shown that the model is sufficient for assessing changes in multiplication factor resulting from rod insertion. In Table 3, the effect of insertion of four control rods (off-centered, as described above) is shown for three different cases. The largest rod mass shown is 3.64 kg (or about 8 pounds). It is clear from these results that four such EM-OSCR rods are sufficient to scram the reactor, as the corresponding reactivity insertion would be of the order of -3.6\$. A set of four of the smallest rod shown would insert merely -0.76\$. Although this would be insufficient for a secure scram, it would be enough to maintain subcriticality after cooling of the core, which is the principal function of the OSCR rods. A higher reactivity hold-down variant of the EM-OSCR rod, for a more secure scram, could easily be devised, merely by increasing the voltage of the power supply to the E-M and hence increasing the E-M pull. These results show that the proposed emergency shutdown system can be devised to provide ample shutdown negative reactivity with control rods that can be supported easily by E-M pull corresponding to low currents and hence low energy dissipation, as discussed in the previous section.

Table 2. Model reactor and shutdown system design parameters.

Reactor and Shutdown System Design Parameters	
Core height	10 m
Core diameter	3 m
Fuel material	UO ₂
Reflector thickness (all around)	1 m
Reflector material	graphite
Control element material	boron carbide (B ₄ C)
Control element diameter	1 cm or 2.5 cm
Control element cladding material	Stainless steel
Control element cladding thickness	1 mm
Control rod guide tube material	Stainless steel
Control rod guide tube thickness	5 mm
Number of control rods	4
Radius of control-rod circle	75 cm
Length of control elements	1 m or 2 m
Packing fraction of pebbles in core	61%

Table 3. MCNP k_{eff} results and control rod masses

k_{eff} and EM-OSCR Rods Worth			
Control element length (m)	1.0	1.0	2.0
Control element diameter (cm)	1.0	2.5	2.5
k_{eff} (rods withdrawn)	1.00441	0.98793	0.98793
k_{eff} (rods inserted)	0.99940	0.97252	0.96452
Reactivity worth of 4 rods (\$)	0.76	1.8	3.6
Mass of one control rod (kg)	0.244	1.82	3.64

5. Rod Time of Descent

The EM-OSCR is expected to drop into the core during any abnormal occurrence in which the temperature in or near the core region exceeds its nominal normal range by more than 50 °C. Assuming that gaseous coolant is present in the guide tube and, conservatively, that no flow takes place, the law governing the fall of the rod is given by

$$M \frac{d^2x}{dt^2} = Mg - \frac{1}{2} C_d A_s \rho v^2, \quad (4)$$

where M is the mass of the rod, x is its displacement from its initial position, t is time, g the acceleration of gravity, C_d the coefficient of friction between the rod and the ambient gas, ρ the gas density, A_s the cross section area of the rod (projection), and v the relative velocity of the rod and the ambient coolant. If the normally downward coolant flow were present in the guide tube, the descent of the rod into the core region would be even faster. At the initiation of abnormal occurrences, the flow would still be downward, thus it is conservative to assume absence of flow. Another conservative assumption is to consider that no depressurization has taken place and that the rod must fall through the tube at full operational coolant pressure. It is noteworthy, however, that in the event of a breach of the pressure boundary, depressurization (the equivalent of the loss-of-coolant accident for a PBR) would be complete in less than 3 seconds [9]. With these assumptions, v reduces to the time derivative of x . Then equation (4) can be solved analytically. The solution,

$$x(t) = \sqrt{\frac{g}{\alpha}} t - \frac{1}{\alpha} \ln \left(\frac{2}{1 + \exp(-\sqrt{\alpha g} t)} \right), \quad (5)$$

where

$$\alpha = \frac{C_d A_s \rho}{2M}, \quad (6)$$

is used to determine the time of descent to any desired final position. For circumstances typical of PBR designs under consideration, such as an operating pressure of 6.99 MPa, the density of helium coolant would be about 3.42 kg/m³. Further, a friction coefficient of 1.0 is arbitrarily assumed (sensitivity calculations show that the results depend negligibly on this parameter). The rod cross section area is taken as 4.91 cm², corresponding to a 2.5-cm diameter. Then, for a mass of 1.8 kg, the descent time for a distance of 10 m is about 1.43 second. This time is hardly distinguishable from the time for free fall in vacuum. Drop times of roughly the same magnitude should be expected for more massive rods. It is clear from these results that the EM-OSCR would drop into the core well in advance of the times when it would be needed for reactivity hold-down.

6. Discussion and Conclusions

This paper has presented the concept and preliminary performance study of a passive, inherently safe, and fail-safe design for an emergency control rod. The functioning of the rod is based solely on inexorable physical laws. The operation of the rod in its emergency function does not require the intervention of a human operator, nor does it rely on any signal from a monitoring or safety system. Although the concept could be applicable to a variety of reactor types, in this paper it is applied to the emergency shutdown of a PBR. It is clear from this study that the EM-OSCR will drop into the core fast enough provide the required scram. It will also be within the core well in advance of the times at which it would be needed to prevent re-criticality following core cooling. Even if the rod were

dropped into the core much slower than the above study shows, it would be effective for this function. In all case, the EM-OSCR would constitute an effective backup system.

The neutronic effectiveness of the OSCR concept has also been demonstrated with a range of rod sizes. It is clear from the examples shown and from the discussion of larger rod masses (via larger currents or EM design modification) that large scrambling reactivities can be achieved. Further optimization of the EM-OSCR are of course possible, including via better positioning of the rods at location of larger neutronic importance or via more massive rods. All of these possible improvements warrant further study.

7. Acknowledgements

We are grateful to Drs. P. Pohl, C. Marnet and S. Storch for bringing reference 2 to our attention. This work was supported by the Department of Energy (DOE) under DOE Idaho Operations Office Contract DE-AC07-99ID13727.

8. References

1. D. R. Nichols, "Status of the Pebble Bed Modular Reactor," Nucl. Energy, 39, 4, 231, (2000).
2. R. Baumer et al., AVR – Experimental High-Temperature Reactor Book on AVR, 21 Years of Successful Operation for a Future Energy Technology, Association of German Engineers (VDI), The Association for Energy Technologies (Publi.), VDI-Verlag GmbH, Dusseldorf, 1990.
3. Krüger, K.J., and G.P. Ivens, "Safety-Related Experiences with the AVR Reactor," pp. 61-70, in IAEA-TECDOC-358, "Gas-Cooled Reactor Safety and Accident Analysis," proceedings of a specialists' meeting on safety and accident analysis for gas-cooled reactors organized by the International Atomic Energy Agency, held at Oak Ridge National Laboratory, Oak-Ridge, 13-15 May, 1985.
4. Krüger K., and J. Cleveland, "Loss-of-Coolant Accident Experiment at the AVR Gas-Cooled Reactor," pp. 455-462 in the "Fifth Proceedings of Nuclear Thermal Hydraulics" 1989 Winter Meeting, November 26-30, 1989, San Francisco, California, Sponsored by the Thermal Hydraulics Division of the American Nuclear Society, ANS 1989.
5. Nakagawa, S., A. Saikusa, and K. Kunitomi, "Development of a Simulation Model and Safety Evaluation for a Depressurization Accident without Scram in an Advanced HTGR," Nuclear Technology, pp. 141-152, Vol. 133, Feb, 2001.
6. Fink, D. G., and J. M. Carroll, "Standard Handbook of Electrical Engineers," 10th Ed., pp. 5-4 through 5-9, McGraw Hill, 1968.
7. Ougouag, A. M., R. R. Schultz, W. K. Terry, and A. G. Stephens, "Preliminary investigation of an Optimally Scramming Control Rod for Gas-Cooled Reactors," paper ICONE 10-22778, accepted for publication in proceedings of ICONE-10, International Conference on Nuclear Energy, April 14-18, 2002, Arlington, Virginia.
8. Ougouag, A.M. and W. K. Terry, "A Preliminary Study of the Effect of Shifts in Packing Fraction on k-effective in Pebble-Bed Reactors," American Nuclear Society Mathematics & Computation Division Conference, Salt Lake City, Utah, September 9-13, 2001.
9. D. A. Petti, et al., Modular Pebble-Bed Reactor Project, W. K. Terry, Editor, p. 65, INEEL/EXT-2001-1623, December 2001.

**AN INHERENT SAFE HTGR POWER PLANT:
AN INNOVATIVE DESIGN CONCEPT**

A. Hodzic, Environment & Energy Engineering EEE, Germany

Paper will be handed out separately

AN IN-DEPTH STUDY ON OSCILLATION PECULIARITIES BY STEP-INPUT OF REACTIVITY AND FREQUENCY OF HELIUM FAN'S TRANSDUCER OF 10 MW HIGH TEMPERATURE GAS-COOLED REACTOR AND ITS CONTROL STRATEGY

XIAOJIN HUANG

*Department 401, INET
Tsinghua University, 100084 Beijing - China*

ABSTRACT

In order to know more deeply about dynamic characteristics of 10 MW High Temperature Gas-Cooled Reactor (HTR-10), the dynamic math model of HTR-10 is established. On the basis of this model, the paper simulates and studies on the main dynamic processes of HTR-10, especially the oscillation peculiarities that are very different from PWR. The conclusions are: the main reason of oscillation caused by step reactivity disturbing is that the special structure of HTR-10's fuel component causes fuel granule's temperature to change slower than nuclear power; the main reasons of oscillation caused by step-input frequency disturbing of helium fan's transducer are the structure, flux and pressure peculiarities of HTR-10 primary loop, and synchronous vibration between HTR-10 primary and secondary loop. In order to make reactor running smoother and safety, the multi-layer harmony control strategy is adopted. This paper also discusses the design outlines of the under layer controllers.

1. Introduction

High Temperature Gas-Cooled Reactor is a kind of advanced new-style nuclear reactor. 10 MW High Temperature Gas-Cooled Reactor (HTR-10) has been built and reached critical in China at the end of 2000 year. In order to aim at the rating power and continued running and also to satisfy analysis and design on I&C system of HTR-10, knowing more deeply about its dynamic characteristics is pressed for.

2. Dynamic math model of HTR-10

The dynamic math model of HTR-10^[1] shown in figure 1 is composed of reactor core model, once-through steam generator model, helium fan model, feed water pump model, pipe model, and turbine-power generator model, etc. The four input variables are reactivity, transducer frequency of helium fan and feed water pump, steam regulator valve. The model's dynamic characteristics are multi-variables, strong coupling, non-linear and distributed parameters. In figure1, the solid arrowhead represents flowing direction of helium gas and water or steam. The hollow arrowhead represents heat

exchange between primary and secondary loop of HTR-10.

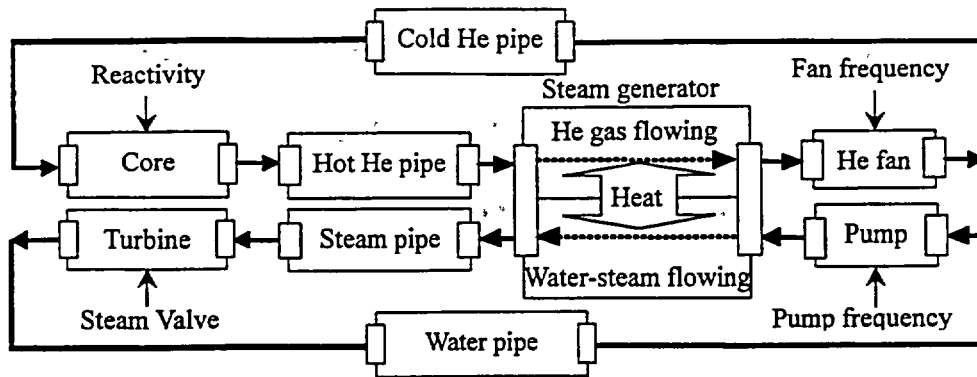


Fig 1. The math model of HTR-10

3. Dynamic characteristics simulated of HTR-10 by step reactivity disturbing

The computing initial conditions are: a) steady system status at 30% rating power, b) 2×10^{-4} reactivity step-input at 100s. The curve of relative power increment ΔP , whose definition is power increment divided by 30% rating power, is shown in figure 2.

4. Simulating results

Figure 2 clearly indicates that the relative power increment presents a decreasing amplitude oscillation. Its oscillation period is about 400s and the ΔP oscillates about 6 times. Because HTR-10 has large negative temperature reactivity coefficient and the negative temperature reactivity feedback can compensate the input reactivity disturbing, the amplitude of power change decreases gently and finally reaches the steady status. On the other hand, because negative temperature reactivity coefficient also causes large initial error of power at the beginning of dynamic process, the ΔP 's transitional process time is very long from oscillation to steady status.

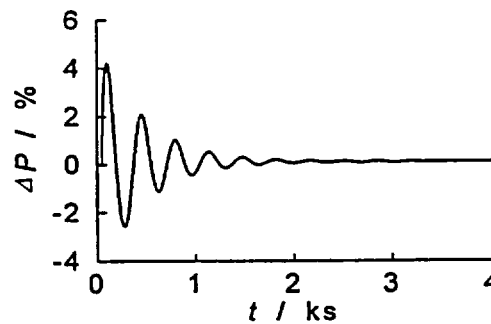


Fig2. 30% rating power, 2×10^{-4} reactivity step-input at 100s, curve of ΔP

5. Reasons discussed and analyzed of oscillation peculiarity

The structure and techniques of HTR-10's global fuel component differs greatly from PWR's fuel module. Because the fuel and moderator is separate in PWR, the heat exchange area is relative small. When power changes, the fuel temperature almost changes immediately. Because the response of fuel temperature is very quickly, the negative temperature reactivity feedback can quickly and effectively restrain the change of nuclear power.

HTR-10's global fuel component is composed of very small fuel granule which dispersing in the black lead moderator. It has two distinct structure characteristics: a) because fuel granule is very small and disperses inside the global fuel component and contacts closely with surrounding black lead moderator, the heat exchange area is relative large and heat exchange is plenty. b) The proportion of black lead

moderator is bigger than that of fuel granule in the global fuel component. The fission energy produced in the fuel granule is absorbed quickly by surrounding black lead moderator, thus the temperature difference between fuel granule and surrounding black lead moderator is very small. Compared with PWR's fuel module, the fuel granule temperature changing time is delayed. Therefore, the slow change of fuel granule temperature lags behind the fast change of nuclear power, and the negative temperature reactivity feedback cannot restrain the change of nuclear power in time. The above-mentioned analysis explains why the nuclear power has an oscillation peculiarity.

6. Dynamic characteristics simulated of HTR-10 by step frequency disturbing of helium fan's transducer

In order to concentrate on characteristics by step-input frequency disturbing of helium fan's transducer, the influence of power oscillation on the nuclear system, which caused by reactivity disturbing, must be eliminated or greatly weakened. So the nuclear power regulator is added into HTR-10's math model. The computing initial conditions are: a) steady system status at 30% rating power, b) 2% frequency step-input of helium fan's transducer at 100s. The curve of outlet helium flux of reactor core Q is show in figure 3.

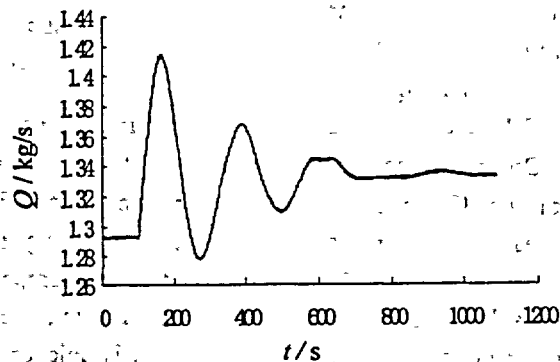


Fig3. 30% rating power, 2% frequency step-input of helium fan's transducer at 100s. curve of Q

7. Simulating results

Figure 3 clearly indicates that even though nuclear power regulator is added and power oscillation caused by reactivity disturbing is greatly weakened, however, the large decreasing amplitude oscillation process of helium flux appears. The oscillation period of helium flux is about 220s and Q oscillates about three times. Because oscillation period and times are all shorter than that of power oscillation caused by reactivity disturbing which mentioned in section 4, and the additional power regulator also greatly weakens the power oscillation, so their reasons of oscillation are different to a certainty.

8. Reasons discussed and analyzed of oscillation peculiarity

Firstly, the system structure and technical flow of HTR-10 primary loop is analyzed. a) HTR-10 primary loop is a close helium loop. Only a gas gate is put into the inlet of helium fan, whose function is preventing nature cycling flow of helium in the reactor core, and does not function during the normal reactor-running period. Thus HTR-10 primary loop lacks resistance component, which stabilizes helium flux in primary loop system. b) The regulation of system helium gas completely depends on transducer of helium fan. Though helium system absolute pressure is very high (about 3 MPa), relative pressure is very low (about 50KPa at rating power) and the properties of helium are compressible, easily flowing, sensitive to temperature and pressure. Thus, the helium flux of primary loop is sensitive to some disturbing factor. When input frequency of helium fan's transducer changes, helium flux fluctuation will present easily. Therefore, the structure and technical flow of HTR-10 primary loop system causes the helium flux to fluctuate very easily.

Secondly, the physical property of HTR-10 primary loop is analyzed. The influence factors on resistance-flux-relative pressure property of primary loop are very complicated. When helium gas flows smoothly, it can be considered as incompressible liquid. When helium gas does not flow smoothly or its flux is in a dynamic process, its compressible property must be considered. For example, because some component such as reactor core or steam generator stores a large number of helium gas, changing inlet helium temperature of these components will cause a typical taking in and sending out process of the outlet helium flux. One of the typical processes of reactor core is shown in figure 4. Figure 4 shows the outlet helium flux Q dynamic curve of reactor core at 30% rating power when its inlet helium temperature has 5% step-input change at 100s. This taking in and sending out process of the outlet helium flux is explained as follows. When inlet helium temperature has a step change, the density of inlet helium gas decreases. But the inlet helium mass flux does not change, so the velocity of flow of inlet helium gas increases. Because flow process is quicker than heat exchange of helium gas, the change of outlet helium temperature lags behind velocity of flow of outlet helium gas. Thus, the change of outlet density of helium is delayed and the outlet helium flux increases at the beginning. According to the law of conservation of mass, because the inlet helium mass flux does not change, the outlet helium flux finally comes back to its original value. Therefore, a typical taking in and sending out process of the outlet helium flux is formed.

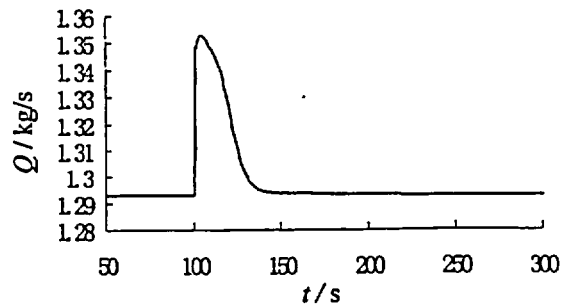


Fig4. 30% rating power, 5% inlet helium temperature step-input of reactor core at 100s, curve of its outlet helium flux Q

Finally, the strong coupling between HTR-10 primary and secondary loop is analyzed. Because complicated and strong coupling exists between HTR-10 primary and secondary loop, the sympathetic vibration phenomenon occurs. The outline of coupling process is as follows: when helium flux oscillation of primary loop happens by some disturbing, the outlet steams flux and temperature of the steam generator will change greatly; then because the outlet of steam generator is steam turbine, the feed water flux of second loop also changes; then the heat exchange condition changes between helium gas of primary loop and water of secondary loop in the steam generator; then the outlet helium temperature of steam generator changes; because of the gas compressible property, the taking in and sending out processes of the helium gas flux in some devices are formed and are added on the original helium flux oscillation of primary loop. Thus, the helium flux oscillation amplitude of primary loop is greater than before. Therefore, the complicated oscillation process with feedback coupling is formed.

9. Control strategy

When HTR-10 nuclear system is running, it is not allowed that the important system variables, such as nuclear power and helium flux etc, presenting oscillation with long time and large amplitude. Therefore these factors must be considered sufficiently when designing on I&C system and control strategy of HTR-10. In order to eliminate the loop oscillation during reactor's running such that to make reactor running safety and smoother, aiming at HTR-10's dynamic characteristics, the control strategy of HTR-10 adopts multi-layer and harmony control scheme. The HTR-10 automatic control system is divided into two layers: under layer local control loop and super layer harmony control loop.

The main purpose of introducing under layer local control loop is to improve dynamic quality of HTR-10 system, to eliminate or greatly weaken system oscillation peculiarity, and to well bottom the design of super layer harmony control loop.

Aiming at power oscillation caused by reactivity disturbing, the under layer PID regulator of nuclear power can be introduced to overcome power oscillation. Aiming at HTR-10 primary loop helium flux oscillation caused by input frequency disturbing of helium fan transducer, according to the main reasons of oscillation, the under layer local helium flux PID controller of primary loop and under layer local feed water flux PID controller of secondary loop can be introduced on the precondition of not changing the structure and technical flow of HTR-10 system. The controller design outlines are: a) selecting appropriate parameters of PID controller in order to change the natural frequency of primary and secondary loop and break the condition of sympathetic vibration between them, b) introducing appropriate helium gas temperature compensator to counteract the influence of helium gas temperature change and in order to weaken or eliminate the taking in and sending out process of the helium gas flux, which caused by helium gas temperature fluctuation.

The next in-depth study and simulation indicate that if the above control strategy and design outlines of controller are adopted, the system oscillation will be greatly weakened and thereby the dynamic running quality of HTR-10 will also be distinctly improved.

10. Conclusion

The conclusions of above-mentioned simulating results and analysis are as follows:

- a) The main reason of system oscillation caused by step reactivity disturbing is that the special structure of HTR-10's global fuel component causes fuel granule's temperature inside the component to change slower than nuclear power, and then makes the negative temperature reactivity feedback not to restrain the change of nuclear power in time.
- b) The main reasons of system oscillation caused by step-input frequency disturbing of helium fan's transducer are the structure and technical flow of HTR-10 primary loop, the physical property such as helium flux and relative pressure peculiarities of HTR-10 primary loop, and the synchronous vibration caused by strong coupling between HTR-10 primary loop and secondary loop.

In order to eliminate the loop oscillation during reactor's running such that to make reactor running safety and smoother, the control strategy of HTR-10 adopts multi-layer and harmony control scheme. Through selecting appropriate parameters of under layer local PID controller and introducing appropriate helium gas temperature compensator, the dynamic quality of HTR-10 system is improved, the system oscillation peculiarity is eliminated or greatly weakened, and the design of super layer harmony control loop is well bottomed.

References

- [1] Xiaojin Huang. Dynamic Models of 10MW High Temperature Gas-Cooled Reactor and Studies on its Dynamic Characteristics [D]. Beijing TsingHua University, China, 1998. (In Chinese)

THERMAL INSULATION FOR HOT GAS DUCTS

P. Bröckerhoff, Forschungszentrum Jülich, Germany

Paper will be handed out separately

Stress and Seismic Calculation of HTR-10 SG Accident Discharge System

DONG Jianling¹ Jiyang Fu Suyuan Yu
(INET Tsinghua University Beijing 100084 P.R. of CHINA)

ABSTRACT

Steam Generator (SG) heat transfer tubes of 10MW High Temperature Gas Cooled Reactor (HTR-10) are protective screens between the primary loop of helium and the secondary loop of water and steam. Water and steam will enter into the primary loop from the secondary loop if the SG heat transfer tubes rupture, which lead to increase of the primary loop pressure and discharge of radioactive materials.

Function of the SG accident discharge system (SGADS) is to discharge water and steam, so that the amount of water entering into the primary side could be reduced. The SGADS is connected with the main feedwater piping system. If the pipe ruptures, the coolant of the secondary loop will lose. This might cause unplanned reactor shut down. So it is important to guarantee the integrity of the SGADS. This paper presents stress and seismic calculation and analysis of the SGADS by use of PIPESTRESS. Results show that stress distributions satisfy the requirements of ASME codes for Classes 2 components.

Key words: high temperature gas cooled reactor, SG accident discharge system, pipe, stress

1. Introduction

10MW High Temperature Gas Cooled Reactor (HTR-10) was constructed in Tsinghua University and reached the first criticality in November 21, 2000. In the reactor, steam generator (SG) heat transfer tubes of HTR-10 are protective screens between the primary loop of helium with radioactivity and the secondary loop of feeding water and steam without radioactivity. Water and steam will enter into the primary loop from the secondary loop when rupture of the heat transfer tubes occurs, which lead to increase of the primary loop pressure and discharge of radioactive materials. Therefore, it is important to reduce the amount of water and steam entering into the primary loop.

The principal function of the HTR-10 SG accident discharge system (SGADS) is to discharge water and steam of the secondary loop when the SG heat transfer tubes rupture and water and steam getting into the primary loop from the secondary loop occurs so that the amount of water entering into the primary side could be reduced^[1].

The HTR-10 SGADS is directly connected to the main feedwater pipe of SG. If the pipe of the HTR-10 SGADS ruptures, water and steam will lose, and the heat produced by the reactor could not be carried out normally. This might cause unplanned shut down of the reactor. So to guarantee the integrity of the SGADS is important. This paper conducts stress and seismic calculation and analysis of the SGADS using FEM code of piping stress analysis, PIPESTRESS, under various load cases, such as normal operation loads, seismic loads and the propulsive load produced as the discharge valves open, etc.

2. The SGADS and its working environment

Figure 1 is the layout of the SGADS. It could be seen from the figure that the system consists of a shutoff valve JED-AA01, two discharge valves JED-AA02, JED-AA03, a SG discharge tank JED-BB01, pipe segments and supports H₁~H₁₀. The upper end of the SGADS piping system is directly connected to the feeding water piping system LAB. The joint point of the two systems is located between the shutoff valve JED-AA01 and SG. The lower end of the SGADS piping system is

¹ Correspondent author. Address for correspondence: Beijing 100084, P.R. of CHINA.
Tel: 8610-62784809 Fax: 8610-62771150 E-mail: jianling@mail.inet.tsinghua.edu.cn

Material of the main water feed pipe is 20G, a Chinese low carbon steel, mechanical properties of which are shown in table 1. Material of the SGADS pipe is stainless steel 321^[2], mechanical properties of which are shown in table 2. In table 1 and table 2, allowable stress range $S_A=1.25S_c+0.25S_b$ ^[3].

4. Stress calculations

4.1 FEM model

According to the distribution of the fixed supports shown in figure 1, the SGADS piping system was considered as comprising three parts. The first part was the main feedwater pipe located between the main feedwater nozzle of SG and the first fixed support of the main feedwater piping system. The second part was the SGADS pipe located between the joint point and the support H₇. The third part was the SGADS pipe between the support H₇ and the discharge tank JED-BB01. The discrete piping system were obtained by use of pipe elements, in which one pipe element was connected to the adjacent pipe elements by nodes. Mass of elements was considered to concentrate in nodes. The valves were simulated by rigid elements. The FEM model is shown in figure 2.

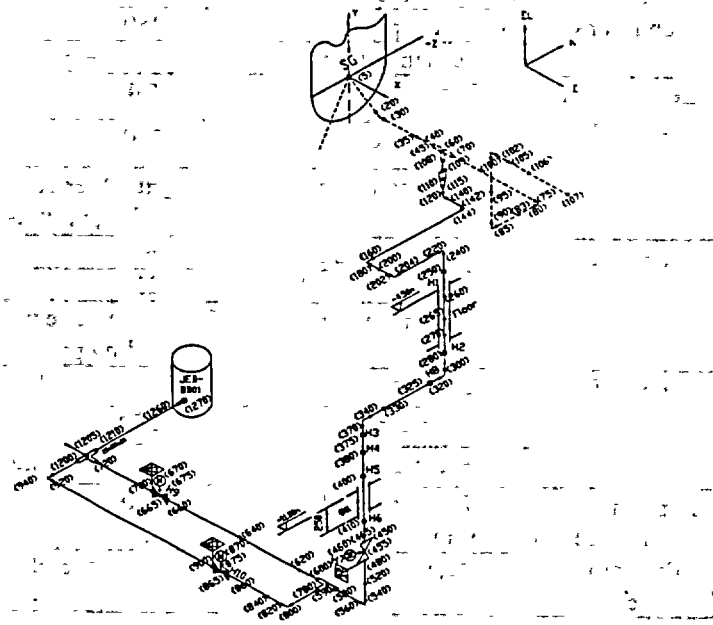


Figure 2 FEM model

4.2 Loads

Loads applied to the SGADS piping system were internal pressure, gravitational force, thermal expansion force, propulsive force, seismic loads or combination loads above, as shown in table 3. In the table, the main feed water pipe I represents the main feedwater system pipe located between the main feedwater nozzle of SG and the joint point, and the main feedwater pipe II represents the main feedwater system pipe located between the joint point and the first fixed support of the main feedwater piping system.

1) Continuous loads

The continuous loads were internal pressure, weight and restrain counterforce. Internal pressure in the SGADS pipe was determined by that of the main feedwater pipe. Weight of the SGADS pipe included that of pipe itself and the insulating layer. Material of the insulating layer was silicate cotton, specific density of which was 207kg/m³, thickness of which was 40mm. The insulating layer was laid down the main feedwater pipe and the SGADS pipe located between the joint point and the shutoff valve JED-AA01.

2) Propulsive force

The SGADS was a kind of closed type discharge equipment. The propulsive force produced by the discharge valve was calculated according to the method of Appendix O^[2]. In reference 5, it had been shown that water hammer produced by switchover of the valves could not make the piping systems ruptured, and the maximum internal pressure were less than the design pressure of the piping system, 6.4MPa.

3) Seismic loads

From section 4.1, it is known that the SGADS piping system was considered as consisting of three parts. Seismic inputs of the first part and the second part was from the main feedwater nozzle of SG, the first fixed support of the main feedwater piping system and the support H₇ of

the SGADS piping system, while seismic inputs of the third part were from the support of the SGADS support H₇ and the SGADS nozzle of the discharge tank JED-BB01.

Table 3 Load conditions

Loads		Discharge system pipe	Main feedwater pipe I	Main feedwater pipe II
Design conditions	Design pressure (MPa)	6.4	6.4	
	Design temperature (°C)	250	250	150
	Mechanical loads	Weight and other continuous loads		
Level A and level B	Pressure (MPa)	6.4	6.4	
	Temperature (°C)	250	250	150
	Mechanical loads	Weight, other continuous loads and accidental loads including propulsive force and seismic load OBE		
Level C	Pressure (MPa)	6.4	6.4	
	Temperature (°C)	250	250	150
	Mechanical loads	Weight, other continuous loads and accidental loads including propulsive force and seismic load SSE		
Level D	Pressure (MPa)	6.4	6.4	
	Temperature (°C)	250	250	150
	Mechanical loads	Weight and limit accidental load cases		
Experimental load case (hydraulic test)	Pressure (MPa)	8.0	8.0	
	Temperature (°C)	20	20	
	Mechanical loads	Weight, other continuous loads		

Reference 6 supplied acceleration spectrums of the positions located fore and after the acceleration input points. For example, the height mark of the SGADS support H₇ was -13m, but reference 6 only supplied the acceleration spectrums of the points height mark of which were -15.3m and -10m, respectively, and the values were OBE ($a_{x1}=0.58g$, $a_{y1}=0.65$, $a_{z1}=0.58g$; and $a_{x2}=0.6g$, $a_{y2}=0.65g$, $a_{z2}=0.65g$). Therefore, the acceleration values were taken as OBE ($a_{x1}=0.6g$, $a_{y1}=0.65$, $a_{z1}=0.65g$). In the same way, the acceleration input values of the other supports were obtained, as shown in table 4, where ratio of damping is 0.2%.

Diameter of the SGADS piping system was less than 60mm. So stress calculation was conducted by equivalent static load method according to reference 7. The equivalent static loads of the systems were obtained by multiplying the acceleration values in table 4 by 1.5 times mass of pipes. Values obtained were used as acceleration inputs in FEM calculations.

Table 4 Seismic input acceleration values

Positions	Acceleration (g)	X	Y	Z
Main feed water nozzle of the SG	OBE	2.6	2.5	2.6
	SSE	2.6	2.45	2.5
First fixed support of the main feed water pipe	OBE	1.0	0.75	1.1
	SSE	1.2	1.2	1.2
Fixed support H ₇	OBE	0.6	0.65	0.65
	SSE	1.2	1.1	1.15
Fixed support between the shutoff valve and the nozzle of the discharge tank	OBE	0.6	0.65	0.65
	SSE	1.2	1.1	1.15

4.3 Displacement boundary conditions

Suppose that the position of the reactor pressure vessel axis does not change. Then expansion of the reactor pressure vessel and the hot gas duct makes the position of the SG pressure vessel axis move.

Linear expansion coefficient of the two pressure vessels and the hot gas duct was $13.6 \times 10^{-6} / ^\circ\text{C}$ at the temperature of 325°C . Therefore, the displacement of the SG pressure vessel axis was 30.36mm. According to the position of the main feed water nozzle in SG, displacement components of the nozzle $\Delta_x = 30.36\text{mm}$, $\Delta_y = -8.16\text{mm}$, $\Delta_z = 2.89\text{mm}$, where the directions of x, y, z were from west to east, south to north and vertically upward, respectively.

4.3 Stress calculations

The stress calculation of the SGADS pipe was conducted in two parts. Part 1 was the pipe located between the joint point and the fixed support H₇. Part 2 was the SGADS pipe part between the fixed support H₇ and the SGADS nozzle in the discharge tank JED-BB01.

The input file of PIPESTRESS could be gotten by use of geometric conditions (length, outer diameter and wall thickness of pipe, etc.), material properties (Young's modulus, allowable stress, linear thermal expansion coefficient, etc.), load cases and displacement boundary conditions. Starting the code, the three force components and moment components could be obtained.

5. Calculation results and analysis

Table 5 gives stress ratios in the two parts of the SGADS. In the table, values in the brackets are node numbers of the FEM model, where the maximum stress ratios equal the maximum stress divided by the stress limit. From table 5, it could be seen that the extremum stresses occur at node 280, 115 and 1270, respectively. Therefore, these positions are dangerous positions. Besides, all the stress ratios in these positions are less than 1, so satisfy the requirements for class 2 components in ASME section III. According to reference 3 and reference 4, the SGADS piping system is safe.

Table 5 Stress ratios

Load cases	Stress limits	Maximum stress ratios	
		Part 1	Part 2
Design condition	$1.5S_h^{[3]}$	0.144(105)	0.09(1270)
Level A and level B	$1.8S_h^{[3]}$	0.946(280)	0.236(480)
Level C	$2.25S_h^{[3]}$	0.737(280)	0.189(480)
Level D	$3.0S_h^{[3]}$	None	None
Thermal expansion load case	$S_A^{[3]}$	0.951(115)	0.971(1270)
Experimental load case	$0.9S_y^{[4]}$	0.139(105)	0.104(1270)

References

- [1] Li Weihua. Design sheets for the HTR-10 SG accident discharge system. HTR-10 Report 4.7.2, 1997.
- [2] ASME Boiler and Pressure Vessel Committee. ASME Boiler and Pressure Vessel Code, Nuclear Equipment Appendix, The American Society of Mechanical Engineers, New York, 1983.
- [3] ASME Boiler and Pressure Vessel Committee. ASME Boiler and Pressure Vessel Code, Nuclear Equipment Class 2 Components, The American Society of Mechanical Engineers, New York, 1992.
- [4] ASME Boiler and Pressure Vessel Committee. ASME Boiler and Pressure Vessel Code, Nuclear Equipment Class 1 Components, The American Society of Mechanical Engineers, New York, 1992.
- [5] Department of Mechanics of Tsinghua University. Water Hammer Analysis on HTR-10 SG Accident Discharge System, 1998.
- [6] Wang Tajun, Zhu Bao, etc. Analysis on Interaction of HTR-10 Reactor Factory Building Soil and Structure and Calculation of Floor Response Spectrum. HTR-10 Report 2.5.2, 1996.
- [7] China National Nuclear Safety Office. Safety Guide Rules: Seismic Design and Verification for Nuclear Power Plant, Nuclear Safety Codes: HAF0215 (1), 1996.

MODELLING OF THE HTTR IN FLOWNET

P.G. ROUSSEAU and G.P. GREYVENSTEIN

*School of Mechanical & Materials Engineering, Faculty of Engineering
Potchefstroom University for CHE, Potchefstroom, 2520 – South Africa*

ABSTRACT

Flownet is a user-friendly software package allowing the dynamic simulation of mass, momentum and energy transfer in thermal-fluid networks integrated with controllers. It is currently used extensively in the modelling and design of the South African Pebble Bed Modular Reactor (PBMR) power plant. The code was recently extended to include a model for the High Temperature engineering Test Reactor (HTTR) that is currently being demonstrated by Japan Atomic Energy Research Institute (JAERI). This paper describes the thermal network and flow path discretization that is used to simulate the physical geometry of the reactor core for the simultaneous solution of the governing equations in the fluid passages and solid structures. The numerical integration and solution scheme for the equations are discussed in an accompanying paper. The current paper also shows results of a preliminary steady-state sample calculation.

Introduction

Flownet is a user-friendly thermo-hydraulic network simulation software package developed at the Engineering Faculty of Potchefstroom University. Flownet allows detailed steady-state and transient thermo-hydraulic simulations fully integrated with PID controller algorithms. The simulation ensures complete conservation of mass, momentum and energy while accounting for non-ideal gas behaviour, compressibility effects such as choked flow through orifices, the dynamics of turbo units as well as thermal storage in heat exchangers and other components. Flownet is currently used extensively in the modelling and design of the South African Pebble Bed Modular Reactor (PBMR) power plant. As part of the IAEA coordinated research program on the evaluation of High Temperature Gas cooled Reactor (HTGR) performance, the code was recently extended to include a model for the helium cooled High Temperature engineering Test Reactor (HTTR) that is currently being demonstrated by Japan Atomic Energy Research Institute (JAERI). The aim of this paper is to describe the thermal network and flow path discretization used to simulate the physical geometry of the reactor core and to present preliminary results of a steady-state sample calculation.

Physical geometry of the reactor core

A detailed description of the reactor geometry and materials as well as the reactor cooling system is provided in reference [1]. The reactor core is contained within a pressure vessel with plenums at the top and bottom. The coolant enters the pressure vessel at the bottom and flows vertically upward outside of the core in a flow passage formed between the reactor core and the pressure vessel. The flow then enters the core from the top plenum. The gas flows downward through cylindrical flow passages in the reflector and plenum blocks and through annular flow passages formed between the fuel rods and the fuel assembly blocks. At the bottom of the core the hot gas flows into a plenum and exits the pressure vessel via a hot pipe at the bottom of the vessel. The reactor core is made up of layers of various different fuel assembly blocks and reflector blocks. A schematic of the reactor core layout is shown in Figure 1. The outside of the core is made up of permanent reflector blocks with a twelve-sided shape when viewed from the top. Inside of the permanent reflector blocks is a single layer of hexagon-shaped replaceable graphite reflector blocks. To the inside of this, there is a layer of hexagon-shaped fuel assembly blocks (numbered 3 and 4 in the figure) each with a height of 580 mm. The next layer contains graphite control rod guide blocks and fuel assembly blocks (numbered 2 in the figure) in an alternating pattern.

The next layer contains only fuel assembly blocks (numbered 1 in the figure) and in the centre is a single control rod guide block. The maximum outer diameter of the core is 4250 mm and the height of the core is 5250 mm.

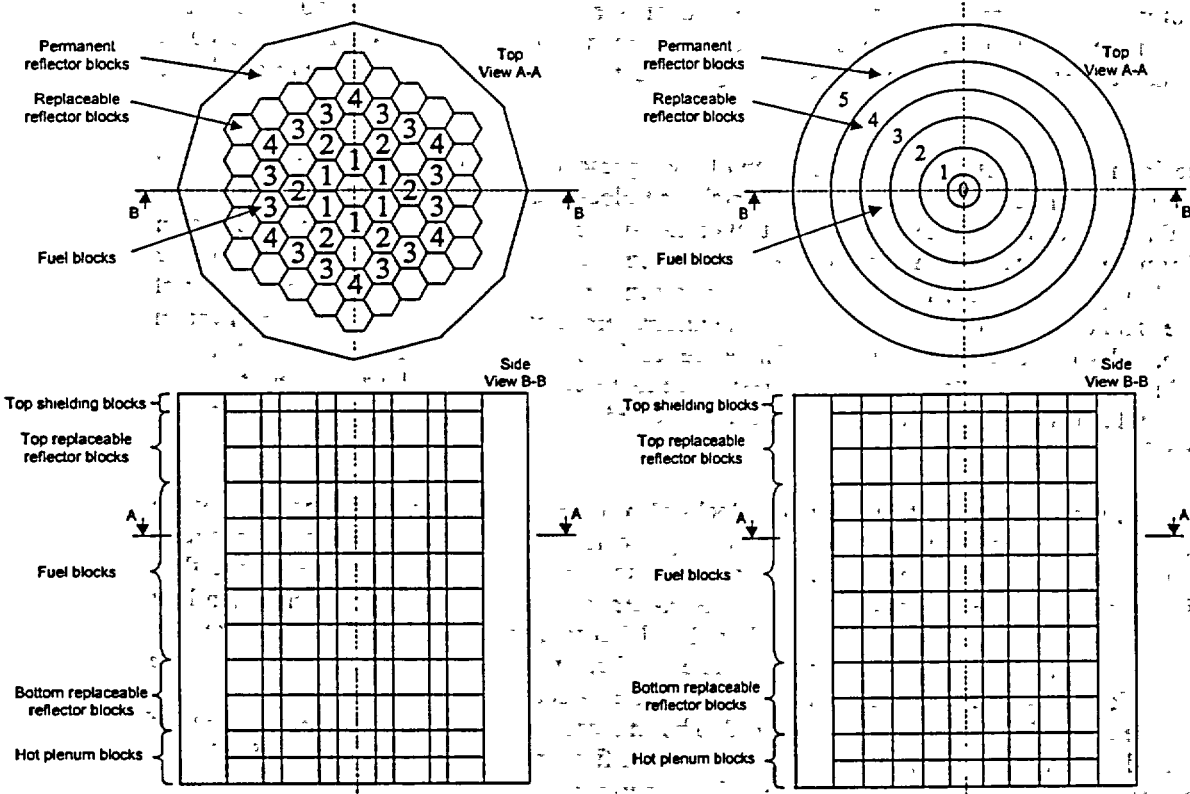


Fig 1. Schematic of reactor core geometry.

Fig 3. Schematic layout of axi-symmetric core.

The fuel assembly blocks numbered 1 and 2 each contain 33 fuel rods while the blocks numbered 3 and 4 each contain 31 fuel rods. The fuel rods are each 577 mm long, i.e. 3 mm shorter than the fuel assembly blocks. Figure 2 shows a three-dimensional schematic of the fuel rod assembly. The fuel rod consists of a fuel compact with inner diameter of 10 mm and outer diameter of 26 mm. The fuel compact is contained in a graphite sleeve with an outer diameter of 34 mm. The fuel rod is inserted into holes with a diameter of 41 mm in the fuel assembly blocks.

Flownet reactor core model

In the Flownet reactor model the reactor core is reduced to the simplified axi-symmetric two-dimensional geometry shown schematically in Figure 3. The outer ring represents the permanent reflector blocks while the ring just inside of that

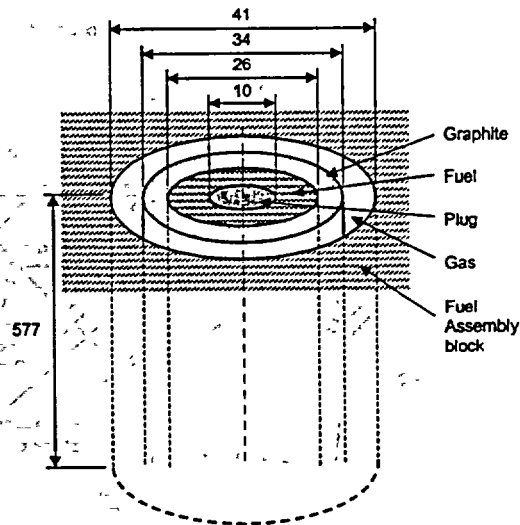


Fig 2. Schematic of fuel rod assembly.

represents the replaceable reflector blocks. The ring numbered 3 represents the fuel assembly blocks numbered 3 and 4, i.e. 18 fuel assembly blocks in total. The ring numbered 2 represents the fuel assembly blocks numbered 2 as well as the reflector blocks in-between the fuel blocks, i.e. a total of 12 blocks. The composition of ring 2 is assumed to be homogeneous with an average of only 16.5 fuel rod per block to account for the reflector blocks in-between. The ring numbered 1 represents the six fuel blocks also numbered 1 and the central cylinder represents the single reflector block at the centre of the original core geometry.

When viewed from the top, the surface area of each of the representative axi-symmetric rings is exactly the same as the total surface area of all the hexagon-shaped blocks represented by that ring. Also, the 'donut-shaped' rings each have the same height as that of the layer of blocks that it represents, as shown in Figure 3. Therefore, the total thermal mass of the axi-symmetric core will be exactly equal to that of the original core during transient events. Each of the rings can be discretized into a number of control volumes in the axial direction to improve accuracy. A uniform temperature distribution is assumed within each of the control volumes at any time step. Therefore, each control volume can be represented by a single thermal mass node connected via a thermal resistance to the adjacent thermal mass nodes at the top, bottom, inside and outside. The thermal resistances are adjusted to account for the porosity of the blocks containing the flow passages.

Each of the nodes representing the fuel assembly blocks also represents the surface temperature of the flow passages inside the fuel assembly block containing the fuel rods. This surface temperature is connected via a forced convection heat transfer resistance to the gas flow passing through the flow passages. The gas flow in the fuel assembly blocks is in-turn connected via a forced convection heat transfer resistance to the outside surface of the graphite shield that forms part of the fuel rod. The graphite shield and fuel compact can in turn be discretized into a number of layers each represented by a single thermal mass node and connected to the adjacent nodes via conduction heat transfer resistances. The innermost surface of the fuel compact can be assumed to be an adiabatic surface since the heat capacity of the gas contained within the inner cylinder is negligible. As a first approximation the effect of radiation between the fuel rod surface and the fuel assembly block surface as well as heat losses on the outside surfaces of the core were neglected. The reactor power is distributed within the fuel compact layers only. Figure 4 shows the thermal network representing the heat transfer for a single fuel assembly block control volume.

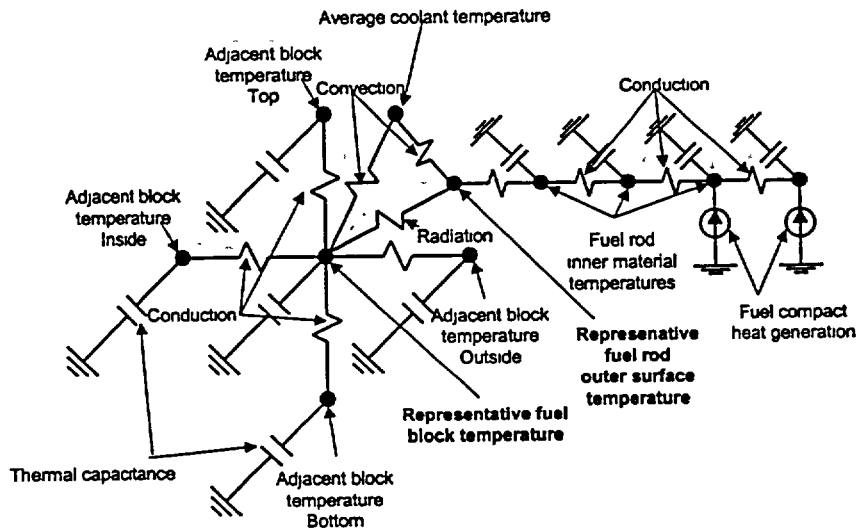


Fig 4. Thermal network representing the heat transfer for a single representative fuel assembly block control volume.

The gas flow path through the core from the plenum at the top to the plenum at the bottom is formed by a combination of cylindrical and annular flow passages. A section through the geometry of a typical flow path is shown schematically in Figure 5. The flow path is discretized as indicated by the node-element-node configuration shown on the right-hand side of Figure 5. A node is represented by a square and an element by a circle. An element represents a single pipe or duct component with a fixed cross-sectional area, wetted perimeter and hydraulic diameter. A node in this case simply represents a connection between two elements. Although only one flow element is shown in the schematic, each block can be discretized into any number of smaller flow elements in order to improve accuracy.

For each flow element the transient fully compressible form of the mass, momentum and energy conservation equations are solved using the so-called Implicit Pressure Correction Method [2]. The frictional losses are determined as a function of Reynolds number based on the Darcy-Weisbach formulation for the friction factor. Specific inlet- and outlet secondary loss coefficients are also specified for each element in both the forward and backward flow direction based on the geometry shown in Figure 5. For the heat transfer calculation heat transfer to the walls are based on the Nusselt number formulations provided in reference [1]. The complete flow element and solid thermal mass node network is shown in Figure 6 for the case where each ring in the axi-symmetric core is only represented by a single control volume.

Based on the neutronic power generated within the fuel elements, a fixed axial power distribution profile is specified along the height of the reactor [1]. The normalised power distribution profile as a function of the normalised position along the height of the fuel block section in the reactor is shown in Figure 7. At present the calculation of the neutronic power is not included in the model. However, for steady-state conditions a fixed value of the total power can be specified and for reactor scram transients a suitable time-dependent decay heat power curve is specified.

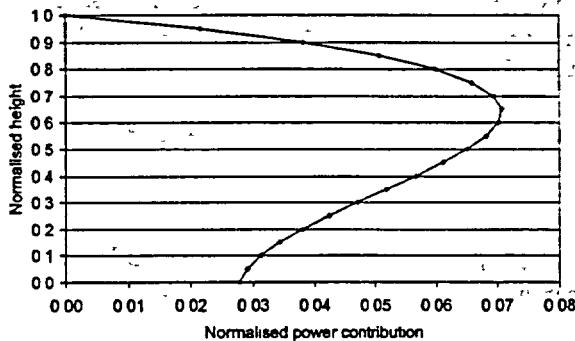


Fig 7. Normalised power distribution profile along the height of the reactor.

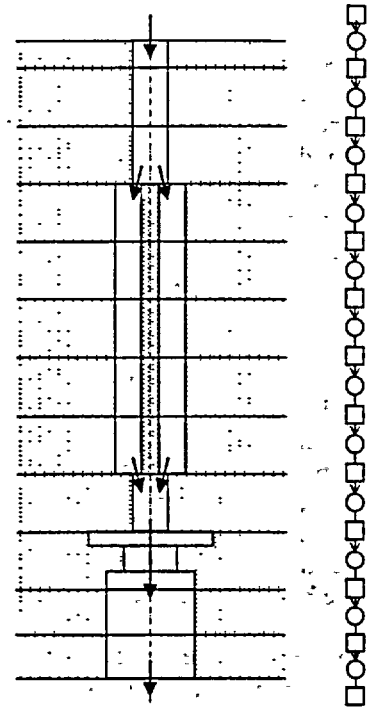


Fig 5. Schematic layout of flow path.

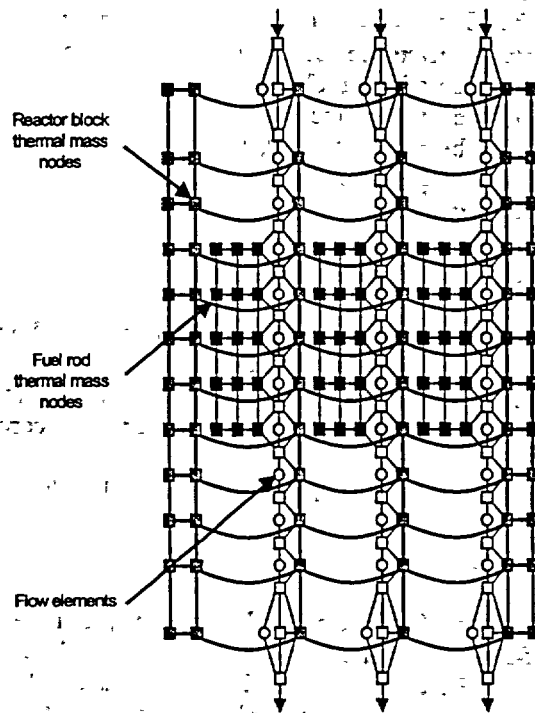


Fig 6. Complete flow element and solid thermal mass node network.

Results

Figure 8 shows the results of a sample steady-state calculation for the temperature distribution within the solid reactor block nodes at the different radial positions along the height of the reactor. In this case the gas temperature at the inlet to the core is 254 °C and the pressure is 3096 kPa. The Helium mass flow rate is 12.25 kg/s. The total neutronic power generation is 15 kW and the gas outlet temperature is 490 °C. The results show that at the inlet the reactor blocks closer to the centre have the lowest temperature due to the cooling effect of the gas. The outer reactor blocks are heated up slightly via conduction from the blocks lower down. On the levels containing the fuel rods, the reactor blocks are heated up swiftly and at the outlet the blocks near the centre are hotter than those on the outside:

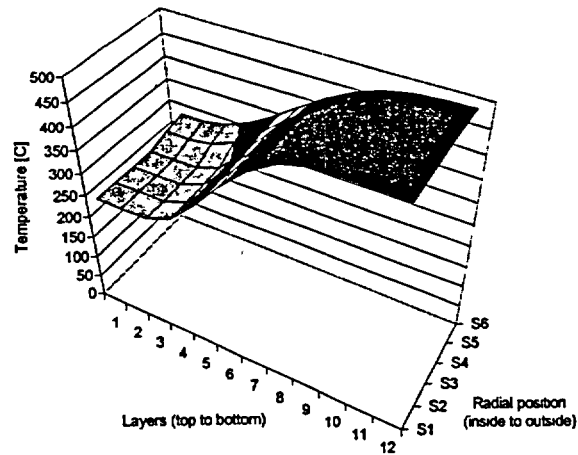


Fig 8. Steady-state temperature distribution within the reactor blocks.

Figure 9 shows the calculated inner (fuel compact) and outer (gas flow) surface temperature distribution in the fuel rods of fuel region 1 along the height of the reactor. The figure clearly shows the large temperature gradient from top to bottom as the gas heats up along the flow path. It also shows a large temperature difference of 56 °C between the outside surface of the fuel rod and the exposed surface of the fuel assembly block. Although it has not yet been investigated, this temperature difference is expected to reduce substantially if the effect of radiation is also taken into account.

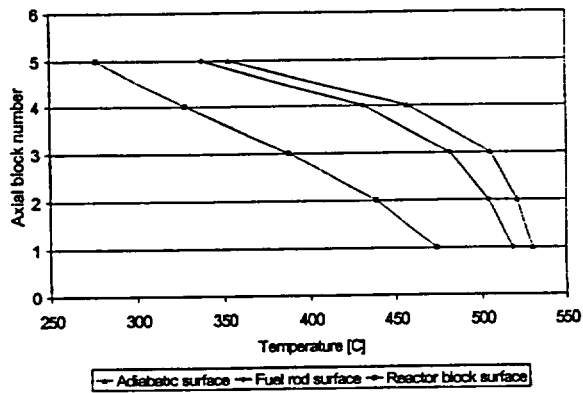


Fig 9. Adiabatic, fuel rod and reactor block surface temperature distribution in fuel region 1 along the height of the reactor.

Conclusion

The preliminary results presented in this clearly showed the effect of convection and conduction within the fuel rods, reactor blocks and flow passages of the HTTR reactor core. However, the effect of radiation between the outside surface of the fuel rods and the exposed surfaces of the fuel assembly block as well as heat losses from the outside surface of the reactor core must still be incorporated.

Acknowledgements: The authors gratefully acknowledge the contributions made by PBMR (Pty) Ltd.

References

- [1] T. Takeda, S. Nakagawa, Y. Tachibana, E. Takada & K. Kunitomi, Analytical evaluation on loss of off-site electrical power simulation of the high temperature engineering test reactor, Japan Atomic Energy Research Institute, 2000-016, March 2000.
- [2] G.P. Greyvenstein, An implicit method for the analysis of transient flows in pipe network, *Int. J. Numer. Meth. Engng*, 53:1127-1143, 2002.

EC-FUNDED PROJECT (HTR-L) FOR THE DEFINITION OF A EUROPEAN SAFETY APPROACH FOR HTR's.

S. EHSTER AND M.T. DOMINGUEZ

I. COE, G. BRINKMANN, W. VON LENZA,
W. VAN DER MHEEN, C. ALESSANDRONI

Respectively from Framatome ANP SAS (France), Empresarios Agrupados Internacional S.A. (Spain), National Nuclear Corporation Limited (England), Framatome ANP GmbH (Germany), Forschungszentrum Juelich GmbH (Germany), Nuclear Research and consultancy Group (Netherlands) and Ansaldo Nucleare (Italy)

And

J. PIRSON

Tractebel Energy Engineering, Nuclear Engineering Department
Avenue Ariane, 7 B-1200 Brussels (Belgium)
jacques.pirson@tractebel.be

Partners of the Safety Working Group of the HTR-TN (1) network

SUMMARY

The inherent safety features of the HTRs make events leading to severe core damage highly unlikely and constitute the main differentiating aspects compared to LWRs. While a known and stable regulatory environment has long been established for Light Water Reactors, a different approach is necessary for the licensing of HTR-based power plants.

Among the R&D projects funded by the European Commission for HTR reactors, the HTR-L project is dedicated to the definition of a common and coherent European safety approach and the identification of the main licensing issues for the licensing framework of the Modular HTRs.

Other specific objectives of this project are :

- *To develop a methodology to classify the accidental conditions*
- *To define the preliminary requirements for the confinement of radioactive products and to assess the need for a "conventional" containment structure*
- *To establish a SSC (2) classification and to define the rules for equipment qualification*
- *To identify the key issues that need to be addressed in the licensing process of the HTRs*
- *To organize a workshop with the concerned Safety Authorities at the end of the project.*

This paper will explain the project objectives and its final expected outcomes.

1. INHERENT SAFETY OF THE HTR REACTORS.

Renewing public acceptance for nuclear technology is one of the main challenges faced in the short term by the nuclear industry if new projects are to be started. The major issues related to public acceptance of nuclear industry are non-proliferation, safety and nuclear waste. It appears that HTRs could generate a significantly improved level of public acceptance compared to existing reactors, especially when taking into account some conclusions of safety analysis to be done in the future licensing framework.

(1) HTR-TN stands for High Temperature Reactor - Technology Network

(2) SSC stands for Systems, Structures and Components

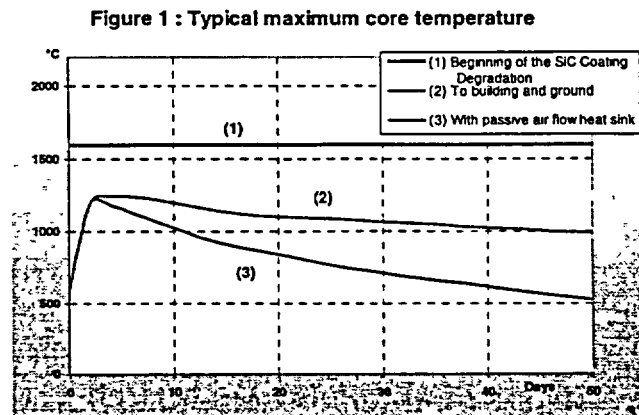
The HTR reactors appear as very simple to operate, with inherent passive safety features, low possibility of reactivity incidents ; decay heat removal can be ensured by natural convection. The main inherent safety characteristics of the HTR are the result of several design features, i.e. :

- the use of coated fuel particles embedded in a graphite matrix which retain the fission products. Kernels coated with carbon and silicon carbide (SiC) have greater heat-resistance than those coated with metallic materials : this provides a unique robustness of the first barrier,

- the strong negative temperature coefficient of the core, which tends to passively shut down the reactor with relatively modest temperature rise above normal temperature,

- a very slow temperature transient of the reactor if the active cooling of the core is lost (see figure 1). This is made possible by the high thermal inertia of the graphite and the core structure, and the low power density of the core (less than 10 MW/m³, compared to at least 50 MW/m³ for a LWR),.

- possibility for passive core cooling. The core can be configured to have a large core surface-to-volume ratio ; combined with the low power density, this makes possible passive heat removal (by thermal radiation, heat conduction and free convection) from the core and the outer surface of the pressure vessel, even under the worst accident conditions. Furthermore, in these conditions the maximum fuel temperature can be maintained below the integrity limit of the ceramic-coated fuel.



In terms of safety, for licensing purposes an analysis has to be made for all "classical" as well as design specific incidents. One of the most severe accidents in the reactor system is expected to be the complete loss of coolant accident (LOCA), which renders all the active cooling systems unavailable ; this is the case of the reactor circuit depressurization and of the loss of forced cooling helium flow.

Other accidents have to be considered, e.g. :

- reactivity accidents due to core or absorbers configuration modifications,
- blockage of coolant channels,
- reactor coolant pressure boundary failure,
- air ingress, with the potential for combustion of the core graphite,
- water ingress, for which the risks seem limited compared to previous HTRs with steam generators, because they concern only low pressure water circuits;
- radiological contamination in normal and accidental conditions, even if the past operating records of HTRs have shown that they were very clean reactors. This can have very significant impacts on the source term in case of accident.
- deblading accident of the gas turbine, which is specific to the direct cycle reactors and which can induce a shock wave causing substantial damage to the core structures of the reactor.

Although detailed safety analysis has still to be performed to demonstrate the fact for a particular design, due to the potential for passive cooling, the HTR reactor can be considered as "core meltdown proof". This makes the safety approach quite different from that developed for LWRs. Furthermore, the behaviour of HTRs in accidental conditions relies on high-quality fuel : the high level of safety of HTRs results from the capability of coated fuel particles to confine the radiological fission products even at high temperatures under the worst postulated accident.

2. HTR-L PROJECT WITHIN THE R&D EC FUNDED PROJECTS.

The high-temperature (HTR) and gas-cooled reactors (GCR) have been developed within Europe over many decades and considerable expertise in this technology is still available within the European Community countries. A common European approach to the renewal of HTR technology under the direction of a European HTR Technology Network (HTR-TN) has been established to enable and encourage work-sharing structures within this nuclear R&D field [1].

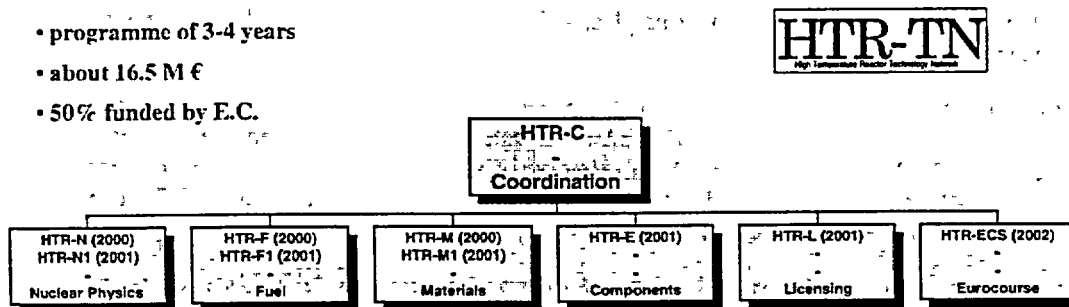
European Community Framework Programmes have been launched to consolidate and press forward the modular HTR technology in Europe. These involve partnerships of principal industrial and research organisations from countries of the European Union, including the JRC, in order to develop and consolidate European expertise and experience.

The partners of HTR-TN⁽³⁾ presented six co-ordinated projects, which were selected for the 5th Framework Programme of the European Commission with a total budget of about 16.5 ME (50% funded by the European Commission) [2]. The HTR-C project deals only with the integration and the co-ordination of the whole cluster and each of the other projects covers a technical area :

- HTR-N Reactor Physics and fuel cycle studies,
- HTR-F Fuel technology,
- HTR-M Material development
- HTR-E Key components of the power conversion system
- HTR-L Key safety issues and Safety approach
- HTR-ECS Eurocourse.

Moreover a task force on accident analysis and fission product transport has been created by HTR-TN in order to start the work in these fields, even though there is no related project funded for the time being by the European Commission, due to funding limitation.

Figure 2 : HTR Projects Cluster



HTR-TN is also looking for the synergy and complementarities of its programme with the present worldwide R&D effort on HTR technology, through the development of international co-operation : some co-operation already started with JAERI (Japan), INET (China), General Atomics (US) and US DOE/NRC, other international co-operative projects are considered.

3. HTR-L PROJECT OBJECTIVES.

The designs of High Temperature Reactors (HTRs) are very different from the ones for Light Water Reactors (LWRs) for which a known and stable regulatory environment has been established for many years. In LWRs the possibility of core meltdown has largely driven the safety philosophy.

(3) Present-day members are Ansaldo, Balcke-Dürr, Belgatom, BNFL, CEA, Cogema, Empresarios Agrupados, FRA-ANP (SAS and GmbH), FZJ (Jülich Centrum) and FZR (Rossendorf), IKE, IPM Zittau, IRI Delft University, NNC, NRG, VTI, JRC and C.E. (DG RTD and TREN)

The unique design of the Modular HTR uses simplicity instead of economy-of-scale to attain economic viability. Its inherent safety features (which make events leading to severe core damage highly unlikely), its potential for use in high temperature industrial processes and the possibility of using direct cycle gas turbines are some of the main aspects that set it apart from LWRs. For all these reasons, the existing regulatory environment is not well suited for the licensing of Modular HTR power plants and, therefore, a different approach is necessary.

The main purpose of HTR-L is to establish a common and coherent European safety approach for the licensing framework of the modular direct cycle HTRs. A large consensus on an approach, which can take into account the specific safety features of modular HTRs and which leads thus to a simplification of the reactor design (e.g. suppression of engineered safety featured systems, limitation of the number of components with a safety classification, reduction of the loads on the third barrier, ...), is very important for consolidating the economic competitiveness of these reactors. Therefore the results of HTR-L will be presented not only to European Safety Authorities, but HTR-TN will also take initiatives to promote extensive international discussions on them in order to broaden the consensus.

The studies will focus on HTRs with direct cycle concept, using both pebble and block type of U-based fuel for electrical power generation. However, exploratory work of the safety impact of Pu burning and other applications (e.g. hydrogen production, combined heat and power production, district heating, desalination) will also be performed.

4. HTR-L PROJECT WORKPACKAGES.

The project started on the 1st of October 2001 and will last 36 months. Its final outcome should constitute the basis for further developments (i.e. the establishment of more detailed requirements similar to those of EUR (4) applicable for LWRs). There are currently five workpackages.

4.1. Definition of the Safety Approach

The purpose of this workpackage is to define the main safety concepts and principles (defence-in-depth, physical barriers, events classification principles, safety functions, target radiological release limits, etc.) applicable to modular HTRs.

The project will be built on basis of the internationally accepted applicable standards, principles and methodologies (e.g. IAEA Safety Guides, OECD/NEA recommendations) and of licensing materials available for old (e.g. HTR-Modul, THTR and other German Projects, MHTGR in the US) and current HTR projects (e.g. PBMR in South Africa and in the US as well as GT-MHR initiative in the US). The EUR requirements will also be considered as a reference.

The general guidelines and principles must be adapted to modular direct cycle HTRs taking into account the inherent and unique safety features of modular HTRs. In particular, the greatly reduced probability of accidents with severe fission products release has to be taken into account.

4.2. Classification of the Operating Conditions

The design basis operating conditions to be considered in the safety analysis will be determined and a classification of these conditions will be proposed according to the associated risks and consequences.

The categorisation principles for Operating Conditions will be applied for two direct cycle modular HTR reactors (one with pebbles and one with blocks as fuel elements).

Moreover, as a preliminary evaluation, a draft list of the safety parameters to be controlled and supervised will be established at the end of the exercise in order to identify potential problems relating to measurement of some of these parameters.

(4) EUR stands for European Utility Requirements. This document giving the design requirements for Light Water Reactors was produced by the utilities from nine European countries.

This exercise will also be very helpful to define some areas to be studied in the other HTR projects or future extensions, in particular for the definition and the development of safety analysis codes. In addition, it is hoped that preliminary work will be undertaken by an NAS (5) organisation to establish the viability of some existing computer codes for HTR safety analysis.

4.3. Confinement Requirements.

Without any doubt, an important issue for the HTR reactors is whether a "conventional" containment structure or some other mitigating system or process should be required in order to provide adequate protection of the public. The decision to stipulate a containment has to be made on the basis of technical judgement, taking into account the design features of the HTR reactors.

One significant advantage of the HTR reactors is the high resistance for fission products release of the fuel particles, as the fuel and its successive protective shells constitute the most effective confinement barrier for the radioactive elements. The requirements for the confinement/containment function provided by the third barrier will therefore be re-assessed considering the properties of the first barrier of HTR fuel, the nature of the design basis accidents to be considered for licensing modular HTRs and the almost complete exclusion of core melting situations for this type of reactors.

The confinement requirements will be closely related with the results of the HTR-F and HTR-F1 projects (fuel barrier efficiency, fuel quality control process) ; furthermore, these requirements may depend on the plant design. Safety analyses results and especially those related to fission products transport are also important data for the definition of quantitative confinement requirements ; unfortunately, such data may be not available and the conclusion of this WP can only be qualitative and preliminary.

The integrity of the safety barriers will be also assessed in relation to accidental events originated outside of the plant (External Events as airplane crashes).

4.4. System, Structure and Component Classification

The goal of this workpackage is to establish a safety classification for the systems, structures and components, and to define the principles, rules and methodology for equipment qualification starting from the applicable international standards. This will be realised with the objectives to either avoid undue cost penalties using unnecessary high quality levels, and to respect the safety criteria during design basis conditions.

For this purpose, the key safety functions with their quality levels will be identified in a first step

4.5. Key licensing issues

The fifth package will try to identify the key safety aspects for which the Safety Authorities may be attentive, in order to consolidate the safety approach developed in the first work package.

For this purpose, on one hand, the review by a company with experience in the defence of safety cases and in dealing with the Safety Authorities in the frame of the licensing process, is considered.

Finally, it is proposed to organise a workshop with the Safety Authorities from the main European countries. The objective is to collect their first reactions to the proposed safety approach. The Safety Authorities of foreign countries (e.g. US, South-Africa, Japan, China and Russia) will also be invited to present their approaches and the international organisations (e.g. IAEA, OECD/NEA) will also be invited to present their approaches and activities on the safety and licensing of HTRs.

(5) NAS stands for Newly Associated States of the European Union.

5. CONCLUSION

It is most likely that HTRs will emerge on the world industrial scene in the next 10 years. The objective of the HTR-L project is to establish a common European safety approach for modular direct cycle HTRs. A substantial pan-European consensus on a safety approach is necessary and very important for consolidating the economic competitiveness of HTRs.

The adaptation of the usual internationally accepted safety guidelines and principles to modular direct cycle HTRs will be examined, taking into account the unique safety features of modular HTRs (exceptional strength of the first barrier, large negative temperature coefficient, very large thermal inertia and inherently safe design).

A way to look into the safety issues and to demonstrate that the safety functions are respected in all conditions will be developed.

The work will constitute a first trial for defining a common European safety approach for the future HTR reactors in Europe : this exercise must be the basis and the input for further more detailed developments and much more detailed requirements, similar to those of EUR applicable to LWRs. The HTR-L project rallies industrial partners (manufacturers and energy producers) and research centres from different countries. Furthermore, it is also open to international co-operation.

References

- [1] The Renewal of HTR Development in Europe (ICONE 10)
D. Hittner Framatome ANP, Paris la Defense.
- [2] Advanced concepts for waste management and nuclear energy production in the EURATOM Fifth Framework Programme - Global 2001 (09/01) – Paris
M. Hugon, V. P. Bhatnagar and J. Martin Bermejo (European Commission).

GRAPHITE MATERIALS TESTING IN THE ATR FOR LIFETIME MANAGEMENT OF MAGNOX REACTORS

S. B. GROVER

Idaho National Engineering and Environmental Laboratory, 2525 North Fremont Ave., Idaho Falls, Idaho 83415, United States of America

and

M. P. METCALFE

British Nuclear Fuels plc, Research and Technology, Berkeley Center, Berkeley, Gloucestershire GL13 9PB, United Kingdom

ABSTRACT

A major feature of the Magnox gas cooled reactor design is the graphite core, which acts as the moderator but also provides the physical structure for fuel, control rods, instrumentation and coolant gas channels. The lifetime of a graphite core is dependent upon two principal aging processes: irradiation damage and radiolytic oxidation. Irradiation damage from fast neutrons creates lattice defects leading to changes in physical and mechanical properties and the accumulation of stresses. Radiolytic oxidation is caused by the reaction of oxidizing species from the carbon dioxide coolant gas with the graphite, these species being produced by gamma radiation. Radiolytic oxidation reduces the density and hence the moderating capability of the graphite, but also reduces strength affecting the integrity of core components. In order to manage continued operation over the planned lifetimes of their power stations, BNFL needed to extend their database of the effects of these two phenomena on their graphite cores through an irradiation experiment. This paper will discuss the background, purpose, and the processes taken and planned (i.e. post irradiation examination) to ensure meaningful data on the graphite core material is obtained from the irradiation experiment.

1. Introduction

BNFL Magnox Generation Business Group in the United Kingdom is currently operating six commercial nuclear power stations, and is undertaking a program of work to underwrite continued operation of these nuclear power stations beyond their original design lifetimes. These are gas-cooled graphite-moderated reactors of the first generation Magnox design that utilize uranium metal fuel in magnesium alloy fuel cans. The reactor design has evolved as each power station in the series has been commissioned, with progressive increases in operating gas pressures and temperatures leading to increased power densities and thermal output.

For economic planning purposes, the reactors were designed with nominal lifetimes of 20-25 years. All the power stations are now operating well beyond their design lifetimes (30-40 years). In order to satisfy the operators and the United Kingdom regulators (HM Nuclear Installations Inspectorate) that the reactors continue to operate safely under normal operating and fault conditions, the reactors are subjected to rigorous periodic assessment. The graphite core of a Magnox reactor not only acts as the moderator which sustains the energy-releasing chain reaction but also serves as the main structural element of the core design, providing a lattice of vertical channels for fuel elements, instrumentation and flow of heat transfer gas. The assessment of the condition and behavior of the graphite moderator is a key part of this periodic safety review process.

With the graphite cores being operated significantly beyond their nominal lifetimes, it has been recognized that additional materials property data on irradiation damage and radiolytic oxidation are required to underwrite safety case assessments which will bound the projected irradiation and environment conditions. To this end, the Industry Management Committee within the United Kingdom (comprising British Energy, British Nuclear Fuels plc and HM Nuclear Installations Inspectorate) has provided funding for a graphite irradiation program. This program will irradiate samples of archive pre-characterized graphite used in the Magnox type reactors in the Advanced Test Reactor (ATR) at the United States Department of Energy's Idaho National Engineering and Environmental Laboratory (INEEL). After irradiation, the graphite will undergo Post Irradiation Examination (PIE) at BNFL Research and Technology's Berkeley Centre in the United Kingdom.

The new Irradiation Test Vehicle (ITV) facility in the ATR was selected for the irradiation to provide the desired irradiation conditions and on-line temperature control of the specimens. The ITV has the capability of irradiating specimens at elevated temperatures in a dry gas environment similar to an HTR. Depending on the amount and type of specimen and capsule material available for gamma heating, specimens may be irradiated in the ITV at temperatures as low as 200 °C or in excess of 800 °C. A new gas environment system was also added to the ITV to provide both oxidizing and inert gas atmospheres for the graphite specimens during irradiation. This will provide specimens with both the oxidation and neutron damage as well as specimens with just neutron damage effects. During PIE, the effect of each type of damage on the graphite can then be assessed.

This paper discusses the irradiation experiment background, purpose and the processes taken and planned to ensure meaningful data on the graphite core material is obtained from the irradiation experiment.

2. Magnox Reactor Graphite Core Design and Operating Conditions

The cores are constructed from graphite bricks stacked in columns, geometrical stability being achieved through axial and lateral keying within the core in combination with a steel core restraint system. The columns of bricks are pierced by cooled vertical channels containing fuel elements, control rods and reactor instrumentation. The heat transfer medium is pressurized carbon dioxide. Pile Grade A (PGA) graphite, an orthotropic extruded needle-coke graphite, was chosen for the active regions of all the Magnox reactor cores, with a less pure graphite from an earlier stage of the same manufacturing process (Pile Grade B) being used for side reflector components.

Operating gas pressures are in the range ~8-27 bar absolute with operating gas temperatures of ~140-370°C. Reactor thermal powers range from ~270-1700MWt. The peak fast neutron dose to the graphite over the planned extended lifetimes of the stations is calculated to be in the region of 7×10^{21} neutrons/cm² Equivalent DIDO Nickel Dose (EDND).

3. Graphite Core Aging Process

There are two principal graphite aging processes: irradiation damage from fast neutrons creates lattice defects leading to dimensional changes and changes in properties including coefficient of thermal expansion, thermal conductivity, modulus and strength; exposure of graphite to carbon dioxide in the presence of gamma irradiation results in radiolytic graphite oxidation. This oxidation process produces changes to the porosity of the material leading principally to changes in modulus, strength and thermal conductivity.

The irradiation behavior of PGA graphite was extensively researched prior to and during the early development/construction period of the Magnox nuclear power stations. Fast neutron effects were studied using Materials Testing Reactors (MTR) principally in the United Kingdom (e.g. DIDO and PLUTO at Harwell, DFR at Dounreay) but also in France and Belgium (Siloe in Grenoble and BR-2 at

Mol). The temperatures and doses achieved in these studies bound Magnox station operating envelopes, even for extended operation. Irradiation damage in Magnox reactor graphite cores leads to a build-up of stored (Wigner) energy, distortion and dimensional change of components and, in combination with temperature and flux gradients, the generation of internal stresses within components. These processes are well understood and the MTR database for PGA graphite provides the means for predicting the effects of irradiation damage on core integrity.

Radiolytic graphite oxidation was studied in low dose experiments in MTRs in the United Kingdom (with samples being annealed to remove the effects of irradiation damage). The process involves the radiolysis of carbon dioxide to produce an oxidizing species. If these reactive oxidizing species impinge on a graphite surface, they gasify it to carbon monoxide. Depending upon the rate of diffusion of the oxidizing species within the pores of the graphite, it may become deactivated before it can react with carbon atoms in the graphite. The radiolytic oxidation of the graphite depends on the energy absorbed by the carbon dioxide (principally gamma) within the pores of the graphite. Oxidation rates increase with gas density – i.e. with increasing pressure and decreasing temperature. The presence of “inhibitors” such as carbon monoxide (a product of the process itself) and hydrogenous material (i.e. hydrogen, water or methane) will reduce oxidation rates. Data for the effects of radiolytic weight loss on PGA graphite properties are available up to weight losses of approximately 35%, with the database being somewhat sparse in the range 20-35% (Figure 1).

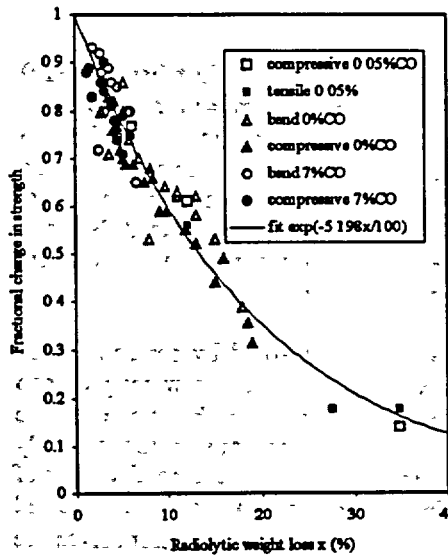


Figure 1: Fractional change in strength of PGA graphite with radiolytic weight loss

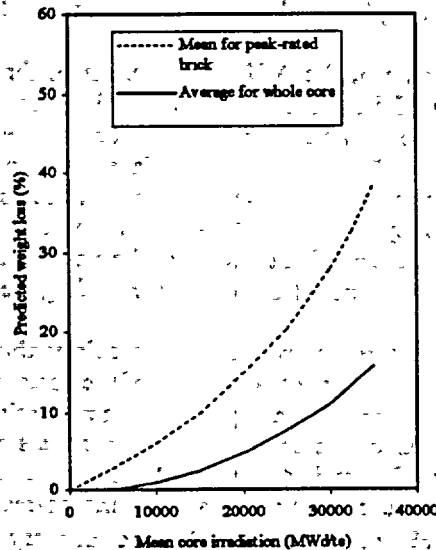


Figure 2: Radiolytic weight loss predictions for the Oldbury reactor graphite core

The adequacy of the database for radiolytic graphite oxidation must be assessed against measured and predicted weight losses in Magnox reactor core components. Figure 2 shows predicted weight losses for the Oldbury reactor core as a function of mean core irradiation. Weight losses have been expressed in two ways: as the average weight loss over the whole active core and as the mean weight loss for a brick in the peak-rated (“worst”) position. The average weight loss of the graphite falls well within the database. For the small number of bricks at the peak-rated position within the core, mean weight losses are expected to lie at the database limit of 35% at a mean core irradiation of approximately 33,500 MWd te⁻¹ (U). It is likely that part of the Oldbury core, the lead reactor on radiolytic graphite weight loss, will be operating during its planned lifetime outside the materials database unless new data from accelerated irradiation experiments can be acquired.

4. Objectives of Graphite Irradiation in ATR

There are two objectives for the graphite irradiation in ATR. The first and principal objective is the extension of the PGA graphite mechanical properties database to higher weight losses to bound reactor material over planned lifetimes for the Magnox nuclear power stations. Samples shall be irradiated in a controlled representative gas environment with target weight losses in the range 20-60%. The second objective is to crosscheck fast neutron damage effects between ATR and the existing MTR database for PGA graphite. In this case, samples shall be irradiated in an inert environment with instrumentation providing the accurate measurement of temperatures and doses.

5. ATR Facilities and Capabilities

The ATR's newly installed Irradiation Test Vehicle (ITV) was chosen as the position to perform the irradiation. The ATR is a premiere MTR capable of accommodating large irradiation specimens (11.5 cm in diameter by 1.22 m long) within very high neutron flux (1×10^{15} neutrons/cm²/sec thermal and 5×10^{14} neutrons/cm²/sec $E \geq 1$ MeV) and gamma heating (~ 20 W/g in stainless steel) environments. The ITV is located at the very center of the ATR core and is an extremely flexible facility designed to support a variety of experiments requiring fast, thermal, or mixed spectrum neutron environments. This facility is capable of providing neutron spectral tailoring and continuous temperature control for up to 15 capsules with inside diameters of 1.35 to 2.21 cm and lengths of 15.2 to 35.6 cm. Smaller numbers of longer length capsules can also be accommodated.

The in-reactor portion of the ATR ITV consists of three closely packed mini-in-pile tubes (MIPTs) running the length of the ATR vessel. The inside bores of the MIPTs are kept dry and test trains are inserted from the top of the reactor into the dry cavities. Temperature control gas lines enter through the bottom of the MIPTs and remain in place between tests. The temperature measurement and any other desired instrumentation or support systems are supplied with the test train and connections are made to the control system at the ATR vessel top head area each time a test train is replaced. Neutron spectral tailoring is accomplished through the use of replaceable filters that are inserted between the reactor fuel and an aluminum filler piece surrounding the MIPTs in the core region.

Independent temperature control of each capsule within the ITV is accomplished by controlling the transfer of the gamma and neutron heating of the capsule and its contents across a narrow gas jacket to the ATR primary coolant. During operation, the precisely sized gas jacket between each capsule and the mini-in-pile tube receives a continuous supply of gas custom blended for heat transfer purposes. By adjusting the ratio of a conductor (helium) gas and an insulator (neon) gas, the thermal conductivity of the gas jacket can be controlled to provide the correct insulating value between the nuclear heated capsules and the relatively cold (60 °C) reactor primary coolant. This controlled heat transfer drives the temperature of the specimens to the desired values during reactor operation. The correct temperature is maintained in each capsule by blending the mixture ratio of the two gases based upon temperature feedback from thermocouples located within each capsule. The blending operations are completely automated and are performed using Mass Flow Controllers (MFCs) that are linked to a computer control console in a manned experiment operation center. The exhaust lines leave the MIPTs at the reactor bottom head, pass through a leak detection panel, and discharge to the reactor ventilation system, which exhausts to the ATR stack.

6. Experiment Description

The graphite irradiation will be performed in MIPT #3, which is in the west position of the ITV. The experiment will consist of a single test train, which will be split into two capsules containing the Magnox graphite specimens. The two capsules are of equal length, separated at the vertical center of the ATR core by a sealed bulkhead, and extend from the center to the upper and lower ends of the active fuelled region of the reactor core. The top capsule, with a flowing inert (helium) gas environment, will contain fast neutron damage control specimens and the bottom capsule, with a

flowing oxidizing (CO₂) gas environment, will contain specimens to be radiolytically oxidized to high weight losses. In both capsules, the graphite will be positioned within a specimen carrier to ensure the applicable gas flow is positively directed over as much of the specimen surface as possible. This was done to minimize the diffusion distance for the gas within the porosity of the graphite specimens. To ensure data from the irradiation specimens would be directly comparable to data obtained from samples trepanned from Magnox reactor cores, the same standard specimen size was used in the irradiation. Other prototypic conditions mandated for the irradiation included specimen temperatures and gas environment (gas composition and gas pressure) of Magnox reactors. The length of irradiation was determined using a radiolytic oxidation model developed in support of the Magnox reactors. This model takes into account the total nuclear (gamma plus neutron) heating of the specimens, the composition of the gas and the desired weight loss of the specimens. Using this input, the model predicted approximately 140 irradiation days in the ATR ITV would lead to radiolytic weight losses which would bound those calculated to arise over the planned lifetimes (including planned life extension) of the Magnox power reactors. If the oxidation specimens reach the desired amount of oxidation prior to the end of the irradiation cycle, the oxidation system will be flushed with an inert (helium) gas and then purged with the same gas throughout the remainder of the irradiation cycle.

Extreme care was taken in the design of the experimental hardware to maintain prototypic chemistry control of the specimen environment to limit the unknown variables and prevent any unwanted chemical reactions during the irradiation. Materials that could either affect (e.g. catalyze or block) or mask the oxidation rate (e.g. carbon deposition) were excluded from the experimental hardware and all communicating systems. The major component of most ATR test trains and capsule shells, stainless steel, was excluded due to its nickel content. To satisfy the chemistry requirements, the capsule material was researched extensively and 9Cr 1Mo alloy steel was selected. This material was able to meet the chemistry requirements and also survive the high neutron flux environment of the ATR without experiencing a significant increase in its brittle fracture transition temperature. However, since the design code required a post weld heat treatment for this material, special techniques were needed to prevent melting of the aluminum specimen carrier during this process.

A vertical section of the experimental hardware is shown in Figure 3, and a horizontal cross-section at the top of the capsules is shown in Figure 4. The specimen carrier consists of two clamshell halves that are held together by thin aluminum straps. These straps also hold the thermocouple leads, gas lines and flux monitors in grooves machined in the outer surface of the carrier. Aluminum was chosen for the specimen carrier material for several reasons including chemistry control, low neutron absorption rate, high thermal conductivity and a high thermal expansion rate. The last two properties enable the carrier to provide an excellent heat transfer path between the specimens and the capsule wall. The high thermal expansion rate also helps in the assembly and later disassembly of the capsules by providing needed clearance between the carrier and the capsule wall at room temperature. However, during irradiation the aluminum expands to provide positive thermal contact between the carrier and the

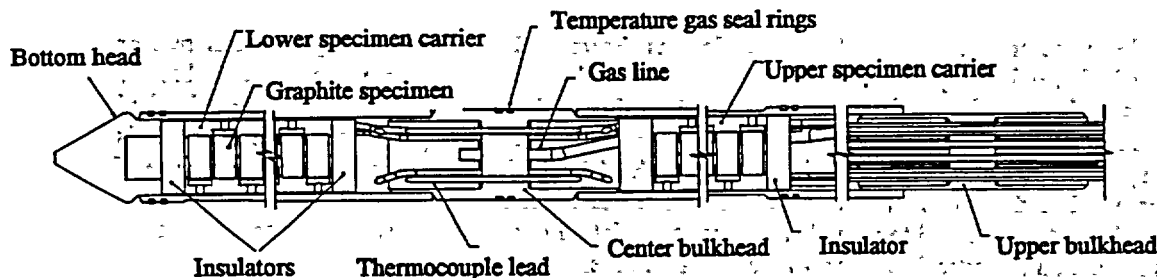


Figure 3: Vertical section of the experiment capsule showing the orientation of the capsules and the bulkhead separating the two capsules.

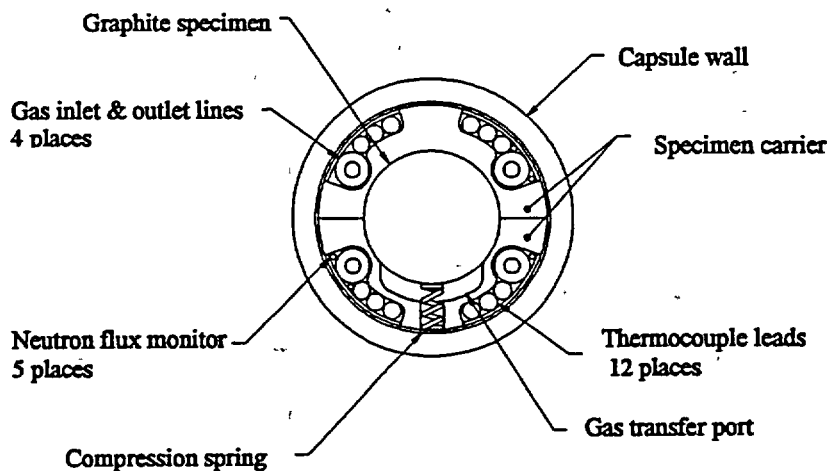


Figure 4: Cross-section of the experiment capsule showing the graphite specimens located in the center of the capsule and surrounded by the specimen carrier and other key components.

capsule wall. Nonetheless, the carrier's main role is to provide support for the graphite specimens, whilst separating them by a 1-mm gas space between adjacent top and bottom surfaces of the specimens. The gas spaces (or gas path) between the specimens are connected by gas ports located on alternating sides of the specimens. The specimens are held against the side of the carrier opposite the gas port by a compression spring to ensure a good thermal contact between the specimen and the carrier for heat transfer purposes. Thermocouples are located at the top, middle and bottom of each capsule for both temperature control and recording the temperature of the specimens. At each of these locations there are two thermocouple junctions located diametrically opposite each other: one measuring the centerline temperature of a graphite specimen and one measuring the temperature of the specimen carrier. Neutron flux monitors were installed to measure both the fast and thermal neutron fluences. Iron, nickel, and niobium wires measure the fast spectrum, whilst cobalt-aluminum alloy wires measure the thermal spectrum. Two iron flux monitors were also positioned diametrically opposite each other in each capsule to measure the fast neutron flux gradient across the capsules. Bare monitor wires were utilized in the upper inert capsule, but to prevent any unknown chemical effects on the specimens or wires, the monitors were encapsulated in a sealed aluminum tube in the lower oxidation capsule. Since each capsule has a different gas environment, there are separate gas inlet and outlet lines for each capsule. The inlet gas lines terminate at the bottom and the outlet gas lines are located at the top of the capsules. The gas (either oxidizing or inert) enters the gas plenum from the inlet gas line at the bottom of each capsule. It then traverses the tortuous path up between the specimens via the spaces between the specimens and the gas ports to enter the outlet line at the top of the capsule.

The outside diameter and profile of the capsule was determined based upon very rigorous reactor physics and thermal analyses. In order to ensure the data from this experiment was directly comparable with the existing database, an equivalent flux and temperature relationship established using data from the DIDO reactor was used to determine the required specimen temperatures. This relationship was applied to the neutron flux profile of the ATR to determine the correct temperature of the specimens based upon their axial position within the ATR core. The outside diameter of the capsule wall was then tapered to provide the correct insulating gas jacket between the capsule and the MIPT as a function of vertical location within the ATR core.

The capsule environment system is a new capability added to the ITV specifically for this project. It consists of the two different gas systems (inert and oxidizing) connected to the inert and oxidizing capsules in the MIPT. The inert gas system contains pure helium gas, and the oxidizing gas system contains a carbon dioxide gas that is blended with a carbon monoxide/hydrogen mixture. A

description of the requirements for and the design of the complex control system are beyond the scope of this paper. Inlet and outlet gas compositions are monitored over the duration of the experiment using a gas chromatograph and oxidizing gas flow rates and composition adjusted to take account of the oxidation of the graphite.

7. BNFL Facilities and Capabilities

BNFL currently operates hot cell facilities in the UK at Berkeley and at Sellafield. The main graphite facilities at Berkeley comprise a suite of cells and glove boxes for medium and low active work. Berkeley has been involved in the characterization of graphites in the UK for many years and has developed considerable expertise and designed specialized equipment for such investigations. Techniques and methods available for irradiated graphite include: precision machining equipment and equipment for mensuration, weighing, high temperature annealing, volume determination, helium pycnometry, strength, dynamic Young's modulus, coefficient of thermal expansion, diffusivity, permeability, thermal conductivity, stored energy measurements and chemical behavior. In addition, a wide range of optical and electron microscopes are available including a shielded scanning electron microscope. The Berkeley capability also includes surface and image analysis instruments.

8. Characterization of Material for Irradiation

Archive graphite retained during the construction of the reactor cores has been used as the source of material for the experiment. For the purposes of the experiment described here, cylinders of graphite were machined from selected heats of archive graphite with the grain direction either perpendicular or parallel to the axis. The cylinders were sectioned to provide discs 12.00mm in diameter and 6.00mm in length (machining tolerances of ± 0.03 mm). Each disc either side of the disc destined for the experiment has been retained as reference material. Standard waisted tensile strength samples were also machined from selected sections of the cylinders for reference. All the graphite discs were subjected to detailed mensuration and weighing and measurement of dynamic Young's modulus. Selected graphite discs were subjected to open-pore volume (helium pycnometry) and coefficient of thermal expansion measurements. All the data were subjected to detailed analysis, with samples with outlying properties being examined for microcracks/flaws and rejected as appropriate. For each heat and for each grain orientation, samples were then paired to match properties. Samples from each pair have been assigned to the oxidation and inert irradiation capsules at symmetrical positions about the center of the ATR core to provide identical irradiation conditions.

9. Summary

Extreme care has been taken in the development of the irradiation experiment to ensure the data will be directly comparable to the existing database. The design of the experiment test train and the capsule environment system has taken all known variables into account and every effort was made to minimize the effects of any items (e.g. chrome, gold, etc.) that were unavoidable. This philosophy together with the nuclear heating and temperature control provided by the ATR IIV facility will provide the irradiation specimens needed to extend the current database on radiolytic oxidation of PGA graphite. This database may then be utilized in underwriting the safety cases for safe continued operation of the Magnox power stations.

ENERGY STORAGE AND RELEASE CALCULATIONS FOR HTR-10 REFLECTOR

U. COLAK, H. DIKMEN, and U.E. SIKIK

*Nuclear Engineering Department
Hacettepe University, Beytepe, 06532 Ankara-Turkey*

ABSTRACT

Significant amount of lattice defects are created in graphite under the exposure of fast neutrons. If irradiation temperature is high enough, in-situ annealing takes place. However, annealing is difficult at low temperatures and excess energy associated with lattice defects tends to be stored in graphite. Uncontrolled release of this energy may cause appreciable temperature increase in the material. The magnitude of energy release and associated temperature increase may be a safety concern and should be assessed during the gas cooled reactor design stage. This study deals with the calculation of stored energy in the reflector during the operation of HTR-10 pebble bed gas cooled reactor and its release upon a temperature increase caused by a transient event.

1. Introduction

There is a renewed interest in gas cooled reactors. This is mainly due to their excellent safety characteristics and better economics with respect to conventional power plants. HTR-10 is a gas cooled pebble bed reactor with 10 MW thermal power output located at the Institute of Nuclear Energy Technology (INET) near Beijing, China. The main purpose of this test reactor is to provide a knowledge base for the design of power reactors.

Graphite in gas cooled reactors is extensively used in different components such as fuel, moderator, and reflector due to excellent nuclear characteristics. It is also a well known characteristics of graphite under irradiation that a fraction of the energy associated with the slowing down of neutrons stored in such materials [1]. This stored energy may be released as heat upon annealing of point defects by increasing the temperature. This phenomenon should be considered during the design of gas cooled reactor since it is directly related to reactor safety. Local temperature increase during any loss of cooling event may be sufficiently high to cause substantial amount of energy release. This, in turn, further increase the temperature.

The energy storage and release characteristics of HTR-10 reactor is analyzed in this study. The analysis is performed by taking temperature and radiation dose distribution in the reflector region. Then, the energy storage and release characteristics are evaluated with reference to the previously obtained data in a standard irradiation facility [2].

2. Energy storage and release in graphite

Energetic neutrons cause significant amount of atomic displacements in the reflector of gas cooled reactors. If irradiation temperature is not high enough, these defects do not anneal out and the heat content of the material increases. This is called "the stored energy". This process is attributed to the formation of complex defect clusters and the difficulty of the dissociation of these clusters due to being trapped in crystals. This is especially important for the reflector region of the reactor since temperatures are relatively low in this region compared with the reactor core. The amount of energy deposition is a function of irradiation dose as well as local temperature. When the temperature increases above the

irradiation temperature, then, some of the defects anneal out and the stored energy is released as heat. The amount of energy release is directly related with the temperature rise. If temperature rise is limited as in the case of operational transients, the amount of energy release will not be so significant. However, there may be significant energy release in case of any loss of cooling transient. During such a transient, uncontrolled temperature rise trigs the energy release and this further increases the temperature.

3. HTR-10

HTR-10 is a gas cooled reactor constructed based on pebble bed concept. The thermal power rating of the reactor is 10 MW. The reactor core is 180 cm in diameter and 197 cm in average height and equilibrium core is made up by 27,000 spherical fuel elements. Reactor core is surrounded by a large graphite reflector. Helium coolant enters the core at 623 K and the outlet temperature is 973 K. Helium pressure is 3 MPa.

4. Thermal-hydraulics calculations

Temperature distribution in HTR-10 core and reflector is calculated by solving mass, momentum, and energy equations. Mass and momentum equations provide the velocity distribution of the helium coolant in the core. The coolant velocity is needed to evaluate the heat transfer coefficient between the coolant and the fuel surface. Calculations are performed in such a manner that mass and momentum equations and heat equations for the coolant and the fuel spheres are coupled independently. Correct velocity and temperature distributions are obtained iteratively.

Thermal-hydraulics calculations are performed in the r-z geometry. Core and reflector regions are divided into radial and axial nodes. Momentum, mass, and heat equations are discretized and solved in this grid. Differential equations are converted into matrices. These matrices are solved by using Gauss-Seidel iteration method. The methodology given by Liem and Sekimoto is used in these calculations [3]

Mass equation is given by

$$\nabla \cdot (\rho v) = 0$$

where ρ and v are the density and velocity of the helium coolant. Pressure gradient is given by

$$\nabla P = -F + \rho v$$

Frictional term F is expressed in terms of the pressure loss coefficient and porosity. Local porosity distribution in the pebble bed is taken into account. [4]

Energy equations are used to represent the heat transfer between the coolant and fuel spheres

$$\nabla k_{He} \nabla T_{He} - \nabla (\rho v C_{p,He} T_{He}) + \alpha h (T_s - T_{He}) = 0$$

$$\nabla k_s \nabla T_s + q''' + \alpha h (T_{He} - T_s) = 0$$

where C_p , T , q''' , k and h are heat capacity, temperature, volumetric heat generation rate, thermal conductivity coefficient, and overall heat transfer coefficient, respectively. Subscripts s and He refer to fuel spheres and helium coolant. Conductivity coefficients for reflector and pebble bed are used as temperature and irradiation dose dependent parameters [5]. Correlations for heat transfer coefficient is taken from the literature [6]. Reflector region is also included in the heat transfer calculations. Conduction is the only heat transfer mode in the reflector. Power produced in each node is calculated by the results

obtained with the VSOP code. The reactor in the model is divided into 20 axial and 31 radial positions. Axial and radial power profiles are evaluated and they are converted to the power produced in each node. Mass and momentum equations are evaluated in a coupled manner. Iterations are performed until the pressure drop and velocity across the core satisfy the conditions. Once velocity distribution is obtained, it is used to obtain heat transfer coefficient. Conduction, convection, and radiation are included as possible mode of heat transfer.

Temperature distribution (in Kelvin) in the core and the reflector regions as calculated is shown in Fig 1.

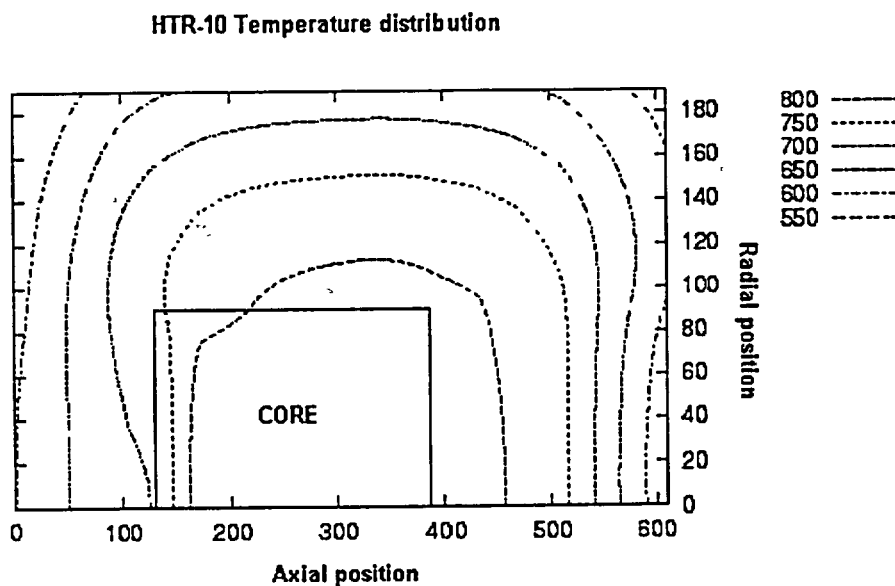


Fig 1. Calculated temperature distribution in HTR-10 core and reflector.

5. Energy storage and release calculations

It is customary to perform irradiation experiments at high flux facilities to establish a database for irradiated material characteristics. Since flux levels are extremely high in these facilities, it takes rather short period of time to achieve reasonable dose levels. Data obtained in such a standard facility are then used for any other facility provided that an appropriate conversion is made. Radiation damage in graphite may be estimated by a parameter named "damage flux". It is expressed in terms of neutron flux and multiplication factor which gives the number of displacements produced per neutron with the energy of E . Such that

$$\phi_d = \int_0^{\infty} \nu(E)\phi(E)dE$$

A correction in damage flux is necessary to include the effect of neutron flux distribution. Another correction is required to include the effect of irradiation rate. If irradiation is completed within a short period of time at high flux, the effect of irradiation will not be the same as it was completed at low flux but longer time. This is due the fact that there is no sufficient time for annealing in the first case. An invariant is proposed by taking the ratio of defect creation rate to defect annealing rate. Thus, the term

$$\phi_d / \exp(-E/kT)$$

is expected to be constant. Hence, two different irradiation conditions can be related by

$$\frac{1}{T_{eq}} - \frac{1}{T_1} = \frac{k}{E} \ln\left(\frac{\phi_d}{\phi_s}\right)$$

where E , k , and T are the activation energy, Boltzmann's constant, and temperature in K. In this equation, equivalent temperature T_{eq} in K is required to obtain a displacement rate in a standard facility with a damage flux of ϕ_s , with compared to a facility with a damage flux ϕ_d and temperature T_1 . The activation energy is somewhat uncertain. However, 1.2 eV and 3 eV are recommended for low temperature and for high dose irradiation, respectively [7]. The activation energy of 3 eV recommended for high dose is used in throughout the calculations in this study.

Local energy storage values at different regions of the reflector is calculated based on the local temperature and irradiation dose. Local temperature values are obtained as previously indicated. Irradiation dose is taken as $25 \cdot 10^{20}$ n/cm² at the interface between the core and reflector. Decrease in the radiation dose along the reflector is accounted with respect to the neutron flux variation as calculated by VSOP.

Reference stored and released energy data are taken from the literature for irradiations performed at Calder Hall reactor [2]. Represented cases are referred to a local power rating of 3.12 MW/t. Accumulated damage is related and represented in terms of the burnup (MWd/t). In order to make a better assessment, dose values for Calder Hall reactor and HTR-10 reactor are converted into equivalent DIDO nickel dose using appropriate conversion factors [7]. Then, equivalent temperatures in each discretized region are obtained by the above given relation using the temperature distribution across the reflector as explained in Section 4. In the next step, energy storage in each computational node is calculated. This is performed by a two dimensional linear interpolation from the table constructed for various equivalent temperature and DIDO nickel dose values.

In order to predict the release of stored energy in the reflector region during a loss of cooling event, one needs to have the temperature distribution during a loss of cooling event. Such an analysis has been performed for HTR-10 reactor [5]. Results show that reflector temperature vary with the axial position and can go up to roughly 970 K. This axial temperature variation may be taken as the representative case and used to express temperature distribution in the reflector region. This approximation may be justified by considering the relatively high thermal conductivity of the graphite. The use of this temperature increase throughout the reflector, also provides a more conservative results from the safety point of view. Increasing temperature will stimulate the energy release. Representative cases in this study are taken as the temperature increases of 100, 150, and 200 K.

5. Results

The results of stored energy calculations is shown in Fig 2. As it is clearly seen that energy storage in the reflector region is concentrated on the bottom part of the core region. Temperature here is relatively low. On the other hand, neutron flux is sufficient enough to generate significant damage. The situation is somewhat different in the side reflector. Regions near the core do show some damage accumulation due to high damage flux. Temperature may not be high enough in this region for complete annealing.

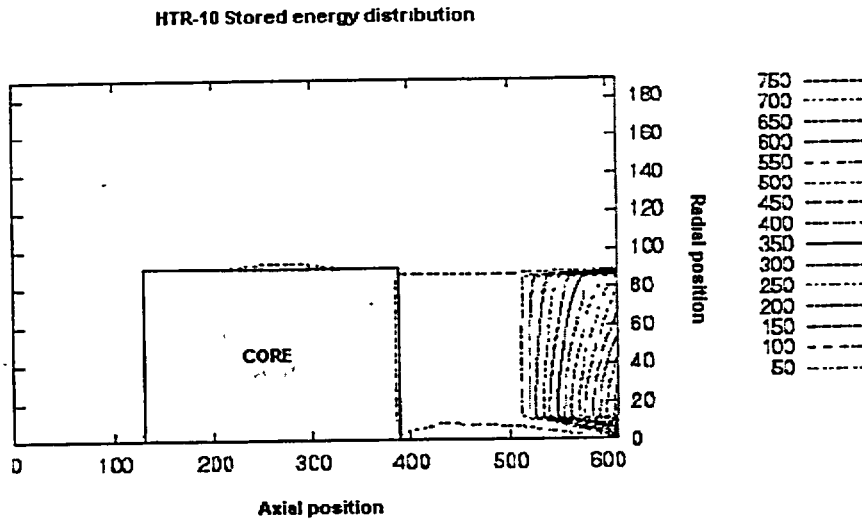


Fig 2. Stored energy (J/g) distribution in HTR-10 reflector

Nevertheless, the neutron flux almost diminishes beyond this region and there is no significant defect formation. Therefore, only central section shows some energy storage, however, it is not so significant. The amount of total stored energy is calculated to be about 7.05 MJ throughout the reflector. Total released energy for transients causing 100, 150, 200 K temperature increase in the reflector correspond to 471.7, 653.1, and 804.6 kJ, respectively.

6. Conclusions

Energy storage and release in HTR-10 reflector does not cause any safety concern since the coolant temperature is kept high enough to avoid any damage accumulation. The most critical part of the reflector is found to be the bottom reflector with regard to the energy storage. Energy release during a postulated loss of cooling event is very limited and low compared to the decay heat of the reactor. Regular engineering safety systems can easily cope with the temperature increase without causing any safety problem.

7. References

- [1] R.E. Nightingale, "Stored energy" in Nuclear Graphite, Academic Press, 1962, p.325.
- [2] H. Bridge, B. T. Kelly, B. S. Gray, "Stored energy in graphite and reactor design" reprint from Nuclear Engineering, March, 1962.
- [3] P. H. Liem and H. Sekimoto, "Neutronic and thermal hydraulic design of the graphite moderated helium-cooled high flux reactor", Nuc. Eng. Des., 139, 1993, p. 221
- [4] S. Liu, J. H. Masliyah, "Non-linear flows in porous media", J. Non-Newtonian Fluid Mechanics, 86, 1999, p.229.
- [5] Heat transport and afterheat removal for gas cooled reactors under accident conditions, IAEA-TECDOC-1163, 2000.
- [6] E. Achenbach, "Helium cooled systems. HTR Pebble Design" in Heat Transfer and Fluid Flow in Nuclear Systems, ed. By H. Fenech, Pergamon Press, 1981, p. 382.
- [7] Irradiation damage in graphite due to fast neutrons in fission and fusion systems, IAEA-TECDOC-1154, 2000.

DR. UNER COLAK

Metallurgical
Engineering (1982)

Istanbul Technical University

M.S. (1986)

IOWA State University
Nuclear Engineering Department

Ph. D. (1989)

IOWA State University
Nuclear Engineering Department

1989- present

Hacettepe University
Nuclear Engineering Department

CEA METHODS IMPROVEMENT IN HTTR MODELLING

F. Damian and X. Raepsaet, CEA, France

Paper will be handed out separately

THE BEHAVIOUR OF FISSION PRODUCTS IN THE HTGR FUEL IRRADIATED IN THE IVV-2M REACTOR

K.N. KOSHCHAYEV

Sverdlovsk Branch of R&D Institute of Power Engineering, Zarechny, P.O.Box 29, 624250 - Russia

and

A.S. CHERNIKOV

RPA "Lutch", Podolsk, 142100 - Russia

ABSTRACT

The results of the post-irradiation investigations of fission products behaviour in HTGR fuel and its main elements such as kernels, protective coatings and matrix graphite are considered. The dominating role of SiC layer in the protective coating of coated particles in the retention of the volatile and solid fission products, being of great radiological importance, is noticed.

1. Introduction

Radioactivity of a HTGR primary circuit is mainly constituted by the release of light volatile (I, Cs, Ag and other) and solid fission products (FP) since their half-life is more than that of the gaseous FP. Therefore the radioactivity is accumulated during the entire reactor campaign.

It is known that the total FP release from spherical fuel elements (SFE) is determined by the efficiency of the diffusion transfer from fuel kernels through the coatings of coated particles (CP) and matrix graphite (MG) of SFE, the level of contamination of SFE matrix graphite and CP coatings with the fissile material (U-235) as well as defects in CP coatings. The FP release in the above SFE design elements has been studied at the post-irradiation stage; the methods used to investigate the FP behaviour in the HTGR SFE were as in [1].

2. Object of Investigation and Test Conditions

The SFE, dia. 60 mm, were manufactured by RPA "Lutch" and tested at the IVV-2M reactor. The investigated SFE were fabricated as based on the CP and MG, whose key data are summarised in Table 1. The irradiation parameters are presented in Table 2.

3. Test Results

3.1. A content of FP in matrix graphite and a failed CP fraction

The FP distribution profiles in MG and IMGA histograms obtained from the tests of two SFE (# 63 and # 88), exposed to electrolytic disintegration, are shown in Fig. 1. A content of solid FP in MG is determined by the amount of failed CP in SFE. Besides, the retention of light volatile FP (like Cs-137 and Cs-134) by MG is weak under the test temperatures. At the irradiation temperatures of 1000-1400°C, a retention capability of MG there was no more than 10 %. The data scattering, observed in the activity ratios of the defective CPs, testifies to a different degree of defectiveness of their coatings, especially of the SiC layer.

3.2. A content of FP in CP

A regular content of FP and U-235 in the CP tested as SFE are shown in Fig. 2. The obtained data prove that the SiC layer is a main diffusion barrier against Cs release at 1000-1400°C and the fuel burn-up of 14-19 % FIMA. The release of Cs from the kernel into internal PyC layers was considerable there. The effective coefficients of Cs diffusion in the different coating layers were calculated from the obtained profiles of Cs distribution along a CP radius and the SFE irradiation modes (see Table 3).

The analysis of the obtained results testifies that the Cs diffusion transfer from the kernel into the coating is the factor determining the release from intact CP. The contribution of the external PyC layer contaminated by U-235 of a concentration of 10^{14} – 10^{15} at./cm³ to the total release is considerably less.

3.3. FP release from kernel

The results on Cs release from the fuel kernels of the intact CP, irradiated as included in both SFE and mock-up samples [2], are in Figures 3 and 4, where each point is determined for every 10 to 15 coated particles controlled in the test.

By the summarised information (presented graphically), the relative Cs release from UO₂-kernels at the end of their exposure is as large as 0.76 to 0.95. It reveals a weak dependence in a burn-up region higher than 10 % FIMA and temperatures over 1000°C. At the irradiation temperature less than 1400°C the release of Ce, Ru, Zr from the kernels is mainly determined by the mechanisms of recoil and knock-out.

3.4. FP release from SFE

Table 4 presents the FP release data for the end of irradiation, they are calculated from the content and distribution of fission products, uranium in the kernels and coatings in SF and CP. When analysing the data, it is necessary to keep in mind the accelerated irradiation modes used for in-pile experiments in the channels "Vostok" to reveal the maximum capabilities of the fuel. Therefore the fuel, supplied for the post-irradiation investigations, has been exposed to the high temperature (1000-1400°C) and the burn-up higher than required.

Conclusion

1. The main factor determining the cesium release from the fuel elements is the portion of coated particles containing the defective SiC coatings.
2. Cesium releases practically fully (80-96 %) from the kernel to the coating; and when the coating is disintegrated, cesium releases outside the coated particles. However, the integrity of the coated particles with respect to gas fission products can be preserved.
3. The graphite matrix and fuel coating are weak diffusion barriers against cesium release; their retention capability is no more than 10 % , and their equilibrium concentration is 10^{-6} to 10^{-4} Ci/g graphite.
4. The intact CP coatings provide a reliable retention of cesium with the relative release being no more than 5×10^{-6} – 6×10^{-5} . The release of Ce, Ru and Zr does not exceed a value of 2×10^{-7} .

Table 1. Data of SFE subjected to complex post-irradiation investigations

Experiment (SFE number)	Coated Particles Data							Matrix graphite density (g/cm ³)
	CP lot	Kernel: diameter (μm) / UO ₂ density (g/cm ³)	Thickness (μm) / Density (g/cm ³) of a layer					
			PyC-1	PyC-2	PyC-3	SiC-4	PyC-5	
"Vostok-2" (SFE-16, -18)	2J25	540 / 10.0	85 / 1.1	30 / 1.5	30 / 1.8	40 / 3.2	95 / 1.95	1.82 - 1.83
"Vostok-3" (SFE-52)	V12	520 / 10.4	80 / 0.8	50 / 1.6	30 / 2.0	55 / 3.2	45 / 1.8	1.82 - 1.83
"Vostok-4" (SFE-63)	2V215	490 / 10.8	100 / 1.0	-	70 / 1.8	55 / 3.2	80 / 1.8	1.82 - 1.84
"Vostok-5" (SFE-88)	2V535	500 / 10.5	120 / 0.9	-	70 / 1.8	60 / 3.2	60 / 1.8	1.83 - 1.88

Table 2. SFE irradiation conditions

SFE number	Temperature (°C)	Fuel burn-up (% FIMA)	Fast neutron ($E > 0.2$ MeV) fluence ($\times 10^{21}$ cm ⁻²)
16	1370 - 1130	17.3	1.8
18	1000 - 1400	14.8	1.3
52	1180	14.2	2.2
63	1100 - 1200	18.7	1.5
88	1300 - 1400	18.5	1.6

Table 3. Effective coefficients of Cs diffusion in CP coatings

SFE number	CP lot	Effective diffusion coefficient, D_{eff} (cm ² /s)	
		PyC layer ($\rho = 1.5 - 1.8$ g/cm ³)	SiC layer ($\rho = 3.2$ g/cm ³)
18	2J25	$(1.5 \pm 0.5) \times 10^{-12}$	$(2.3 \pm 1.0) \times 10^{-13}$
52	V12	$(3.0 \pm 0.9) \times 10^{-13}$	$(5.0 \pm 1.6) \times 10^{-14}$
63	2V215	$(2.5 \pm 0.5) \times 10^{-12}$	$(1.5 \pm 0.3) \times 10^{-13}$
88	2V535	$(3.2 \pm 1.1) \times 10^{-12}$	$(1.4 \pm 0.4) \times 10^{-13}$

Table 4. Cesium release from SFE elements at the irradiation temperatures of 1000 - 1400°C

SFE number	Fission product	Relative Cs release from			Failed CP fraction in SFE	Uranium-235 contamination of SFE free-fuel zone (g ²³⁵ U / g graphite)	Relative Cs release from SFE
		kernel	intact CPs	failed CPs			
16	Cs-134	0.95	6.0×10^{-5}	0.93	4.61×10^{-3}	1.7×10^{-6}	3.6×10^{-3}
	Cs-137	0.90	6.0×10^{-5}	0.90			3.2×10^{-3}
18	Cs-134	0.89	5.0×10^{-5}	0.45	6.63×10^{-4}	1.1×10^{-6}	2.3×10^{-4}
	Cs-137	0.78	5.0×10^{-5}	0.35			2.0×10^{-4}
52	Cs-134	0.94	5.0×10^{-6}	0.65	1.16×10^{-3}	3.0×10^{-7}	7.8×10^{-4}
	Cs-137	0.86	2.0×10^{-6}	0.50			7.6×10^{-4}
63	Cs-134	0.96	1.8×10^{-5}	0.48 - 0.80	1.45×10^{-2}	1.5×10^{-7}	4.3×10^{-3}
	Cs-137	0.93	1.5×10^{-5}	0.45 - 0.76			3.8×10^{-3}
88	Cs-134	0.96	2.0×10^{-5}	0.60 - 0.96	3.43×10^{-2}	6.2×10^{-8}	2.5×10^{-2}
	Cs-137	0.95	1.5×10^{-5}	0.50 - 0.95			2.2×10^{-2}

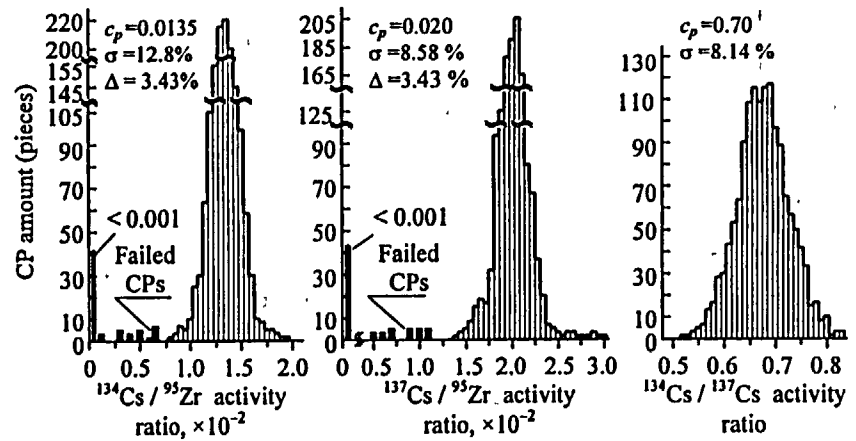
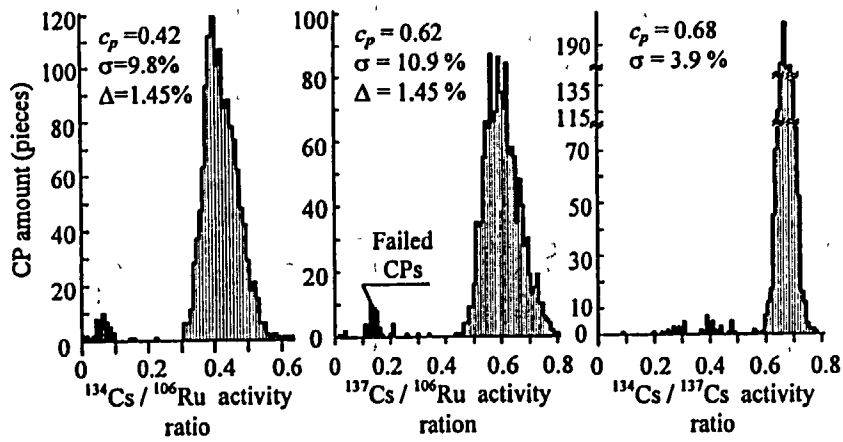
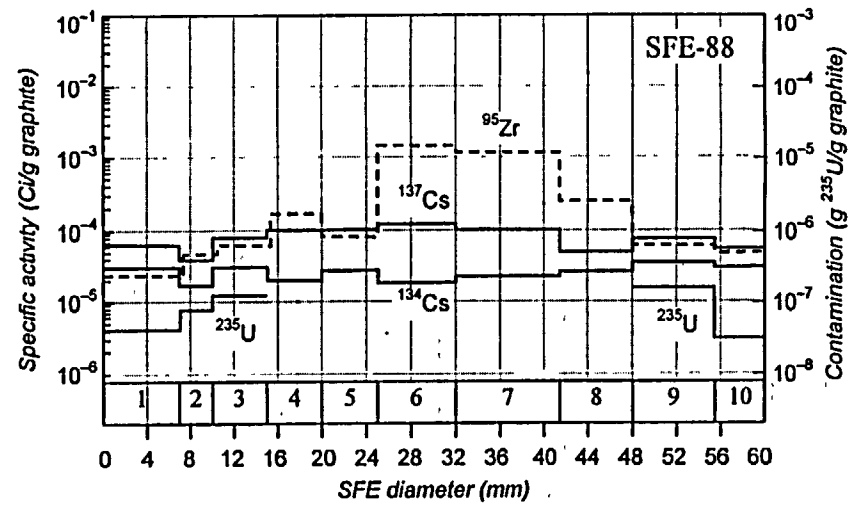
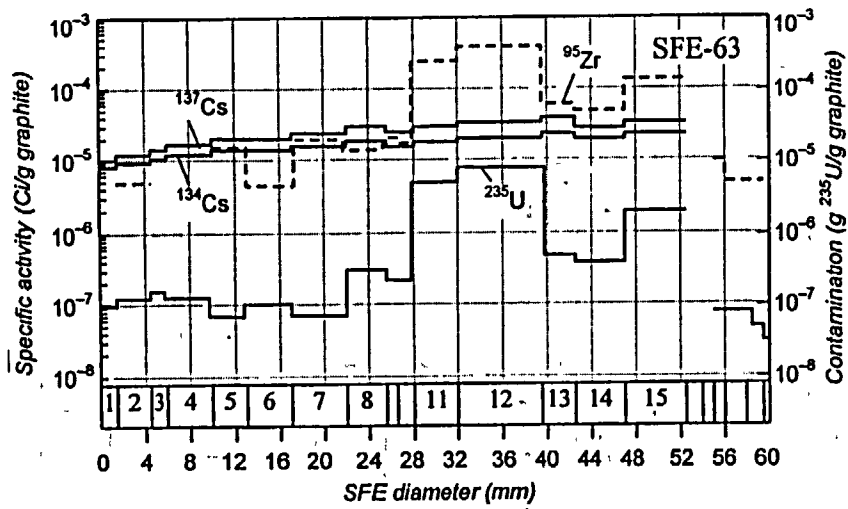


Fig.1. Distribution profiles of U-235, Cs-137, Cs-134, Zr-95 and IMGA histograms for spherical fuel elements 63 and 88.

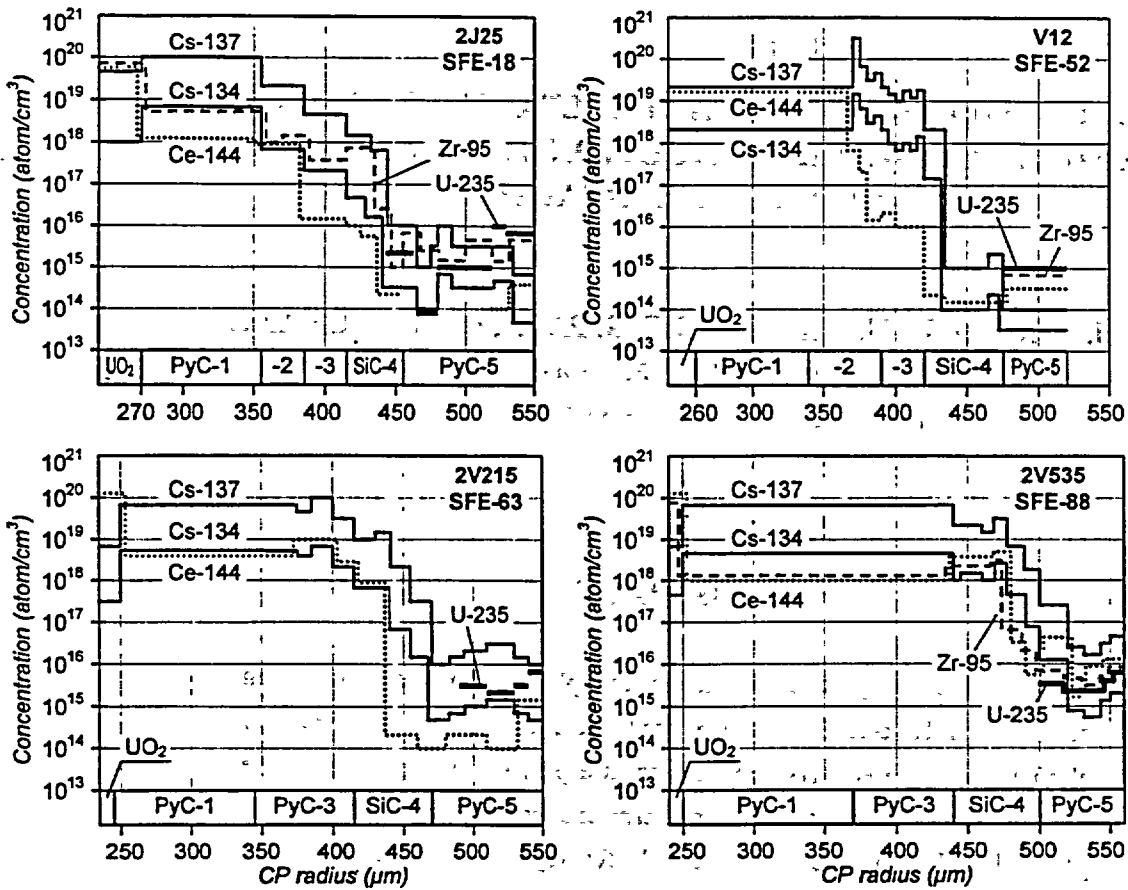


Fig.2. FP distribution profiles in protective coating layers of coated particles.

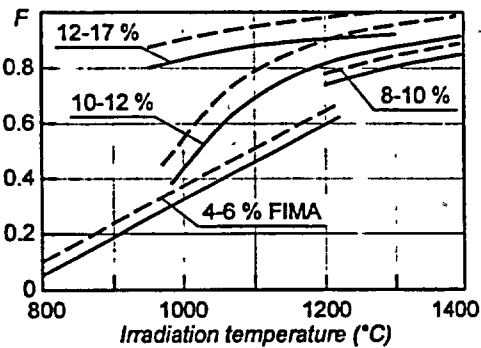


Fig.3. Relative Cs-134 (---) and Cs-137 (—) release from fuel kernel in CP coating.

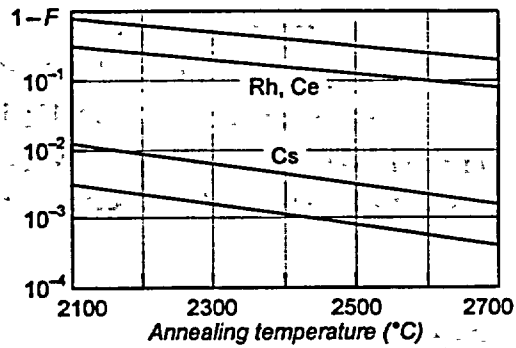


Fig.4. Residual content of FP in CPs after their failures during annealing.

References

- [1] K.N. Koshcheyev, L.I. Menkin, et al. Experimental Capabilities of IVV-2M Reactor and its Research Complex to Determine Workability of Coated Particles and Fuel Elements of High Temperature Gas-Cooled Reactors.— In: "Basic Studies High-Temperature Engineering. First Information Exchange Meeting."— Paris, France, 27-29 September, 1999, p.345.
- [2] K.N. Koshcheyev, A.I. Deryugin, V.A. Kashparov, et al. VANT. Ser.: Atomic and Hydrogen Technology, 1987, No.3, p.7.

CONCEPTUAL DESIGN OF A SIMULTANEOUS HYDROGEN AND HEAVY WATER PRODUCTION SYSTEM FOR HIGH TEMPERATURE REACTORS

H. CHUNG, D. H. AHN, M. LEE, S. PAEK, and J. H. CHANG

Korea Atomic Energy Research Institute

P. O. Box 105, Yuseong, Daejeon, 305-600, Korea

ABSTRACT

High temperature gas-cooled reactors can play a significant role, with respect to a large-scale hydrogen production, if used as a provider of electricity in the electrolysis process or as a provider of high temperature heat in fossil fuel conversion or thermochemical cycles. A variety of potential hydrogen production methods for high temperature gas-cooled reactors were analyzed. They are steam reforming of natural gas, high-temperature electrolysis, thermochemical cycles, and etc. For the simultaneous production of heavy water from the hydrogen plants, Korea Atomic Energy Research Institute has developed a catalyst for the deuterium exchange reaction, which is not wetted by liquid water. The catalyst consists of platinum deposited on a styrene-divinylbenzene copolymer support. Both the catalyst and the combined processes were discussed.

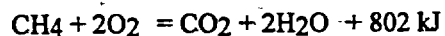
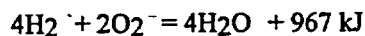
1. Introduction

The high-temperature gas-cooled reactor (HTR) represents one type of the next generation of nuclear reactors for safe and reliable operation as well as for efficient and economic generation of energy [1, 2]. The industrial power plant with HTR can provide three energetical connection points: high-temperature heat up to 1000 °C, high-temperature steam of about 530 °C, and electricity. In heat applications, heat is delivered from the helium coolant with an outlet temperature at the high end of 750 - 950 °C, for the conversion of fossil fuels and/or water into clean hydrogen. In this paper, the authors analyze various potential hydrogen production

methods for high temperature gas-cooled reactors. Furthermore, for the simultaneous production of heavy water from the hydrogen plants, Korea Atomic Energy Research Institute has developed a catalyst for the deuterium exchange reaction, which is not wetted by liquid water. The catalyst consists of platinum deposited on a styrene divinylbenzene copolymer support. Both the catalyst and the combined processes are presented.

2. Hydrogen Production Processes

Potential methods for the production of hydrogen with HTR are the reforming of fossil fuels and water splitting. The non-fossil generation of heat for the endothermal reforming reaction represents a means of reduction of carbon dioxide emissions. The theoretical energies required and CO₂ reduction effects are listed in Table 1. The values of heat of formation at 25 °C were taken from the reference [3]. Theoretical reduction of CO₂ emissions is calculated as follows. In case of methane steam reforming, the heats of combustion for H₂ and CH₄ are:



So, theoretical reduction of CO₂ emissions is $(967/802 - 1)$ or 20.6%.

3. Simultaneous Heavy Water Production

Heavy water is used as moderator and coolant in Pressurized Heavy Water Power Plants. Korea is now operating four Pressurized Heavy Water Power Plants. A small make-up of about one per cent of the heavy water inventory per year is needed to replace losses by leakage. The total make-up is about 18Mg/a. The Combined Electrolysis Catalytic Exchange (CECE) process can be applied to the water electrolysis in Table 1 for the simultaneous hydrogen and heavy water production [4]. In the process, the electrolytic hydrogen steadily loses most of its deuterium as it moves up the catalyst column in counter-current flow with the feed water trickling down into the electrolysis cell. The water becomes enriched in deuterium according to the catalytic isotope exchange reaction as it passes down the catalyst bed. The overall deuterium profile is one in which the deuterium concentration in the water increases along the length of the column from top to bottom, while in the gas phase the deuterium concentration decreases from the bottom to top. The other interesting method applicable to the methane steam reforming plant of Table 1 is the Combined Industrially Reforming and Catalytic Exchange (CIRCE) process [5]. This process operates in conjunction with a hydrogen-producing Steam-Methane Reformer. Another catalytic method (Combined ChloroAlkali Electrolysis and Catalytic Exchange or CAECE) proposed by the authors is suitable to the chloralkali electrolysis process (CAP) in Table 1.

Table 1. Characteristics of potential splitting processes for hydrogen production.

Splitting process	Chemical reactions with enthalpy change [kJ/mol]	Theoretical reduction of CO ₂ emissions [%]	Minimum enthalpy required for the production of hydrogen [kJ/mol]
Methane steam reforming	$\text{CH}_4 + 2\text{H}_2\text{O} = \text{CO}_2 + 4\text{H}_2 - 165$	20.6	41
Butane steam reforming	$\text{C}_4\text{H}_{10} + 8\text{H}_2\text{O} = 4\text{CO}_2 + 13\text{H}_2 - 486$	18.3	37
Coal steam reforming	$\text{C} + 2\text{H}_2\text{O} = \text{CO}_2 + 2\text{H}_2 - 90$	22.8	45
Methane thermal cracking	$\text{CH}_4 = \text{C} + 2\text{H}_2 - 76$	9.5	38
Water electrolysis	$\text{H}_2\text{O} = \text{H}_2 + 1/2\text{O}_2 - 242$	CO ₂ free	242
Chloralkali electrolysis	$2\text{NaCl} + 2\text{H}_2\text{O} = 2\text{NaOH} + \text{H}_2 + \text{Cl}_2 - 453$	CO ₂ free	453
Iodine-sulfur process	$2\text{HI} = \text{H}_2 + \text{I}_2 - 10$ $\text{I}_2 + \text{SO}_2 + 2\text{H}_2\text{O} = 2\text{HI} + \text{H}_2\text{SO}_4 + 40$ $\text{H}_2\text{SO}_4 = \text{H}_2\text{O} + \text{SO}_2 + 1/2\text{O}_2 - 272$	CO ₂ free	282
Sulfuric acid hybrid process	$\text{H}_2\text{SO}_4 = \text{H}_2\text{O} + \text{SO}_2 + 1/2\text{O}_2 - 272$ $\text{H}_2\text{O} + \text{SO}_2 + \text{H}_2\text{O} = \text{H}_2\text{SO}_4 + \text{H}_2 + 30$	CO ₂ free	272
Metal-metal hydride hybrid process	$2\text{Li} + \text{H}_2\text{O} = 2\text{LiH} + 1/2\text{O}_2 - 50$ $2\text{LiH} = 2\text{Li} + \text{H}_2 - 192$	CO ₂ free	242

Figure 1 shows a schematic of one type of CAP after adaptation to the CAECE process. The CAECE process is in three stages, and strictly speaking, CAECE is used only in the first stage where deuterium is extracted from the hydrogen produced in the CAP, via the water feed to the CAP. Hydrogen produced in the CAP is routed to a catalyst column where it contacts a counter-flow of water. The water picks up deuterium from the hydrogen in the column and enters the CAP substantially enriched in deuterium. The deuterated sodium hydroxide is treated with carbon dioxide to recycle the product water. Material balance shows that a plant of 65.4MgH₂/day can co-produce heavy water at the rate of 18MgD₂O/a.

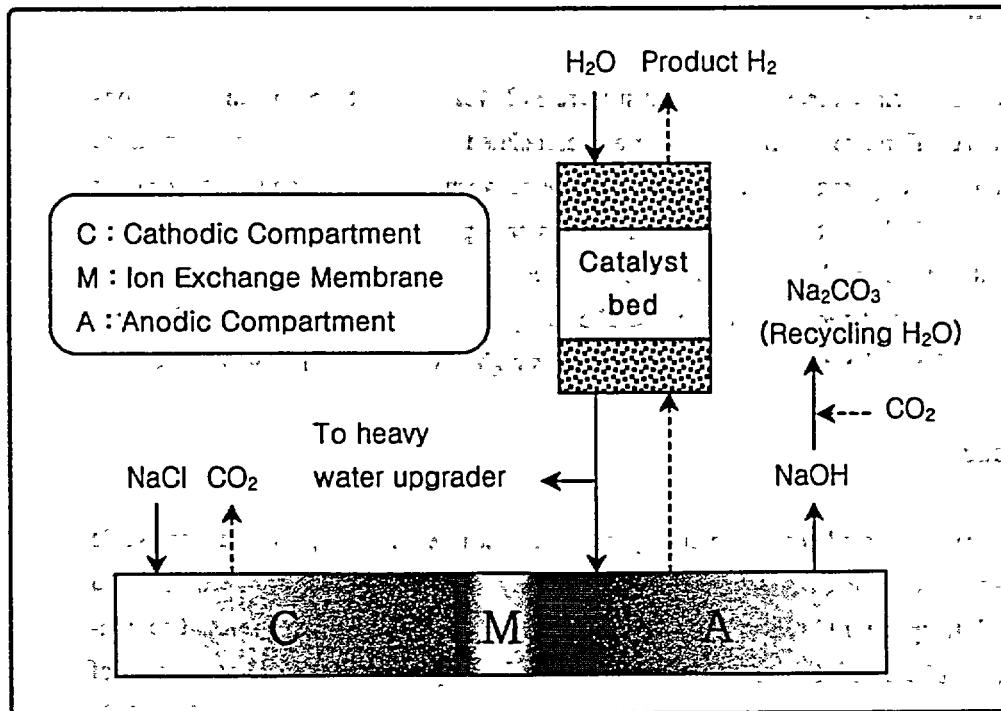


Fig. 1. Schematic of one type of CAP after adaptation to the CAECE process.

4. Experimental

The authors have developed a catalyst for the deuterium exchange reaction, which is not wetted by liquid water [6]. The catalyst is filled up in the catalyst bed of Fig. 1. Macroporous styrene-divinylbenzene copolymer (SDBC) was synthesized and selected as the catalyst support. Solvents such as toluene, n-heptane and 2-ethyl-1-hexanol were used in the synthesis. The specific surface area and the pore volume of the catalyst support could be controlled by the ratio of monomer to solvent. Dissolving hexachloroplatinic acid in ethanol made the platinum precursor solution. After platinum being impregnated over the SDBC support, the sample was directly reduced in flowing hydrogen of 230 °C for 15 hours. The platinum loading on the SDBC support was measured by ICP-MS analytical method. The physical properties of the catalyst, such as BET surface area, pore volume and pore size distribution were measured by physical adsorption of nitrogen gas at liquid nitrogen temperature of 77K using Quantachrom Autosorb-6.

5. Experimental Results and Discussion

The measured BET surface areas of the catalyst were 318–422 m²/g. The platinum dispersions were 32–110%. A differential chemical reactor and associated equipment were used to measure the catalytic activity of hydrogen – deuterium exchange between water vapor and hydrogen over Pt/SDBC catalysts. With mixtures of hydrogen and water vapor of low deuterium content, the exchange activity of the catalyst was characterized by a transfer coefficient k_r , as the moles of HD transferred per second per gram of catalyst. The catalytic activity increased with an increase in the platinum loading. The transfer coefficient k_r was as high as 0.017 mole HD/g-cat. /sec.

6. Conclusions

High temperature gas-cooled reactors can play a significant role, with respect to a large-scale hydrogen production, if used as a provider of electricity in the electrolysis process or as a provider of high temperature heat in fossil fuel conversion or thermochemical cycles. The non-fossil generation of heat with HTR for the endothermal reforming reaction represents a means of reduction of carbon dioxide emissions. The theoretical reduction of CO₂ emissions is about 20% in hydrocarbon steam reforming processes. The simultaneous production of heavy water from the hydrogen plant was also found feasible.

References

- [1] IAEA, Hydrogen as an Energy Carrier and Its Production by Nuclear Power, IAEA-TECDOC-1085, International Atomic Energy Agency, Vienna, May 1999
- [2] J. H. Chang, K. J. Yoo, and C. K. Park, Status of Hydrogen Production by Nuclear Power, KAERI/AR-600/2001, Korea Atomic Energy Research Institute, July 2001
- [3] R. H. Perry and Don W. Green, Perry's Chemical Engineers' Handbook, 6th ed., McGraw-Hill, New York, 1984
- [4] M. Hammerli, W. H. Stevens, and J. P. Butler, Combined Electrolysis Catalytic Exchange Process for Hydrogen Isotope Separation, in Separation of Hydrogen Isotopes, ACS Symposium Series, American Chemical Society, 1978
- [5] C. J. Allan et al., New Heavy Water Processing Technologies, 12th PBNC, Seoul, Korea, October 29 - November 2, 2000
- [6] S. Paek, H. Chung, and S. I. Woo, Preparation, Characterization, and Reactivity of Pt/SDBC Catalysts for the hydrogen-Water Isotopic Exchange Reaction, Journal of Radioanalytical and Nuclear Chemistry, Vol. 242, No. 3, 1999

THERMODYNAMIC ANALYSIS OF PBMR PLANT

S. SEN and O.K.KADIROGLU

*Hacettepe University, Nuclear Engineering Department
06532 Beytepe, Ankara, Turkey*

ABSTRACT

The thermodynamic analysis of a PBMR is presented for various pressures and temperatures values. The design parameters of the components of the power plant are calculated and an optimum cycle for the maximum thermal efficiency is sought for.

1. Introduction

The thermodynamic analysis of a PBMR is of importance at the design stage. Such an analysis will not be complete if the component design is not included in the analysis as well as the economic analysis. Unfortunately a complete set of design and economical data are not easy to acquire. There are various design parameters available in the open literature that are not in agreement with each other [1,2]. Thus a detailed analysis of the thermodynamic cycle and design of the components of such a cycle is of academic interest as well as practical use. A computer program capable of optimizing a PBMR plant for a limited amount of input parameters is presented as a preliminary result of an ongoing project.

2. Modeling

The PBMR power plant has two turbocompressors, a power turbine, a recuperator and two coolers and the pebble bed reactor. The simplified block diagram of the plant is shown in fig. 1. The T-s diagram of the Brayton cycle of this power plant is presented in fig 2. All heat exchangers, recuperator and two coolers, are designed in such a way that they have the physical dimensions very similar to ones given in the literature [1].

3. Calculations

The computer code requests the properties at the inlet of the low pressure compressor and at the outlet of the reactor core. Then the code calculates the number of compressors needed to achieve the required compression ratio and the design parameters of the compressors, like number of stages, blade angles, etc. Intercooler design parameters, like the dimensions of the intercooler, pressure drops of both sides, water flow rate, etc. are also calculated. A rough calculation for the recuperator design parameters are performed to determine core inlet properties.

A detailed core thermal hydraulic modeling of the core is not performed at this point of time but will be added to the code in the near future. The core inlet and outlet temperatures are taken as metallurgical and radiation damage limits for the graphite internals.

Thermodynamic state and design parameters of the turbines driving the compressors and the generator and the recuperator inlet properties are calculated. The exhaust pressure of the power turbine is changed such that the new cycle has a better thermal efficiency than the initial guess.

This iterative procedure is terminated when the highest thermal efficiency is obtained for the given input temperatures and pressures.

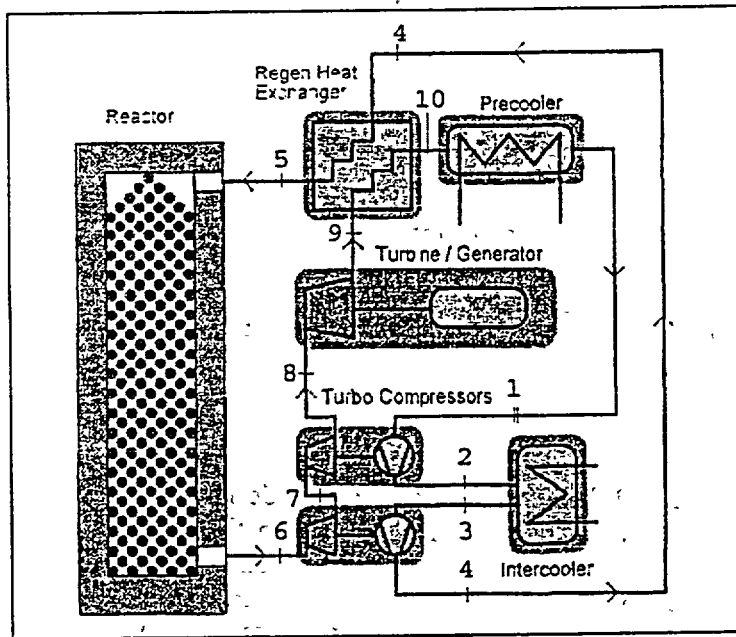


Fig 1. Layout of a Typical PMBR Power Conversion System [1]

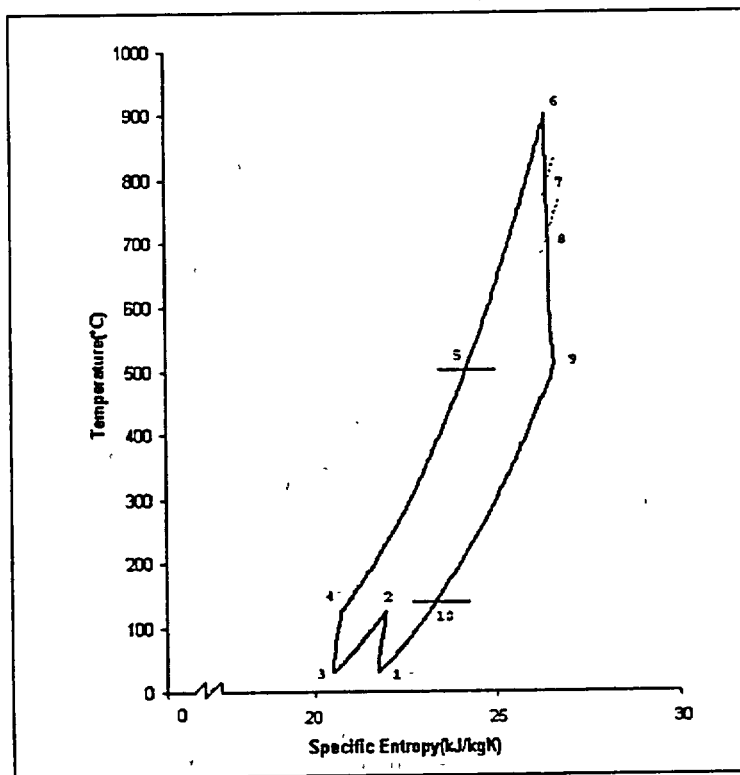


Fig 2. T-S Diagram of a typical PBMR system

4. Results

A sample case for the maximum operation pressures of 7, 8.5, 10 MPa and 30°C low pressure compressor inlet temperature are run for the core outlet temperature of 900°C and 950°C and core inlet temperature of 500°C. The results, pressure and temperature values of each points on the Brayton cycle, required and generated power for compressors, coolant pumps and turbines and the overall thermal efficiency are presented in table 1.

Table 1. Thermodynamic Analysis of PBMR System

P_{max} (MPa)	7.0		8.5		10.0		
T_{max} (°C)	900.00	950.00	900.00	950.00	900.00	950.00	
1	P (MPa)	2.1800	1.9500	2.6700	2.3700	3.1700	2.8000
	T (°C)	30.00	30.00	30.00	30.00	30.00	30.00
2	P (MPa)	3.9064	3.6946	4.7639	4.4883	5.6303	5.2915
	T (°C)	123.02	144.23	125.91	136.63	124.52	136.24
3	P (MPa)	3.9062	3.6944	4.7638	4.4882	5.6302	5.2914
	T (°C)	30.00	30.00	30.00	30.00	30.00	30.00
4	P (MPa)	7.0052	7.0033	8.5038	8.5036	10.0024	10.0034
	T (°C)	127.43	136.20	125.41	137.34	124.00	135.71
5	P (MPa)	7.0000	7.0000	8.5000	8.5000	10.0000	10.0000
	T (°C)	500.00	500.00	500.00	500.00	500.00	500.00
6	P (MPa)	6.8250	6.8250	8.3250	8.3250	9.8250	9.8250
	T (°C)	900.00	950.00	900.00	950.00	900.00	950.00
7	P (MPa)	5.3743	5.3133	6.5897	6.4628	7.8052	7.6582
	T (°C)	802.57	843.80	804.59	842.66	805.99	844.29
8	P (MPa)	4.0468	3.8818	5.0260	4.8258	5.9801	5.7274
	T (°C)	697.29	723.56	703.63	730.42	706.51	732.46
9	P (MPa)	2.1814	1.9513	2.6712	2.3712	3.1709	2.8011
	T (°C)	509.11	511.49	509.78	510.05	512.00	509.81
10	P (MPa)	2.1803	1.9504	2.6703	2.3703	3.1702	2.8002
	T (°C)	134.68	144.82	133.85	145.02	135.78	144.69
W_{c1} (MW)	72.71	83.04	69.73	77.51	68.71	77.24	
W_{c2} (MW)	70.83	77.20	69.36	78.03	68.34	76.85	
W_{p1} (MW)	4.86	7.03	4.33	5.80	4.15	5.75	
W_{p2} (MW)	5.09	7.06	4.68	6.26	4.65	6.20	
W_t (MW)	123.46	139.13	127.18	144.58	127.61	146.07	
η	0.390	0.382	0.406	0.405	0.409	0.410	

5. References

- [1] "Review of the Pebble Bed Modular Reactor (PBMR) Plant" Current Status and Future Development of Modular High Temperature Gas Cooled Reactor Technology, p.21, IAEA-TECDOC-1198, 2000.
- [2] Introduction to the Pebble Bed Modular Reactor (PBMR), Document No: 009949-185, Rev.1, p.43-49, 2001